Climate–dependent phosphorus forms and their utilization by plants and microorganisms

Inauguraldissertation
der Philosophisch–naturwissenschaftlichen Fakultät
der Universität Bern

vorgelegt von

Moritz Johannes Köster

aus Deutschland

LeiterInnen der Arbeit:

Prof. Dr. Sandra Spielvogel
Institut für Pflanzenernährung und Bodenkunde,
Christian–Albrechts–Universität zu Kiel, vormals Professur für Bodenkunde,
Geographisches Institut, Universität Bern

Prof. Dr. Michaela Dippold
Biogeochemie der Agrarökosysteme,
Georg-August-Universität Göttingen

Climate–dependent phosphorus forms and their utilization by plants and microorganisms

Inauguraldissertation
der Philosophisch–naturwissenschaftlichen Fakultät
der Universität Bern

vorgelegt von

Moritz Johannes Köster

aus Deutschland

LeiterInnen der Arbeit:

Prof. Dr. Sandra Spielvogel
Institut für Pflanzenernährung und Bodenkunde,
Christian–Albrechts–Universität zu Kiel, vormals Professur für Bodenkunde,
Geographisches Institut, Universität Bern

Prof. Dr. Michaela Dippold
Biogeochemie der Agrarökosysteme,
Georg-August-Universität Göttingen

Von der Philosophisch–naturwissenschaftlichen Fakultät angenommen.

Bern, 11.10.2021

Der Dekan

Prof. Dr. Martin Grosjean

This is a human-readable summary of (and not a substitute for) the license. Disclaimer.

You are free to:

Share — copy and redistribute the material in any medium or format The licensor cannot revoke these freedoms as long as you follow the license terms.

Under the following terms:

Attribution — You must give appropriate credit, provide a link to the license, and indicate if changes were made. You may do so in any reasonable manner, but not in any way that suggests the licensor endorses you or your use.

NonCommercial — You may not use the material for commercial purposes.

NoDerivatives — If you remix, transform, or build upon the material, you may not distribute the modified material.

No additional restrictions — You may not apply legal terms or technological measures that legally restrict others from doing anything the license permits.

Notices:

You do not have to comply with the license for elements of the material in the public domain or where your use is permitted by an applicable exception or limitation.

No warranties are given. The license may not give you all of the permissions necessary for your intended use. For example, other rights such as publicity, privacy, or moral rights may limit how you use the material.

Table of contents

List of Figures

List of Supplementary Figures

List of Tables

List of supplementary Tables

Abbreviations

C	Carbon
C_{mic}	Microbial biomass carbon
CO_2	Carbon dioxide
DCB	Dithionite–citrate–bicarbonate
GC	Gas–chromatography
ddH_2O	Double distilled water (ultrapure)
LMWOA	Low–molecular weight organic acids (in this work often used as a collective term for oxalic, malic, and citric acid)
MS	Mass–spectrometer
N	Nitrogen
NH_4–oxalate	Ammonium–oxalate
P	Phosphorus
P_{mic}	Microbial biomass phosphorus
SRO	Short–range order
TOC	Total soil organic carbon
XANES	X–ray absorption near edge structure

Summary

Phosphorus (P) in soil is an important nutrient for biological activity and often limits plant and microbial growth in natural ecosystems. Due to its chemical nature and conditions in soil, its mobility in soil is limited by strong sorption to metal(hydr)oxides and precipitation with calcium (Ca), iron (Fe), and aluminum (Al) ions. P speciation and fixation in soil changes during pedogenesis from mainly Ca-bound P in early developmental stages to Fe-, and Al-bound P and organic P in more weathered soils. The rate of mineral weathering and soil development strongly depend on climatic conditions. Therefore, ecosystems under varying climate, but with soils that originate from similar parent material, are expected to show different states of weathering and P speciation in soil. Plants and microorganisms possess adaptations to mobilize P from various sources. It is believed that P cycling mechanisms and processes change with the P species that are available in soil.

The aim of this work was to determine climate-dependent P speciation and biotic P cycling strategies along an aridity gradient in the Chilean Coastal Cordillera. The study sites comprised a sequence of ecosystems from an arid shrubland in the north to a Mediterranean woodland as intermediate site and a humid-temperate forest in the south. The studies of this work focused on the question whether P nutrition in a given ecosystem depends mainly on the acquisition of P from mineral sources, or if recycling of organic P is the main P source. Moreover, the focus was on the impact of root-derived labile C on P cycling under varying climatic conditions. The contribution of low-molecular-weight organic acids (LMWOAs) to mineral weathering (weathering agents) but also to organic P recycling was scrutinized. This work consists of four studies that investigated P speciation in soil and the mechanisms driving P cycling within the plant-soil-microbe system. P speciation in the rhizosphere and bulk soil was determined by X-ray absorption near edge structure (XANES), a powerful tool to determine the speciation of inorganic P in soil. Moreover, P was extracted as operationally defined P pools as water extractable, $NaHCO_3$ extractable, ammonium-oxalate extractable (NH_4-oxalate), and dithionite-citrate-bicarbonate (DCB) extractable P. The sorption capacity of soils for P was determined by ^{33}P application. The adsorption of the tracer to the soil solid phase was measured and the sorption capacity of soils was calculated. Microbial uptake of sorbed inorganic P was quantified under steady state conditions and under the addition of glucose (rhizosphere conditions). A method to extract low-molecular-weight organic acids was adapted to measure the ^{13}C content in these weathering agents. LMWOA were extracted after ^{13}C enriched CO_2 application (pulse labeling). This allowed not only to relate P species to the exudation of organic acids in general, but also to quantify plant and microbial C allocation to these weathering agents.

Primary Ca-bound P contents were highest in the arid shrubland ecosystem and declined towards the Mediterranean woodland and humid-temperate forest. Secondary precipitated Fe- and Al-P followed the same trend, while inorganic P sorbed to Fe- and Al-(hydr)oxides and organic P increased with decreasing aridity. Accumulation of organic P in root proximity was detected in the Mediterranean woodland and humid-temperate forest, reflecting high biological activity at these sites. P speciation was correlated with LMWOA contents, phosphatase kinetics and microbial biomass carbon. It was demonstrated, that under arid climate and in the subsoil of the Mediterranean woodland, LMWOA contributed to mineral weathering. They fundamentally changed their role in the Mediterranean woodland's topsoil and humid-temperate forest soil, where LMWOA liberated organic P, likely for enzymatic degradation. It was inferred that P cycling under arid conditions is driven by the acquisition of mineral inorganic P but towards decreasing aridity, the importance of organic P recycling increases.

The P sorption capacity of soils was highest under a humid climate and highly weathered soils and was explained by high contents of ferrihydrite, ammonium-oxalate leachable Al and clay. Microbial uptake of sorbed inorganic P from the soil's solid phase was highest in the A-horizon of the Mediterranean woodland soil and was low in the humid-temperate forest. In the latter, phosphatase activity was high, indicating organic P recycling and a low relevance of sorbed inorganic P to meet the P requirements of the biota. Inorganic P sorbed to the soil solid phase was most intensively utilized in the Mediterranean woodland soil and microbial uptake of sorbed inorganic P increased when glucose was added. This demonstrates that P limitation in the Mediterranean woodland soil can be reduced when readily available C is exuded in the rhizosphere. In contrast, microbiota in the other ecosystems along the ecosequence were either not primarily P limited or relied on different P sources. Moreover, in the humid-temperate forest a plethora of C compounds are available for microbial utilization, reducing the importance of labile root exuded C.

In accordance with the XANES results, operationally defined P pools showed an increase of plant available P and a decrease of precipitated P with decreasing aridity. While the content of LMWOA in soil was higher in the humid-temperate forest than the Mediterranean woodland and arid shrubland, ^{13}C allocation to LMWOA was of equal magnitude in the humid-temperate forest and Mediterranean woodland. High enzyme activities in the humid-temperate forest imply the utilization of organic P. A variety of P mobilizing processes can be assumed as weathering agents were only partly derived from recently exuded root C but also from unlabeled C sources. For the arid shrubland and Mediterranean woodland it was shown that the content of fungi-derived oxalic acid is positively correlated with well crystallized inorganic P (DCB leachable P),

pointing to fungi as important organisms to mobilize hardly available P sources in these ecosystems. ^{13}C allocation patterns in the arid shrubland are similar to those in the Mediterranean woodland, even though contents are on a lower level. This is interpreted as adaption to drought in both off these ecosystems and an indication that aridity is driving belowground C allocation.

In summary it was demonstrated that biological weathering is an important process of P acquisition under arid and Mediterranean climate, but not under humid-temperate climate, where P recycling becomes more important. At the same time, LMWOA are important P cycling agents in soil; under arid conditions they support mineral weathering, while under humid climate they facilitate organic P recycling. C limitation of P acquisition is high under arid and Mediterranean climate and relieved under humid climate. With respect to climate dependent P cycling in soil it is concluded that each site has its specific P speciation, P availability, and stoichiometric nutrient constraints. It was, therefore, not possible to identify a systematic trend of these parameters along the ecosequence. Abiotic changes (i.e., climate change) likely result in nonlinear changes in P speciation, P availability, and stoichiometric nutrient limitations, impeding our ability to predict changes in P cycling as a result of changing abiotic conditions at a site.

Zusammenfassung

Phosphor (P) im Boden ist ein wichtiger Nährstoff für die biologische Aktivität, welcher in natürlichen Ökosystemen häufig das Wachstum von Pflanzen und Mikroorganismen limitiert. Aufgrund seiner chemischen Eigenschaften und der physikochemischen Gegebenheiten im Boden ist seine Mobilität im Boden durch starke Sorption an Metall(hydr)oxide und Ausfällung mit Calcium (Ca), Eisen (Fe) und Aluminium (Al) eingeschränkt. Die P-Speziierung und -Fixierung im Boden ändert sich während der Pedogenese von hauptsächlich Ca-gebundenem P in frühen Entwicklungsstadien zu Fe-, und Al-gebundenem- und organischem P in stärker verwitterten Böden. Die Geschwindigkeit der Mineralverwitterung und der Bodenentwicklung hängt stark von den klimatischen Bedingungen ab. Daher ist zu erwarten, dass Ökosysteme mit unterschiedlichem Klima, aber mit Böden, die aus ähnlichem Ausgangsmaterial entstanden sind, unterschiedliche Zustände der Verwitterung und P-Speziierung im Boden aufweisen. Pflanzen und Mikroorganismen verfügen über Mechanismen, um P aus verschiedenen Quellen zu akquirieren. Es wird angenommen, dass sich die biotischen Mechanismen und Prozesse des P-Kreislaufs den im Boden verfügbaren P-Spezies anpassen.

Ziel dieser Arbeit war es, die klimaabhängige P-Speziierung und die biotischen P-Mobilisierungsstrategien entlang eines Ariditätsgradienten in der chilenischen Küstenkordillere zu bestimmen. Die Untersuchungsstandorte bildeten eine Ökosystem- Sequenz von einem ariden Strauchland im Norden über ein mediterranes Waldgebiet zu einem feucht-temperierten Wald im Süden. Die Studien dieser Arbeit konzentrierten sich insbesondere auf die Frage, ob die pflanzliche P-Ernährung in einem gegebenen Ökosystem hauptsächlich auf der Aufnahme von P aus mineralischen Quellen beruht oder ob die Mineralisierung von organischem P die Haupt-P-Quelle darstellt. Darüber hinaus lag der Fokus der Arbeit auf den Auswirkungen von aus Wurzeln stammendem leicht verfügbarem Kohlenstoff (C) auf den P-Kreislauf unter variierenden klimatischen Bedingungen. Der Beitrag von niedermolekularen organischen Säuren (LMWOAs) zur mineralischen Verwitterung, aber auch zur Mineralisierung organischen Ps wurde untersucht. Diese Arbeit besteht aus vier Studien, die die P-Speziierung im Boden und die Mechanismen, die den P-Kreislauf innerhalb des Systems Pflanze-Boden-Mikrobe antreiben, untersuchten. Die P-Speziierung in der Rhizosphäre und im Boden wurde mittels Röntgen-Nahkanten-Absorptions-Spektroskopie (XANES) bestimmt, einer leistungsfähigen Methode zur Bestimmung der Speziierung anorganischen Ps im Boden. Darüber hinaus wurde P als Löslichkeits-definierte P-Formen als wasser-extrahierbares-, Natriumhydrogencarbonat-extrahierbares-, Ammonium-Oxalat-extrahierbares- und Dithionit-Citrat-Bikarbonat (DCB)-extrahierbares P bestimmt. Die Sorptionskapazität von Böden für P wurde mittels Applikation

von ^{33}P untersucht. Die mikrobielle Aufnahme von sorbiertem anorganischem P wurde unter stationären Bedingungen und unter Zugabe von Glukose (Bedingungen ähnlich denen der Rhizosphäre) quantifiziert. Eine Methode zur Extraktion niedermolekularer organischer Säuren wurde adaptiert, um den ^{13}C-Gehalt in diesen, die mineralische Verwitterung befördernden Stoffen zu messen. LMWOA wurden nach der Applikation von ^{13}C-angereichertem CO_2 extrahiert. Dies ermöglichte einerseits P-Spezies mit der Exsudation von organischen Säuren im Allgemeinen in Beziehung zu setzen, und andererseits auch die pflanzliche und mikrobielle C-Allokation zu diesen Verwitterungsmitteln zu quantifizieren.

Die primären Ca-gebundenen P-Gehalte waren im ariden Strauchland-Ökosystem am höchsten und nahmen zum mediterranen Waldgebiet und feucht-temperierten Wald hin ab. Sekundär gebundenes Fe- und Al-P folgte dem gleichen Trend, während anorganisches P, das an Fe- und Al-(Hydr)oxiden sorbiert ist, und organisches P mit abnehmender Trockenheit zunahmen. Eine Akkumulation von organischem P in der Nähe der Wurzeln wurde im mediterranen Wald und im feucht-temperierten Wald festgestellt, was eine hohe biologische Aktivität an diesen Standorten widerspiegelt. Die P-Speziierung wurde mit dem LMWOA-Gehalt, der Phosphatase-Kinetik und dem mikrobiellen Biomasse-Kohlenstoff korreliert. Es konnte gezeigt werden, dass LMWOA unter aridem Klima und im Unterboden des mediterranen Waldes zur Mineralverwitterung beitrugen. Ihre Rolle änderte sich jedoch grundlegend im Oberboden des mediterranen Waldes und im Boden des feucht-temperierten Waldes, wo LMWOA organisches P freisetzten, was dann für den enzymatischen Abbau zur Verfügung stand. Daraus wurde gefolgert, dass der P-Zyklus unter ariden Bedingungen durch die Aufnahme von mineralischem, anorganischem P angetrieben wird, mit abnehmender Trockenheit nimmt die Bedeutung der organischen P-Mineralisierung jedoch zu.

Die P-Sorptionskapazität der Böden war unter feuchtem Klima und stark verwitterten Böden am höchsten und wurde durch hohe Gehalte an Ferrihydrit, Ammonium-Oxalat-löslichem-Al und Ton erklärt. Die mikrobielle Aufnahme von sorbiertem anorganischem P von der Bodenfestphase war im A-Horizont des mediterranen Waldes am höchsten. Im feucht-temperierten Wald hingegen war die mikrobielle Aufnahme von sorbiertem anorganischem P gering, die Phosphataseaktivität jedoch hoch. Dies deutet auf die Mineralisierung organischen Ps und eine geringe Relevanz sorbierten anorganischem Ps zur Deckung des P-Bedarfs der Pflanzen und Mikroorganismen hin. An die Bodenfestphase sorbiertes anorganisches P wurde im Boden des mediterranen Waldes am intensivsten verwertet und die mikrobielle Aufnahme von sorbiertem anorganischem P erhöhte sich bei Zugabe von Glukose. Dies zeigt, dass die P-Limitierung im mediterranen Waldboden aufgehoben wird, wenn leicht verfügbarer C in der

Rhizosphäre ausgeschieden wird. Im Gegensatz dazu waren die Mikroorganismen in den anderen Ökosystemen entlang der Ökosequenz entweder nicht primär P-limitiert oder sie waren auf andere P-Quellen angewiesen. Darüber hinaus ist im feucht-temperierten Wald eine Vielzahl von C-Verbindungen für die mikrobielle Verwertung verfügbar, was die Bedeutung des von Wurzeln ausgeschiedenen Cs reduziert.

In Übereinstimmung mit den XANES-Ergebnissen zeigten Löslichkeits-definierte P-Pools eine Zunahme des pflanzenverfügbaren P und eine Abnahme des ausgefällten P mit abnehmender Trockenheit. Während der Gehalt an LMWOA im Boden im feucht-gemäßigten Wald höher war als im mediterranen Wald und im trockenen Buschland, war die ^{13}C-Allokation zu LMWOA im feucht-gemäßigten Wald und im mediterranen Wald gleich groß. Hohe Enzymaktivitäten im feucht-gemäßigten Wald deuten auf die Verwertung von organischem P hin. Es ist anzunehmen, dass in diesem Ökosystem eine Vielzahl von P-mobilisierenden Prozessen anzutreffen ist, da die Verwitterungsstoffe nur teilweise aus kürzlich ausgeschiedenem Wurzel-C, aber auch aus anderen C-Quellen des Bodens stammen. Für das aride Strauchland und die mediterranen Wälder wurde gezeigt, dass der Gehalt an pilzlich erzeugter Oxalsäure positiv mit gut kristallisiertem anorganischem P (DCB lösliches P) korreliert ist, was auf Pilze als wichtige Organismen zur Mobilisierung schwer verfügbarer P-Quellen in diesen Ökosystemen hinweist. Die ^{13}C-Allokation im ariden Strauchland ähnelt derjenigen im mediterranen Wald, auch wenn die Gehalte auf einem niedrigeren Niveau liegen. Dies wird als Anpassung an die Trockenheit in diesen beiden Ökosystemen interpretiert und ist ein Hinweis darauf, dass die Trockenheit die pflanzliche C-Allokation im Boden antreibt.

Zusammenfassend wurde gezeigt, dass die biologische Verwitterung ein wichtiger Prozess der P-Gewinnung unter aridem und mediterranem Klima ist, aber nicht unter feucht-gemäßigtem Klima, wo die Mineralisierung organischen Ps eine bedeutende Rolle spielt. Gleichzeitig sind LMWOAs wichtige Stoffe der P Mobilisierung im Boden; unter ariden Bedingungen dienen sie der mineralischen Verwitterung, während sie unter feuchtem Klima die Mineralisierung organischen Ps unterstützen. Die C-Limitierung der P-Aufnahme ist unter aridem und mediterranem Klima hoch und unter feuchtem Klima gering. In Bezug auf den klimaabhängigen P-Kreislauf im Boden wird geschlossen, dass jeder Standort seine spezifische P-Speziation, P-Verfügbarkeit und stöchiometrische Nährstoffverfügbarkeiten hat. Es war nicht möglich, einen systematischen Trend dieser Parameter entlang der Ökosequenz zu identifizieren. Abiotische Veränderungen (d. h. der Klimawandel) führen wahrscheinlich zu nichtlinearen Veränderungen der P-Speziation, der P-Verfügbarkeit und der stöchiometrischen Nährstoffverfügbarkeit, was

unsere Fähigkeit zur Vorhersage von Veränderungen des P-Kreislaufs als Folge veränderter abiotischer Bedingungen an einem Standort erschwert.

1. Extended summary

1.1. Context and rationale for investigating P cycling mechanisms in soil

Soil is formed by weathering of rocks and minerals on the Earth's surface. Weathering is mainly divided into physical and chemical weathering processes (Anderson et al. 2007). Living organisms contribute to both, physical and chemical weathering processes by a variety of mechanisms. Biota proliferate in protected places such as fissures and disintegrated areas of the parent material (e.g., algae, bacteria, saprotrophic fungi, protozoa) or penetrate such structures (e.g., roots, mycelium) and impose physical stress on the surrounding rock (Silverman 1979). In addition, biota introduce organic compounds into the soil and parent material, some of which help to dissolve minerals (Jones and Darrah 1994). Accumulation of organic compounds is one component for the formation of a broad variety of soil types. Not surprisingly, already at the rise of modern soil science it was recognized that biota are one of the five soil–forming factors (Dokuchaev 1883; Jenny 1941).

An inherent aspect of living organisms is the need for nutrients to maintain their metabolism. With exception of nitrogen (N), which is captured from the atmosphere, all crucial nutrients (macronutrients) are mainly rock derived (e.g., P, Mg, K, Ca, Si). Among rock born nutrients phosphorus (P) plays a crucial role as it often, together with N, limits productivity in terrestrial ecosystems (Vitousek and Farrington 1997). It's mobility in soil is commonly low as it sorbs strongly to calcium (Ca) at high pH and to iron (Fe) and aluminum (Al) at low pH (Penn and Camberato 2019). Plants and microorganisms, therefore, developed strategies to solubilize P from parent rock material and to liberate sorbed P (Marschner and Marschner 2012). Moreover, more than 80% of plants form a symbiosis with arbuscular mycorrhizal (AM) fungi (Parniske 2008; Brundrett and Tedersoo 2018) which has been shown to improve plants P uptake (Smith et al. 2003). This work aims to investigate the role of plants, bacteria, and fungi for P cycling in incipient but also developed soils under changing climates. It focuses on the role of low–molecular weight organic acids (LMWOA) for plant induced mineral weathering (biological weathering) and organic P recycling. The pathway of C through the plant–microbe–soil system and to LMWOA is examined and interpreted in terms of energy investments in P acquiring/cycling processes. These objectives were studied along a climatic gradient in the Chilean Costal Cordillera, forming a sequence of ecosystems (ecosequence; more details in Section 1.2.1)

In the following, the topic will be approached by summarizing the state of knowledge on how plants and associated microorganisms affect weathering in terrestrial ecosystems. P

transformation during pedogenesis is then discussed before research on the role of biota in the P cycle is briefly reviewed.

1.1.1. Impact of plants and microorganisms on weathering in terrestrial ecosystems

Roots enable mass exchange between aboveground plant biomass and soil. About 20–30% of assimilated C is translocated below ground as root biomass or root exudates (Farrar and Jones 2000). Plant roots take up nutrients from the deep soil and saprolite as well as from the topsoil, thereby acting as a bidirectional pump for C and nutrients between the atmosphere and the lithosphere. In this sense, the soil is a bioreactor that is created at the interface between the atmosphere and the lithosphere, forming a habitat that is completely different from the first two (Anderson et al. 2007). Plants and their associated microorganisms actively control soil chemical conditions (Dakora and Phillips 2011), thereby controlling mineral weathering, particularly in the rhizosphere (Kuzyakov and Razavi 2019). Biochemical weathering is highly complex and occurs through a wide variety of processes. Roots are known to cause mechanical stress on rocks when penetrating cracks, which enlarges the surface area of minerals and facilitates mineral weathering (Roering et al. 2010). On the contrary, plants can slow erosion because a dense root network prevents particle transport and allows better exploitation of minerals, i.e., complete dissolution, than without a dense root network. Enhanced chemical weathering in the rhizosphere is mainly induced by root exudates such as organic anions, rhizosphere acidification by proton excretion and root respiration (Figure 1.1.4). The rhizosphere is also the place in soil with highest microbial activity (Kuzyakov and Razavi 2019). Rhizosphere microbes release a plethora of chemical compounds, some of which release scarce nutrients from soil minerals. Moreover, it was shown that plant roots and mycorrhizal fungi selectively dissolve nutrient rich minerals (Berner 2004). Mycorrhizal fungi further enhance mineral weathering by enlarging the soil volume exploited for nutrients and the surface area for nutrient uptake (Parniske 2008). Glomalin production by mycorrhizal fungi and mucilage excretion by plants, conversely, stabilizes the soil and favors the formation of aggregates, resulting in decreased erosion but increased chemical weathering as the contact time between minerals and the soil solution is extended (Taylor et al. 2009; Chen et al. 2018; Zhong et al. 2021). These examples are mentioned here to illustrate that there is no linear relationship between plant growth and mineral weathering. Thus, it is not to be expected that higher net primary productivity will simply enhance biological weathering rates. Rather, there will be a particular state of plant density that will allow the highest rates of weathering under a given climate. Since plant density itself depends on climate, it is reasonable to assume that climate will determine maximum biological weathering rates.

1.1.2. P speciation development during pedogenesis and along climosequences

The outstanding importance of P for ecology was realized by Thomas William Walker already in 1965 when he claimed: "In these studies [of soil chronosequences], phosphorus emerges as perhaps the key element in pedogenesis, because of its great ecological significance. It is the one major element in soil organic matter that must be supplied almost entirely from the parent material" (Walker 1965; Turner and Condron 2013). With few exceptions (Kurtz et al. 2001; Chadwick et al. 1999; Ziółek and Melke 2014), all P involved in biological processes in natural soils is rock born. Unlike C or N, the transport of P depends solely on water and (with exception of very old volcanic and tropical sites as well as rare sites where a major input of P origins from seabird feces) input via the atmosphere is negligible. At the same time, its mass share in the Earth's crust is only 0.09 wt.% (Filippelli 2008). The chemical properties of P include susceptibility to precipitation with numerous cations common in soil, most prominently with Fe, Al, and Ca. When primary P minerals are dissolved it is likely to rapidly adsorb to reactive surfaces within soil or precipitate with various cations (Tiessen et al. 1984). Figure 1.1.1 depicts the P availability in soil and indicates highest P availability at about pH 6.5.

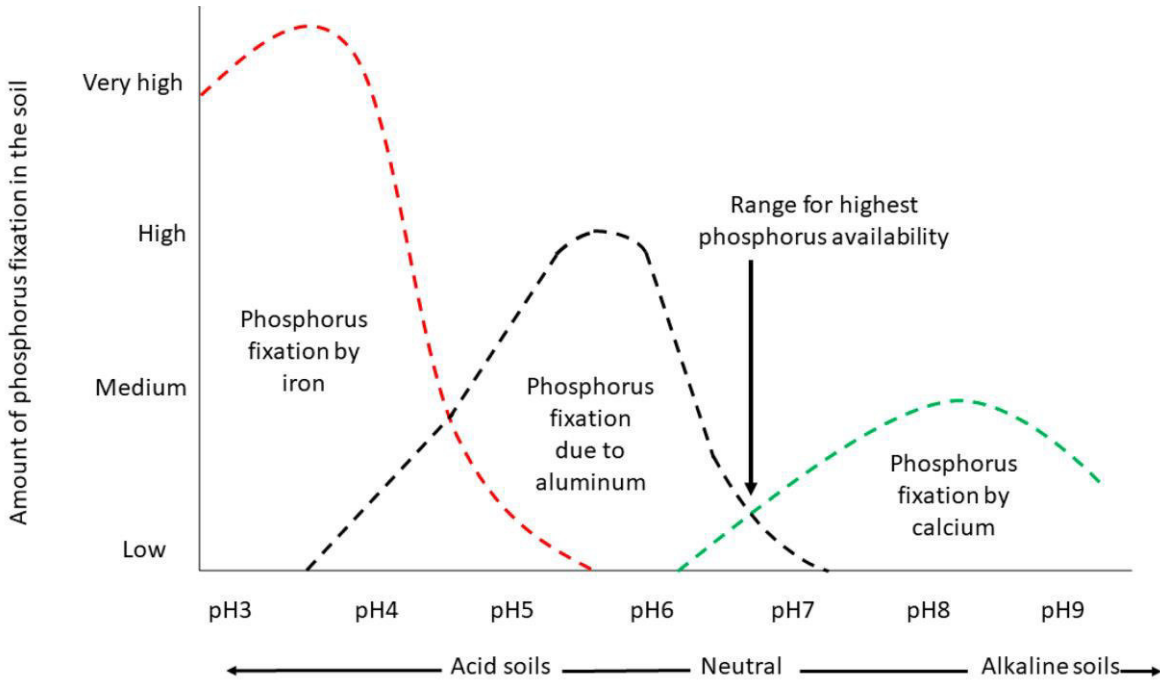

Figure 1.1.1: Phosphorus availability in soil depending on soil pH and the most important binding elements of P. P availability in soil is relatively high at a pH of about 6.5 and declines towards lower and higher pH (Penn and Camberato 2019).

The most abundant primary minerals in which P occurs in soil is apatite (hydroxyapatite $Ca_{10}(PO_4)_6(OH)_2$; fluorapatite $Ca_{10}(PO_4)_6F_2$, and chlorapatite $Ca_{10}(PO_4)_6Cl_2$) (Blume et al. 2010; Jones and Oburger 2011; Sims and Pierzynski 2005). During pedogenesis, P is transformed into a variety of pedogenic Ca–, Fe–, and Al–P. Walker and Syers (1976) formulated a model of P

transformation during pedogenesis which postulates that P is gradually transformed to secondary inorganic P minerals (Figure 1.1.2, Turner and Condron 2013). At the beginning of pedogenesis, in young incipient soils, most of the P remains in the primary apatite form, whereas at later stages of soil development P is either precipitated with Fe and Al, occluded in Fe– and Al–(hydr)oxides or bound as organic P. This model reaches an equilibrium for very old, P–depleted soils where all losses of P are replenished by atmospheric inputs (Crews et al. 1995; Peltzer et al. 2010). Although the original authors were very cautious about applying the theory to ecosystems outside the humid climate for which it was developed, it has proven to be applicable under other climates from subtropical to semiarid (Peltzer et al. 2010; Tiessen et al. 1984; Crews et al. 1995; Cross and Schlesinger 1995).

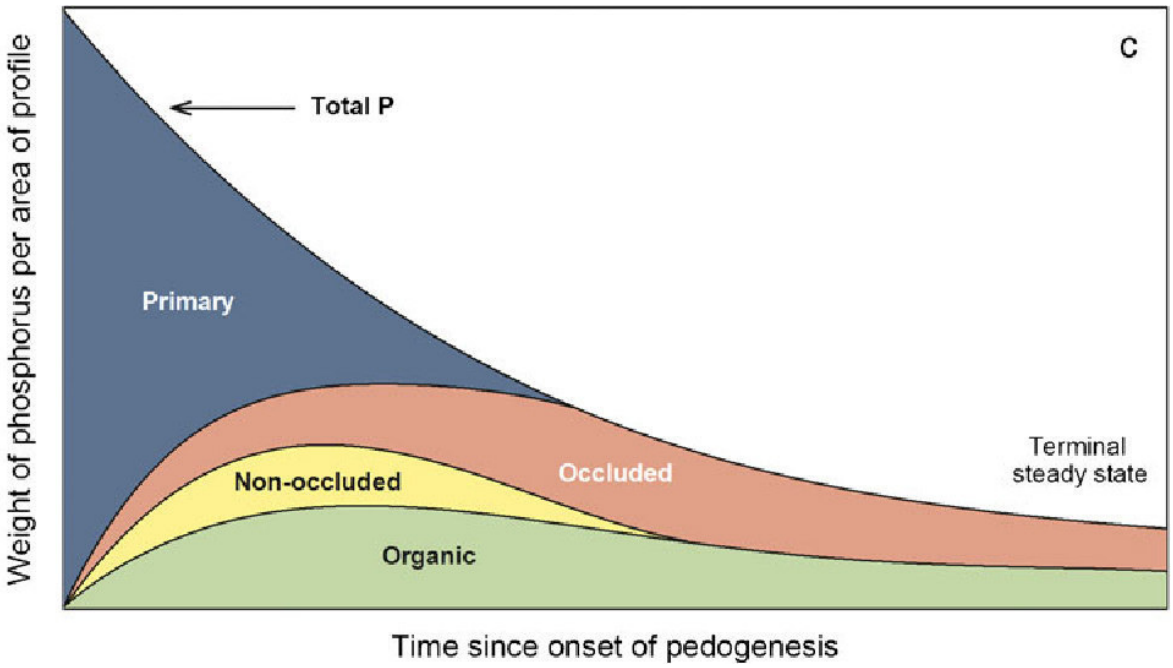

Figure 1.1.2: Development of P speciation during pedogenesis (Turner and Condron 2013; Williams and Walker 1969 and references therein).

The Walker and Syers model was tested in a space–for–time approach for its validity in soils along a climate gradient (Feng et al. 2016). The study postulated that decreasing aridity would accelerate pedogenesis and, therefore, it could substitute the time factor in the Walker and Syers model. Indeed, they found that primary P was declining with decreasing aridity and that organic P follows the reverse trend. However, they investigated only arid and semiarid environments. A global compilation of Hedley P fractions (Hedley et al. 1982) found that in a range from hyperarid to humid climate primary P decreases while secondary mineral P, occluded P, and organic P increase (Hou et al. 2018b). However, it is questionable whether a space for time approach in natural ecosystems can be realized because changes in climate are always associated with changes in the plant– and microbial community-composition. For this

reason, it might not be possible to design an experiment where climate is allowed to change while the other four soil forming factors (biota, relief, parent material, and time) are kept constant.

1.1.3. P cycling in soils and the (myco−)rhizosphere

P always occurs in soils as phosphate. Depending on the pH of the soil, inorganic P in the soil solution occurs as one of the anions of phosphoric acid (H_3PO_4, $H_2PO_4^-$,HPO_4^{2-}, and PO_4^{3-}) which are the sole forms that can be taken up by plants and microorganisms (Pierzynski et al. 2005). P is transferred between the various P pools in soil by physicochemical and biological processes (Figure 1.1.3). Important P pools in soil are P dissolved in the soil solution, organic P (mainly inositol phosphates, Jones and Oburger 2011), inorganic P (mainly precipitates of phosphates with Ca, Fe, Al and P sorbed to Fe− and Al−(hydr)oxides), and P within the microbial biomass (P_{mic}), micro− and macro fauna (mainly phospholipids and nucleic acids). The organic P pool is differentiated into rapidly and slowly mineralizable organic P. The inorganic P pool is separated into rapidly and slowly exchangeable P. The pool of P actively cycling within the

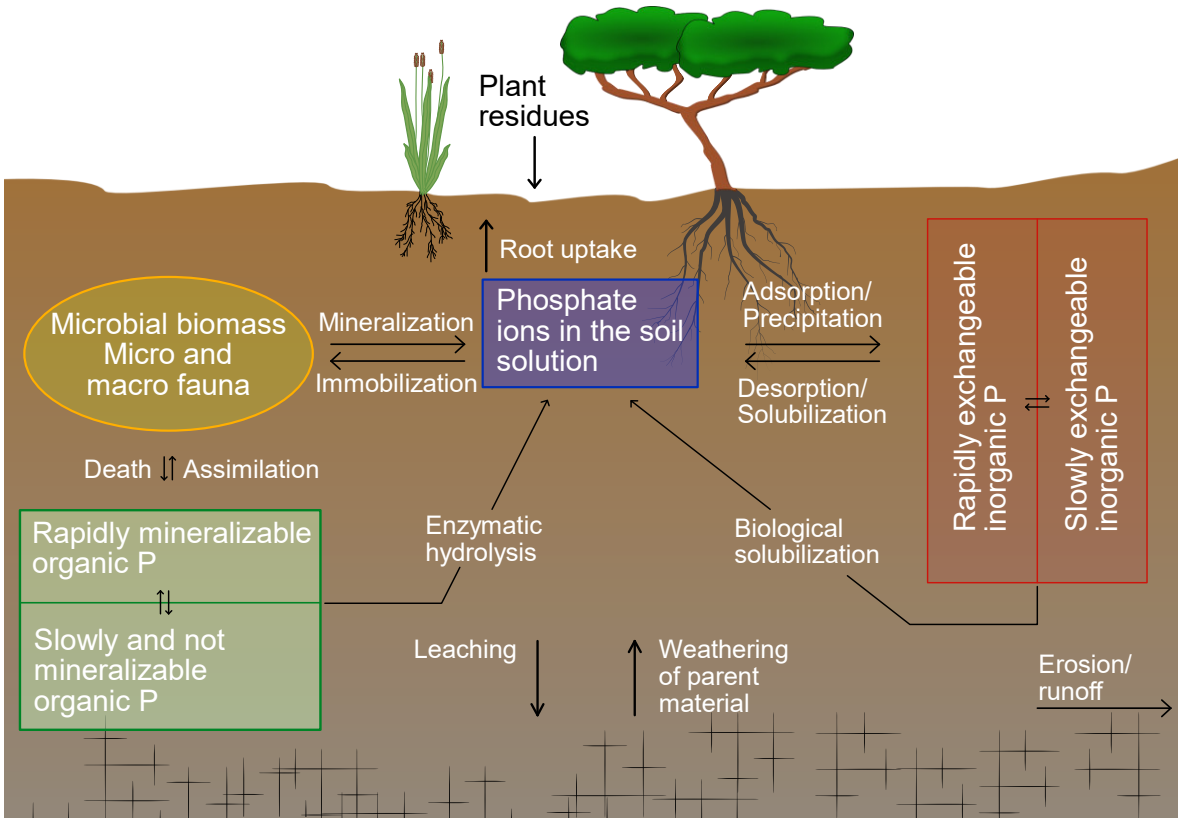

Figure 1.1.3: P transformations in a soil−plant−microorganisms system. Biological hydrolysis of organic P and solubilization of inorganic P are strong drivers of P cycling within soils, along with abiotic sorption/precipitation and desorption/solubilization. Modified after Frossard et al. (2011).

soil−plant system is at least an order of magnitude smaller than the total content (Frossard et al. 2011). Turnover rates of the various P pools are highly variable and in the range of minutes

for dissolved P (Helfenstein et al. 2018a) but in the range of millennia for P occluded in metal oxides (Helfenstein et al. 2018b).

P is often scarcely soluble in soil and consequently in most soils its availability is low. Plants and microorganisms have developed a broad set of mechanisms to access P from otherwise unavailable sources. Figure 1.1.4 depicts mechanisms of plants and microorganisms to access P that would be unavailable if dissolution were only driven by abiotic processes.

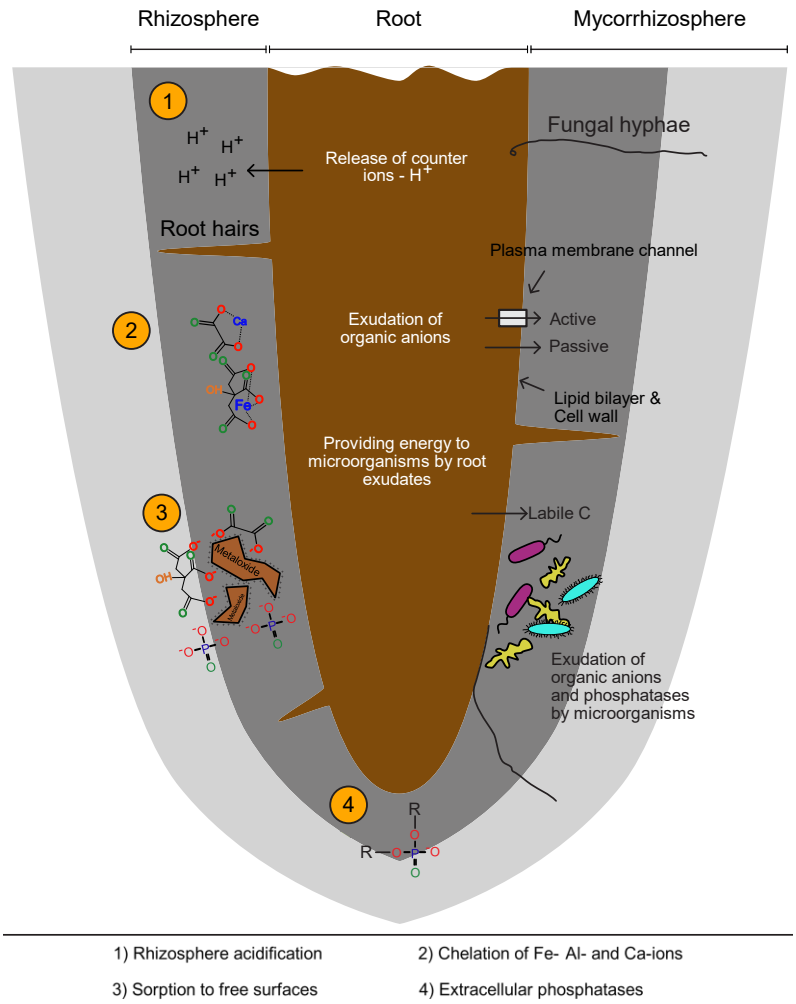

Figure 1.1.4: P mobilization processes in the rhizosphere and mycorrhizosphere.

The area around roots, the rhizosphere, is a hotspot of microbial activity and thereby of high P availability (Kuzyakov and Razavi 2019). The area explored by mycorrhizal fungi, the mycorrhizosphere, extends even further away from roots. One of the main benefits plants gained when entering the symbiosis with mycorrhizal fungi was the extension of the soil volume that can be scavenged for nutrients (Finlay 2008). Plants release labile C compounds to the soil to feed microorganisms near the root. Exudation of organic C is not only important as a source of energy for the surrounding microbes, but plants and microorganisms also release low–molecular–weight organic acids (LMWOAs) and extracellular enzymes (phosphatases) into the rhizosphere to solubilize P from soil minerals and mineralize organic P (Tarafdar and Claassen 1988). LMWOAs enhance the dissolution of P minerals by three mechanisms and extracellular phosphatases support the degradation of organic P compounds (processes are shown in Figure 1.1.4 and indicated by the numbers in the orange circles). (1) The exudation of organic anions, associated with the

exudation of a proton as counterion, lowers the rhizosphere pH (Ma et al. 2019) and thereby dissolves Ca–phosphates (Ca–P). (2) Organic anions chelate bi– and trivalent cations, which decreases the concentrations of iron (Fe^{3+}), aluminum (Al^{3+}), and calcium (Ca^{2+}) in the soil solution (Jones 1998). Their effect on P mobilization is altered by the number and position of their functional groups. LMWOAs have been shown to release more P per added proton in comparison to mineral acids, suggesting effective chelating of P–associated metals (Kpomblekou and Tabatabai 1994). (3) Organic anions block sorption sites, especially at sesquioxides, thereby desorbing phosphate ions (Hinsinger 2001; Jones and Darrah 1994; Jones 1998). (4) Extracellular phosphatases are exuded to hydrolyze phosphate esters which are common in organic P compounds. Phosphatase activity s inversely correlated to the availability of P in soil (Olander and Vitousek 2000).

The mechanisms by which plants mobilize P and if they follow an acquisitive (biological weathering of P–containing minerals) or recycling (organic P mineralization) strategy to meet their P demand is a vital information to understand P cycling in soil. Moreover, the understanding of P cycles and the conditions and mechanisms that lead to P limitation are crucial to understand ecosystem development. The extent to which C availability (e.g., root exudates) influences P mobilization and limitation is not well understood.

1.1.4. Objectives & Hypotheses

The overarching aim of this work was to examine how climatic conditions drive biological P mobilization and utilization in soil. Three hypotheses were formulated to build the backbone of this work:

- H1: Ecosystem P nutrition shifts from acquiring P from mineral sources under dry climates and initially developed soils to recycling of P from accumulated organic compounds as humidity increases and soils become more developed.
- H2: Biological P weathering is maximal at intermediate humidity because water availability is high enough to overcome transport limitation of soluble substances in soil, while the organic P content is still low.
- H3: The importance of labile C (root exudates) for P mobilization is greatest under an arid climate. Under humid climates the abundance of organic C in soil decouples microbial energy demand from fresh C inputs.

The investigations and experiments in this work focused on two main aspects. First, P speciation (Study 1) and abiotic P sorption (Study 2) were characterized in soils along a climate gradient to determine whether these are driven by climatic conditions. Second, key P cycling

mechanisms and climate–dependent shifts of the P sources preferred by plants and microbes (Studies 1, 3 and 4) were scrutinized. This was investigated by determining contents of LMWOA (Studies 1 and 3) and phosphatase activity (Studies 1 and 4) in soils. Samples were taken from rhizosphere and bulk soil (Study 1) and labile C was added to the soil (Study 2) to gain insight into the role of root–released C for biological P utilization and differences in P speciation between the rhizosphere and bulk soil. Furthermore, the partitioning of photosynthetically fixed C between plants, bacteria and fungi was investigated in a ^{13}C field labeling experiment (Study 3). Examining the pathway of C through the plant–soil–microbe system allowed to differentiate between plant–, bacteria–, or fungi–released weathering agents under different climates. By evaluating correlations between P mobilizing compounds and operationally determined P pools, it was possible to infer the preferred P source under a given climate.

1.2. Research approach and Methods

1.2.1. Study sites

The study sites were located along the Chilean Coastal Cordillera and covered a large spatial range from 26° to 38° southern latitude (Figure 1.2.1). A distinctive feature of the study design was that the variation in parent material was kept low by choosing soils that all developed on granodioritic material. This was ensured by staying in the area of the Coastal Cordillera (Hervé et al. 1988). Moreover, none of the sites were glaciated during the last glacial maximum, this was important to avoid fluvial overprinting of the bedrock material. The sites were characterized by differences in climate and vegetation and provided the unique opportunity to study different ecosystems developed from the same parent material. The climate in the study area is determined by the South Pacific anticyclone. The rainfall distribution over the year is similar in the four sites, with most precipitation in the austral winter months of May to August (Muñoz et al. 2007). Because climate changes between the study sites and, therefore, different ecosystems developed at each site, the four study sites were termed an 'ecosequence'. They covered a gradient of mean annual precipitation (MAP) and mean annual temperature (MAT) ranging from 12 mm yr^{-1} and 16.8 °C in the north to 1469 mm yr^{-1} and 6.6 °C in the south (Table 1.2.1, Fick and Hijmans 2017).

The northernmost site was located in the National Park *'Pan de Azúcar'* (26.112 S, 70.551 W) with an aridity index of 0.0047 (Trabucco and Zomer 2018) and was classified as hyperarid ('*hyperarid desert*'). The study site was located about 10 km inland from the Pacific Ocean. The very scarce vegetation was dominated by biocrusts, which covered large areas. Sparsely distributed small bushes were the only vascular plants at this site (*Tetragonia maritima, Nolana*

mollis, Perityle sp. and Stipa plumosa, Cristaria integerrima) (Bernhard et al. 2018). The soils at this site were classified as Regosols (IUSS Working Group WRB 2015) with A horizons ranging from 2 to 5 cm thickness and B horizons ranging from 18 to 45 cm thickness (pH 8.1) (Bernhard et al. 2018). This site was only considered in Study 2 where microbial P utilization was investigated. As vascular plants were very scarce at this site, it was excluded from the studies where sampling of roots or CO_2 labeling were conducted.

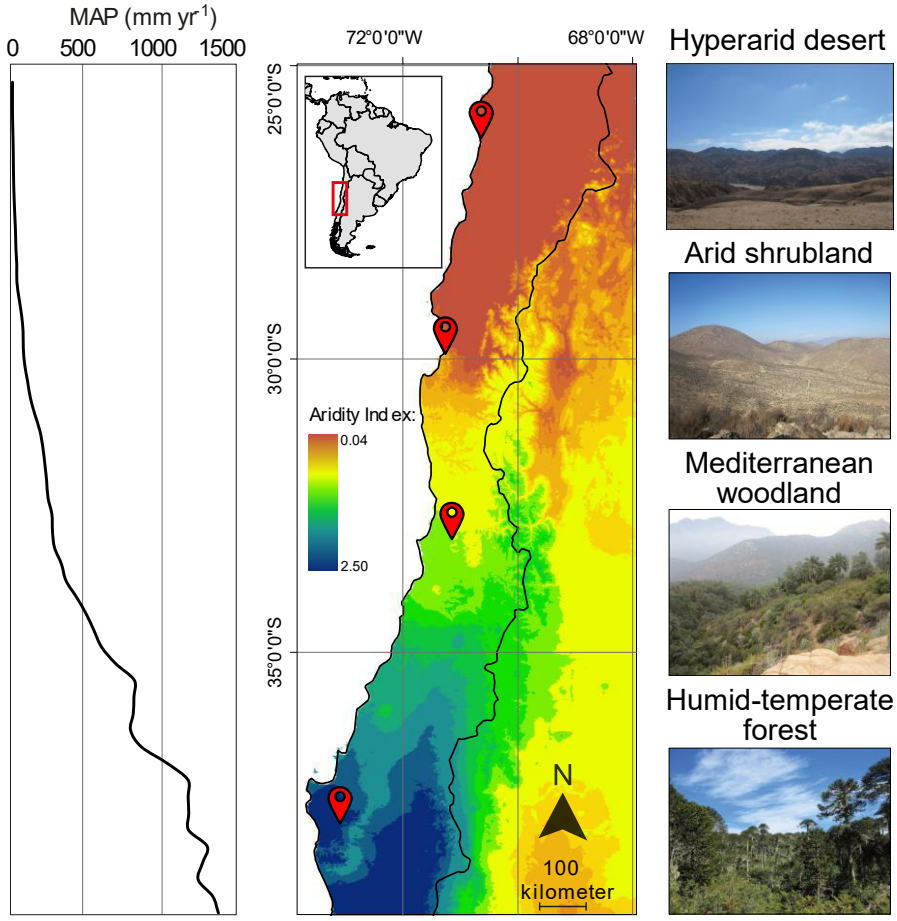

Figure 1.2.1: Map section of Chile from about 25° to 38° southern latitude. The field sites are marked by black tack symbols. Map color corresponds to the aridity index, which is calculated as the quotient of mean annual precipitation and potential mean annual evapotranspiration (Trabucco and Zomer 2018). Mean annual precipitation after Fick and Hijmans (2017).

The investigations at the *'arid shrubland'* were done at two sites, located close to each other. The sites were close to the city of La Serena, had aridity indices of 0.06 and 0.05 and were classified as arid. One of the sites was in the *'Natural Reserve Santa Gracia'* (29.76 S, 71.14 W), about 23 km from the Pacific Ocean and at an elevation of 680 m a.s.l. The other site was located in an area named *'Quebrada de Talca'* ((30.05 S, 71.09 W) where grazing was excluded for the previous ten years. The Pacific Ocean was 23 km away and the altitude was 645 m a.s.l. MAP and MAT were similar at both sites with 66 mm yr^{-1} and 13.7 °C. The vegetation was composed of drought−deciduous shrubs (*Proustia cuneifolia, Balbisia peduncularis, Senna cumingii, Cordia decandra, Adesmia sp. and Baccharis paniculatum*) and cacti (*Eulychnia acida* and *Cumulopuntia sphaerica*) and covered 30−40% of the area (Bernhard et al. 2018). The

vegetation was standing upon Cambisols (IUSS Working Group WRB 2015) with pH 5.9 – 7 (Bernhard et al. 2018).

The Mediterranean site (*'Mediterranean woodland'*) was located in the *'National Park La Campana'* (32.96 S, 71.06 W) with an aridity index of 0.24 (Trabucco and Zomer 2018). It was about 43 km from the Pacific Ocean and at an altitude of 730 m a.s.l. MAP and MAT were 367 mm yr^{-1} and 14.1 °C (Fick and Hijmans 2017). The soils were Cambisols (IUSS Working Group WRB 2015) with a pH of 4.7 – 6.2 and were 100% covered by vegetation which consisted of evergreen–sclerophyllous trees (*Lithraea caustica and Colliguaja odorifera*), palm trees (*Jubaea chilensis*), deciduous shrubs (*Podanthus mitiqui and Aristeguietia salvia*) and a dense understory herb layer (*Alstroemeria sp., Geranium robertianum, Stellaria media, Adiantum chilense*) (Bernhard et al. 2018).

The most southern site was classified as humid (*'humid–temperate forest'*) with an aridity index of 1.4 (Trabucco and Zomer 2018) and located in the *'National Park Nahuelbuta'* (37.81 S, 73.01 W). Soils were Umbrisols and Podzols (pH 3.9–5.3) (IUSS Working Group WRB 2015) covered again 100% by a mixed forest, consisting of evergreen and winter–deciduous broadleaved trees (*Araucaria araucana* (Mol.) K. Koch, *Nothofagus antarctica, Nothofagus obliqua*) and a dense understory vegetation of grasses (*Chusquea coleu*), bushes (*Gaultheria mucronata*), and herbs (*Stipa sp.* and *Mutisia decurrens*) (Bernhard et al. 2018).

Important site characteristics are shown in Table 1.2.1. For a comprehensive description of vegetation, soils and geology see Bernhard et al. (2018) and Oeser et al. (2018).

Table 1.2.1: Site characteristics of the four study sites along the Chilean Coastal Cordillera. Mean annual precipitation (MAP) and mean annual temperature (MAT) are taken from (Fick and Hijmans 2017). The aridity index and climate classification are derived from Trabucco and Zomer (2018), soil type (IUSS Working Group WRB 2015) and soil pH are after Bernhard et al. (2018).

Site	MAP [mm]	MAT [°C]	Aridity index	Climate	Vegetation	Soil–type	pH
Hyperarid desert	12	16.8	0.0047	Hyperarid	Biocrusts, small desert shrubs	Regosol	8.1
Arid shrubland	66	13.7	0.05 – 0.06	Arid	Sclerophyllous shrubs, cacti	Cambisol/ Leptosol	5.9 – 7
Mediterranean woodland	367	14.1	0.24	Mediterr–an ean	Deciduous forest, sclerophyllous shrubs	Cambisol	4.7 – 6.2

Humid–temperate forest	1469	6.6	1.4	Humid	Coniferous forest	Orthodystric Umbrisol/ umbric Podzol	3.9 – 5.3

1.2.2. Research design

The research approach of this work is based on the idea to investigate changes in soil P cycling along a climatic gradient with constant lithology. In terms of the five soil forming factors, the aim was to keep as many variables constant as possible. At each site, sampling was done at a north– and south facing slope with slope inclination between 12° and 25° at midslope position (Bernhard et al. 2018). The basis of this work was to determine the state of P weathering along the climatic gradient. Settled upon this, biological parameters influencing P weathering were investigated. Table 1.2.2 gives an overview of the applied methods and how they relate to the hypotheses stated earlier. In addition, Table 1.2.2 shows which analysis were carried out with which set of samples. In total three sets of samples were taken to comprehensively answer the questions addressed by this work (samples were always taken in the arid, Mediterranean, and humid sites for Studies 1, 3, and 4 and at all sites for Study 2):

- Rhizogradient sampling.
- Laboratory incubation of A and B horizons from each site: observation period of 25 days.
- ^{13}C field labeling: bulk samples from soil around labeled plants: observation period of 14days.

The rhizogradient sampling was done at soil profiles in three depths increments which were determined relative to the total soil thickness (100%) at each site. Samples were taken from 0–50% (*'topsoil'*), 50–100% of soil depth (*'subsoil'*), and >100% (*'saprolite'*). This approach was chosen over horizon–specific sampling in order to compare sites with each other. A gradient from rhizosphere to bulk soil was obtained by sampling soil around young living roots (diameter ≤ 2 mm) at three distances to roots (0–2 mm, 2–4 mm, 4–6 mm). The 0–2 mm and 2–4 mm distance increments were defined as rhizosphere soil, the distance 4–6 mm was considered as bulk soil. Roots were not distinguished on a species level but a pooled sample from roots occurring in the respective soil pit and depth was taken.

For the laboratory experiment soil was collected at each site from a south facing soil profile in midslope position. An aliquot from each site and horizon was sterilized by gamma–irradiation (min. 50 kGy, STERIS, Radeberg, Germany). The sterile soil was used to determine ion–exchange kinetics (IEK) of ^{33}P, thereby the soil was labeled for a consecutive incubation experiment. The labeled sterile soil was mixed with the non–sterile soil for the incubation study.

The incubation lasted for 25 days; samples were collected on days 1, 5, 7, 12, and 25 of the incubation period.

The last set of samples came from a field labeling experiment where site specific plant species were exposed to a pulse of $^{13}CO_2$. Soil samples from beneath each specimen were collected over a period of two weeks.

Table 1.2.2: Main study objects presented in this work and their connection to the hypotheses. A short description of the purpose and the method is also given.

Study object	Study and sampling	Connects to Hypothesis	Purpose	Method
Biological weathering agents *Section 1.2.3*	Study 1: rhizogradient sampling. Study 3: bulk sampling, several timepoints.	H1; H2	Intensity of biological mineral weathering. Abbundance of weathering agents in rhizosphere vs. bulk soil. ^{13}C in LMWOA to trace origin of weathering agents (plants, bacteria, or fungi).	Extraction of LMWOA from soil: ▪ water extractable "free" acids ▪ HCl extractable "sorbed" acids
P speciation *Section 1.2.4*	Study 1: rhizogradient sampling.	H1; H2	Determine climate dependent chemical structure of P in soil. Root impact on P speciation. Correlate with weathering agents to infer preferred P source.	P K−edges X−ray absorption near edge structure (XANES). Samples taken as a gradient from rhizosphere to bulk soil "Rhizogradient sampling" (Study 1).
Operational P pools *Section 1.2.4*	Study 3: bulk sampling, several timepoints.	H2; H3	Determine P availability in soil. ▪ High throughput method to determine P availability in a large number of samples Correlate with ^{13}C allocation to roots, bacteria, fungi, and LMWOA to infer plants investment in P mobilization.	Plant available P: ▪ Water extractable P ▪ $NaHCO_3$ extractable P Hardly available: ▪ Ammonium−oxalate extractable P ▪ Dithionite−citrate−bicarbonate extractable P
P sorptivity of the soil *Section 1.2.5*	Study 2: laboratory experiment.	Indirectly to H1 and H3.	Determination of physicochemical P sorption in soil. ▪ Determine sorption capacity of soils. ▪ Correlate with soil properties to infer which parameters determine climate dependent P sorption in soil.	Ion−exchange kinetics (IEK). ^{33}P tracer application to unlabeled sterile soil.
Microbial element contents and respiration *Section 1.2.6*	Study 2: laboratory incubation study, serveral timepoints.	H3	Determine microbial P uptake (^{33}P in P_{mic}). Determine microbial growth under addition of labile C.	Microbial biomass P (P_{mic}): hexanol fumigation extraction. Microbial biomass C (C_{mic}): chloroform−fumigation extraction.
Phosphatase activity *Section 1.2.7*	Study 4: rhizogradient sampling.	H1; H3	Indications of organic P utilization. Rhizosphere impact on P recycling.	Extracellular phosphatase assay.
Moessbauer spectroscopy and free surface area *Section 1.2.8*	Study 2: laboratory experiment.	Indirectly to H1 and H3.	Explaining physicochemical P sorption in soi by Fe−mineralogy and free surface area in soil.	Moessbauer spectroscopy N_2 monolayer sorption to soil ("Free surface area").

Rhizosphere P speciation was determined by X−ray absorption near edge structure (XANES) (Study 1). On the same samples, the amounts of LMWOA (oxalic−, malic−, and citric acid) (Study 1) and phosphatase kinetics (Study 4) were quantified to gain insight in the investment of plants in mineral weathering or P recycling as a function of P speciation. The results gave

first indications to answer the question if biological P weathering varies with climate and whether P recycling is enhanced under increased humidity.

As P cycling in soil is strongly determined by the availability and mobility of P, it is necessary to understand the abiotic boundary conditions determining the soil's capacity to adsorb P. Using radioactive isotopes with a short half–life allows to derive precise conclusions about the path of an element through biological pools, while the background concentration of the isotope is low. For these reasons IEK of ^{33}P with the soil solid phase under sterile conditions were determined for the three sites in the A and B horizon, respectively (Study 2). By doing so, soil enriched in sorbed inorganic ^{33}P was produced and used in a consecutive incubation study, in which mesocosms were prepared to investigate microbial inorganic P utilization. Incubation studies in environmental science allow control of environmental factors (soil moisture, temperature, light, basal soil respiration) and provide a reduced model of real–world conditions that allows manipulations and process observations that would not be possible under field conditions (Verhoef 1996). While all other parameters were kept constant, half of the mesocosms received a labile C source (glucose) to model rhizosphere conditions of C availability and derive implications for P cycling under varying substrate availability. This approach was designed to investigate the C limitation of microbial inorganic P acquisition.

The third pillar of this work was a field labeling study where plants were exposed to a $^{13}CO_2$ enriched atmosphere in a pulse labeling experiment (Study 3). The stable isotope ^{13}C was used

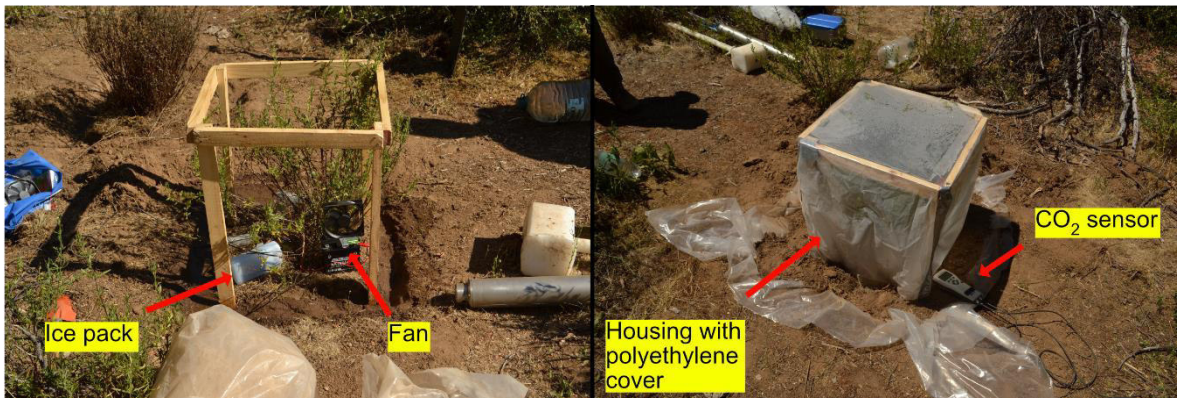

Figure 1.2.2: Field labeling setup. The labeling chamber was constructed as a wooden frame around the investigated specimens which were covered by polyethylene foil for the labeling. An ice pack and fan were placed in the labeling chamber to keep temperatures inside at ambient level. The CO_2 concentration in the labeling chamber was monitored with a CO_2 sensor.

to trace the path of freshly assimilated C through the plant–microbe–soil system and in LMWOAs. The setup allowed to determine plant and microbial investment in LMWOA production for mineral weathering. This study setup allowed to draw concise conclusion about the climate dependent C investment in biological weathering agents.

To make clear the limitations of the research approach presented in this work: It is not assumed, that climate substitutes for time and that one of the dry ecosystems presented here would eventually converge to a state that one of the more humid ecosystems is in today. Rather, each ecosystem is considered as a unique entity in which the Walker and Syers transformations occur at different rates, and which therefore has its own P–cycle mechanisms.

1.2.3. Weathering agents exuded by plants

LMWOA were extracted from soil, purified, and derivatized for gas–chromatography (GC) after Szmigielska et al. (1997). The extraction method was considerably modified. In short, soil (stored at −20 °C after sampling until analysis) was sequentially extracted with double distilled H_2O (ddH_2O) and in a second step with 0.5 M HCl, which allowed free and sorbed LMWOA to be distinguished. The extract was purified by liquid–liquid extraction and subsequently organic acids were methylated to their corresponding methyl–esters. GC–mass spectrometer (MS) settings were also adjusted from the original method (Szmigielska et al. 1997). Samples were reduced in volume and measured on a GC–MS (GC 7890A, MS 7000A Series Triple Quad, Agilent Technologies, Waldbronn, Germany) with a capillary column (DB–FFAP, 30 m length, 1 µm film thickness, 0.25 mm diameter, Agilent Technologies, Waldbronn, Germany).

1.2.4. P speciation and operational P pools

P speciation in the rhizosphere and bulk soil (Study I) was determined by P K–edge XANES. The XANES technique allows to determine the chemical speciation of elements. It is a powerful technique to determine "the oxidation state, coordination chemistry, and the distances, coordination number and species of the atoms immediately surrounding the selected element" (Newville 2014). The energy necessary to produce a photoelectron from the core shell, the absorption edge, is specific for each element. Modulations in the absorption edge energy reveal the chemical surrounding of an atom (Newville 2014; Varma et al. 2011). In soil science the technique is often applied to determine inorganic P speciation (e.g., Prietzel et al. 2016; Hesterberg et al. 2017; Hesterberg et al. 1999). For organic P species it is less powerful and does not allow to distinguish between different organic P species (Varma et al. 2011). For the measurement, samples were homogenized by milling and applied to a P–free *'Kapton tape'* (Lanmar Inc., Northbrook, IL, USA) (area 2.0 cm x 0.5 cm). The samples were measured in fluorescence mode. A detailed description of the fitting and standards is provided in Section 2.2.3. For result presentation the single standards were grouped in six soil P classes: calcium P (Ca–P), precipitated Fe–P ('*Fe–P*'), precipitated Al–P ('*Al–P*'), sorbed Fe–P ('*sorb Fe–P*'), sorbed Al–P ('*sorbAl–P*'), and '*organic P*'.

Operational P pools were determined in Study 3 to assess P availability in soil. In this study H_2O (H_2O-P), $NaHCO_3$ ($NaHCO_3$-P) (Olsen et al. 1954), Ammonium-oxalate (NH_4–P, Tamm 1922; Schwertmann 1964), and dithionite–citrate–bicarbonate leachable P (DCB–P; Mehra and Jackson 1958) were determined. These extraction methods were preferred over the common extraction procedure of Hedley et al. (1982) to provide comparability with P speciation determined by XANES (Prietzel et al. 2016). To better distinguish between Fe and Al bound P the NH_4–oxalate and DCB extractions were performed for parallel samples instead of a sequential extraction. This is because NH_4–oxalate is more effective in dissolving Al–(hydr)oxides than DCB and the latter is more effective for Fe–(hydr)oxides.

1.2.5. P sorption kinetics determined by isotope exchange kinetics (IEK)

The P sorptivity of soil A and B horizons was determined by quantification of ^{33}P isotope exchange kinetics with the unlabeled P pool adsorbed to the soil solid phase. Measuring isotope exchange kinetics (IEK) of sterilized or microbially inhibited soils is a powerful tool to determine sorptivity while excluding biological P immobilization (Lopez-Hernandez et al. 1998; Fardeau 1993; Randriamanantsoa et al. 2015). For the IEK determination, ^{33}P suspended in 0.1 M H_3PO^{4-} solution (carrier solution) was mixed with the soil. The suspension was placed on a shaker and samples were taken at 1, 5, 10, 30, 70, and 100 minutes after addition of the tracer. The exchange between solution and soil solid phase was stopped by centrifugation. The radioactivity remaining in the supernatant was measured on a scintillation counter (HIDEX 300 SL, Hidex Deutschland Vertrieb GmbH, Germany). The exchange kinetics of ^{33}P with the unlabeled soil solid phase provides information about the sorptivity and sorption strength of a soil for P.

1.2.6. Microbial element contents

Microbial biomass phosphorus (P_{mic}) contents (^{31}P and ^{33}P) were determined by hexanol–fumigation extraction (Bünemann et al. 2016; Kouno et al. 1995). Each sample was aliquoted in two subsamples and an anion–exchange membrane in bicarbonate form was added to the soil. The fresh soil was mixed with ddH_2O, additionally, one aliquot received hexanol. Samples were placed on a shaker for 16 hours. The anion–exchange membranes were removed, and the adhering orthophosphate eluted by 0.5 M HCl. During the extraction parts of the liberated P get adsorbed to the soil, therefore, a P spike was used to correct for this adsorption. Total inorganic P was determined photometrically by the malachite green method (Ohno and Zibilske 1991). To measure the ^{33}P content in fumigated and unfumigated samples, 3 ml of sample and 8 ml of scintillation cocktail (Rotiscint eco plus, Carl Roth GmbH & co. KG, Karlsruhe, Germany) were mixed in a plastic vial. Quantification was done with a scintillation

counter (HIDEX 300 SL, Hidex Deutschland Vertrieb GmbH, Germany). The P_{mic} content was calculated as the difference between the fumigated and the unfumigated sample, corrected by the adsorption of liberated P that occurred during the extraction-(Bünemann et al. 2016). The uptake of labeled P in the incubation experiment (Study 2) was calculated as the ratio of ^{31}P to ^{33}P in the supernatant multiplied by the ^{33}P content in P_{mic}. This is based on the assumption, that the isotopic ratio of the supernatant and the soil are the same (Bünemann et al. 2016).

Microbial biomass carbon (C_{mic}) was extracted by chloroform–fumigation extraction, following the procedure of (Vance et al. 1987). One sample of each sample pair was held under a chloroform ($CHCl_3$) atmosphere for 24 h. Afterwards both samples were extracted with 0.05 mol l^{-1} K_2SO_4 for 1h. The supernatant was filtered, and the total soil organic carbon content (TOC) was determined on a TOC/TIC analyzer (Multi N/C2100, Analytik Jena, Germany). C_{mic} was calculated as the difference between the fumigated and unfumigated sample and a correction factor of 0.45 (Wu et al. 1990) was applied.

1.2.7. Phosphatase assay

Activity of the extracellular acid phosphatase was determined using synthetic fluorogenic 4–methylumbelliferone–phosphate (substrate solution) (Marx et al. 2001). Soil samples were stored at 4°C until analysis. The samples were pre–incubated for 24 h in sterile 100 ml jars. Subsequently, sterile water was added to the jars and samples were shaken for 30 min. The soil solution was sonicated (40 J s^{-1} for 2 min) before aliquots of 50 µl were pipetted into black polystyrene 96–well microplates (Brand, Germany). A pH buffer (0.1 M 2–(N–morpholino)ethanesulfonic acid (MES) (pH 6.1)) was added together with 100 µl of substrate solution (0, 10, 20, 30, 40, 50, 100, and 200 µmol g^{-1}). Three analytical replicates were measured for each sample at each substrate concentration. Fluorescence was measured by a microplate reader (Victor³ 1420–050 Multi label Counter; extinction: 355 nm, emission: 460 nm) immediately after substrate addition (t_0) and 2 h after addition (t_1). For calibration and accounting for quenching, standard plates were prepared with 50 µl of a composite soil solution (for each site and depth), with 150, 145, 140, 130, 100, 70, and 30 µl of buffer (MES) and 0, 5, 10, 20, 50, 80, and 120 µl standard (methylumbelliferone), respectively. Plates were measured at t_0 and t_1. With the regression slopes of the standard measurements, enzyme activities of the samples were calculated [nmol substrate g^{-1} soil h^{-1}]. Activities were fitted by the Michaelis–Menten Equation, which describes non–linear saturation curves. The parameters V_{max} as the maximal rate of enzymatic activity under optimum substrate conditions, and K_m as the half–saturation constant as indicator for substrate affinity were determined.

1.2.8. Moessbauer spectroscopy and total free surface area

Fe speciation in soils was measured by Moessbauer spectroscopy. Samples were ball milled to obtain a homogenous powder, subsequently the spectra were recorded at 4.2 K. The method allows to distinguish between Fe^{II+} and Fe^{III+} integrated in silicate minerals (FeSi) and four Fe–(hydr)oxides: ferrihydrite (FeFH), goethite (FeGOE), hematite, and magnetite (grouped in results as FeHM).

The total "free surface area" (Chiou et al. 1990) was measured according to the method described by Brunauer et al. (1938). It serves as one parameter determining the sorption capacity for P in soil. The method determines the amount of N_2 that is adsorbed to a soil sample. The free surface area was calculated from the N_2–soil sorption.

1.3. Study results and discussion

In the following sub–sections, climate–dependent P-cycling mechanisms in the three studied ecosystems will be summarized. First the arid shrubland ecosystem is discussed, followed by the humid–temperate forest. After describing these endmembers of the ecosequence, the Mediterranean forest, which combines elements of the first two ecosystems, is reviewed. In general, P speciation and abiotic conditions are presented first, followed by a discussion of the implications for what this means for P cycling processes. Staying with this result–presentation pattern should make it easy for the reader to follow the argumentation.

Overall, P speciation along the ecosequence from arid to humid climate was characterized by a decrease of primary P and precipitated Al– and Fe-P and an increase of organic P and sorbed Fe– and Al–P (Figure 2.2.4). This pattern reflects enhanced weathering with decreasing aridity (Hou et al. 2018a) and the accumulation of organic P from the more productive vegetation in more humid climates (Lang et al. 2016). At the same time, the abiotic sorption capacity for inorganic P followed a unimodal distribution, with highest sorption capacities in the hyperarid desert and the humid–temperate forest. As the hyperarid desert was only included in Study 2 it will not be discussed more extensively here. Moreover, this site may receive considerable amounts of sea spray (Oeser et al. 2018) which might have a strong impact on nutrient dynamics at this site.

1.3.1. P cycling in the arid shrubland

On average, hydroxyapatite in the arid shrubland accounted for 40% of total P (Figure 1.3.1) as determined by XANES. The content of hydroxyapatite was highly variable, with a minimum of 7% and a maximum of 70% (Table 2.2.3). This is likely to result from the heterogenous distribution of P in soils, especially in its primary mineral form (Adediran et al. 2020) which is

exacerbated by the small volumes of soil used for the XANES measurement. The remaining P was mostly in crystalline Al– and Fe–P. Fe– and Al–P together accounted for 40% to 60% of total P, but again were highly variable. Fe–P was absent in about half of the samples but contributed up to 38% of total P in other samples.

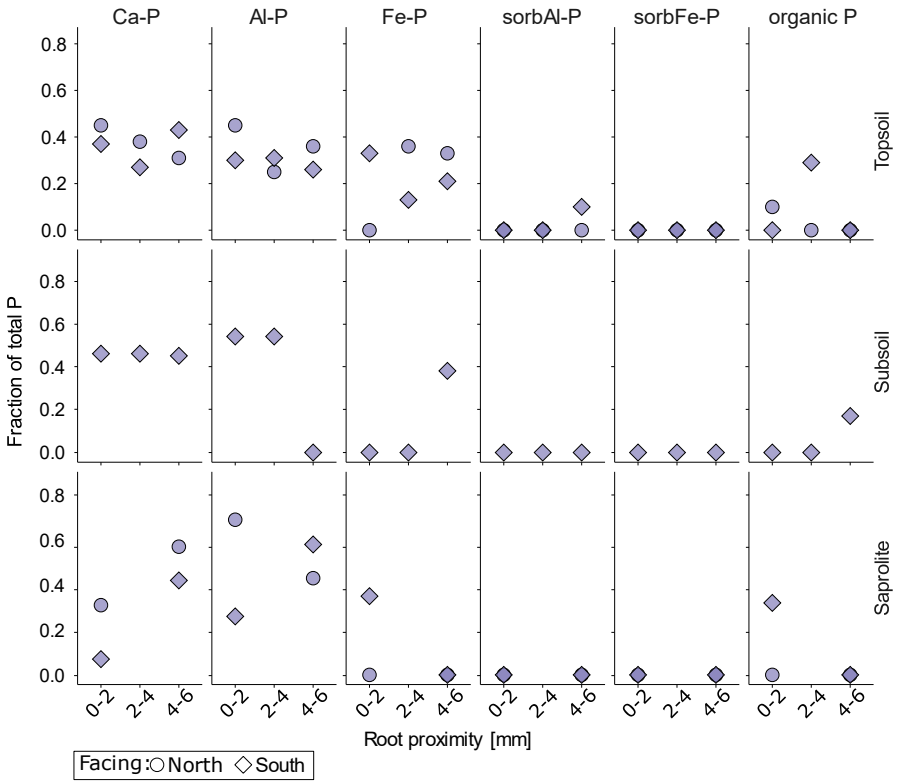

Figure 1.3.1: P speciation in de arid shrubland as determined by XANES spectroscopy. Samples from north facing profiles are depicted as circles, from south facing profiles as diamonds.

P sorbed to Fe– or Al–(hydr)oxides was absent at this site. In line with these results the sorption capacity for P was low (Figure 1.3.2). Low contents of NH_4–oxalate leachable Al indicated a low content of short–range–order Al–(hydr)oxides in the arid shrubland soils. Fe speciation determined by Moessbauer spectroscopy identified most of the Fe bound in silicates, indicating that Fe, like P, was mostly present in crystalline structures. The sorption capacity in the B horizon was slightly higher than in the A horizon, which was associated with a higher ferrihydrite content than in the A horizon. The $NaHCO_3$ extractable P was low, in accordance with the low P sorption capacity and P bound in primary minerals and crystalline metal–(hydr)oxides (Tiessen and Moir 2008). As a result, P sorption capacity in the arid shrubland was low (Figure 1.3.2).

The pH value indicated a high combined solubility of Fe–, Al–, and Ca–P (pH 6.5) (Penn and Camberato 2019). Therefore, the availability of P is likely transport–limited —due to the lack of water— in this ecosystem, and P minerals would readily dissolve if water were available. The pH value also favors the formation of crystalline Fe– and Al–(hydr)oxides (Cornell et al. 1989). For Fe this can be explained by the high solubility of ferrihydrite which favors the formation of well

ordered FeO(OH) and Fe_2O_3 (Cornell et al. 1989). In addition, low contents of P and organic matter in soil facilitate the formation of well crystalline Fe(hydr)oxides (Cornell et al. 1989).

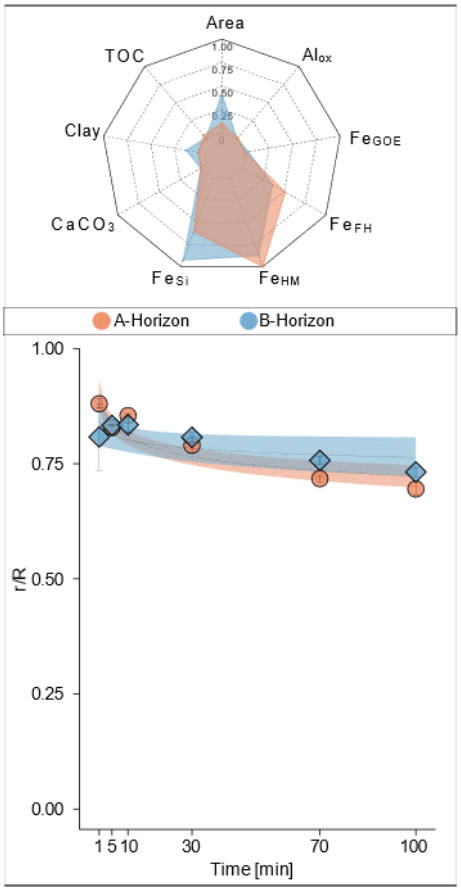

Figure 1.3.2: P sorption kinetics (lower subfigure) and explaining variables of P sorption (upper subfigure) in the arid shrubland. The y–axis of the sorption kinetics figure shows the ratio of radioactivity remaining in soil solution after a given time to the total added radioactivity. Thus, high values indicate low sorption capacity (sorptivity) of the soil. Sorption explaining variables are shown as relative values (relative to the highest value of the respective variable along the ecosequence).

In Study 1 an RDA was calculated to investigate the relationship between P speciation determined by XANES and biological parameters involved in biological P weathering and organic P recycling. Independent variables in the RDA, thus, were P species and explaining variables were oxalic–, malic–, citric acid, C_{mic} (MBC), maximal phosphatase activity (V_{max}), and phosphatase half saturation constant (K_m). The result of the RDA for the arid shrubland is presented as a biplot in Figure 1.3.3. The RDA revealed a strong correlation between hydroxyapatite and variscite, and LMWOA, indicating that organic acids are responsible to dissolve P minerals at this site (biological weathering). The importance of biological weathering at this site was corroborated by Study 3, where it was found that freshly assimilated C is allocated to fungi in places where crystalline P minerals (DCB-P) were present (Figure 2.4.5), suggesting that fungi play an important role in mineralizing those P forms. Only four out of 13 samples contained organic P. When present, organic P was between 10% and 32% of total P. This points to substantial accumulations of organic P at some places, while at other places it is completely absent. This might be due to spatial heterogeneity of microbial activity and P mineralization (Kuzyakov and

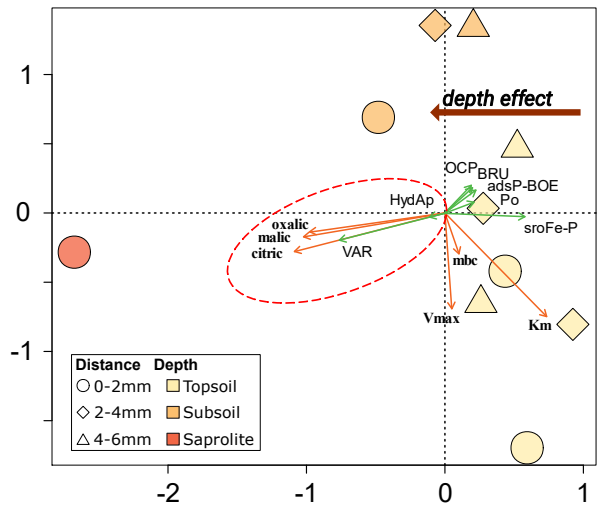

Figure 1.3.3: Biplot of the RDA for the arid shrubland, relating P speciation to biological parameters of P weathering and P recycling. The data are presented in type II scaling, the angles between the arrows can be interpreted in terms of correlation strength between variables.

Blagodatskaya 2015). Study 3 showed that the addition of labile organic C increased P_{mic} and the uptake of sorbed inorganic P over two days (Figure 1.3.4). At later timepoints, uptake of sorbed inorganic P fell below control level, while P_{mic} remained high. This suggests that, after labile C has boosted microbial activity (confirmed by the elevated CO_2 release, Figure: S 2.3.3), the microbial community switches back to the P sources that are preferentially utilized under conditions of scarce labile C. It was not possible to disentangle the individual contributions of primary and organic P to microbial P nutrition in this case, but it cannot be excluded, that hotspots of fast organic P mineralization occur when environmental conditions are favorable, e.g., water and labile C are available. In Study 4 it was shown that phosphatase activity, and hence organic P turnover, is strongly C limited in the arid shrubland. This provides a convincing explanation for the highly heterogeneous distribution of organic P by two mechanisms. On the one hand, organic P is accumulated at sites with high biological activity. On the other hand, organic P is utilized when water supply and C availability allow organic matter degradation, but retained when spatially separated from such hotspots of microbial activity (Kuzyakov and Blagodatskaya 2015). These two processes do not necessarily have to occur at the same sites. Thus, heterogeneous accumulation of organic P is amplified by selective degradation at sites where conditions are favorable for microbial P mineralization. With field labeling experiment (Study 3) it was found that ^{13}C enrichment in bacteria and fungi, was highest immediately after labeling (1 day, Figure 2.4.3), pointing to a fast transfer of freshly assimilated C to the microbial community and, therefore, a tight temporal coupling of root exudates and microbial activity (Spohn et al. 2013). Microorganisms in the rhizosphere are main drivers of nutrient mineralization in soil (e.g. Marschner and Marschner 2012; Kuzyakov and Blagodatskaya 2015). Therefore, a tight coupling of root exudation and microbial activity indicates that the mineralization of organic nutrients is closely linked in time to the availability of root C.

A general conclusion for the arid shrubland ecosystem is that inorganic P species are the most important P source under this climate. It has been shown that biological weathering by LMWOA is an important process in this ecosystem. Although it seems that in some microenvironments, mineralization of organic P is a relevant process when abiotic conditions allow for organic matter degradation.

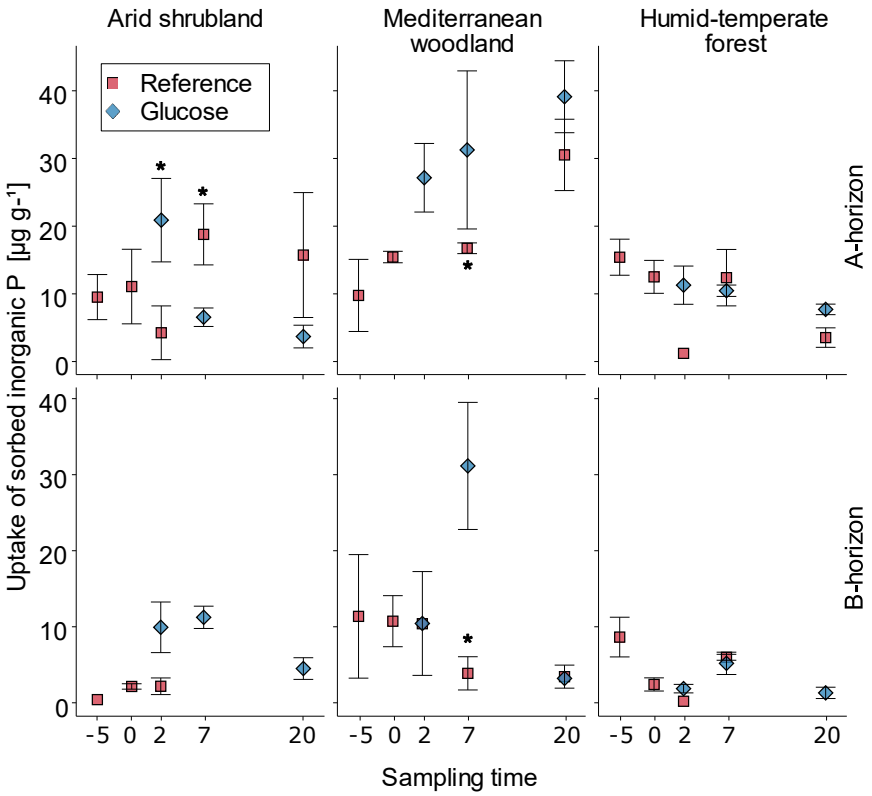

Figure 1.3.4: Microbial inorganic P uptake under steady state conditions (red markers) and under the addition of glucose (blue markers) in the arid shrubland, Mediterranean woodland, and humid–temperate forest. Significant differences between treatments are indicated by an asterisk ($p<0.05$).

1.3.2. P cycling in the humid–temperate forest

In the humid–temperate forest soils and saprolite, no primary P minerals (Ca–P) were found based on the XANES analysis. All P in the soil and the upper part of the weathered bedrock had been transformed to secondary forms associated with Fe and Al or organic compounds. Soil pH in the humid–temperate forest (pH 4.5) favored the sorption of P to Fe– and Al–(hydr)oxides (Schlesinger and Bernhardt 2020), which was reflected by the low abundance of P precipitated with Al– and Fe– at this site (Study 1, Figure 1.3.5). The predominance of Al–P over Fe–P was corroborated by the higher content of NH_4–P than DCB–P (Study 3, Figure 2.4.1) (Prietzel 2017). In line with these results, the P sorption capacity of the soil was very high, with up to 98% of added P sorbed within 100 min (Study 2, Figure 1.3.6).

This indicated a low mobility of inorganic P which may be a result of the formation of Al–humus complexes (Takahashi und Dahlgren 2016), possibly favored by volcanic ashes (i.e., imogolite, allophane). The high sorption capacity coincided with a high clay content at the humid–temperate forest (Figure 1.3.6). However, although the clay content in the B horizon was lower than in the A horizon, the sorption capacity did not differ between the two horizons (Figure 1.3.6). This might result from a higher content of negatively charged organic compounds, occupying binding sites in the A horizon (Warrinnier et al. 2019). In Study 2 it was shown, that

the amount of P which can be released to the soil solution within one minute was highest for the B horizon of the humid–temperate forest, suggesting a good supply of P to the soil solution for plants and microbial uptake (Figure: S 2.3.2, Bünemann et al. 2007).

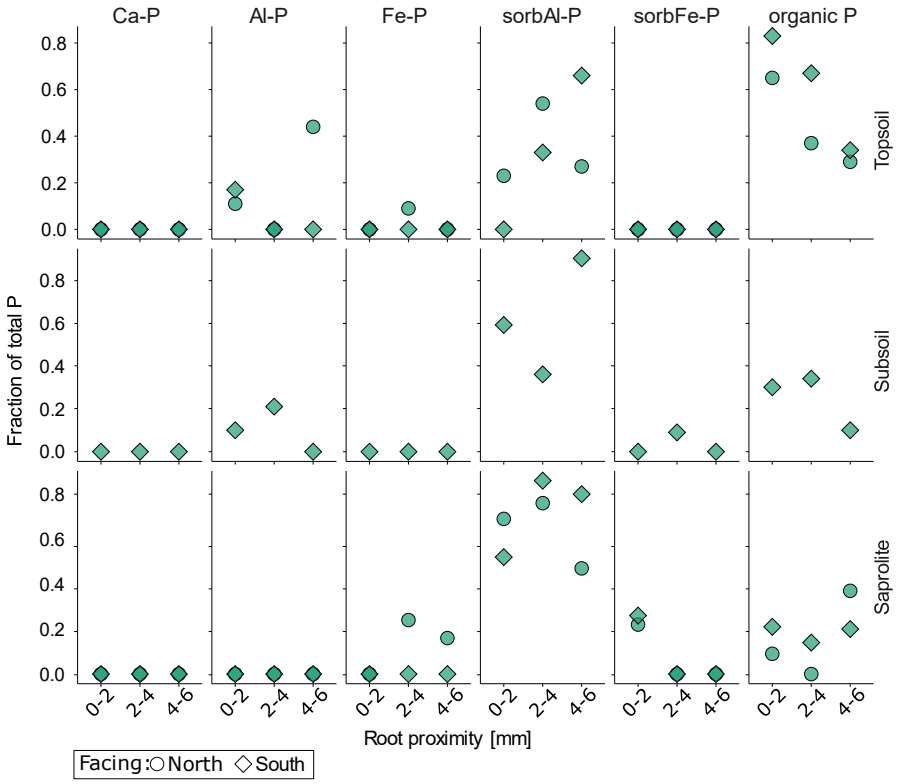

Figure 1.3.5: P speciation in the humid–temperate forest as determined by XANES spectroscopy. Samples from north facing profiles are depicted as circles, from south facing profiles as diamonds.

However, the calculation assumes that the sorption of P to the soil solid phase is a reversible process. It is highly questionable whether this assumption is met for the humid–temperate forest soil. Rather, it can be expected that P desorption from the soil solid phase shows a hysteresis effect with regard to the adsorption of P, i.e., not all the P adsorbed over a defined time is desorbable within the same period of time (Okajima et al. 1983).

Kinetics of C allocation to bacteria and fungi (determined as ^{13}C enrichment) in the humid–temperate forest were highest three days after labeling (Figure 2.4.3), indicating a rather slow release of photosynthetically fixed C as root exudates. The absolute incorporation of fresh root exudates into microorganisms, however, was low, i.e., at about the level of the highly water–limited arid shrubland (Figure 2.4.3). Also, microbial inorganic P uptake was not affected by glucose amendment (Figure 1.3.4). Hence, microbial P supply was not C limited (Study 3). Microbial activity (CO_2 respiration, Figure: S 2.3.3) and abundance (C_{mic} content (named MBC in this figure), Figure 2.3.4) in the humid–temperate forest soil was high. Despite low utilization of fresh root exudates (Figure 2.4.3, Study 3) and inorganic P uptake (Figure 1.3.4 Study 2), the soil houses a thriving microbial community (as seen by highest C_{mic} among the three sites (named MBC in this table; Study 1 Table: S 2.2.8). Moreover, activity of acid phosphatase was highest

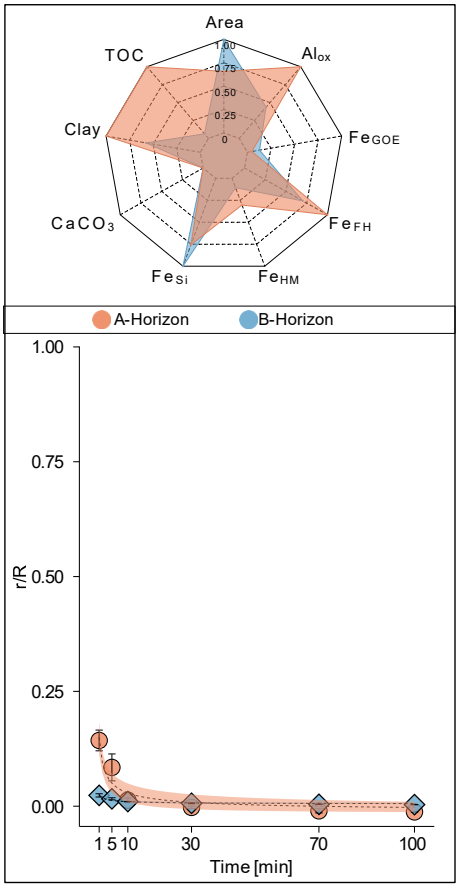

Figure 1.3.6: P sorption kinetics (lower subfigure) and explaining variables of P sorption (upper subfigure) in the humid-temperate forest. The y-axis of the sorption kinetics figure shows the ratio of radioactivity remaining in soil solution after a given time to the total added radioactivity. Thus, high values indicate low sorption capacity (sorptivity) of the soil. Sorption explaining variables are shown as relative values (relative to the highest value of the respective variable along the ecosequence).

in the humid–temperate forest, compared to the other sites (Figure 2.5.3) and the high availability of C compounds likely induced nutrient limitation (N and P, Study 4) in microorganisms. At the same time, organic P was the second largest P pool (Figure 1.3.5) and is likely to be recycled within plants. This was corroborated by Oeser and Blanckenburg (2020) who found a recycling factor of 30 for P at this site (compared to 5 and 9 in the arid, shrubland and the Mediterranean woodland, respectively), which means that a P atom that enters the biological cycle is on average recycled 30 times within the soil plant system before it is lost by erosion or leaching. LMWOA did not correlate with inorganic P species at this site but with enzyme kinetics and C_{mic} (MBC;) and are therefore likely involved in the mobilization of organic P for subsequent enzymatic degradation. The ability of organic acids, especially citric acid, to liberate organic P for enzymatic attack (Wei et al. 2010) seems to play a major role for P cycling in the humid–temperate forest.

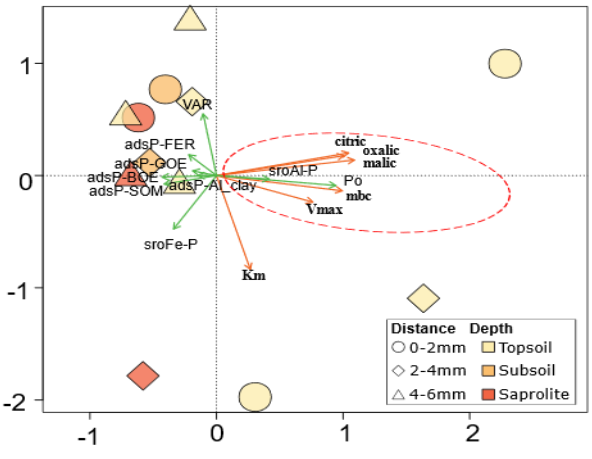

Figure 1.3.7: Biplot of the RDA for the humid–temperate forest, relating P speciation to biological parameters of P weathering and P recycling. The data are presented in type II scaling, the angles between the arrows can be interpreted in terms of correlation strength between variables.

P nutrition in the humid temperate forest is based on recycling of organic P. LMWOA mobilize organic P and thereby foster P mineralization. In summary, plants in this ecosystem benefit from an active microbial community, which does not directly depend on root exudates, as nutrients are mineralized and provided for plant uptake by bacteria and fungi.

1.3.3. P cycling in the Mediterranean woodland

Primary P (hydroxyapatite) was the dominant P species in the Mediterranean woodland soil, where it was highest in the saprolite and decreased towards the topsoil (Figure 1.3.8). Primary P in the topsoil was not detected close to roots (0–2 mm) but accounted for up to 24% in bulk soil (4–6 mm distance to roots). Secondary inorganic P was largely precipitated in Fe- and Al-(hydr)oxides and accounted for up to 56% of total P. The content varied greatly among the samples and was even absent in some topsoil samples. P sorbed to short-range-order Fe- and Al-(hydr)oxides was only found in 6 out of 15 samples and was also highly variable in amount. In accordance with the low content of sorbed P species, the sorption capacity for inorganic P in the soil was low (Sanyal and Datta 1991). Fe-speciation data from Moessbauer spectroscopy in Study 2 also indicated a low sorption capacity, as most Fe was bound in silicates. The B horizon had slightly higher ferrihydrite contents and, consequently, a higher P

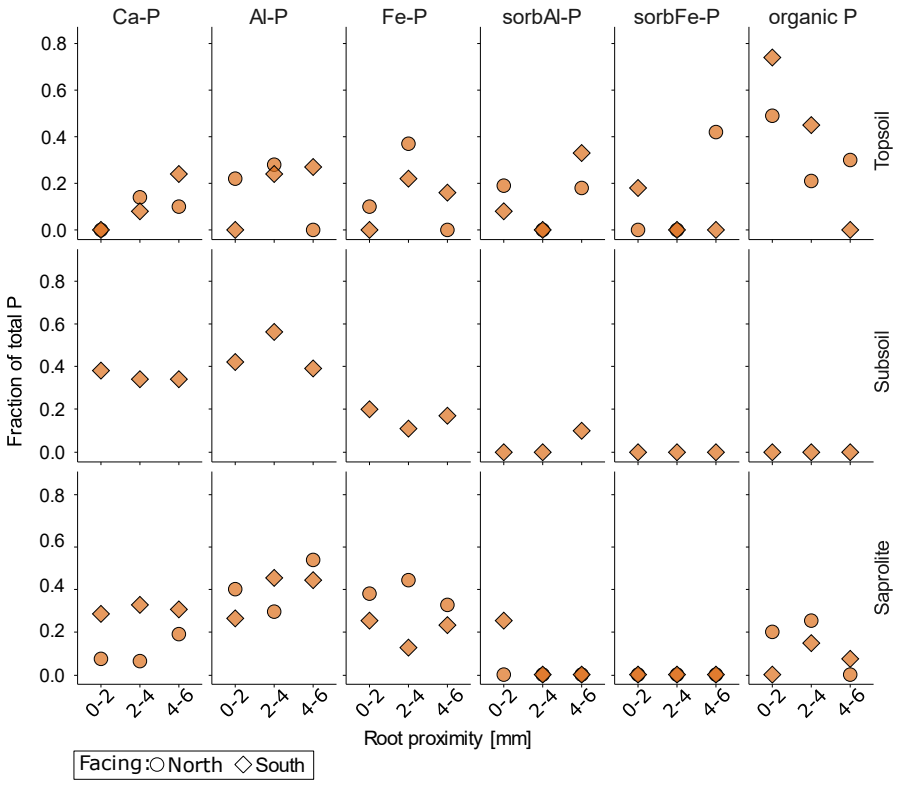

Figure 1.3.8: P speciation in the Mediterranean woodland as determined by XANES spectroscopy. Samples from north facing profiles are depicted as circles, from south facing profiles as diamonds.

sorption capacity than the A horizon (Figure 1.3.9).

Organic P was highest in the topsoil and accounted for up to 74% of total P. Regarding rhizogradients, organic P was highest in root proximity in the topsoil and strongly declined towards the bulk soil, corroborating high P turnover in root vicinity (Figure 1.3.8). The RDA exploring the relationship between P speciation (independent variables), organic acid contents and phosphatase activity (explained variables, Study 1, Figure 1.3.10), showed a strong

correlation of organic P with oxalic acid, phosphatase kinetic parameters, and C_{mic}. Moreover, the arrows representing these variables overlapped mainly with topsoil samples in the biplot. This indicated that organic acids in the topsoil of the Mediterranean woodland were involved in the recycling of organic P.

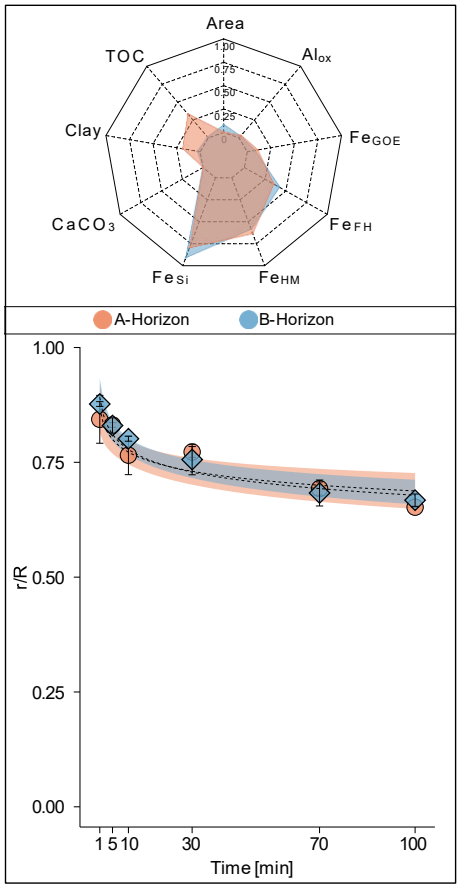

Figure 1.3.9: P sorption kinetics (lower subfigure) and explaining variables of P sorption (upper subfigure) in the Mediterranean woodland. The y-axis of the sorption kinetics figure shows the ratio of radioactivity remaining in soil solution after a given time to the total added radioactivity. Thus, high values indicate low sorption capacity (sorptivity) of the soil. Sorption explaining variables are shown as relative values (relative to the highest value of the respective variable along the ecosequence).

Allocation of plant-derived ^{13}C to organic acids was at a similar level as in the humid-temperate forest, but the kinetics were slower with highest amounts of ^{13}C in free LMWOAs two weeks after labeling (Study 3; Figure 2.4.4). The tracer enrichment in roots followed a similar pattern, indicating that non-sorbed LMWOA were of plant origin (Figure 2.4.3). However, ^{13}C in sorbed oxalic acid showed the same pattern as ^{13}C in fungi (Figure 2.4.3 and Figure 2.4.4). A PCA with supplementary variables (PCA on ^{13}C enrichment in roots, bacteria, and fungi; operational P pools as supplementary variables: H_2O-P, $NaHCO_3$-P, NH_4-P, DCB-P) revealed that ^{13}C allocation to sorbed LMWOA and fungi was closely correlated with DCB-extractable P (Figure 2.4.5). Hence, sorbed oxalic acid exudated by fungi appears to be responsible for the dissolution of crystalline P minerals in the Mediterranean woodland soils and, thus, an important agent for mineral P weathering. Moreover, the RDA (Figure 1.3.10) emphasized the ambiguous role of LMWOA in this ecosystem as it showed a strong correlation of citric and malic acid with Fe-, Al-P and Ca-P. Consequently, LMWOA seem to support P recycling in the topsoil and contribute to mineral weathering in the subsoil. Precipitated P species are likely to be an important P source for plants and microorganisms in the Mediterranean woodland. This is because the easily bioavailable inorganic P pool (H_2O-P + $NaHCO_3$-P) and organic P (except for the soil's thin A horizon) were small. Moreover, the sorption capacity for P was low (Figure 1.3.9). Nevertheless, microbial uptake of sorbed inorganic P is high (Study 2; Figure 1.3.4). Microbial inorganic P uptake was improved when glucose was added, indicating that despite low P availability, the microbial community is C, and not P limited. The C limitation was validated

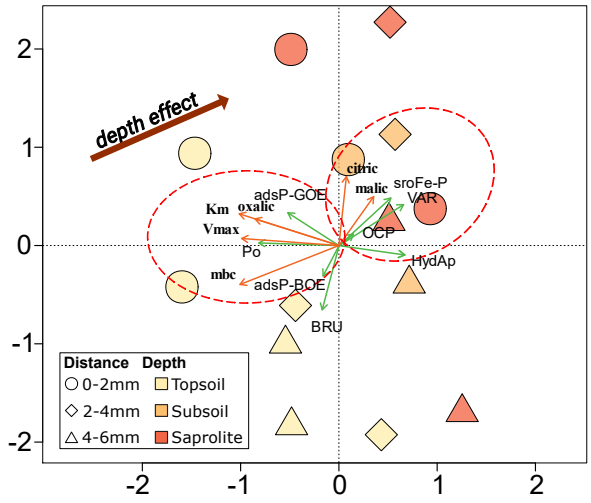

Figure 1.3.10: Biplot of the RDA for the Mediterranean woodland relating P speciation to biological parameters of P weathering and P recycling. The data are presented in type II scaling, the angles between the arrows can be interpreted in terms of correlation strength.

by the acid phosphatase maximal activity, which was higher close to roots and in the topsoil (high C availability) than in bulk soil, subsoil or saprolite (low C availability) (Figure 2.5.5 and Figure 2.5.6). These findings confirm that the system is C limited, likely due to high denudational losses and erosion rates (Schaller et al. 2018; van Dongen et al. 2019; Oeser and Blanckenburg 2020).

Conclusively it was found that LMWOA in the Mediterranean woodland are involved in both, biological P weathering and P recycling. It is likely that mineral P species are of great importance for biotas' P nutrition as losses expected to be high and only a thin A horizon exists where organic P accumulates. Microbial activity was limited by the availability of labile C, as well indicating a low relevance of nutrients from organic matter mineralization.

1.4. Synthesis and Conclusion

In Table 1.4.1 summarizes the research aims addressed in the four studies of this work and the main conclusion that were drawn from the studies.

Table 1.4.1: Summary of the four studies: research aims and main conclusion.

Study I: From rock eating to vegetarian ecosystems — Disentangling processes of phosphorus acquisition across biomes	
Research aim:	Determine plant P acquisition strategies across three dimensions; along a sequence of ecosystems (aridity gradient); from the rhizosphere to bulk soil (C–input gradient); with soil profile depth (expected P availability gradient)
Conclusions:	The P acquisition strategy shifts across biomes from mineral weathering in arid conditions to recycling of organic phosphorus under a temperate climate
	LMWOAs exuded by roots induce biochemical weathering of P minerals under dry climate, but support organic phosphorus mobilization under humid climate.
Study 2: Microbial mobilization and utilization of sorbed inorganic phosphorus in soils of granodioritic origin formed under hyperarid to humid–temperate climate	
Research aim:	Determine soil sorption strength for inorganic P along an aridity gradient.
	Quantify microbial uptake of sorbed inorganic P from the soil solid phase along an aridity gradient.
	Determine how labile root–derived carbon affects microbial P uptake.
Conclusions:	P sorption follows a unimodal distribution with strong sorption in the hyperarid desert (driven by accumulation of $CaCO_3$) and the humid–temperate forest (due to a high clay content and accumulation of Al–humus complexes).
	Microbial inorganic P uptake is highest in the Mediterranean woodland; P utilization is limited by the availability of labile C at this site.
	Organic P is preferred over sorbed inorganic P by microorganisms in the humid–temperate forest. Moreover, microbial activity is decoupled from the input of labile C but is likely P limited.
Study 3: Plant allocation of freshly assimilated C to roots, microorganisms, and weathering agents along an aridity gradient depends on prevailing P forms	
Research aim:	Determine belowground allocation of freshly assimilated C into P weathering agents, microbial functional groups, and roots.
	Characterize P availability by sequential extraction.
	Relate P availability to the amount of C incorporated in roots, microorganisms, and weathering agents.
Conclusions:	Bioavailable P is highest in the humid–temperate forest. The arid shrubland and Mediterranean woodland have equal ammounts of bioavailable and hardly–bioavailable P.
	Allocation of recently fixed plant C to LMWOA is similarly high in the Mediterranean woodland and humid–temperate forest soils but low in the arid shrubland soils.
	C allocation to oxalic acid is an indicator for biological weathering of precipitated and sorbed inorganic P in the Mediterranean woodland and arid shrubland.
	P mobilization in the Mediterranean woodland and the arid shrubland soils is dominated by roots and fungi.
Study 4: Environmental drivers and stoichiometric constraints on enzyme activities in soils from rhizosphere to continental scale	
Research aim:	Determine activities of extracellular enzymes involved in C, N, and P cycling across scales: ecosequence (water availability gradient), depth profile (nutrient availability gradient), rhizosphere/bulk soil (C input gradient).
	Effects of substrate availability and stoichiometric constraints on enzyme activities.
Conclusions:	Maximal activity of C, N, and P acquring enzymes in soils increases with increasing mean annual precipitation.
	Maximal activity of C, N, and P acquring enzymes decreases with soil depth.
	Maximal activity of C, N, and P acquring enzymes decreases from rhizosphere to bulk soil.
	Maximal activity of N and P acquiring enzymes is controlled by nutrient limitation.
	Nutrient limitation is induced by input of labile C (primarily in the rhizosphere and topsoil).

Much is known about the effect of time (e.g. Walker and Syers 1976; Crews et al. 1995; Chen et al. 2015) and climate on P forms in soil (e.g. Feng et al. 2016; Ippolito et al. 2010; Hou et al. 2018a). The effect of climate determined by earlier studies in fact is a mixed effect of climate and biota on soil P speciation and cycling. To which extent biota control P speciation and soil P cycling, however, was never systematically investigated. The inherent problem of disentangling the effect of biota on soil P cycling from that of climate, is that biota is directly dependent on climate. This makes it impossible to change one parameter while keeping the other constant. This problem could not be overcome by this study, nevertheless, some conclusions about the strength of either parameter on P cycling can be drawn.

For further studies it remains to quantify the rates of P transformation that are solely caused by biological activity. It would also be of great importance to disentangle the contributions of plants, bacteria, and fungi to P mobilization under different climatic conditions. This would support to improve our understanding of the P cycle in natural ecosystems and could also contribute to the development of strategies to improve P nutrition of crops.

1.4.1. Integration of P cycling processes across the ecosystem gradient

Figure 1.4.1 shows a compilation of the outcomes of this work. As stated in Hypothesis 1, primary P in soil declined along the climatic gradient from the arid shrubland to the humid–temperate forest. At the same time, organic P increased, reflecting increased biological activity and, therefore, the conversion of primary into organic P. Secondary pedogenic Fe– and Al–P minerals occurred mainly in precipitated forms in the arid shrubland soils. With decreasing aridity, the proportion of P sorbed to Fe– and Al–P increased, most likely favored by the more advanced formation of pedogenic Fe- and Al-(hydr)oxides (sorption sites for P). P speciation along the ecosequence indicated that the arid shrubland and Mediterranean woodland ecosystems are still in an early state of pedogenic P transformation, both sites still contain primary P, while the humid–temperate forest soils are deeply weathered and depleted in primary P.

By relating amounts and ^{13}C incorporation in LMWOA, acid phosphatase activity and C_{mic} to the chemical P speciation along the ecosequence, LMWOA were shown to function as biological weathering agents in the arid shrubland ecosystem, whereas in the humid–temperate forest LMWOA are predominantly involved in organic P recycling. In the Mediterranean woodland the data suggest that LMWOA are involved in both processes, mineral weathering in the subsoil and organic P recycling in the topsoil. It is known that LMWOA can facilitate mineral weathering (e.g. Jones 1998; Hinsinger 2001; Dechassa and Schenk 2004) but also mobilize organic P for

subsequent enzymatic degradation (e.g. Giles et al. 2012; Wei et al. 2010). With respect to Hypothesis 2 it must be concluded that biological weathering was likely to be highest in the Mediterranean woodland. Hence P speciation determines whether LMWOA act as biological weathering agents or facilitate enzymatic degradation of organic P (Figure 1.4.1). If LMWOA are involved in mineral weathering, they themselves exert an influence on P speciation by aiding in the dissolution of mineral inorganic P species and initiating P transformation (centuries to millennia). This, in turn means, that climate and biota determine P cycling mechanisms in soil on a centennial to millennial scale. Since climate not only sets the abiotic conditions for mineral weathering and erosion, but also determines net primary productivity through solar radiation, temperature, precipitation, etc., it is concluded that the rate of P transformation in soil is mainly determined by climate. However, it is left to biota what mechanisms are at play to mobilize the P sources present in soil. This was demonstrated in the arid shrubland soils. Under conditions of low C availability microorganisms utilized primary- and/or organic P. When the C limitation of microorganisms was alleviated by the addition of glucose, microorganisms began to utilize the sorbed inorganic P pool.

Hypothesis 3 addressed the question whether microbial P uptake is limited by the availability of labile C. It was shown that microorganisms depend strongly on easily available C (i.e., root exudates) to maintain inorganic P uptake in the arid shrubland and Mediterranean woodland soils. The addition of labile C in the incubation study enhanced microbial inorganic P uptake in these ecosystems. Also, ^{13}C incorporation in oxalic acid in the arid shrubland and Mediterranean woodland ecosystems correlated with well–crystallized P minerals and ^{13}C incorporation in fungi. In the humid–temperate forest, however, microbial uptake of sorbed inorganic P is decoupled from the input of readily available C, probably due to the rich reservoir of C compounds in the soil. It was therefore concluded that microbial P uptake under arid shrubland and Mediterranean woodland is C limited.

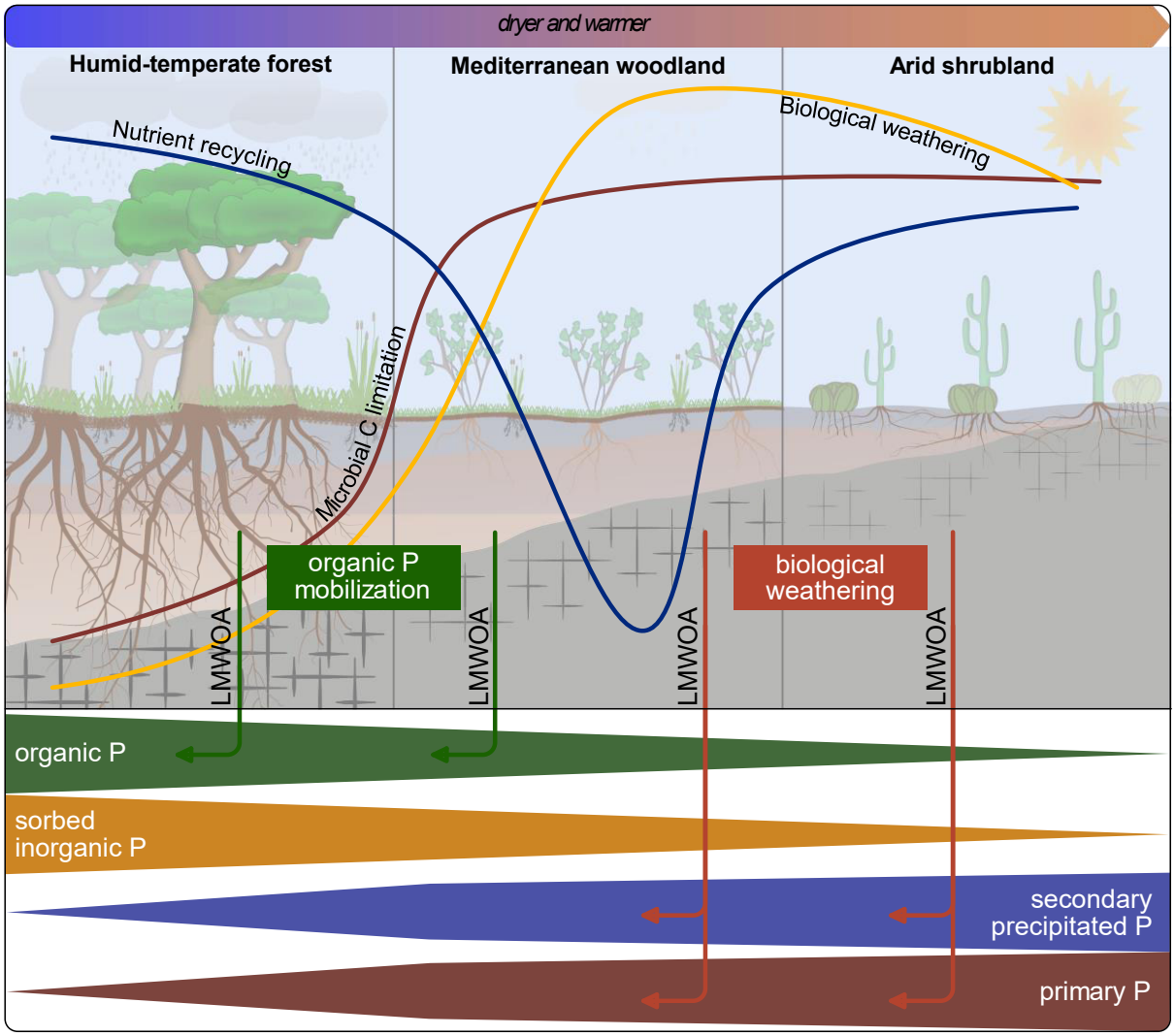

Figure 1.4.1: Conceptual figure of the whole ecosystem gradient. Relevant processes of P cycling in soil are schematically depicted.

It was demonstrated that climatic conditions determine the P speciation in soil and that biota react to these conditions, by adapting P cycling mechanisms. It can be assumed that adaptation to changing conditions occurs more readily in less developed soils, where most of the P is in primary and precipitated secondary P forms. With higher proportions of organic P in soil the recycling mechanisms probably become more specific and alternative P sources exploited. This is valuable information to predict the P availability in ecosystems under climate change. However, it was shown that P sorption and C limitation of P microbial P mobilization are not linearly correlated with aridity. It is, therefore, likely, that under changing climate ecosystems will reach tipping points where established P cycling mechanisms fail. To ensure P nutrition of ecosystems, it is crucial how fast climate change occurs so that ecosystems can adapt to new conditions and adjust P cycling mechanisms. Climate change is projected to change the annual distribution of precipitation and increase precipitation variability (IPCC 2014). For the regions investigated in this study a reduction in MAP of >50% is predicted within the next 50 years, with

greatest reductions in the southern study sites (Garreaud 2011; IPCC 2007). This will reduce soil moisture and consequently lead to a limitation of enzymatic nutrient mineralization. It is likely, that the most developed ecosystems with the highest contents of organic P but depleted mineral P stocks will suffer greatest from more arid conditions.

1.5. References

Adediran, Gbotemi A.; Tuyishime, J. Marius R.; Vantelon, Delphine; Klysubun, Wantana; Gustafsson, Jon Petter (2020): Phosphorus in 2D: Spatially resolved P speciation in two Swedish forest soils as influenced by apatite weathering and podzolization. In *Geoderma* 376, p. 114550. DOI: 10.1016/j.geoderma.2020.114550.

Anderson, S. P.; Blanckenburg, F. von; White, A. F. (2007): Physical and Chemical Controls on the Critical Zone. In *Elements* 3 (5), pp. 315–319. DOI: 10.2113/gselements.3.5.315.

Berner, Robert A. (2004): The phanerozoic carbon cycle: CO2 and O2. New York: Oxford Univ Press.

Bernhard, Nadine; Moskwa, Lisa-Marie; Schmidt, Karsten; Oeser, Ralf A.; Aburto, Felipe; Bader, Maaike Y. et al. (2018): Pedogenic and microbial interrelations to regional climate and local topography: New insights from a climate gradient (arid to humid) along the Coastal Cordillera of Chile. In *CATENA* 170, pp. 335–355. DOI: 10.1016/j.catena.2018.06.018.

Blume, Hans-Peter; Brümmer, Gerhard W.; Horn, Rainer; Kandeler, Ellen; Kögel-Knabner, Ingrid; Kretzschmar, Ruben et al. (2010): Lehrbuch der Bodenkunde. 16. Auflage. Heidelberg: Spektrum Akademischer Verlag. Available online at http://site.ebrary.com/lib/alltitles/docDetail.action?docID=10359930.

Brunauer, Stephen; Emmett, P. H.; Teller, Edward (1938): Adsorption of Gases in Multimolecular Layers. In *J. Am. Chem. Soc.* 60 (2), pp. 309–319. DOI: 10.1021/ja01269a023.

Brundrett, Mark C.; Tedersoo, Leho (2018): Evolutionary history of mycorrhizal symbioses and global host plant diversity. In *New Phytologist* 220 (4), pp. 1108–1115. DOI: 10.1111/nph.14976.

Bünemann, E.; Marschner, P.; McNeill, A.; McLaughlin, M. (2007): Measuring rates of gross and net mineralisation of organic phosphorus in soils. In *Soil Biology and Biochemistry* 39 (4), pp. 900–913. DOI: 10.1016/j.soilbio.2006.10.009.

Bünemann, E. K.; Augstburger, S.; Frossard, E. (2016): Dominance of either physicochemical or biological phosphorus cycling processes in temperate forest soils of contrasting phosphate availability. In *Soil Biology and Biochemistry* 101, pp. 85–95. DOI: 10.1016/j.soilbio.2016.07.005.

Chadwick, O. A.; Derry, L. A.; Vitousek, P. M.; Huebert, B. J.; Hedin, L. O. (1999): Changing sources of nutrients during four million years of ecosystem development. In *Nature* 397 (6719), pp. 491–497. DOI: 10.1038/17276.

Chen, C. R.; Hou, E. Q.; Condron, L. M.; Bacon, G.; Esfandbod, M.; Olley, J.; Turner, B. L. (2015): Soil phosphorus fractionation and nutrient dynamics along the Cooloola coastal dune chronosequence, southern Queensland, Australia. In *Geoderma* 257-258, pp. 4–13. DOI: 10.1016/j.geoderma.2015.04.027.

Chen, Min; Arato, Miguel; Borghi, Lorenzo; Nouri, Eva; Reinhardt, Didier (2018): Beneficial Services of Arbuscular Mycorrhizal Fungi - From Ecology to Application. In *Front. Plant Sci.* 9, p. 1270. DOI: 10.3389/fpls.2018.01270.

Chiou, Cary T.; Lee, Jiunn Fwu; Boyd, Stephen A. (1990): The surface area of soil organic matter. In *Environ. Sci. Technol.* 24 (8), pp. 1164–1166. DOI: 10.1021/es00078a002.

Cornell, Rochelle M.; Giovanoli, Rudolf; Schneider, Walter (1989): Review of the hydrolysis of iron(III) and the crystallization of amorphous iron(III) hydroxide hydrate. In *J. Chem. Technol. Biotechnol.* 46 (2), pp. 115–134. DOI: 10.1002/jctb.280460204.

Crews, Timothy E.; Kitayama, Kanehiro; Fownes, James H.; Riley, Ralph H.; Herbert, Darrell A.; Mueller-Dombois, Dieter; Vitousek, Peter M. (1995): Changes in Soil Phosphorus Fractions and Ecosystem Dynamics across a Long Chronosequence in Hawaii. In *Ecology* 76 (5), pp. 1407–1424. DOI: 10.2307/1938144.

Cross, Anne Fernald; Schlesinger, William H. (1995): A literature review and evaluation of the. Hedley fractionation: Applications to the biogeochemical cycle of soil phosphorus in natural ecosystems. In *Geoderma* 64 (3-4), pp. 197–214. DOI: 10.1016/0016-7061(94)00023-4.

Dakora, Felix D.; Phillips, Donald A. (2011): Root exudates as mediators of mineral acquisition in low-nutrient environments. In J. J. Adu-Gyamfi (Ed.): Food security in nutrient-stressed environments. Exploiting plants' genetic capabilities, vol. 248. Dordrecht, London: Springer (Developments in plant and soil sciences, 95), pp. 201–213.

Dechassa, Nigussie; Schenk, Manfred K. (2004): Exudation of organic anions by roots of cabbage, carrot, and potato as influenced by environmental factors and plant age. In *J. Plant Nutr. Soil Sci.* 167 (5), pp. 623–629. DOI: 10.1002/jpln.200420424.

Dokuchaev, V. V. (1883): Russian Chernozem, in Selected Works of V.V. Dokuchaev, Kaner, N. (Trans.), publ.1967: International Program for Scientific Translations.

Fardeau, J. C. (1993): Le phosphore assimilable des sols : sa représentation par un modèle fonctionnel à plusieurs compartiments. In *Agronomie* 13 (4), pp. 317–331. DOI: 10.1051/agro:19930409.

Farrar, J. F.; Jones, D. L. (2000): The control of carbon acquisition by roots. In *New Phytologist* 147 (1), pp. 43–53. DOI: 10.1046/j.1469-8137.2000.00688.x.

Feng, Jiao; Turner, Benjamin L.; Lü, Xiaotao; Chen, Zhenhua; Wei, Kai; Tian, Jihui et al. (2016): Phosphorus transformations along a large-scale climosequence in arid and semiarid grasslands of northern China. In *Global Biogeochem. Cycles* 30 (9), pp. 1264–1275. DOI: 10.1002/2015GB005331.

Fick, Stephen E.; Hijmans, Robert J. (2017): WorldClim 2: new 1-km spatial resolution climate surfaces for global land areas. In *Int. J. Climatol* 37 (12), pp. 4302–4315. DOI: 10.1002/joc.5086.

Filippelli, G. M. (2008): The Global Phosphorus Cycle: Past, Present, and Future. In *Elements* 4 (2), pp. 89–95. DOI: 10.2113/GSELEMENTS.4.2.89.

Finlay, Roger D. (2008): Ecological aspects of mycorrhizal symbiosis: with special emphasis on the functional diversity of interactions involving the extraradical mycelium. In *J Exp Bot* 59 (5), pp. 1115–1126. DOI: 10.1093/jxb/ern059.

Frossard, Emmanuel; Achat, David L.; Bernasconi, Stefano M.; Bünemann, Else K.; Fardeau, Jean-Claude; Jansa, Jan et al. (2011): The Use of Tracers to Investigate Phosphate Cycling in Soil–Plant Systems. In Ajit Varma, Else Bünemann, Astrid Oberson, Emmanuel Frossard (Eds.): Phosphorus in Action, vol. 26. Berlin, Heidelberg: Springer Berlin Heidelberg (26), pp. 59–91.

Garreaud, René D. (2011): Cambio Climático: Bases Físicas e Impactos en Chile. In *Revista Tierra Adentro – INIA* 93.

Giles, Courtney D.; Richardson, Alan E.; Druschel, Gregory K.; Hill, Jane E. (2012): Organic Anion–Driven Solubilization of Precipitated and Sorbed Phytate Improves Hydrolysis by Phytases and Bioavailability to Nicotiana tabacum. In *Soil Science* 177 (10), pp. 591–598. DOI: 10.1097/SS.0b013e318272f83f.

Hedley, M. J.; Stewart, J. W. B.; Chauhan, B. S. (1982): Changes in Inorganic and Organic Soil Phosphorus Fractions Induced by Cultivation Practices and by Laboratory Incubations. In *Soil Science Society of America Journal* 46 (5), pp. 970–976. DOI: 10.2136/sssaj1982.03615995004600050017x.

Helfenstein, Julian; Jegminat, Jannes; McLaren, Timothy I.; Frossard, Emmanuel (2018a): Soil solution phosphorus turnover: derivation, interpretation, and insights from a global compilation of isotope exchange kinetic studies. In *Biogeosciences* 15 (1), pp. 105–114. DOI: 10.5194/bg-15-105-2018.

Helfenstein, Julian; Tamburini, Federica; Sperber, Christian von; Massey, Michael S.; Pistocchi, Chiara; Chadwick, Oliver A. et al. (2018b): Combining spectroscopic and isotopic techniques gives a dynamic view of phosphorus cycling in soil. In *Nature communications* 9 (1), p. 3226. DOI: 10.1038/s41467-018-05731-2.

Hervé, F.; Munizaga, F.; Parada, M. A.; Brook, M.; Pankhurst, R. J.; Snelling, N. J.; Drake, R. (1988): Granitoids of the Coast Range of central Chile: Geochronology and geologic setting. In *Journal of South American Earth Sciences* 1 (2), pp. 185–194. DOI: 10.1016/0895-9811(88)90036-3.

Hesterberg, D.; Zhou, W.; Hutchison, K. J.; Beauchemin, S.; Sayers, D. E. (1999): XAFS study of adsorbed and mineral forms of phosphate. In *Journal of synchrotron radiation* 6 (Pt 3), pp. 636–638. DOI: 10.1107/S0909049599000370.

Hesterberg, Dean; McNulty, Ian; Thieme, Juergen (2017): Speciation of Soil Phosphorus Assessed by XANES Spectroscopy at Different Spatial Scales. In *Journal of Environmental Quality* 46 (6), pp. 1190–1197. DOI: 10.2134/jeq2016.11.0431.

Hinsinger, Philippe (2001): Bioavailability of soil inorganic P in the rhizosphere as affected by root-induced chemical changes: a review. In *Plant and soil* 237 (2), pp. 173–195. DOI: 10.1023/A:1013351617532.

Hou, Enqing; Chen, Chengrong; Luo, Yiqi; Zhou, Guoyi; Kuang, Yuanwen; Zhang, Yuguang et al. (2018a): Effects of climate on soil phosphorus cycle and availability in natural terrestrial ecosystems. In *Global change biology* 24 (8), pp. 3344–3356. DOI: 10.1111/gcb.14093.

Hou, Enqing; Tan, Xiang; Heenan, Marijke; Wen, Dazhi (2018b): A global dataset of plant available and unavailable phosphorus in natural soils derived by Hedley method. In *Sci Data* 5 (1), p. 180166. DOI: 10.1038/sdata.2018.166.

IPCC (2007): Climate Change 2007: Synthesis Report. Contribution of Working Groups I, II and III to the Fourth Assessment Report of the Intergovernmental Panel on Climate Change [Core Writing Team, Pachauri, R.K and Reisinger, A. (eds.)]. IPCC. Geneva, Switzerland.

IPCC (2014): IPCC, 2014: Climate Change 2014: Synthesis Report. Contribution of Working Groups I, II and III to the Fifth Assessment Report of the Intergovernmental Panel on Climate Change [Core Writing Team, R.K. Pachauri and L.A. Meyer (eds.)]. IPCC. Geneva, Switzerland.

Ippolito, J. A.; Blecker, S. W.; Freeman, C. L.; McCulley, R. L.; Blair, J. M.; Kelly, E. F. (2010): Phosphorus biogeochemistry across a precipitation gradient in grasslands of central North America. In *Journal of Arid Environments* 74 (8), pp. 954–961. DOI: 10.1016/j.jaridenv.2010.01.003.

IUSS Working Group WRB (2015): World Reference Base for Soil Resources 2014, update 2015. International soil classification system for naming soils and creating legends for soil maps. Rome: FAO (World soil resources reports, 106).

Jenny, Hans (1941): Factors of soil formation. New York and London: McGraw Hill Book Company, Inc. Ed.

Jones, D. L. (1998): Organic acids in the rhizosphere - A critical review. In *Plant Soil* 205, pp. 25–44. DOI: 10.1023/A:1004356007312.

Jones, David L.; Darrah, Peter R. (1994): Role of root derived organic acids in the mobilization of nutrients from the rhizosphere. In *Plant Soil* 166 (2), pp. 247–257. DOI: 10.1007/BF00008338.

Jones, David L.; Oburger, Eva (2011): Solubilization of Phosphorus by Soil Microorganisms. In Ajit Varma, Else Bünemann, Astrid Oberson, Emmanuel Frossard (Eds.): Phosphorus in Action, vol. 26. Berlin, Heidelberg: Springer Berlin Heidelberg (26), pp. 169–198.

Kouno, Kenji; Tuchiya, Yasuhiro; Ando, Tadao (1995): Measurement of soil microbial biomass phosphorus by an anion exchange membrane method. In *Soil Biology and Biochemistry* 27 (10), pp. 1353–1357. DOI: 10.1016/0038-0717(95)00057-L.

Kpomblekou, A. K.; Tabatabai, M. A. (1994): Effect of Organic Acids on release of Phosphorus from Phosphate rocks. In *Soil Science* 158 (6), pp. 442–453, checked on 4/6/2021.

Kurtz, Andrew C.; Derry, Louis A.; Chadwick, Oliver A. (2001): Accretion of Asian dust to Hawaiian soils: isotopic, elemental, and mineral mass balances. In *Geochimica et Cosmochimica Acta* 65 (12), pp. 1971–1983. DOI: 10.1016/S0016-7037(01)00575-0.

Kuzyakov, Yakov; Blagodatskaya, Evgenia (2015): Microbial hotspots and hot moments in soil: Concept & review. In *Soil Biology and Biochemistry* 83, pp. 184–199. DOI: 10.1016/j.soilbio.2015.01.025.

Kuzyakov, Yakov; Razavi, Bahar S. (2019): Rhizosphere size and shape: Temporal dynamics and spatial stationarity. In *Soil Biology and Biochemistry* 135, pp. 343–360. DOI: 10.1016/j.soilbio.2019.05.011.

Lang, Friederike; Bauhus, Jürgen; Frossard, Emmanuel; George, Eckhard; Kaiser, Klaus; Kaupenjohann, Martin et al. (2016): Phosphorus in forest ecosystems: New insights from an ecosystem nutrition perspective. In *J. Plant Nutr. Soil Sci.* 179 (2), pp. 129–135. DOI: 10.1002/jpln.201500541.

Lopez-Hernandez, Danilo; Brossard, M.; Frossard, E. (1998): P-Isotopic exchange values in relation to Po mineralisation in soils with very low P-sorbing capacities. In *Soil Biology and Biochemistry* 30 (13), pp. 1663–1670. DOI: 10.1016/S0038-0717(97)00255-1.

Ma, Xiaomin; Mason-Jones, Kyle; Liu, Yuan; Blagodatskaya, Evgenia; Kuzyakov, Yakov; Guber, Andrey et al. (2019): Coupling zymography with pH mapping reveals a shift in lupine phosphorus acquisition strategy driven by cluster roots. In *Soil Biology and Biochemistry* 135, pp. 420–428. DOI: 10.1016/j.soilbio.2019.06.001.

Marschner, Petra; Marschner, Horst. Mineral nutrition of higher plants (Eds.) (2012): Marschner's mineral nutrition of higher plants. 3rd ed. Amsterdam, London: Academic Press.

Marx, M.-C; Wood, M.; Jarvis, S.C (2001): A microplate fluorimetric assay for the study of enzyme diversity in soils. In *Soil Biology and Biochemistry* 33 (12-13), pp. 1633–1640. DOI: 10.1016/S0038-0717(01)00079-7.

Mehra, O. P.; Jackson, M. L. (1958): Iron Oxide Removal from Soils and Clays by a Dithionite-Citrate System Buffered with Sodium Bicarbonate. In *Clays and Clay Minerals* 7 (1), pp. 317–327. DOI: 10.1346/CCMN.1958.0070122.

Muñoz, José F.; Fernández, Bonifacio; Varas, Eduardo; Pastén, Pablo; Gómez, Diego; Rengifo, Pablo et al. (2007): Chilean water resources: The Geological Society of London. Available online at https://pubs.geoscienceworld.org/books/book/1529/chapter/107227077/Chilean-water-resources.

Newville, M. (2014): Fundamentals of XAFS. In *Reviews in Mineralogy and Geochemistry* 78 (1), pp. 33–74. DOI: 10.2138/rmg.2014.78.2.

Oeser, Ralf A.; Blanckenburg, Friedhelm von (2020): Do degree and rate of silicate weathering depend on plant productivity? In *Biogeosciences* 17 (19), pp. 4883–4917. DOI: 10.5194/bg-17-4883-2020.

Oeser, Ralf A.; Stroncik, Nicole; Moskwa, Lisa-Marie; Bernhard, Nadine; Schaller, Mirjam; Canessa, Rafaella et al. (2018): Chemistry and microbiology of the Critical Zone along a steep climate and vegetation gradient in the Chilean Coastal Cordillera. In *CATENA* 170, pp. 183–203. DOI: 10.1016/j.catena.2018.06.002.

Ohno, Tsutomu; Zibilske, Larry M. (1991): Determination of Low Concentrations of Phosphorus in Soil Extracts Using Malachite Green. In *Soil Sci. Soc. Am. J.* 55 (3), pp. 892–895. DOI: 10.2136/sssaj1991.03615995005500030046x.

Okajima, Hideo; Kubota, Hiroyuki; Sakuma, Toshio (1983): Hysteresis in the phosphorus sorption and desorption processes of soils. In *Soil Science and Plant Nutrition* 29 (3), pp. 271–283. DOI: 10.1080/00380768.1983.10434628.

Olander, Lydia P.; Vitousek, Peter M. (2000): Regulation of soil phosphatase and chitinase activityby N and P availability. In *Biogeochemistry* 49 (2), pp. 175–191. DOI: 10.1023/A:1006316117817.

Olsen, S. R.; Cole, C.V.; Watanabe, F. S.; Dean, L. A. (1954): Estimation of available phosphorus in soils by extraction with sodium bicarbonate. With assistance of of the UN FAO. Washington DC, USA: U.S. Dept. of Agriculture (Circular 939).

Parniske, Martin (2008): Arbuscular mycorrhiza: the mother of plant root endosymbioses. In *Nat Rev Microbiol* 6 (10), pp. 763–775. DOI: 10.1038/nrmicro1987.

Peltzer, Duane A.; Wardle, David A.; Allison, Victoria J.; Baisden, W. Troy; Bardgett, Richard D.; Chadwick, Oliver A. et al. (2010): Understanding ecosystem retrogression. In *Ecological Monographs* 80 (4), pp. 509–529. DOI: 10.1890/09-1552.1.

Penn, Chad; Camberato, James (2019): A Critical Review on Soil Chemical Processes that Control How Soil pH Affects Phosphorus Availability to Plants. In *Agriculture* 9 (6), p. 120. DOI: 10.3390/agriculture9060120.

Pierzynski, Gary M.; McDowell, Richard W.; Sims, J. Thomas (2005): Chemistry, Cycling, and Potential Movement of Inorganic Phosphorus in Soils. In J. Thomas Sims, Andrew N. Sharpley (Eds.): Phosphorus: Agriculture and the Environment. Madison, WI, USA: American Society of Agronomy, Crop Science Society of America, and Soil Science Society of America, pp. 51–86.

Prietzel, Jörg (2017): Mobilization of X-ray amorphous and crystalline aluminum and iron phosphates by common soil extraction procedures. In *J. Plant Nutr. Soil Sci.* 180 (1), pp. 14–17. DOI: 10.1002/jpln.201600374.

Prietzel, Jörg; Klysubun, Wantana; Werner, Florian (2016): Speciation of phosphorus in temperate zone forest soils as assessed by combined wet-chemical fractionation and XANES spectroscopy. In *J. Plant Nutr. Soil Sci.* 179 (2), pp. 168–185. DOI: 10.1002/jpln.201500472.

Randriamanantsoa, Lalajaona; Frossard, Emmanuel; Oberson, Astrid; Bünemann, Else K. (2015): Gross organic phosphorus mineralization rates can be assessed in a Ferralsol using an isotopic dilution method. In *Geoderma* 257-258, pp. 86–93. DOI: 10.1016/j.geoderma.2015.01.003.

Roering, Joshua J.; Marshall, Jill; Booth, Adam M.; Mort, Michele; Jin, Qusheng (2010): Evidence for biotic controls on topography and soil production. In *Earth and Planetary Science Letters* 298 (1-2), pp. 183–190. DOI: 10.1016/j.epsl.2010.07.040.

Sanyal, S. K.; Datta, S. K. de (1991): Chemistry of Phosphorus Transformations in Soil. New York: Springer-Verlag New York Inc. (17).

Schaller, M.; Ehlers, T. A.; Lang, K.A.H.; Schmid, M.; Fuentes-Espoz, J. P. (2018): Addressing the contribution of climate and vegetation cover on hillslope denudation, Chilean Coastal Cordillera (26°–38°S). In *Earth and Planetary Science Letters* 489, pp. 111–122. DOI: 10.1016/j.epsl.2018.02.026.

Schlesinger, William H.; Bernhardt, Emily S. (2020): Biogeochemistry. An analysis of global change. Fourth edition / by William Schlesinger, Emily S. Bernhardt. Amsterdam: Academic Press (Developments in plant and soil sciences).

Schwertmann, U. (1964): Differenzierung der Eisenoxide des Bodens durch Extraktion mit Ammoniumoxalat-Lösung. In *J. Plant Nutr. Soil Sci.* 105 (3), pp. 194–202. DOI: 10.1002/jpln.3591050303.

Silverman, M. P. (1979): Chapter 7.2 Biological and Organic Chemical Decomposition of Silicates. In Philip Alan Trudinger, Dalway John Swaine (Eds.): Biogeochemical cycling of mineral-forming elements, vol. 3. Amsterdam, Oxford: Elsevier (Studies in environmental science, vol.3), pp. 445–465.

Sims, Thomas J.; Pierzynski, Gary M. (2005): Chemistry of Phosphorus in Soils. In M. A. Tabatabai, D. L. Sparks (Eds.): Chemical Processes in Soils. Madison, WI, USA: Soil Science Society of America, pp. 151–192.

Smith, Sally E.; Smith, F. Andrew; Jakobsen, Iver (2003): Mycorrhizal fungi can dominate phosphate supply to plants irrespective of growth responses. In *Plant physiology* 133 (1), pp. 16–20. DOI: 10.1104/pp.103.024380.

Spohn, Marie; Ermak, Anton; Kuzyakov, Yakov (2013): Microbial gross organic phosphorus mineralization can be stimulated by root exudates – A 33P isotopic dilution study. In *Soil Biology and Biochemistry* 65, pp. 254–263. DOI: 10.1016/j.soilbio.2013.05.028.

Szmigielska, A. M.; Van Rees, K. C. J.; Cieslinski, G.; Huang, P. M. (1997): Comparison of liquid and gas chromatography for analysis of low molecular weight organic acids in rhizosphere soil. In *Communications in Soil Science and Plant Analysis* 28 (1-2), pp. 99–111. DOI: 10.1080/00103629709369775.

Tamm, O. (1922): Eine Methode zur Bestim mung der anorganischen Komponenten des Gelkomplexes im Boden. In *Meddel. Statens Skogsforsoksanst.* 19, pp. 385–404. Available online at https://ci.nii.ac.jp/naid/10006129139/en/.

Tarafdar, J.C; Claassen, N. (1988): Organic phosphorus compounds as a phosphorus source for higher plants through the activity of phosphatases produced by plant roots and microorganisms. In *Biol Fert Soils* 5 (4), pp. 308–312. DOI: 10.1007/BF00262137.

Taylor, L. L.; Leake, J. R.; Quirk, J.; Hardy, K.; Banwart, S. A.; Beerling, D. J. (2009): Biological weathering and the long-term carbon cycle: integrating mycorrhizal evolution and function into the current paradigm. In *Geobiology* 7 (2), pp. 171–191. DOI: 10.1111/j.1472-4669.2009.00194.x.

Tiessen, H.; Moir, J. O. (2008): Characterization of Available P by Sequential Extraction. In Martin R. Carter, E. G. Gregorich (Eds.): Soil sampling and methods of analysis. 2nd ed. Pinawa Manitoba, Boca Raton FL: Canadian Society of Soil Science; CRC Press.

Tiessen, H.; Stewart, J. W. B.; Cole, C. V. (1984): Pathways of Phosphorus Transformations in Soils of Differing Pedogenesis. In *Soil Sci. Soc. Am. J.* 48 (4), pp. 853–858. DOI: 10.2136/sssaj1984.03615995004800040031x.

Trabucco, Antonio; Zomer, Robert (2018): Global Aridity Index and Potential Evapotranspiration (ET0) Climate Database v2. DOI: 10.6084/M9.FIGSHARE.7504448.V3.

Turner, Benjamin L.; Condron, Leo M. (2013): Pedogenesis, nutrient dynamics, and ecosystem development: the legacy of T.W. Walker and J.K. Syers. In *Plant Soil* 367 (1-2), pp. 1–10. DOI: 10.1007/s11104-013-1750-9.

van Dongen, Renee; Scherler, Dirk; Wittmann, Hella; Blanckenburg, Friedhelm von (2019): Cosmogenic 10 Be in river sediment: where grain size matters and why. In *Earth Surf. Dynam.* 7 (2), pp. 393–410. DOI: 10.5194/esurf-7-393-2019.

Vance, E. D.; Brookes, P. C.; Jenkinson, D. S. (1987): An extraction method for measuring soil microbial biomass C. In *Soil Biology and Biochemistry* 19 (6), pp. 703–707. DOI: 10.1016/0038-0717(87)90052-6.

Varma, Ajit; Bünemann, Else; Oberson, Astrid; Frossard, Emmanuel (Eds.) (2011): Phosphorus in Action. Berlin, Heidelberg: Springer Berlin Heidelberg (26).

Verhoef, Herman A. (1996): The Role of Soil Microcosms in the Study of Ecosystem Processes. In *Ecology* 77 (3), pp. 685–690. DOI: 10.2307/2265492.

Vitousek, Peter M.; Farrington, Heraldo (1997): Nutrient limitation and soil development: Experimental test of a biogeochemical theory. In *Biogeochemistry* 37 (1), pp. 63–75. DOI: 10.1023/A:1005757218475.

Walker, T. W. (1965): The significance of phosphorus in pedogenesis. In E. G. Hallsworth (Ed.): Experimental pedology. London: Butterworths, pp. 295–315.

Walker, T. W.; Syers, J. K. (1976): The fate of phosphorus during pedogenesis. In *Geoderma* 15 (1), pp. 1–19. DOI: 10.1016/0016-7061(76)90066-5.

Warrinnier, Ruben; Goossens, Thomas; Amery, Fien; Vanden Nest, Thijs; Verbeeck, Mieke; Smolders, Erik (2019): Investigation on the control of phosphate leaching by sorption and colloidal transport: Column studies and multi-surface complexation modelling. In *Applied Geochemistry* 100, pp. 371–379. DOI: 10.1016/j.apgeochem.2018.12.012.

Wei, Lili; Chen, Chengrong; Xu, Zhihong (2010): Citric acid enhances the mobilization of organic phosphorus in subtropical and tropical forest soils. In *Biol Fertil Soils* 46 (7), pp. 765–769. DOI: 10.1007/s00374-010-0464-x.

Williams, J D H; Walker, T W (1969): Fractionation of phosphate in a maturity sequence of New Zealand basaltic soil profiles: I. In *Soil Science* 107 (1), pp. 22–30.

Wu, J.; Joergensen, R. G.; Pommerening, Birgit; Chaussod, R.; Brookes, P. C. (1990): Measurement of soil microbial biomass C by fumigation-extraction—an automated procedure. In *Soil Biology and Biochemistry* 22 (8), pp. 1167–1169. DOI: 10.1016/0038-0717(90)90046-3.

Zhong, Xiao-lan; Li, Jiang-tao; Naveed, Muhammad; Raffan, Annette; Hallett, Paul D. (2021): A laboratory study to disentangle hydrological, mechanical and structural mechanisms of soil stabilization by plant mucilage between eroding and depositional zones of a slope. In *Eur J Soil Sci* 72 (1), pp. 125–140. DOI: 10.1111/ejss.12955.

Ziółek, Marta; Melke, Jerzy (2014): The impact of seabirds on the content of various forms of phosphorus in organic soils of the Bellsund coast, western Spitsbergen. In *1* 33 (1), p. 19986. DOI: 10.3402/polar.v33.19986.

2. Publications and manuscripts

2.1. Contributions to the included manuscripts

Study 1: From rock eating to vegetarian ecosystems — disentangling key processes of phosphorus acquisition along a precipitation gradient across biomes in the Chilean Coastal Cordillera

Status: Published in *Geoderma (2021)*, Volume 388, 15 April 2021, 114827. DOI: https://doi.org/10.1016/j.geoderma.2020.114827

Authors	Contribution
Moritz Koester	Field work; Laboratory work; Data analysis; Writing
Svenja C. Stock	Field work; Data contribution; Commenting
Francisco Nájera	Field work; Commenting
Khaled Abdallah	Data contribution; Commenting
Anna A. Gorbushina	Commenting
Jörg Prietzel	Supporting data analysis; Commenting
Francisco Matus	Field work, Commenting
Wantana Klysubun	Supporting data analysis; Commenting
Jens Boy	Commenting
Yakov Kuzyakov	Commenting
Michaela A. Dippold	Study design; Field Work; Supporting data analysis; Commenting
Sandra Spielvogel	Study design; Field Work; Supporting data analysis; Commenting

Study 2: Microbial uptake and utilization of inorganic phosphorus in soils of granodioritic origin formed under hyperarid to humid temperate climate

Status: Submitted to *Geoderma* (GEODER-D-21-01336)

Authors	Contribution
Moritz Koester	Field work; Laboratory work; Data analysis; Writing
Michaela Dippold	Study Design; Supporting data analysis, Commenting
Yue Hu	Laboratory work, Data analysis, Commenting
Werner Häusler	Fe–speciation meassurements; Commenting
Francisco Matus	Field work; Commenting
Francisco Nájera	Field work; Commenting
Svenja C. Stock	Field work; Supporting Data Analysis; Commenting
Sandra Spielvogel	Study Design; Commenting

Study 3: Below ground carbon allocation to low–molecular–weight organic acids and relation to phosphorus availability across biomes

Status: manuscript in preparation

Authors	Contribution
Moritz Koester	Field work; Laboratory work; Data analysis; Writing
Svenja C. Stock	Field work; Laboratory work; Data analysis; Commenting
Francisco Nájera	Field work; Commenting
Francisco Matus	Field work; Commenting
Yakov Kuzyakov	Study design; Field work; Commenting
Sandra Spielvogel	Study design; Field work; Supporting data analysis; Commenting
Michaela A. Dippold	Study design; Field work; Supporting data analysis; Commenting

Study 4: Environmental drivers and stoichiometric constraints on enzyme activities in soils from rhizosphere to continental scale

Status: Published in *Geoderma* (2019), 337, 973–982, doi: 10.1016/j.geoderma.2018.10.030

Authors	Contribution
Svenja C. Stock	Field work; Laboratory work; Data analysis; Writing
Moritz Koester	Field work; Commenting
Michaela A. Dippold	Study design; Field work; Supporting data analysis; Commenting
Francisco Nájera	Field work; Commenting
Francisco Matus	Field work; Commenting
Carolina Merino	Field work; Commenting
Jens Boy	Study design; Commenting
Sandra Spielvogel	Study design; Field work; Commenting
Anna A. Gorbushina	Study design; Commenting
Yakov Kuzyakov	Study design; Supporting data analysis; Commenting

2.2. From rock eating to vegetarian ecosystems — disentangling processes of phosphorus acquisition across biomes (Study 1)

Published in *Geoderma* (2021), Volume 388, 15 April 2021, 114827, DOI: https://doi.org/10.1016/j.geoderma.2020.114827

Authors: Moritz Koester[a,b], Svenja C. Stock[b,c], Francisco Nájera[d,e], Khaled Abdallah[f], Anna Gorbushina[f,g], Jörg Prietzel[h], Francisco Matus[i,j], Wantana Klysubun[k], Jens Boy[l], Yakov Kuzyakov[c,m], Michaela A. Dippold[b], Sandra Spielvogel[a,n]

Affiliations:

[a]Instiute of Geography, University of Bern, Bern, Switzerland

[b]Biogeochemistry of Agroecosystems, University of Goettingen, Goettingen, Germany

[c]Soil Science of Temperate Ecosystems, Agricultural Soil Science, University of Goettingen, Goettingen, Germany

[d]Department of Chemical Sciences and Natural Resources, Universidad de La Frontera, Temuco, Chile

[e]Faculty of Agricultural Sciences, Universidad de Chile, Santiago, Chile

[f]Federal Institute for Material Research and Testing, Berlin, Germany

[g]Department of Earth Sciences & Department of Biology Chemistry Pharmacy, Freie Universität Berlin, Malterserstr. 74–100, D–12249 Berlin, Germany

[h]Research Department Ecology and Ecosystem Management, Chair of Soil Science, Technical University of Munich, Freising, Germany

[i]Laboratory of Conservation and Dynamics of Volcanic Soils, Universidad de La Frontera, Temuco, Chile

[j]Network for Extreme Environment Research, NEXER–Chile, Universidad de La Frontera, Temuco, Chile

[k]Synchrotron Light Research Institute, Nakhon Ratchasima, Thailand

[l]Institute of Soil Science, Leibniz Universität Hannover, Hannover, Germany

[m]Institute of Environmental Sciences, Kazan Federal University, Kazan, Russia

[n]Institute for Plant Nutrition and Soil Science, Christian–Albrechts University Kiel, Kiel, Germany

2.2.1. Abstract

Low–molecular–weight organic acids (LMWOAs) are crucial for the mobilization and acquisition of mineral phosphorus by plants. However, the role of LMWOAs in mobilizing organic phosphorus, which is the predominant phosphorus form in at least half of the world's ecosystems, especially in humid climates, is unclear. The mechanisms of phosphorus mobilization by LMWOAs depend on climate, mainly precipitation, and shape the phosphorus nutrition strategies of plants.

We disentangled the impact of roots and associated microorganisms on mechanisms of phosphorus cycling mediated by LMWOAs by studying soils along an ecosystem–sequence (ecosequence): from arid shrubland (~70 mm yr^{-1}), and Mediterranean woodland (~370 mm yr^{-1}) to humid–temperate forest (~1470 mm yr^{-1}). Phosphorus speciation in soil was examined by X–ray absorption near edge structure analysis (XANES). LMWOAs were quantified as biological rock–weathering and organic phosphorus mobilization agents and compared with kinetics of acid phosphatase as a proxy for organic phosphorus mineralization.

Calcium–bound phosphorus in topsoils decreased from 126 mg kg^{-1} in the arid shrubland, to 19 mg kg^{-1} in the Mediterranean woodland and was undetectable in the humid–temperate forest. In contrast, organic phosphorus in topsoils in close root proximity (0–2 mm distance to roots) was absent in the arid shrubland but raised to 220 mg kg^{-1} in the Mediterranean woodland and to 291 mg kg^{-1} in the humid–temperate forest. The organic phosphorus content in topsoils was 1.6 to 2.4 times higher in close root proximity (0–2 mm distance to roots) compared to bulk soil (4–6 mm distance to roots) in the Mediterranean woodland and humid–temperate forest, showing intensive phosphorus bioaccumulation in the rhizosphere. Redundancy analysis (RDA) revealed that LMWOAs were explained by the content of hydroxyapatite and variscite phosphorus–species in the arid shrubland, indicating that LMWOAs contribute to mineral weathering in this soil. LMWOA contents, phosphatase activity, and microbial biomass carbon correlated strongly with organic phosphorus in the humid–temperate forest soil, which implies a high relevance of LMWOAs for organic phosphorus recycling. In the Mediterranean woodland soil, however, oxalic acid correlated with organic phosphorus in the topsoil (suggesting phosphorus recycling), whereas in the subsoil malic and citric acid were correlated with primary and secondary phosphorus minerals (implying mineral weathering). We conclude that phosphorus acquisition and cycling depend strongly on climate and that the functions of LMWOAs in the rhizosphere change fundamentally along the precipitation gradient. In the arid shrubland LMWOAs facilitate biochemical

weathering (rock eating), while in the humid–temperate forest their functions change towards supporting organic phosphorus recycling (vegetarian).

Keywords: rhizosphere processes; phosphorus K–edge–XANES spectroscopy; low–molecular–weight organic substances; organic phosphorus breakdown; biogenic weathering; climate gradient

Conceptual Figure:

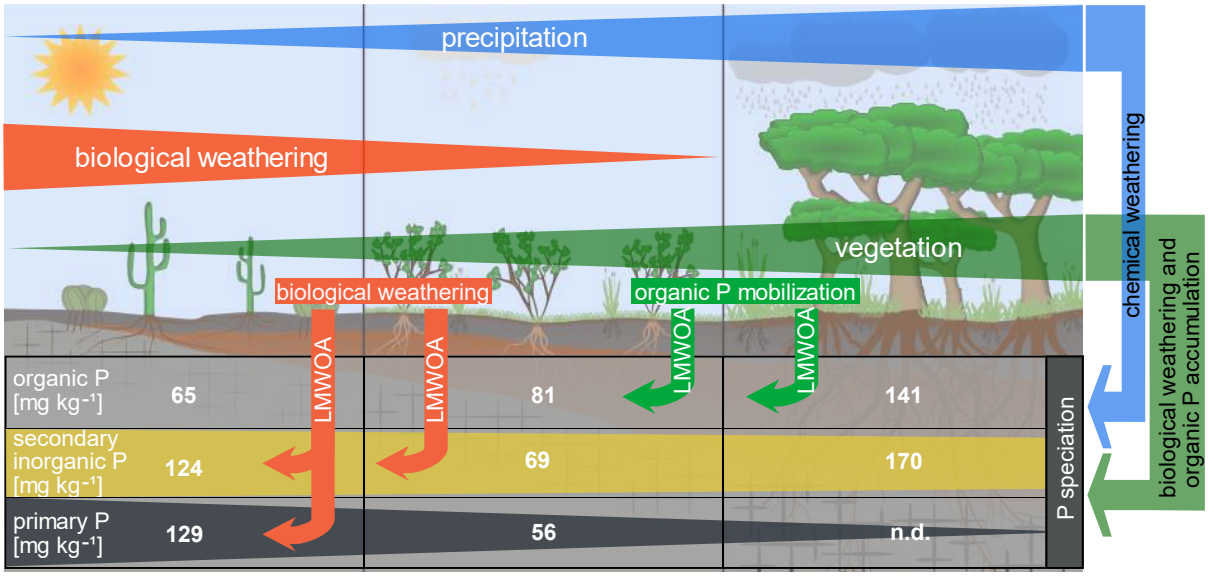

Figure 2.2.1: Conceptual Figure for study 1.

2.2.2. Introduction

Chemical and physical weathering depend on climate and have a strong control over plant's phosphorus (P) accessibility. In general, apatite weathering is strongly driven by water availability (Maher, 2010). Phosphate ($H_2PO_4^-$, HPO_4^{2-}, and PO_4^{3-}) concentrations in soil solution are low and constantly have to be replenished from undissolved pools to sustain plant's P demands (Kirkby and Johnston, 2008). Beyond abiotic dissolution by water, plants and associated microorganisms modify biochemical conditions in the rhizosphere (Kuzyakov and Razavi, 2019), e.g. by the exudation of low–molecular–weight organic acids (LMWOAs) and simultaneous release of protons. Thereby, plants and microorganisms enhance mineral weathering (biochemical weathering) in root proximity and the mobilization of scarce nutrients, but also facilitate the uptake of organic P.

There are three mechanisms by which LMWOAs enhance the dissolution of P minerals. (1) The exudation of organic anions, associated with the exudation of a proton as counterion, lowers rhizosphere pH (Ma et al., 2019) and, subsequently, leads to the dissolution of calcium–phosphates (Ca–P). (2) Organic anions chelate bi– and trivalent cations and decrease

the concentration of iron (Fe^{3+}), aluminum (Al^{2+}), and calcium (Ca^{2+}) in soil solution (Jones, 1998). This process forces the dissolution of Ca–, Fe– and Al–P and hampers phosphate precipitation. (3) Organic anions block sorption sites, especially at sesquioxides, and desorb phosphate ions (Hinsinger, 2001; Jones, 1998; Jones and Darrah, 1994). Several authors have reported that LMWOAs are also capable of organic P mobilization (Giles et al., 2014; Lan et al., 1995), especially citric acid was demonstrated to be highly effective in liberating organic P species in tropical natural and plantation soils (Wei et al., 2010). Because sorption of organic P species to metal ions occurs analogous to that of free phosphates, it was suggested that the liberating mechanisms are similar (Wei et al., 2010). LMWOAs could on the one hand serve to desorb organic P, exposing it to enzymatic attack, and on the other hand hamper the precipitation of liberated P by keeping Fe and Al concentrations in the soil solution low. Different LMWOAs are differently effective in dissolving the various P forms in soils. Johnson and Loeppert (2006) showed that citrate is the most effective LMWOA in desorbing P from Fe surfaces. This is likely due to its tricarboxylic structure and the ability to complex trivalent metal cations. On the other hand, oxalate is most effective in releasing P from Ca–phosphates (Jones, 1998). The effect of malate was only tested in mixtures with other organic acids and never for this acid alone (e.g., Fox et al., 1990).

To date it is unclear how crucial LMWOAs are for biochemical weathering (Jones, 1998; López–Arredondo et al., 2014; Ryan et al., 2001). Furthermore, there are only few data on the concentrations of LMWOAs in soil under field conditions. It was demonstrated that oxalate at concentrations of about 1 mM effectively dissolves feldspars in a batch experiment (Hinsinger, 2001). However, LMWOAs' concentrations in bulk soil in most cases are lower than the concentrations used in batch experiments to dissolve pure minerals (Neaman et al., 2006). Nevertheless, concentrations in some microenvironments such as the rhizosphere, can exceed by far those in bulk soil (Drever, 1994; Neaman et al., 2006).

It has repeatedly been shown that P starvation enhances the exudation of LMWOA by roots (Hedley et al., 1982; Kirk et al., 1999; Lipton et al., 1987). More specifically, citric acid exudation was high under P deficiency in rhizosphere soil under cabbage, but not in rhizosphere soil under carrot and potato (Dechassa and Schenk, 2004). A study by Gaume et al. (2001) comparing a low–P resistant maize (*Zea mays* L.) cultivar with a non–low–P resistant breed showed that the ability to exude organic acids in response to P deficiency can vary even among genotypes of the same species.

Several studies that investigated the change in P speciation along climosequences conclude that climate, mediated by vegetation, is the main driver of apatite transformation to secondary

Fe– and Al–phosphates, phosphates adsorbed to sesquioxides, and organic P (Feng et al., 2016; Ippolito et al., 2010; Pinheiro Junior et al., 2019). Precipitation is particularly important because the addition of water with low ion concentrations (P, Fe, Al, Ca) to the soil solution promotes the abiotic dissolution of P minerals and desorption of P due to concentration gradients. Ippolito et al. (2010) found that the loss of Ca–P from soil was related to mean annual precipitation (MAP) and explained this by the loss of Ca. On the other hand, Walker and Syers (1976) postulate highest P leaching rates at the beginning of pedogenesis. This implies that MAP needs to exceed a certain threshold for P leaching to occur, but weathering and soil mineral composition has to be in a state where P retention by sesquioxides is still low.

It is widely understood that different ecosystems have contrasting strategies to acquire nutrients. Moreover, it has been demonstrated that during ecosystem development a change from acquisition to recycling of nutrients within an ecosystem often occurs via a transition of the plant community from short living individuals to a more complex, interacting community (Lambers et al., 2008; Odum, 1969). Under arid conditions P must largely be acquired from the parent material, because low primary productivity transforms only a small amount of mineral P to organic P. Moreover, physical- and chemical weathering, but also enzymatic processes, are restricted by water limitation under arid and semiarid climate for most of the time. In periods when water is available, it is mandatory for plants to accelerate mineral weathering by the production of weathering agents (Banfield et al., 1999; Lenton and Watson, 2004). Recycling of organic P becomes increasingly important with increasing humidity of the climate, as it can help to prevent leaching and associated P–losses caused by precipitation (Feng et al., 2016; Hou et al., 2018). Moreover, humid climates are correlated with high primary productivity and thus a higher proportion of P is bound in the organic pool as compared to arid ecosystems (Feng et al., 2016). The amount of total P decreases with proceeding soil development (Turner et al., 2018; Yang and Post, 2011 Walker and Syers, 1976). At the same time the proportion of P occluded in organomineral-complexes was highest in the most weathered soils (Yang and Post, 2011). Lang et al. (2017) indicate that deeply weathered humid ecosystems intensively recycle P within the organic pool, rather than acquiring it from the parent material.

We address the concept of acquiring versus recycling ecosystems (Lang et al., 2017) and propose that the P–source preferred by the ecosystems depends on mean annual precipitation, as driver of the biotas' productivity and, thus, P demand. We hypothesize that (1) under arid climate LMWOAs facilitate the dissolution of primary P species (weathering), with partial re–precipitation of the P as secondary inorganic P minerals. (2) In soils under humid conditions, we expect LMWOAs to support recycling of organic P species, induced by a high risk for P losses

by precipitation. This would indicate a high importance of nutrient recycling under humid conditions because suggested weathering rates are too low to provide sufficient P to the ecosystems' biota. This is supported by a study of Oeser and Blanckenburg (2020), who examined the same study sites, and found no increase in weathering depths with increasing precipitation. At the same time, net primary productivity, and thus, P demand along the ecosequence increased strongly from arid to humid ecosystems (Werner et al., 2018).

Table 2.2.1: Characteristics of the three study sites. Mean annual precipitation (MAP) and mean annual temperature (MAT) are derived from Fick and Hijmans (2017). Climate classifications from (Trabucco and Zomer, 2019). Vegetation type, soil type, pH (determined with a 0.01M CaCl2 solution; soil–to–solution ratio 1:2.5), and grain size distribution (sand–, silt–, and clay shares) are taken from Bernhard et al. (2018b). Grain size classes and pH were calculated as mean over the respective soil depths. Soil types refer to soil pits from midslope position at north– and south–facing soil pits. The sampling depth (by soil region) is given in percent classes as they were used for result presentation throughout the present work and in absolute values. Absolute sampling depth is given for the soil pit at the north facing slope in midslope position and for the south facing slope for the soil pits at top– mid– and toeslope position.

Site	Soil region	Percentage soil depth (%)	Absolute depth [cm]				MAP[a] [mm yr^{-1}]	MAT[a] [°C]	Climate[b]	Vegetation[c]	Soil–type[c]	pH[c]	Sand[c] (%)	Silt[c] (%)	Clay (%)
			North		South										
			Mid	Top	Mid	Toe									
Arid shrubland	topsoil	0–50	15	15	22.5	25	66	13.7	Arid	Sclerophyllous	Cambisol/	6.4	77.4	14.6	8.0
	subsoil	50–100	30	30	45	50				shrubs	Leptosol	6.3	73.4	14.3	11.4
	saprolite	>100	>30	>30	>45	>50				cacti		6.4	78.5	13.0	8.6
Mediterranean	topsoil	0–50	30	15	24	35	367	14.1	Semiarid	Deciduous forest	Cambisol	5.5	73.0	17.6	9.5
woodland	subsoil	50–100	70	30	48	70				sclerophyllous		5.0	78.0	13.4	8.6
	saprolite	>100	>70	>30	>48	>70				shrubs		5.4	88.3	7.6	4.1
Humid–temperate	topsoil	0–50	57.5	45	80	65	1469	6.6	Humid	Coniferous forest	Orthodystric	4.3	56.4	21.1	22.5
forest											Umbrisol/				
											Umbric				
											Podzol				
	subsoil	50–100	115	90	160	130						4.6	81.7	11.1	7.3
	saprolite	>100	>115	>90	>160	>130						4.6	84.6	10.1	5.3

a) (Fick, 2017)

b) (Trabucco and Zomer, 2019)

c) (Bernhard et al., 2018b)

2.2.3. Material and Methods

Experimental sites

We focused on three study sites that represent a gradient across biomes (ecosequence) and extend from 29 ° to 38 ° of southern latitude. They are located along the Coastal Cordillera of Chile, and all soils have developed from granodioritic parent material. Mean annual precipitation (MAP) increases from 66 mm yr^{-1} to 1469 mm yr^{-1} and mean annual temperature (MAT) decreases from 13.7 °C to 6.6 °C, from north to south (Fick and Hijmans, 2017) (Table 2.2.1). The study sites comprise an ecosequence from *arid shrubland* (Reserva Nacional Santa Gracia) in the north to *Mediterranean woodland* (Parque Nacional La Campana) and *humid–temperate forest* (Parque Nacional Nahuelbuta) in the most southern site. Important site specifics are shown in Table 2.2.1. For a comprehensive description of vegetation, soils and geology see Bernhard et al. (2018b) and Oeser et al. (2018).

Soil sampling and sample preparation

Soil sampling was done in austral summer 2016. At each site samples were taken from three soil pits on a south–facing slope, arranged as a catena (top–, mid–, and toe–slope), and one soil pit at the opposing north–facing slope (mid–slope) (Bernhard et al., 2018b). Soil pits were sampled at three depths. To compare sites and profiles among each other, depth increments were determined in percent of the total soil depth; with 100% defined as the boundary of soil to saprolite. Samples were taken from 0–50% (*'topsoil'*), 50–100% of soil depth (*'subsoil'*), and >100% (*'saprolite'*). For absolute sampling depths in each soil pit see Table 2.2.1. To obtain a gradient from rhizosphere to bulk soil, samples were taken at three distances (0–2 mm, 2–4 mm, 4–6 mm) from root channels of young living roots. The 0–2 mm and 2–4 mm distance increments were defined as rhizosphere soil, the distance 4–6 mm was considered as bulk soil. Due to the coarse texture of the parent material in the arid shrubland saprolite, it was not possible to accurately sample increments of two millimeters. Therefore, only distance increments 0–2 mm and 4–6 mm were sampled. Roots were found in all sampled horizons, but in different abundances. Rooting density decreased with increasing soil depth and increased with increasing MAP. For more details about the rooting density and pictures of the soil pits the reader is referred to Oeser et al. (2018). We did not distinguish roots on species level but sampled an average of all roots occurring in the respective soil pit and depth. Roots with a diameter of ≤ 2 mm were considered as young roots. To confirm that the sampled roots were still active, we removed the root bark to observe if the underlying tissues was moist, hence, transporting water.

All analyses were run in all three depth increments for south−facing slopes (with mentioned exception for the arid shrubland ecosystem) and depth increments 0−50% (e.g., topsoil) and >100% (e.g., saprolite) for north facing slopes. We aliquoted the samples and immediately froze and stored the samples meant for DNA analyses and LMWOA measurement at −20 °C. Samples for X−ray absorption near edge structure (XANES) analysis were dried and ball milled at 200 rpm for 2 min. Gravimetric water content was measured by drying the samples at 105 °C until weight constancy. Total P content was determined by pressure digestion with HNO_3 (König et al., 2014). Briefly, samples (100 mg) were placed into Teflon beakers and 2 ml of 65 % HNO_3 were added. Beakers were tightly closed and heated to 190 °C for 12 h. Subsequently, the extract was diluted with double distilled water (ultrapure) and analyzed on an inductively coupled plasma−optical emission spectrometer (ICP−OES) (Thermo Scientific iCap 6000 Series, Bremen, Germany).

DNA content and phosphatase kinetics

Total genomic DNA extraction for soil samples was performed using the FastDNA SPIN Kit for Soil (MP Biomedicals, Solon, USA) following the manufacturer's instructions. Samples of maximally 0.25 g were homogenized in three processing cycles with 2 min ice incubations between cycles. The extracted DNA was eluted in 80 µL sterile ultrapure water and quantified with a NanoDrop 2000C (Thermo Fisher Scientific, Bremen, Germany). Diluted DNA extracts were stored at −80°C until qPCR analyses. Bacterial and fungal DNA content was used to calculate microbial biomass carbon (MBC) in the samples by using a conversion factor of 5 (Anderson and Martens, 2013). Besides DNA contents, kinetics of acid phosphatase, determined by Stock et al. (2019) from the same sample set, were included in the multivariate statistical approaches (see section “Statistical analysis”). To describe phosphatase kinetics from a Michaelis−Menten fit, the maximum phosphatase reaction rate V_{max} and the half−saturation constant K_m, were reported. V_{max} represents the maximum enzyme activity at substrate saturation and K_m the substrate concentration required for half−maximal activity.

LMWOA extraction

LMWOAs were extracted based on a method after Szmigielska et al. (1997), with modifications. LMWOAs were extracted with 0.5 M HCl in methanol (MeOH) with a soil to solution ratio of 1:1 (v/v) by shaking for one hour. After centrifugation at 950 *g* for 15 min the supernatant was transferred to a reaction vessel and dried under a gentle stream of N_2. For derivatization, 3 ml of MeOH and 300 µl of H_2SO_4 (50%) were added to the samples which then were placed in a heating block at 60 °C for 30 min. Analytes were purified by liquid−liquid extraction using chloroform ($CHCl_3$) as final solvent. Samples were analyzed on a GC−MS (GC 7890A, MS 7000A

Series Triple Quad, Agilent Technologies, Waldbronn, Germany) with a capillary column (DB−FFAP, 30 m length, 1 µm film thickness, 0.25 mm diameter; Agilent Technologies, Waldbronn, Germany). Standard solutions contained the following organic acids: oxalic−, malonic−, fumaric−, succinic−, maleic−, malic− and citric acid (Table: S 2.2.1). Contents of LMWOAs were determined for three south−facing and one north−facing soil pit in each ecosystem, respectively. As organic acids as well as their anions are co−extracted by the presented approach, the abbreviation for LMWOAs refers to acids and their respective anions.

P speciation by XANES P K−edge spectroscopy

Spectra at the P K−edge were measured at the Beamline 8 of the electron storage ring (1.2 GeV; bending magnet; beam current: 80 – 150 mA; 1.1 to 1.7 x 10^{11} photons s^{-1}) at the Synchrotron Light Research Institute (SLRI), Nakhon Ratchasima, Thailand (Klysubun et al., 2012). Air dried, milled samples were homogenized and applied to P free *'Kapton tape'* (Lanmar Inc., Northbrook, IL, USA) (area 2.0 cm x 0.5 cm). Samples were measured in fluorescence mode. The chamber was flushed with He 2 min before, and during measurements. The energy of the X−ray beam was modulated by an InSb (111) double crystal monochromator, with an energy resolution ($\Delta E/E$) of 3 x 10^{-4} (i.e., about 0.6 eV at the P K−edge). Energy calibration was done with elemental P powder (E_0 = 2145.5 eV; precision 0.11 eV). Depending on the P content of the sample, 3 to 5 scans were recorded.

Evaluation of the XANES spectra was done using the software R Version 3.4.3 (R Core Team, 2017) and the LCF package for linear combination fitting (LCF) (Werner, 2017). Spectra of the samples were background corrected and edge−step normalized by allowing energy levels to float in a defined range. For the lower pre−edge point this was between −48 eV to −28 eV and for the upper pre−edge point between −18 eV to −8 eV, relative to E_0, with energy steps of 1 eV. The post−edge energy was allowed to vary between 29 eV to 39 eV, energy steps of 0.5 eV, for the lower point and 60 eV to 70 eV, energy steps of 1 eV, for the upper point, relative to E_0. All fits which deviated from 1 by less than 0.0005 were chosen and those with the lowest R values selected as to best fit the data. In a second step the optimized background correction and normalization parameters were used in the *fit_athena* environment of the LCF package (which uses the same algorithm as the Athena Software (Ravel and Newville, 2005)). The number of total standards allowed in the final fit was constrained to 4, the sum of weights of the standards was forced to one. If the second−best fit diverged from the best fit in at least one P species by more than five percent, out of these two fits, we selected the one that was most similar to the third−best fit. For the fitting process a total of 13 standards (Table 2.2.2) was selected (Gustafsson et al., 2020; Prietzel et al., 2016).

The 13 P species used for the fitting procedure were summarized in six soil P classes: Ca–bound P (Ca–P), Fe– and Al–phosphates (Fe–P, Al–P), P adsorbed to Fe– and Al–oxyhydroxides (sorbFe–P, sorbAl–P), and organic P (P_o). The Ca–P class contained the P species hydroxyapatite (*HydAp*), octacalciumphosphate (*OCP*) and brushite (*BRU*) as they represent the most important primary P mineral (*HydAp*) and secondary calcium–phosphates in these granodiorite–derived neutral to acidic soils. The Fe–P class consists only of a standard for short–range order Fe–phosphates (*sroFe–P*) (which was the only P standard available in the fitting that accounts for Fe–phosphates) while the Al–P class was composed of short–range order Al–phosphates (*sroAl–P*), and variscite (*VAR*). Both classes were included to account for secondary P minerals. The sorbFe–P compound class entailed P sorbed to ferrihydrite (*adsP–FER*), and P sorbed to goethite (*adsP–GOE*), whereas the sorbAl–P compound class consisted of P sorbed to Al saturated clay (*adsP–Al_clay*), P sorbed to Al–hydroxides (*adsP–AlOH*), P sorbed to boehmite (*adsP–BOE*), and P sorbed to Al saturated soil organic matter (SOM) (*adsP–SOM*). P_o is represented by a standard of pure Inositol hexakisphosphate. An overview over P standards and how they were classified is given in Table 2.2.2. A total of 43 samples were specifically chosen to cover gradients in three dimensions (climate, soil depth, and rhizosphere to bulk soil), and to be most representative for the respective site. Therefore, always the north– and south–facing mid–slope profiles from each site were analyzed.

To be able to combine the P contents in the different distances to roots the '*rhizosphere P per root length segment*' was calculated as total P content in a cylindrical shaped volume around roots with a length of 1 cm and an outer diameter of 8 mm. We assumed an average root thickness of 2 mm to calculate the volume of the cylinder, sheathing the roots, e.g., the cylinder volume in 0–2 mm root distance was calculated as the difference of a cylinder with a radius of 4 mm minus a cylinder with a radius of 2 mm, and so forth. The total P content (in mg P per kg soil) and the content in the P compound classes, respectively, were multiplied by the bulk density (derived from Bernhard et al. (2018a)) and multiplied by the volume of the cylinder in the respective root distance (0–2 mm = 0.38 cm^3, 2–4 mm = 0.63cm^3, 4–6 mm = 0.88 cm^3).

Statistical analyses

All statistical analyses were conducted using R Version 3.4.3 (R Core Team, 2017). Principal component analysis (PCA) was carried out by using the function *prcomp()* of the *'stats'* package of R. Data from all soil pits were included and were normalized to a mean of zero and a standard deviation of one. Linear models for LMWOAs and P speciation, respectively, at each depth, and with root distance as explaining variable, where calculated using the *lm()* function, as well of the package *'stats'*. The linear model was fitted separately for north– and south–facing slopes.

Differences in all three LMWOAs, MBC, Vmax, Km, and P speciation with depth and between sites at one depth were also tested by a linear model. Pairwise comparison between the sites or depths was done by the function *lsmeans()* of the *'lsmeans'* package (Lenth, 2016) with Tukey adjustment. The Redundancy analysis (RDA) was calculated by the *rda()* function of the package *'vegan'* (Oksanen et al., 2018). An RDA was calculated separately for each site and included samples from all soil pits and depths at each site. Explaining and explained variables were normalized to a mean of zero and standard deviation of one. For the RDA, any sample with a missing value in one of the explanatory variables was excluded from the analysis in the respective site. Data are presented in type II scaling, hence, angles between arrows can directly be interpreted in terms of correlation. The correlation between variables is expressed as the cosine (cos(α)) of the angle between the arrows of two variables. Except for the RDA plots (done by the *plot()* function of R) the package *'ggplot2'* was used to produce all graphical outputs of data (Wickham, 2016). Considering an ongoing debate about the meaning of *p* values and their interpretation, and our study design with highly variable parameters of natural ecosystems, the threshold for significance was set to $p < 0.1$ (Amrhein et al., 2019).

Table 2.2.2: Standards included in the Linear combination fitting (LCF) for P species characterization of phosphorus K–edge X–ray absorption near edge structure (XANES) spectra are given in the first column. Characterization of each standard in the second column. Abbreviations as used in the redundancy analysis (RDA) are written in the third column. Standards were grouped to P classes which are presented in column four.

P class	Standard[a]	Description	Abbreviation
calcium phosphates (Ca–P)	Hydroxyapatite[a]	Primary P mineral in the soils of this study.	HydAp
	Brushite[b]	Secondary Ca–phosphate.	BRU
	Octa–Ca–phosphate[b]	Secondary Ca–phosphate	OCP
Al phosphates (Al–P)	$AlPO_4$–amorphous[a]	Secondary Al phosphates with short range ordered crystal lattice.	sroAl–P
	Variscite[b]	Secondary Al phosphate.	VAR
orthophosphate sorbed to Al–(oxy)hydroxides (sorbAl–P)	Boehmite–PO_4[a]	Phosphate adsorbed to Boehmite.	adsP–BOE
	adsP–$AlOH_3$[b]	Phosphate adsorbed to Al–hydroxide.	adsP–AlOH
	adsP–Al–Montmorillonite[a]	Phosphate adsorbed to Al saturated clay.	adsP–Al_clay
	adsP–Al–SOM[a]	Phosphate adsorbed to soil organic matter.	adsP–SOM
Fe–phosphates (Fe–P)	FePO4–amorphous[a]	Secondary Fe phosphates with short range ordered crystal lattice.	sroFe–P
orthophosphate sorbed to Fe–(oxy)hydroxides (sorbFe–P)	adsP–Ferrihydrite[a]	Phosphate adsorbed to Ferrihydrite.	adsP–FER
	adsP–Goethite[b]	Phosphate adsorbed to Goethite.	adsP–GOE
organically bound P (P_o)	Inositol hexakisphosphate[a]	Organic P: the spectrum was obtained from inositolhexakisphosphate. Due to missing characteristics of organic P species in XANES spectra it was used in this study to represents organic P in general.	Po

a) (Prietzel et al. 2016a)
b) (Gustafsson et al. 2020)

2.2.4. Results

Two PCAs were calculated to identify the influence of P speciation alone and the influence of P speciation together with LMWOA contents on the variability within the dataset. The PCA for P speciation alone (Figure 2.2.2 A) explained on the first principal component axis 49.5% and on the second axis 17.2% of the total variance within P species. The humid–temperate forest and the arid shrubland samples were clearly separated along PC 1. In the Mediterranean woodland some topsoil samples forced the woodland polygon to overlap with the polygon comprising samples from the humid–temperate forest soil, whereas all subsoil and saprolite and some topsoil samples of the Mediterranean woodland ecosystem overlapped with the arid shrubland. When LMWOAs (oxalic, malic, citric) were included in the PCA (Figure 2.2.2 B) the clear separation of ecosystems along PC 1 was less expressed, but more variance was explained by PC 2, resulting in a more equally distributed explained variance among the two axes. PC 2 ordinated the samples from the humid–temperate forest and Mediterranean woodland by sampling depth, which was not discerned when only P species were used for the PCA. The latter PCA clearly indicated a systematic, presumably process–based, interaction between P–speciation and LMWOAs, since the separation was kept, and the explained variance was more evenly distributed between the first two principal components.

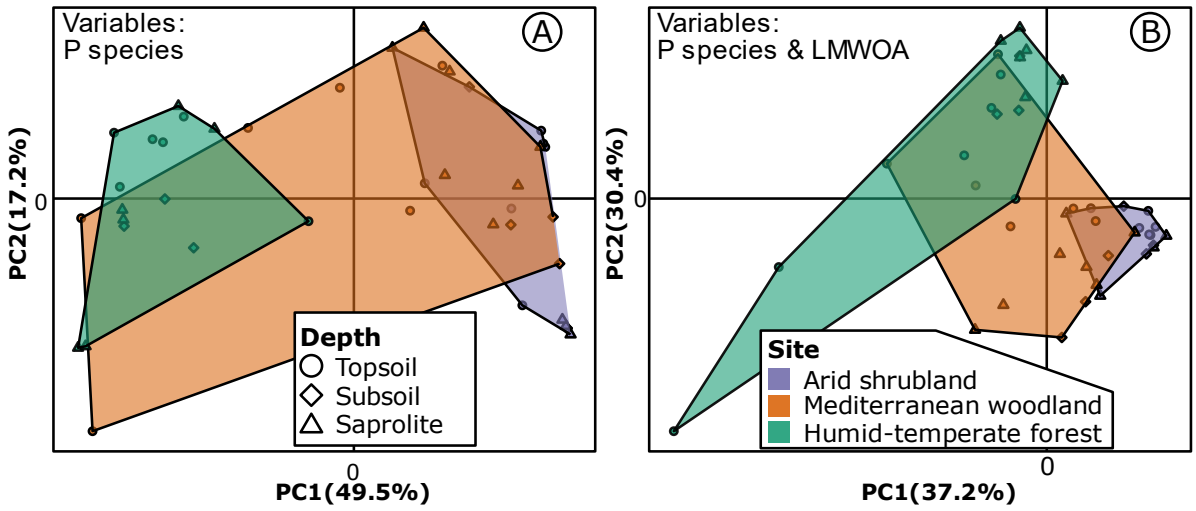

Figure 2.2.2: PCAs for (A) P species and (B) P species and low–molecular–weight organic acids (LMWOA) as variables. Sampling sites are indicated by color, arid shrubland in purple, Mediterranean woodland in orange and humid–temperate forest in turquoise. Marker type denotes the sampling depth: circles = topsoil, diamonds = subsoil, and saprolite = triangles.

Microbial biomass carbon and enzyme kinetics

MBC content (in µg MBC per g soil) in the topsoil increased with increasing precipitation along the ecosequence (Table: S 2.2.8, Table: S 2.2.12). Within the soil profile, MBC content decreased in all three sites with greater soil depth (Table: S 2.2.8). Furthermore, in all sites the MBC content was always significantly different when comparing the topsoil with the saprolite ($p<0.01$). In the

humid–temperate forest, the content of MBC was higher in root proximity compared to bulk soil (Table: S 2.2.8). Along the ecosequence, the maximum reaction rate of acid phosphatase (V_{max}, in nmol substrate g^{-1} soil h^{-1}) increased with increasing humidity (Table: S 2.2.8, after Stock et al., 2019). The V_{max} was lower in the topsoil and saprolite of the Mediterranean woodland and the topsoil of the Arid shrubland, compared to the humid–temperate forest.

LMWOA contents

Contents of oxalic, malic, and citric acid together accounted for more than 97% of all extracted LMWOAs. These acids also represent the most–efficient P dissolving di– and tricarboxylic acids in soils (Gerke et al., 2000). Therefore, we only present the results for these three acids (Figure 2.2.3 and Table: S 2.2.8). When comparing between sites, only malic acid contents in the topsoil were higher in the humid–temperate forest compared to the arid shrubland (Figure 2.2.3). No difference in terms of acid contents in the topsoil were found between the humid temperate forest and the Mediterranean woodland. Next, when assessing the differences with soil depth, the contents of malic and citric acid increased significantly from the topsoil to the saprolite in the arid shrubland soil. LMWOA contents in the Mediterranean woodland ecosystem were more uniformly distributed with soil profile depth (only malic acid increased significantly from the topsoil to the subsoil). Malic acid contents under humid–temperate forest strongly decreased from the topsoil to the saprolite. Finally, when comparing by root proximity we found higher citric acid content in root proximity compared to bulk soil in the topsoil at the south–facing slope of the Mediterranean woodland, and in the saprolite at the north–facing slope of the humid–temperate forest (Figure 2.2.3, red and blue arrows). Contents of malic acid were higher in root proximity (0–2 mm) than bulk soil in the subsoil of the south–facing slope under humid–temperate forest. Oxalic acid contents were higher in root proximity than bulk soil in the subsoil of the arid shrubland's south–facing profile. The same was true in all three depths at the south–facing slope in the Mediterranean woodland, and in the saprolite at the south–facing slope of the humid–temperate forest.

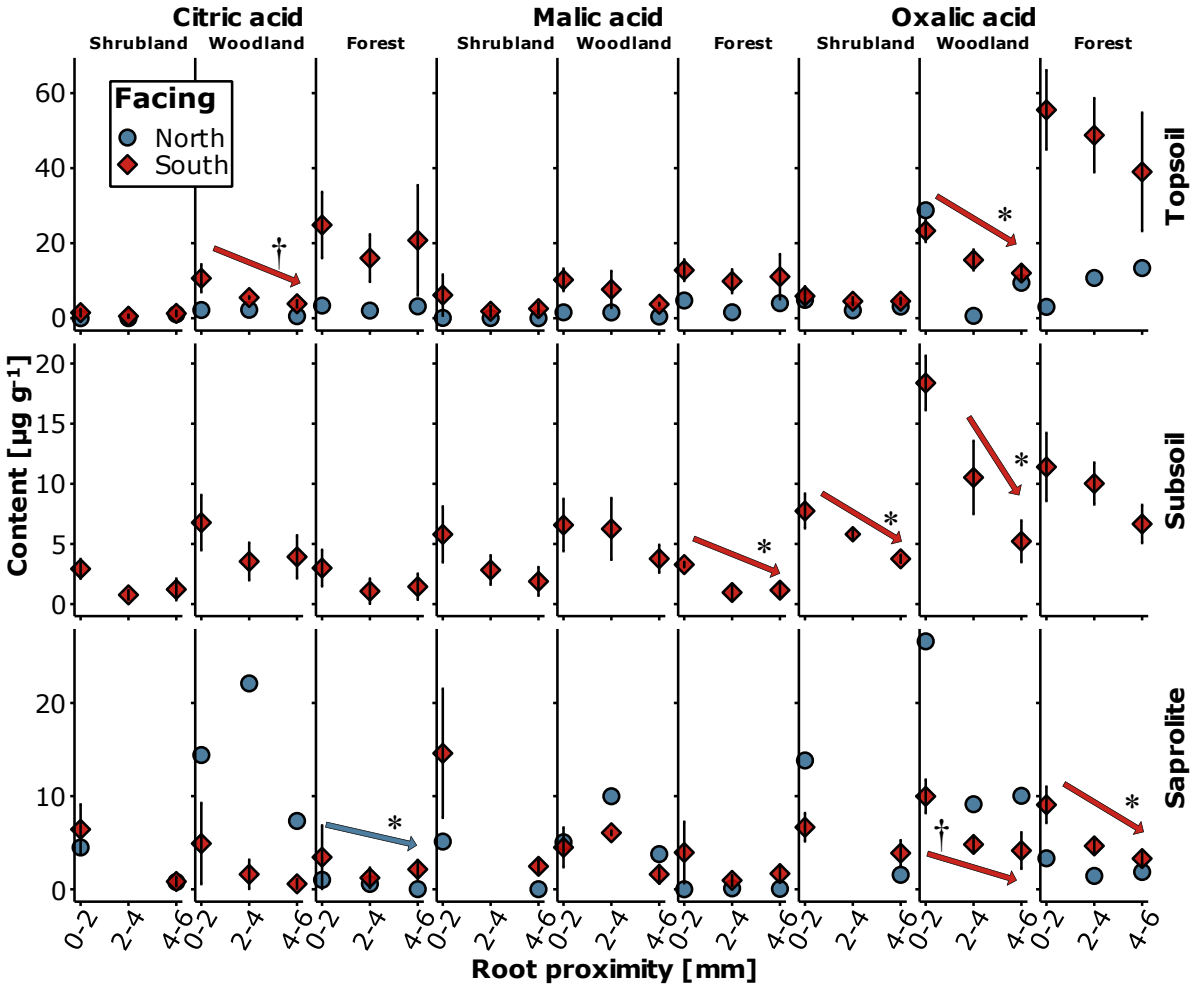

Figure 2.2.3: Content of low-molecular-weight organic acids (LMWOA) (citric-, malic- and oxalic acid) for north (blue circles) and south (red diamonds) facing slopes for all three sites (arid shrubland ('shrubland'), Mediterranean woodland ('woodland') and humid-temperate forest ('forest')) and three sampling depths (topsoil, subsoil and saprolite) separated by the three horizontal panels. Whiskers indicate the magnitude of the standard error from the mean. The x-axis shows root proximity (intervals of 2 mm from 0-2 mm, 2-4 mm, and 4-6 mm), y-axis plots the content of organic acids per gram soil dry weight. Sample size on the south facing slope is n=3, on the north facing slope single replicates are shown (n=1). Arrows indicate significant changes with distance to the roots, the color of the arrow was chosen according to the respective data row. Level of significance is indicated by asterisk ($p < 0.05$) and cross ($p < 0.1$).

P XANES K-edge measurements

When comparing between sites, Ca-P generally declined with increased precipitation, except for the saprolite of the Mediterranean woodland and the arid shrubland (Figure 2.2.4, Table 2.2.3). When focusing on the differences by soil depth, the Ca-P content increased from topsoil to subsoil and saprolite in the Mediterranean woodland. There was no difference in Ca-P content between the subsoil and the saprolite in the Mediterranean woodland and no effect of soil depth in the arid shrubland. In the humid-temperate forest Ca-P was only found in two samples in the saprolite. When assessing the differences with root proximity, the Ca-P content in the topsoil declined with increasing distance from the root at the north-facing slope of the arid shrubland (Figure 2.2.4, Table: S 2.2.7).

Fe–P and Al–P in the topsoil were higher in the arid shrubland than in the humid–temperate forest. In the saprolite Al–P was higher in both, the arid shrubland and Mediterranean woodland, compared to the humid–temperate forest (Figure 2.2.4, Table: S 2.2.7). P sorbed to Al–(oxy)hydroxides (sorbAl–P) was significantly higher in the humid–temperate forest than in the two other sites. In the topsoil at the south–facing slope of the humid–temperate forest the sorbAl–P contents increased with increasing distance from the root.

The P_o content in the topsoil was lower under arid shrubland than under Mediterranean woodland and humid–temperate forest. P_o decreased from topsoil to saprolite in the humid–temperate forest. In the topsoil at the south–facing slope of the Mediterranean woodland P_o was higher in the rhizosphere than bulk soil.

Rhizosphere P per root segment in soils decreased with increasing precipitation. Average values were: 440 µg cm^{-1}, 238 µg cm^{-1}, and 216 µg cm^{-1} in the topsoil, for the arid shrubland, Mediterranean woodland and humid–temperate forest, respectively. In the saprolite, the rhizosphere P per root segment was 418 µg cm^{-1} in the arid shrubland, 296 µg cm^{-1} in the Mediterranean woodland and 497 µg cm^{-1} in the humid–temperate forest.

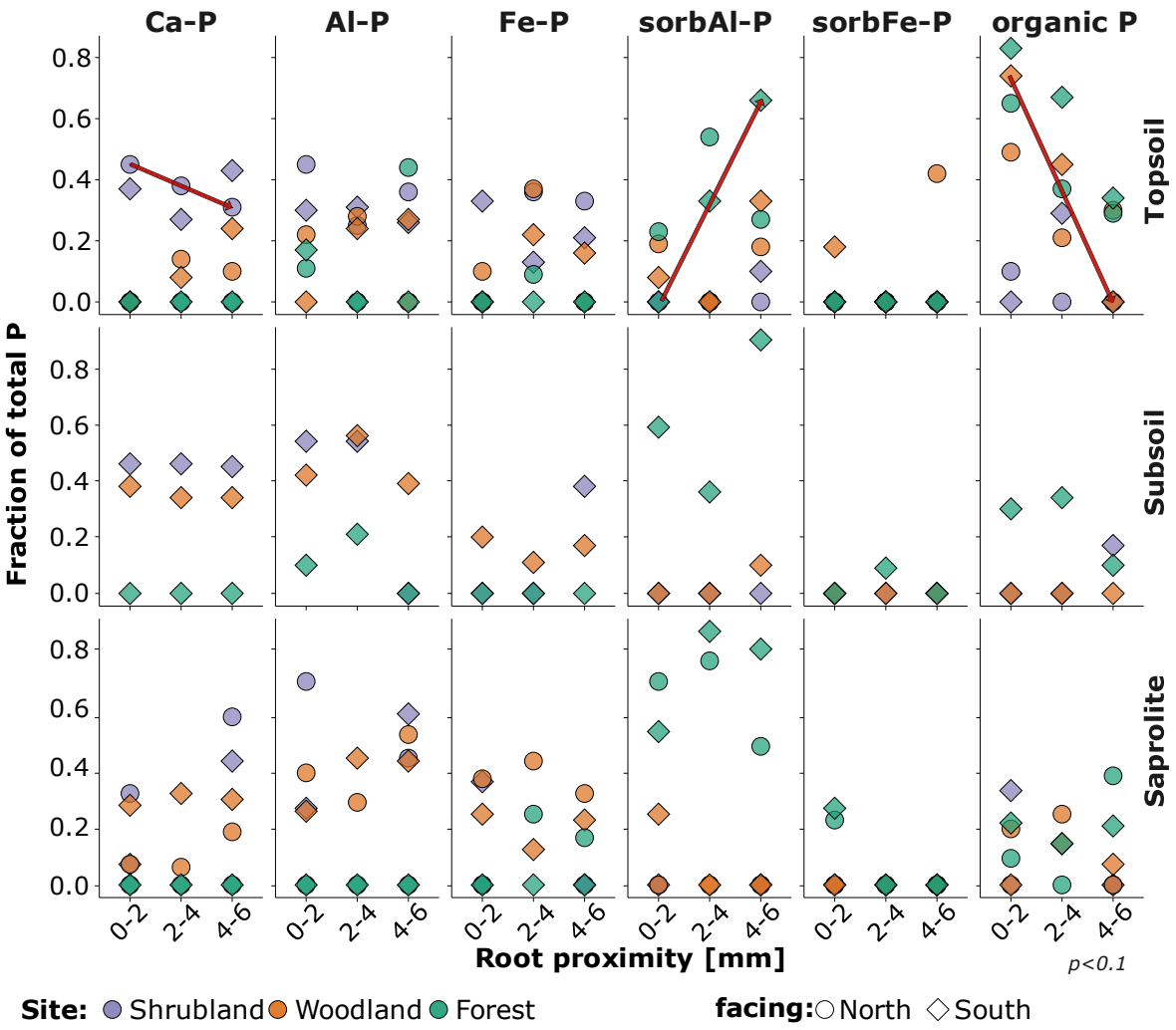

Figure 2.2.4: Contents of P compound classes from phosphorus K−edge X−ray absorption near edge structure (XANES) analysis: calcium phosphates(Ca−P), Al− and Fe phosphates (Al−P and Fe−P), orthophosphate sorbed to Al− and Fe−(oxy)hydroxides (sorbAl−P and sorbFe−P) and organic P, split by slope facing (circles = north facing; diamonds = south facing) and by site (arid shrubland ('shrubland') in purple, Mediterranean woodland ('woodland') in orange and humid−temperate forest ('forest') in turquoise. Samples from different depths are separated by the three horizontal panels (topsoil, subsoil and saprolite). The x−axis shows root proximity (0−2 mm, 2−4 mm, and 4−6 mm), the y−axis plots the fractions of the respective P class on total P. Red arrows indicate significant changes with root proximity ($p < 0.1$). The markers present individual replicates (n=1).

Relating P speciation to P mobilizing processes

Based on the outcomes of the PCA (Figure 2.2.2) and the expected site−specific relations between P speciation, LMWOAs, phosphatase kinetics (V_{max}, K_m), and MBC (Figure 2.2.3, Figure 2.2.4, and Table: S 2.2.8), a RDA was calculated for each of the sites separately (Figure 2.2.5). P species were taken as explanatory variables and LMWOAs, MBC, acid phosphatase activity (V_{max}), and acid phosphatase half saturation constant (K_m) as explained variables. The explanatory variables constrained 75%, 67%, and 80% of the variance for the arid shrubland, the Mediterranean woodland, and the humid−temperate forest, respectively.

In the arid shrubland, variscite and hydroxyapatite were highly correlated with LMWOA contents. Hydroxyapatite shows values of cos(α)=0.99, 0.98, 0.92 for oxalic, malic, and citric acid, respectively. Variscite correlation values (cos(α)) were 0.99, 1.00, 1.00, for oxalic, malic, and citric acid, respectively (Table: S 2.2.6). Variscite and hydroxyapatite together accounted for 61%, 66%, and 82% of total P content in the arid shrubland's topsoil, subsoil and saprolite, respectively. Biotic parameters V_{max}, K_m, and MBC were mainly independent of P speciation under arid shrubland.

In the Mediterranean woodland soils V_{max}, K_m, MBC, and oxalic acid showed the strongest positive correlation with P_o and P sorbed to goethite. The correlation parameter cos(α) was 0.92, 1.0, 0.96, 0.96, for Po and 0.59, 0.88, 0.97, 0.97 for P sorbed to goethite, each for MBC, V_{max}, K_m, and oxalic acid, respectively, (Table: S 2.2.6). P_o was mostly found in the topsoil and was absent in the subsoil at this site (Table: S 2.2.7). In the Mediterranean woodland subsoil and saprolite hydroxyapatite, variscite and short−range order Fe−P together made up at least 70% of total P in each root distance (Table: S 2.2.7). Malic and citric acid were highly to moderately correlated with variscite and short−range order Fe−P (cos(α)= 0.93, and 0.62 for variscite and 0.98, and 0.75 for short−range order Fe−P, each for malic− and citric acid, respectively; Figure 2.2.5 and Table: S 2.2.6).

The RDA for the humid−temperate forest soils revealed a strong (except for Km) positive correlation of all dependent variables with P_o (cos(α)= 0.96, 0.98, 0.96, 1.00, 0.98, 0.39, for oxalic−, malic−, citric acid, MBC, V_{max}, and K_m, respectively; Figure 2.2.5, Table: S 2.2.6). P_o represented on average 51% of the total P in the topsoil and 17% in the saprolite. LMWOAs, MBC, and V_{max} were strongly positively correlated with P_o. All explained variables showed moderate to strong negative correlations with all other P species in the humid−temperate forest ecosystem (Figure 2.2.5, Table: S 2.2.6, Table: S 2.2.7, and Table: S 2.2.8).

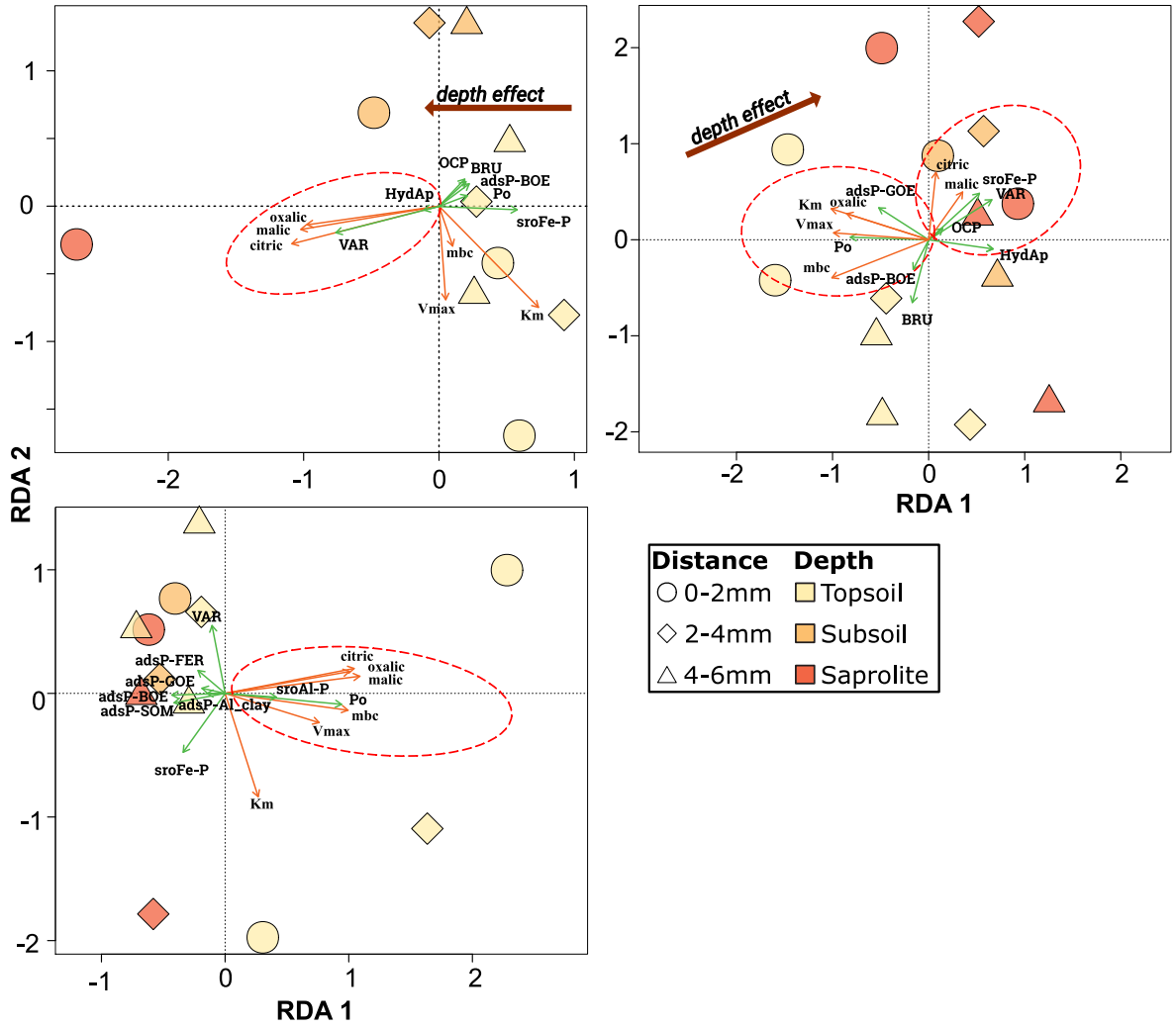

Figure 2.2.5: Triplots of the redundancy analysis (RDA) for the arid shrubland, Mediterranean woodland, and humid–temperate forest ecosystems. With P species as explanatory variables and microbial biomass carbon, low–molecular–weight organic acids, phosphatase activity and –affinity as explained variables. Green arrows indicate direction of the respective explaining variables, orange arrows of explained variables. The name of the respective variable is plotted at each arrowhead. Samples from all three sampling depths (topsoil = light yellow; subsoil = orange; saprolite = red) and root proximities (intervals of 2 mm: 0–2 mm = circles, 2–4 mm = diamonds and 4–6 mm = triangles) were included in the RDA. Red dotted ellipsoids were included to guide the reader to the main messages of the respective figure, which are discussed in the text. The bold arrows in the subfigure of the arid shrubland and the Mediterranean woodland ecosystem point out the effect of soil depth on the outcome of the RDA. The sample size for each RDA was 10, 14, and 12 for the arid shrubland, Mediterranean woodland, and humid–temperate forest ecosystems, respectively.

Table 2.2.3: Six P pools as a sum of single standards from linear combination fitting (LCF) are shown. Values from the LCF are given in percent of total P (Ca–P = calcium phosphates, Al–P = Al–phosphates, sorb Al–P = orthophosphate sorbed to Al–(oxy)hydroxides, Fe–P = Fe–phosphates, sorb Fe–P = orthophosphates sorbed to Fe–(oxy)hydroxides, Po = organically bound P). The LCF was restricted to a maximum of four standards per sample. If a P pools was not detected in a sample this is indicated by 'n.d.' (not determined). Absolute values of P species were calculated by multiplying the share of a P pool with total P (P_{tot}) (Ca–P_{abs} = calcium phosphates, Al–P_{abs} = Al–phosphates, sorb Al–P_{abs} = orthophosphate sorbed to Al–(oxy)hydroxides, Fe–P_{abs} = Fe–phosphates, sorb Fe–P_{abs} = orthophosphates sorbed to Fe–(oxy)hydroxides, Po_{abs} = organically bound P). Rhizosphere P per root segment was calculated as total P content in a cylinder around root with a length of 1 cm and a radius of 6 mm, the inner diameter was set to 2 mm (average root thickness (Ca–PRP = calcium phosphates, Al–PRP = Al–phosphates, sorb Al–PRP = orthophosphate sorbed to Al–(oxy)hydroxides, Fe–PRP = Fe–phosphates, sorb Fe–PRP = orthophosphates sorbed to Fe–(oxy)hydroxides, Po_{RP} = organically bound P).

Site	Facing	Depth	Root proximity	Ca–P	Fe–P	Al–P	sorb Fe–P	sorb Al–P	P_o	P_{tot}	$Ca–P_{abs}$	$Fe–P_{abs}$	$Al–P_{abs}$	$sorbFe–P_{abs}$	$sorbAl–P_{abs}$	Po_{abs}	P_{totRP}	$Ca–P_{RP}$	$Fe–P_{RP}$	$Al–P_{RP}$	$sorbFe–P_{RP}$	$sorbAl–P_{RP}$	Po_{RP}
			[mm]	(%)	(%)	(%)	(%)	(%)	(%)	[mg kg^{-1}]	[mg kg^{-1}]	[mg kg^{-1}]	[mg kg^{-1}]	[mg kg^{-1}]	[mg kg^{-1}]	[mg kg^{-1}]	[µg cm^{-1}]	[µg cm^{-1}]	[µg cm^{-1}]	[µg cm^{-1}]	[µg cm^{-1}]	[µg cm^{-1}]	[µg cm^{-1}]
Arid shrubland	South	Topsoil	0–2	37	33	30	*n.d.*	*n.d.*	*n.d.*	304.5	112.7	100.5	91.4	*n.d.*	*n.d.*	*n.d.*							
			2–4	27	13	31	*n.d.*	*n.d.*	29	295.8	79.9	38.5	91.7	*n.d.*	*n.d.*	85.8	910.6	335.6	189.6	258.0	*n.d.*	45.1	82.4
			4–6	43	21	26	*n.d.*	10	*n.d.*	335.7	144.3	70.5	87.3	*n.d.*	33.6	*n.d.*							
		Subsoil	0–2	46	*n.d.*	54	*n.d.*	*n.d.*	*n.d.*	359.3	165.3	*n.d.*	194.0	*n.d.*	*n.d.*	*n.d.*							
			2–4	46	*n.d.*	54	*n.d.*	*n.d.*	*n.d.*	363.4	167.2	*n.d.*	196.2	*n.d.*	*n.d.*	*n.d.*	869.8	396.6	131.5	282.9	*n.d.*	*n.d.*	58.8
			4–6	45	38	*n.d.*	*n.d.*	*n.d.*	17	273.2	122.9	103.8	*n.d.*	*n.d.*	*n.d.*	46.4							
		Saprolite	0–2	7	35	26	*n.d.*	*n.d.*	32	308.6	21.6	108.0	80.2	*n.d.*	*n.d.*	98.8							
			4–6	42	*n.d.*	58	*n.d.*	*n.d.*	*n.d.*	293.1	123.1	*n.d.*	170.0	*n.d.*	*n.d.*	*n.d.*	536.9	167.1	58.4	258.0	*n.d.*	*n.d.*	53.4
	North	Topsoil	0–2	45	*n.d.*	45	*n.d.*	*n.d.*	10	293.9	132.3	*n.d.*	132.3	*n.d.*	*n.d.*	29.4							
			2–4	38	36	25	*n.d.*	*n.d.*	*n.d.*	419.7	159.5	151.1	104.9	*n.d.*	*n.d.*	*n.d.*	1156.7	412.4	336.3	386.3	*n.d.*	*n.d.*	17.5
			4–6	31	33	36	*n.d.*	*n.d.*	*n.d.*	404.6	125.4	133.5	145.7	*n.d.*	*n.d.*	*n.d.*							
		Saprolite	0–2	31	*n.d.*	69	*n.d.*	*n.d.*	*n.d.*	439.6	136.3	*n.d.*	303.3	*n.d.*	*n.d.*	*n.d.*							
			4–6	57	*n.d.*	43	*n.d.*	*n.d.*	*n.d.*	336.3	191.7	*n.d.*	144.6	*n.d.*	*n.d.*	*n.d.*	766.0	365.1	n.d.	400.9	*n.d.*	*n.d.*	n.d.
Mediterranean woodland	South	Topsoil	0–2	*n.d.*	*n.d.*	*n.d.*	18	8	74	297.7	*n.d.*	*n.d.*	*n.d.*	53.6	23.8	220.3							
			2–4	8	22	24	*n.d.*	*n.d.*	45	160.6	12.8	35.3	38.5	*n.d.*	*n.d.*	72.3	319.7	34.9	39.6	54.0	19.6	46.0	124.6
			4–6	24	16	27	*n.d.*	33	*n.d.*	132.4	31.8	21.2	35.7	*n.d.*	43.7	*n.d.*							
		Subsoil	0–2	38	20	42	*n.d.*	*n.d.*	*n.d.*	339.9	129.2	68.0	142.7	*n.d.*	*n.d.*	*n.d.*							
			2–4	34	11	56	*n.d.*	*n.d.*	*n.d.*	262.0	89.1	28.8	146.7	*n.d.*	*n.d.*	*n.d.*	780.1	272.6	123.9	350.2	*n.d.*	35.8	*n.d.*
			4–6	34	17	39	*n.d.*	10	*n.d.*	281.6	95.8	47.9	109.8	*n.d.*	28.2	*n.d.*							
		Saprolite	0–2	27	24	25	*n.d.*	24	*n.d.*	197.3	53.3	47.4	49.3	*n.d.*	47.4	*n.d.*	821.5	240.1	162.4	328.2	*n.d.*	26.7	64.1

		2–4	31	12	43	*n.d.*	*n.d.*	14	218.9	67.9	26.3	94.1	*n.d.*	*n.d.*	30.6								
		4–6	29	22	42	*n.d.*	*n.d.*	7	383.9	111.3	84.5	161.3	*n.d.*	*n.d.*	26.9								
		0–2	*n.d.*	10	22	*n.d.*	19	49	282.3	*n.d.*	28.2	62.1	*n.d.*	53.6	138.3								
	Topsoil	2–4	14	37	28	*n.d.*	*n.d.*	21	288.5	40.4	106.7	80.8	*n.d.*	*n.d.*	60.6	819.0	76.9	115.2	109.9	164.9	100.6	251.5	
North		4–6	10	*n.d.*	*n.d.*	42	18	30	301.1	30.1	*n.d.*	*n.d.*	126.4	54.2	90.3								
		0–2	7	36	38	*n.d.*	*n.d.*	19	241.4	16.9	86.9	91.7	*n.d.*	*n.d.*	45.9								
	Saprolite	2–4	6	42	28	*n.d.*	*n.d.*	24	191.2	11.5	80.3	53.5	*n.d.*	*n.d.*	45.9	555.5	65.4	197.4	227.4	*n.d.*	n.d.	65.3	
		4–6	18	31	51	*n.d.*	*n.d.*	*n.d.*	205.7	37.0	63.8	104.9	*n.d.*	*n.d.*	*n.d.*								
		0–2	*n.d.*	*n.d.*	17	*n.d.*	*n.d.*	83	350.5	*n.d.*	*n.d*	59.6	*n.d.*	*n.d.*	290.9								
	Topsoil	2–4	*n.d.*	*n.d.*	*n.d.*	*n.d.*	*n.d.*	67	249.6	*n.d.*	*n.d.*	*n.d.*	*n.d.*	82.4	167.2	342.8	*n.d.*	*n.d.*	18.5	*n.d.*	112.1	212.3	
		4–6	*n.d.*	*n.d.*	*n.d.*	*n.d.*	*n.d.*	34	145.8	*n.d.*	*n.d.*	*n.d.*	*n.d.*	96.2	49.6								
		0–2	*n.d.*	*n.d.*	10	*n.d.*	59	30	505.7	*n.d.*	*n.d.*	50.6	*n.d.*	298.4	151.7								
South	Subsoil	2–4	*n.d.*	*n.d.*	21	9	36	34	353.7	*n.d.*	*n.d.*	74.3	31.8	127.3	120.3	590.9	*n.d.*	*n.d.*	64.1	19.5	357.2	148.2	
		4–6	*n.d.*	*n.d.*	*n.d.*	*n.d.*	90	10	219.9	*n.d.*	*n.d.*	*n.d.*	*n.d.*	197.9	22.0								
		0–2	*n.d.*	*n.d.*	*n.d.*	26	52	21	281.9	*n.d.*	*n.d.*	*n.d*	73.3	146.6	59.2								
	Saprolite	2–4	*n.d.*	*n.d.*	*n.d.*	*n.d.*	86	14	290.6	*n.d.*	*n.d.*	*n.d.*	*n.d.*	249.9	40.7	475.8	*n.d.*	*n.d.*	*n.d.*	24.0	364.3	86.6	
		4–6	*n.d.*	*n.d.*	*n.d.*	*n.d.*	80	20	294.8	*n.d.*	*n.d.*	*n.d.*	*n.d.*	235.9	59.0								
		0–2	*n.d.*	*n.d.*	11	*n.d.*	23	65	620.4	*n.d.*	*n.d.*	68.2	*n.d.*	142.7	403.3								
	Topsoil	2–4	*n.d.*	*n.d.*	*n.d.*	*n.d.*	54	37	385.7	*n.d.*	34.7	*n.d.*	*n.d.*	208.3	142.7	719.9	*n.d.*	20.8	141.6	*n.d.*	247.8	307.5	
		4–6	*n.d.*	*n.d.*	44	*n.d.*	27	29	317.7	*n.d.*	*n.d.*	139.8	*n.d.*	85.8	92.1								
North		0–2	*n.d.*	*n.d.*	*n.d.*	22	69	9	349.9	*n.d.*	*n.d.*	*n.d.*	77.0	241.5	31.5								
	Saprolite	2–4	*n.d.*	24	*n.d.*	*n.d.*	76	*n.d.*	829.4	*n.d.*	199.1	*n.d.*	*n.d.*	630.3	*n.d.*	1816.4	*n.d.*	316.1	*n.d.*	35.9	1076.6	387.8	
		4–6	*n.d*	16	*n.d.*	*n.d.*	47	37	926.4	*n.d.*	148.2	*n.d.*	*n.d.*	435.4	342.8								

Humid-temperate rainforest

2.2.5. Discussion

Mature ecosystems are characterized by well–established nutrient cycles, i.e. each atom of a certain nutrient is used by the vegetation multiple times, thereby passing through various nutrient pools (Chadwick et al., 1999; Lang et al., 2017). As the focus of this study was on plant P acquisition and recycling strategies along an ecosequence, we first explored specifics and common features of P speciation and LMWOAs in the soils of the study sites, i.e. the arid shrubland, the Mediterranean woodland, and the humid–temperate forest ecosystem, by performing a PCA (Figure 2.2.2). The PCA confirmed a clear separation of the soils from the most arid and most humid ecosystems in terms of P speciation. If LMWOA contents were included, the separation of the humid–temperate forest and the Mediterranean woodland ecosystems improved. The samples were ordered by soil depth along PC 2. The overall variance accounted for by the PCA remained constant but was more evenly distributed among the two axes. Thus, we conclude that LMWOAs display an ecosystem specific interaction with P speciation, which points toward a systematic dependency of LMWOAs on P minerals in the respective ecosystems. Along the ecosequence (arid to humid), the vegetation–community changes from shrub to tree dominated, at the same time the belowground carbon allocation and leaf area index increase (Bernhard et al., 2018). The PCA (including both P speciation and LMWOAs) clearly separated top– from subsoils in the humid–temperate forest and the Mediterranean woodland, indicating that P mobilization mechanisms are different in the various soil layers. Although it is likely that all plants possess the ability to exudate LMWOAs, it can be speculated that soil regions with low P availability provide an ecological niche for species with an exceptionally high ability to exudate LMWOAs.

The arid shrubland ecosystem

The most important finding for the arid ecosystem is the strong dependence of LMWOA contents on hydroxyapatite and variscite in the subsoil and saprolite. This suggests a mechanistic relation between primary P (hydroxyapatite), which is still available in high amounts, secondary Al–P, and LMWOAs of biotic origin (Figure 2.2.5). Therefore, the arid shrubland is considered to be a rock eating ecosystem. Contents of LMWOAs always increased in root proximity, except for citric acid in the topsoils of the arid shrubland (Figure 2.2.3). This results from the fact that roots exude these acids, which is in accordance with many other studies (e.g. Cieśliński et al., 1998; Hinsinger, 2001; Szmigielska et al., 1996). However, biotic activity in these soils is rather low, which can be explained by the low vegetation cover (30–40%) (Table 2.2.1) (Bernhard et al., 2018b) leading to low microbial biomass in the soils of the arid ecosystem (Table: S 2.2.8).

Ecosystems with low and seasonally variable water availability are characterized by vegetation that produces nutrient–poor litter which is resistant to decomposition (Becker and Kuzyakov, 2018; Makkonen et al., 2012). As expected, the pool of organically bound P in these soils was small (Figure 2.2.4). Abiotic processes involved in the dissolution of P minerals are strongly influenced by the availability of water and, thus, limited under arid shrubland (Maher, 2010). However, the high hydroxyapatite (Table: S 2.2.7) contents in the arid shrubland ecosystem compared to the two other sites indicates that not only net primary productivity and vegetation cover, but also overall weathering is generally low. Additionally, enzymatic activity (Stock et al., 2019) and MBC are also low, suggesting that all biotic processes occur at a low rate. Biota–driven mineral dissolution processes include the exudation of organic anions and the release of protons (Banfield et al., 1999; Drever and Stillings, 1997; Neaman et al., 2006; Plassard et al., 2011), but only occur in root proximity, where plants can partially control the microenvironmental conditions, e.g. by maintaining a moist soil via mucilage exudation (Carminati and Vetterlein, 2013; Kroener et al., 2018). Therefore, it is likely that plants growing under such conditions have to acquire most of their mineral nutrients, through biochemical weathering, from the subsoil and saprolite where P minerals are still abundant.

In contrast to the subsoil and saprolite, the RDA does not resolve which processes are involved in the topsoil at this site. Despite of low enzymatic activities it cannot be excluded that organic P plays a certain role in the topsoil. Low contents of organic P could also be an indication for strong utilization, i.e., rapid turnover, or mineralization of these compounds.

Humid–temperate forest ecosystem

In this site, the weathering of granodioritic parent material is most advanced compared to the two northern ecosystems. This is reflected by the absence of hydroxyapatite and other Ca–phosphates in the top– and subsoil of the humid–temperate forest (Figure 2.2.4 & Table: S 2.2.7). Brucker and Spohn (2019), who investigated the same ecosequence, reported lowest apatite contents, and highest contents of secondary P minerals in the soils of the humid–temperate forest. Rhizosphere P per root segment was lowest in the top– and subsoils of this ecosystem (Figure: S 2.2.2) compared to the two northern ecosystems. This demonstrates the general pattern of decreasing P contents with increasing precipitation and, thus, soil development (Hou et al., 2018; Turner et al., 2018; Walker and Syers, 1976). This interpretation is supported by the fact that the rhizosphere P per root segment in the saprolite of the humid–temperate forest is highest among the three ecosystems, suggesting that this depletion is not due to a lower P content in the parent material, but indeed results from the processes that take place during ecosystem and soil development.

As shown by Stock et al. (2019), phosphatase kinetics indicate the highest relevance of breakdown of organic compounds (recycling) for P nutrition in the humid–temperate forest compared to the two other ecosystems. The RDA supports these previous results and, most importantly, implies that LMWOAs in the humid–temperate forest serve to support plant P_o mobilization, therefore we classify the humid temperate forest as a vegetarian ecosystem. Thus, the function of LMWOAs is, in contrast to the arid shrubland, neither the weathering nor the mobilization of hydroxyapatite or variscite (Figure 2.2.5). Alternatively, increased P_o in root proximity of this ecosystem's topsoil reflects the accumulation of P_o around roots, likely from a thriving microbial community (Figure 2.2.3 for P_o and Table: S 2.2.8 for MBC contents), induced by high root exudation rates. Therefore, it is reasonable to assume that more frequent recycling occurs within the topsoil of the humid–temperate forests. However, even if a tight P cycle is established, there will still be leaching and erosional losses that have to be replenished by P acquisition from mineral sources (Uhlig et al., 2017).

P losses due to leaching affect not only inorganic P in the soil solution, but also dissolved inorganic and organic P species. This results from the increase in the breaking up of organic P and the leaching of dissolved inorganic P and particulate organic or inorganic P species transported in the soil pore system after heavy rainfall (Bol et al., 2016). Finer grain sizes in the humid–temperate forest compared to the two other sites (Bernhard et al., 2018b) are a factor that may contribute to reduced P losses e.g. by leaching or particulate transport (Hou et al., 2018; Sims et al., 1998). This is because they have a higher specific surface area, which provides sorption sites for P in the soil. Moreover, from P adsorption experiments (data not shown) it is clear that P availability in this site is lowest along the ecosequence. On the other hand, MAP is more than three times higher compared to the Mediterranean woodland. MAP is a strong driver of abiotic P weathering and is negatively correlated with primary P and plant available P. This is also shown for primary P in this study and for plant available P in Bernhard et al. (2018a). On the contrary, increased MAP enhances primary production and thus the C availability in soils, which is positively correlated with organic P accumulation.

Higher C availability results in microbial growth and P uptake and consequently organic P accumulation in soils and enhanced P flux through the soil solution. In general soil pH is negatively correlated with the solubility of Ca–phosphates and the degradation of organic P, whereas it is positively correlated with the formation of secondary P minerals (Hou et al., 2018). The positive effect on secondary P minerals originates from decreasing solubility of Fe and Al with decreasing pH. In this study, the pH in topsoils dropped from 6.4 in the arid shrubland to 5.5 in the Mediterranean woodland and 4.3 in the humid–temperate forest (Table 2.2.1). P

sorbed to Al–(oxy)hydroxides was in all three sampling depths lower in the arid shrubland or the Mediterranean woodland compared to the humid–temperate forest (Figure 2.2.4, Table 2.2.3 (for absolute values), Table: S 2.2.14 for p values). Consequently, it seems that a high flux of P through the soil solution, due to elevated C availability and related biological activity, in concert with stabilizing conditions for Al and Fe–(oxy)hydroxides, caused by a low pH, enhances P sorption to Al–(oxy)hydroxides. Because rhizosphere P per root segment in the topsoil of the humid–temperate forest is low, it seems likely that the elevated P flux in combination with high water availability in soil also causes high P leaching losses despite a high sorption capacity.

As indicated by lower plant available P in the humid–temperate forest compared to the two other sites (Bernhard et al., 2018a) the sorption seems to be rather strong and only a small proportion of the sorbed P can be expected to contribute to plant nutrition under these circumstances. A strategy to overcome P limitation due to leaching losses is biological uplift (Gao et al., 2019). As implied by the RDA (Figure 2.2.5) in the humid–temperate forest, primary P acquisition happens in the deep subsoil and saprolite. This interpretation is supported by the fact that LMWOA contents per MBC ratios (Table: S 2.2.8) increased with soil depth (this was true in all ecosystems), pointing towards an intended higher exudation of acids deeper in the soil profile to gain access to this P source (Table S8).

Mediterranean woodland ecosystem

The vegetation in the Mediterranean woodland ecosystems is generally adapted to seasonal rainfall and longer droughts (Amigo Vázquez and Flores Toro, 2013; Nardini et al., 2014). Plants reduce water loss through transpiration during these dry and mostly hot periods by producing sclerophyllous leaves (Nardini et al., 2014). Litterfall is higher than in the arid shrubland, leaving a bigger pool of organically bound nutrients to be cycled within the Mediterranean woodland ecosystem (Figure 2.2.3). The PCA results support the theoretical assumption that this ecosystem is in an intermediate state between the two endmembers of the studied ecosequence (Figure 2.2.2), which were discussed in the previous paragraphs. This theory is verified by the RDA, which identifies recycling of P in the topsoil and biochemical weathering of secondary P minerals in the subsoil (Figure 2.2.5). The RDA also provides indications about several underlying processes. Phosphatase kinetics (V_{max}, K_m), MBC, oxalic acid (explained variables), and P_o (explaining variable) have high values in samples from topsoil and root proximity. The clear correlation between P_o and the explained variables V_{max}, K_m, MBC, and oxalic acid verifies that P recycling is the main process in the topsoil, and it is driven by roots. Surprisingly, in contradiction to Wei et al. (2010), it also implies that oxalic acid in the topsoil of this ecosystem is involved in the recycling of organic P. In contrast, biochemical weathering of

short–range order Fe–P (sroFe–P) and variscite (VAR) in the subsoil and saprolite is mediated by malic and citric acid as biotic drivers (Figure 2.2.5, inferred from the strong correlation between these variables). We found a weak correlation, however, of malic and citric acid with hydroxyapatite, which all showed high contents in samples from the subsoil and saprolite in the Mediterranean woodland. It is, therefore, reasonable to assume that biochemical weathering also contributes to mineral dissolution in this ecosystem. Hence, P dynamics in this ecosystem might be controlled by biological uplift of P (Bullen and Chadwick, 2015; Gao et al., 2019) from subsoil horizons and recycling of these nutrients, once they entered the biological cycle. It has been shown that deep–rooting plants can act as nutrient pumps, that lift up nutrients from the subsoil, subsequently accumulating in the topsoil as organically bound nutrients, after they have undergone transformation within plants (Bullen and Chadwick, 2015; Gao et al., 2019; Wu et al., 2019). Nutrient uplift is driven by plants demand and mediated via roots.

Soil erosion rates in the Mediterranean woodland were highest among all sites (Schaller et al., 2018; van Dongen et al., 2019), which leads to a rapid removal of the upper soil layer. This may explain why intense recycling only occurs in the upper soil layer. This is because with high erosion only a shallow soil horizon with organic P accumulation remains. However, it is unclear to what extend P is lost from the system by erosion and runoff, but they are most likely not identical between the two investigated slopes (north– and south–facing). At the north–facing slope, total rhizosphere P per root segment decreased with depth (819 µg cm^{-1} in the topsoil and 556 µg cm^{-1} in the saprolite), whereas at the south–facing slope it increased from 320 µg cm^{-1} in the topsoil to 822 µg cm^{-1} in the saprolite (Table 2.2.3). The higher content of sand at the south–facing soil (>70%), combined with a MAP of about 370 mm yr^{-1} (Table 2.2.1) likely facilitates the leaching and erosion of plant available P from the soil on the south–facing slope. Hou et al. (2018) have shown that coarse grain sizes and high MAP are key factors determining P losses.

2.2.6. Conclusions

This study elucidates plant strategies for phosphorus nutrition across ecosystems and shows that balance between phosphorus acquisition and cycling along the investigated ecosequence strongly depend on climate. It contributes to resolve plant strategies of phosphorus nutrition under natural conditions.

Low–molecular–weight organic acids (LMWOAs) exuded by roots induce not only biochemical weathering of phosphate minerals, but also support organic phosphorus mobilization. The functions of LMWOAs change with increasing precipitation. Under arid shrubland oxalic, malic, and citric acid support the dissolution of phosphorus minerals, whereas under Mediterranean

woodland malic and citric acid accelerate biochemical weathering in the subsoil and oxalic acid mobilizes organic phosphorus in the topsoil. All LMWOAs support the mobilization of organic phosphorus in the topsoil under humid–temperate forest. Consequently, phosphorus acquisition strategy shifts across biomes from mineral weathering to recycling of organic phosphorus corresponding to increasing precipitation from 70 mm yr^{-1} to 1470 mm yr^{-1}. In the soils under arid shrubland, phosphorus acquisition is actively driven by biochemical weathering of parent material (rock eating ecosystem). In the soils under humid–temperate forest, however, there was no direct evidence for biochemical weathering but intensive phosphorus recycling (vegetarian ecosystem). Phosphorus losses in the Mediterranean woodland are likely to be very high and the demand for it creates an incentive for a strong phosphorus supply through (biological) weathering in the subsoil, while at the same time organic phosphorus in the topsoil is recycled.

2.2.7. Acknowledgement

We thank the Chilean National Park Service Corporación Nacional Forestal (CONAF) for granting permission to work in the National parks Nahuelbuta and La Campana. We also thank the Center for Advanced Research in Arid Zones (CEAZA) for the opportunity to work in the Nacional Reserve Santa Gracia. We express gratitude to the team of Beamline 8 at the Synchrotron Light Research Institute Nakhon Ratchasima. Without their help in setting up the beamline we would not have been able to produce high quality spectra. We thank the Robert Bosch Foundation for supporting this research within the framework of the junior professorship in 2017. Last but not least we thank Karin Schmidt for her help with laboratory analysis.

2.2.8. Funding

This study was funded by the German Research Foundation (DFG) within the frame of the priority program 1803, EarthShape: Earth surface shaping by biota (DFG SPP 1803; project number 255469939) under the subprojects KU 1184/36–1 and DI 2136–11

2.2.9. Conflict of interest

The authors have no conflict of interest to declare, the research was conducted in the absence of any commercial or financial relationships that could be construed as a potential conflict of interest.

2.2.10. References

Amigo Vázquez, F.J., Flores Toro, L., 2013. A new contribution to the syntaxonomy of the sclerophyllous forests and pre–forests of Central Chile: the Lithraeion causticae alliance. International Journal of Geobotanical Research 3 (1), 47–67.

Amrhein, V., Greenland, S., McShane, B., 2019. Scientists rise up against statistical significance. Nature 567 (7748), 305–307.

Anderson, T.-H., Martens, R., 2013. DNA determinations during growth of soil microbial biomasses. Soil Biology and Biochemistry 57, 487–495.

Banfield, J.F., Barker, W.W., Welch, S.A., Taunton, A., 1999. Biological impact on mineral dissolution: application of the lichen model to understanding mineral weathering in the rhizosphere. Proceedings of the National Academy of Sciences 96 (7), 3404–3411.

Becker, J.N., Kuzyakov, Y., 2018. Teatime on Mount Kilimanjaro: Assessing climate and land-use effects on litter decomposition and stabilization using the Tea Bag Index. Land Degrad Dev 29 (8), 2321–2329.

Bernhard, N., Moskwa, L.-M., Schmidt, K., Oeser, R.A., Aburto, F., Bader, M.Y., Baumann, K., Blanckenburg, F. von, Boy, J., van den Brink, L., Brucker, E., Büdel, B., Canessa, R., Dippold, M.A., Ehlers, T.A., Fuentes, J.P., Godoy, R., Jung, P., Karsten, U., Köster, M., Kuzyakov, Y., Leinweber, P., Neidhardt, H., Matus, F., Mueller, C.W., Oelmann, Y., Oses, R., Osses, P., Paulino, L., Samolov, E., Schaller, M., Schmid, M., Spielvogel, S., Spohn, M., Stock, S., Stroncik, N., Tielbörger, K., Übernickel, K., Scholten, T., Seguel, O., Wagner, D., Kühn, P., 2018a. Data supplement to "Pedogenic and microbial interrelations to regional climate and local topography: New insights from a climate gradient (arid to humid) along the Coastal Cordillera of Chile".

Bernhard, N., Moskwa, L.-M., Schmidt, K., Oeser, R.A., Aburto, F., Bader, M.Y., Baumann, K., Blanckenburg, F. von, Boy, J., van den Brink, L., Brucker, E., Büdel, B., Canessa, R., Dippold, M.A., Ehlers, T.A., Fuentes, J.P., Godoy, R., Jung, P., Karsten, U., Köster, M., Kuzyakov, Y., Leinweber, P., Neidhardt, H., Matus, F., Mueller, C.W., Oelmann, Y., Oses, R., Osses, P., Paulino, L., Samolov, E., Schaller, M., Schmid, M., Spielvogel, S., Spohn, M., Stock, S., Stroncik, N., Tielbörger, K., Übernickel, K., Scholten, T., Seguel, O., Wagner, D., Kühn, P., 2018b. Pedogenic and microbial interrelations to regional climate and local topography: New insights from a climate gradient (arid to humid) along the Coastal Cordillera of Chile. CATENA 170, 335–355.

Bol, R., Julich, D., Brödlin, D., Siemens, J., Kaiser, K., Dippold, M.A., Spielvogel, S., Zilla, T., Mewes, D., Blanckenburg, F. von, Puhlmann, H., Holzmann, S., Weiler, M., Amelung, W., Lang, F., Kuzyakov, Y., Feger, K.-H., Gottselig, N., Klumpp, E., Missong, A., Winkelmann, C., Uhlig, D., Sohrt, J., Wilpert, K. von, Wu, B., Hagedorn, F., 2016. Dissolved and colloidal phosphorus fluxes in forest ecosystems–an almost blind spot in ecosystem research. J. Plant Nutr. Soil Sci. 179 (4), 425–438.

Brucker, E., Spohn, M., 2019. Formation of soil phosphorus fractions along a climate and vegetation gradient in the Coastal Cordillera of Chile. CATENA 180, 203–211.

Bullen, T., Chadwick, O., 2015. Evidence for Nutrient Biolifting in Hawaiian Climosequence Soils as Revealed by Alkaline Earth Metal Stable Isotope Systematics. Procedia Earth and Planetary Science 13, 312–315.

Carminati, A., Vetterlein, D., 2013. Plasticity of rhizosphere hydraulic properties as a key for efficient utilization of scarce resources. Ann Bot 112 (2), 277–290.

Chadwick, O.A., Derry, L.A., Vitousek, P.M., Huebert, B.J., Hedin, L.O., 1999. Changing sources of nutrients during four million years of ecosystem development. Nature 397 (6719), 491–497.Cieśliński, G., van Rees, K.C.J., Szmigielska, A.M., Krishnamurti, G.S.R., Huang, P.M., 1998. Low-molecular-weight organic acids in rhizosphere soils of durum wheat and their effect on cadmium bioaccumulation. Plant and soil 203 (1), 109–117.

Dechassa, N., Schenk, M.K., 2004. Exudation of organic anions by roots of cabbage, carrot, and potato as influenced by environmental factors and plant age. J. Plant Nutr. Soil Sci. 167 (5), 623–629.

Drever, J.I., 1994. The effect of land plants on weathering rates of silicate minerals. Geochimica et Cosmochimica Acta 58 (10), 2325–2332.

Drever, J.I., Stillings, L.L., 1997. The role of organic acids in mineral weathering. Colloids and Surfaces A: Physicochemical and Engineering Aspects 120 (1–3), 167–181.

Feng, J., Turner, B.L., Lü, X., Chen, Z., Wei, K., Tian, J., Wang, C., Luo, W., Chen, L., 2016. Phosphorus transformations along a large-scale climosequence in arid and semiarid grasslands of northern China. Global Biogeochem. Cycles 30 (9), 1264–1275.

Fick, S.E., Hijmans, R.J., 2017. WorldClim 2: new 1−km spatial resolution climate surfaces for global land areas. Int. J. Climatol 37 (12), 4302–4315.

Gao, X.−L., Li, X.G., Zhao, L., Kuzyakov, Y., 2019. Regulation of soil phosphorus cycling in grasslands by shrubs. Soil Biology and Biochemistry 133, 1–11.

Gaume, A., Mächler, F., León, C. de, Narro, L., Frossard, E., 2001. Low−P tolerance by maize (Zea mays L.) genotypes: Significance of root growth, and organic acids and acid phosphatase root exudation. Plant and soil 228 (2), 253–264.

Gerke, J., Beißner, L., Römer, W., 2000. The quantitative effect of chemical phosphate mobilization by carboxylate anions on P uptake by a single root. I. The basic concept and determination of soil parameters. J. Plant Nutr. Soil Sci. 163 (2), 207–212.

Giles, C.D., Hsu, P.−C., Richardson, A.E., Hurst, M.R.H., Hill, J.E., 2014. Plant assimilation of phosphorus from an insoluble organic form is improved by addition of an organic anion producing Pseudomonas sp. Soil Biology and Biochemistry 68, 263–269.

Gustafsson, J.P., Braun, S., Tuyishime, J.R.M., Adediran, G.A., Warrinnier, R., Hesterberg, D., 2020. A Probabilistic Approach to Phosphorus Speciation of Soils Using P K−edge XANES Spectroscopy with Linear Combination Fitting. Soil Syst. 4 (2), 26.

Hedley, M.J., White, R.E., Nye, P.H., 1982. Plant−Indced Changes in the Rhizosphere of Rape (Brassica napus Var. Emerald) Seedlings. III. Changes in L Value, Soil Phosphate Fractions and Phosphatase Activity. New Phytol 91, 45–56.

Hinsinger, P., 2001. Bioavailability of soil inorganic P in the rhizosphere as affected by root−induced chemical changes: a review. Plant and soil 237 (2), 173–195.

Hou, E., Chen, C., Luo, Y., Zhou, G., Kuang, Y., Zhang, Y., Heenan, M., Lu, X., Wen, D., 2018. Effects of climate on soil phosphorus cycle and availability in natural terrestrial ecosystems. Global change biology 24 (8), 3344–3356.

Ippolito, J.A., Blecker, S.W., Freeman, C.L., McCulley, R.L., Blair, J.M., Kelly, E.F., 2010. Phosphorus biogeochemistry across a precipitation gradient in grasslands of central North America. Journal of Arid Environments 74 (8), 954–961.

Johnson, S.E., Loeppert, R.H., 2006. Role of Organic Acids in Phosphate Mobilization from Iron Oxide. Soil Science Society of America Journal 70 (1), 222–234.

Jones, D.L., 1998. Organic acids in the rhizosphere − A critical review. Plant Soil 205, 25–44.

Jones, D.L., Darrah, P.R., 1994. Role of root derived organic acids in the mobilization of nutrients from the rhizosphere. Plant Soil 166 (2), 247–257.

Kirk, G., Santos, E., Findenegg, G., 1999. Phosphate solubilization by organic anion excretion from rice (Oryza sativa L.) growing in aerobic soil. Plant Soil 211, 11–18.

Kirkby, E.A., Johnston, A.E., 2008. Soil and fertilizer phosphorus in relation to crop nutrition, in: Hammond, J.P., White, P.J. (Eds.), The Ecophysiology of Plant−Phosphorus Interactions, vol. 7. Springer, Dordrecht, pp. 177–223.

Klysubun, W., Sombunchoo, P., Deenan, W., Kongmark, C., 2012. Performance and status of beamline BL8 at SLRI for X−ray absorption spectroscopy. Journal of synchrotron radiation 19 (6), 930–936.

König, N., Blum, U., Symossek, F., Bussian, B., Furtmann, K., Gärtner, A., Groeticke, K., Gutwasser, F., Höhle, J., Hauenstein, M., Kiesling, G., Klingenberg, U., Klinger, T., Nack, T., Stahn, M., Trefz−Malcher, G., Wies, K., 2014. Handbuch Forstliche Analytik.

Kroener, E., Holz, M., Zarebanadkouki, M., Ahmed, M., Carminati, A., 2018. Effects of Mucilage on Rhizosphere Hydraulic Functions Depend on Soil Particle Size. Vadose Zone Journal 17 (1), 170056.

Kuzyakov, Y., Razavi, B.S., 2019. Rhizosphere size and shape: Temporal dynamics and spatial stationarity. Soil Biology and Biochemistry 135, 343–360.

Lambers, H., Raven, J.A., Shaver, G.R., Smith, S.E., 2008. Plant nutrient−acquisition strategies change with soil age. Trends in ecology & evolution 23 (2), 95–103.

Lan, M., Comerford, N.B., Fox, T.R., 1995. Organic Anions' Effect on Phosphorus Release from Spodic Horizons. Soil Science Society of America Journal 59 (6), 1745–1749.

Lang, F., Krüger, J., Amelung, W., Willbold, S., Frossard, E., Bünemann, E.K., Bauhus, J., Nitschke, R., Kandeler, E., Marhan, S., Schulz, S., Bergkemper, F., Schloter, M., Luster, J., Guggisberg, F., Kaiser, K., Mikutta, R., Guggenberger, G., Polle, A., Pena, R., Prietzel, J., Rodionov, A., Talkner, U., Meesenburg, H., Wilpert, K. von, Hölscher, A., Dietrich, H.P., Chmara, I., 2017. Soil phosphorus supply controls P nutrition strategies of beech forest ecosystems in Central Europe. Biogeochemistry 136 (1), 5–29.

Lenth, R.V., 2016. Least–Squares Means: The R Package lsmeans, Journal of Statistical Software.

Lenton, T.M., Watson, A.J., 2004. Biotic enhancement of weathering, atmospheric oxygen and carbon dioxide in the Neoproterozoic. Geophys. Res. Lett. 31 (5).

Lipton, D.S., Blanchar, R.W., Blevins, D.G., 1987. Citrate, Malate, and Succinate Concentration in Exudates from P–Sufficient and P–Stressed Medicago sativa L. Seedlings. Plant physiology 85 (2), 315–317.

López–Arredondo, D.L., Leyva–González, M.A., González–Morales, S.I., López–Bucio, J., Herrera–Estrella, L., 2014. Phosphate nutrition: improving low–phosphate tolerance in crops. Annual review of plant biology 65, 95–123.

Ma, X., Mason–Jones, K., Liu, Y., Blagodatskaya, E., Kuzyakov, Y., Guber, A., Dippold, M.A., Razavi, B.S., 2019. Coupling zymography with pH mapping reveals a shift in lupine phosphorus acquisition strategy driven by cluster roots. Soil Biology and Biochemistry 135, 420–428.

Maher, K., 2010. The dependence of chemical weathering rates on fluid residence time. Earth and Planetary Science Letters 294 (1–2), 101–110.

Makkonen, M., Berg, M.P., Handa, I.T., Hättenschwiler, S., van Ruijven, J., van Bodegom, P.M., Aerts, R., 2012. Highly consistent effects of plant litter identity and functional traits on decomposition across a latitudinal gradient. Ecology letters 15 (9), 1033–1041.

Nardini, A., Lo Gullo, M.A., Trifilò, P., Salleo, S., 2014. The challenge of the Mediterranean climate to plant hydraulics: Responses and adaptations. Environmental and Experimental Botany 103, 68–79.

Neaman, A., Chorover, J., Brantley, S.L., 2006. Effects of organic ligands on granite dissolution in batch experiments at pH 6. American Journal of Science 306 (6), 451–473.

Odum, E.P., 1969. The strategy of ecosystem development. Science (New York, N.Y.) 164 (3877), 262–270.

Oeser, R.A., Blanckenburg, F. von, 2020. Decoupling silicate weathering from primary productivity – how ecosystems regulate nutrient uptake along a climate and vegetation gradient. Biogeosciences 17 (19), 4883–4917.

Oeser, R.A., Stroncik, N., Moskwa, L.–M., Bernhard, N., Schaller, M., Canessa, R., van den Brink, L., Köster, M., Brucker, E., Stock, S., Fuentes, J.P., Godoy, R., Matus, F.J., Oses Pedraza, R., Osses McIntyre, P., Paulino, L., Seguel, O., Bader, M.Y., Boy, J., Dippold, M.A., Ehlers, T.A., Kühn, P., Kuzyakov, Y., Leinweber, P., Scholten, T., Spielvogel, S., Spohn, M., Übernickel, K., Tielbörger, K., Wagner, D., Blanckenburg, F. von, 2018. Chemistry and microbiology of the Critical Zone along a steep climate and vegetation gradient in the Chilean Coastal Cordillera. CATENA 170, 183–203.

Oksanen, J., Blanchet,, F.G., Friendly, M., Kindt, R., Legendre, P., McGlinn, D., Minchin, P.R., O'Hara, R.B., Simpson, G.L., Solymos, P., Stevens, M.H.H., Szoecs, E., Wagner, H., 2018. vegan: Community Ecology Package. R package version 2.5–3. https://CRAN.R–project.org/package=vegan.

Pinheiro Junior, C.R., Pereira, M.G., Fontana, A., Luz, L.R.Q.P.d., Corrêa Neto, T.d.A., 2019. Pedogenesis in a topo–climosequence in the Agreste region of Pernambuco. Revista Ciência Agronômica 50 (2).

Plassard, C., Louche, J., Ali, M.A., Duchemin, M., Legname, E., Cloutier–Hurteau, B., 2011. Diversity in phosphorus mobilisation and uptake in ectomycorrhizal fungi. Annals of Forest Science 68 (1), 33–43.

Prietzel, J., Harrington, G., Häusler, W., Heister, K., Werner, F., Klysubun, W., 2016. Reference spectra of important adsorbed organic and inorganic phosphate binding forms for soil P speciation using synchrotron–based K–edge XANES spectroscopy. Journal of synchrotron radiation 23 (2), 532–544.

R Core Team, 2017. R: A Language and Environment for Statistical Computing. R Foundation for Statistical Computing, Vienna, Austria.Ravel, B., Newville, M., 2005. ATHENA, ARTEMIS, HEPHAESTUS: data analysis for X−ray absorption spectroscopy using IFEFFIT (eng).

Ryan, P.R., Delhaize, E., Jones, D.L., 2001. Function and mechanism of organic anion exudation from plant roots. Annual Review of Plant Physiology and Plant Molecular Biology 52, 527–560.

Schaller, M., Ehlers, T.A., Lang, K.A.H., Schmid, M., Fuentes−Espoz, J.P., 2018. Addressing the contribution of climate and vegetation cover on hillslope denudation, Chilean Coastal Cordillera (26°–38°S). Earth and Planetary Science Letters 489, 111–122.

Sims, J.T., Simard, R.R., Joern, B.C., 1998. Phosphorus Loss in Agricultural Drainage: Historical Perspective and Current Research. Journal of Environment Quality 27 (2), 277–293.

Stock, S.C., Köster, M., Dippold, M.A., Nájera, F., Matus, F., Merino, C., Boy, J., Spielvogel, S., Gorbushina, A., Kuzyakov, Y., 2019. Environmental drivers and stoichiometric constraints on enzyme activities in soils from rhizosphere to continental scale. Geoderma 337, 973–982.

Szmigielska, A.M., Van Rees, K. C. J., Cieslinski, G., Huang, P.M., 1997. Comparison of liquid and gas chromatography for analysis of low molecular weight organic acids in rhizosphere soil. Communications in Soil Science and Plant Analysis 28 (1–2), 99–111.

Szmigielska, A.M., Van Rees, Ken C. J., Cieslinski, G., Huang, P.M., 1996. Low Molecular Weight Dicarboxylic Acids in Rhizosphere Soil of Durum Wheat. J. Agric. Food Chem. 44 (4), 1036–1040.

Trabucco, A., Zomer, R., 2019. Global Aridity Index and Potential Evapotranspiration (ET0) Climate Database v2. Figshare. doi:10.6084/M9.FIGSHARE.7504448.V3.

Turner, B.L., Hayes, P.E., Laliberté, E., 2018. A climosequence of chronosequences in southwestern Australia. Eur J Soil Sci 69 (1), 69–85.

Uhlig, D., Schuessler, J.A., Bouchez, J., Dixon, J.L., Blanckenburg, F. von, 2017. Quantifying nutrient uptake as driver of rock weathering in forest ecosystems by magnesium stable isotopes. Biogeosciences 14 (12), 3111–3128.

van Dongen, R., Scherler, D., Wittmann, H., Blanckenburg, F. von, 2019. Cosmogenic 10 Be in river sediment: where grain size matters and why. Earth Surf. Dynam. 7 (2), 393–410.

Walker, T.W., Syers, J.K., 1976. The fate of phosphorus during pedogenesis. Geoderma 15 (1), 1–19.

Wei, L., Chen, C., Xu, Z., 2010. Citric acid enhances the mobilization of organic phosphorus in subtropical and tropical forest soils. Biol Fertil Soils 46 (7), 765–769.

Werner, C., Schmid, M., Ehlers, T.A., Fuentes−Espoz, J.P., Steinkamp, J., Forrest, M., Liakka, J., Maldonado, A., Hickler, T., 2018. Effect of changing vegetation and precipitation on denudation – Part 1: Predicted vegetation composition and cover over the last 21 thousand years along the Coastal Cordillera of Chile. 2196632X 6 (4), 829–858.

Werner, F., 2017. LCF: Linear Combination Fitting: R package version 1.7.0. https://CRAN.R−project.org/package=LCF

Wickham, H., 2016. ggplot2: Elegant Graphics for Data Analysis. Springer−Verlag New York, 2016.

Wu, H., Xiang, W., Chen, L., Ouyang, S., Xiao, W., Li, S., Forrester, D.I., Lei, P., Zeng, Y., Deng, X., Zeng, L., Kuzyakov, Y., 2019. Soil Phosphorus Bioavailability and Recycling Increased with Stand Age in Chinese Fir Plantations. Ecosystems 12, 5635.

Yang, X., Post, W.M., 2011. Phosphorus transformations as a function of pedogenesis: A synthesis of soil phosphorus data using Hedley fractionation method. Biogeosciences 8 (10), 2907–2916.

2.2.11. Supplementary

Table: S 2.2.1: External standards included in the low–molecular–weight organic acids method. Retention time with a capillary column DB–FFAP, 30 m, 0.25 mm diameter and a film thickness of 1 µm. For settings of the gas chromatograph contact the authors. The limit of detection was calculated as the amount of analyte in the smallest standard before derivatization.

Analyte	Retention time [min]	Limit of detection [µg]
Oxalic acid	6.6	5.5
Malonic acid	8.8	5.5
Fumaric acid	9.5	5.5
Succinic acid	10.6	5.5
Maleic acid	12.5	5.5
Malic acid	19.1	5.5
Citric acid	26.3	5.5

Table: S 2.2.2: Total and constrained variance by the redundancy analysis (RDA). For the semiarid shrubland, Mediterranean woodland and humid–temperate forest.

Site		Inertia	Proportion
Arid shrubland	Total	5.96	1.00
	Constrained	4.49	0.75
	Unconstrained	1.47	0.25
Mediterranean woodland	Total	6.20	1.00
	Constrained	4.16	0.67
	Unconstrained	2.04	0.33
Humid–temperate forest	Total	6.67	1.00
	Constrained	5.34	0.80
	Unconstrained	1.33	0.20

Table: S 2.2.3: Scores of predictor variables (loadings) on redundancy analysis (RDA) axes. The values are a measure for how much variance of the variable is represented by the respective axis. Results are shown for the arid shrubland, Mediterranean woodland and humid–temperate forest.

Site	Variable	RDA1	RDA2	RDA3	RDA4	RDA5	RDA6
Semiarid shrubland	HypAp	−0.11	−0.03	0.17	−0.07	−0.51	−0.13
	BRU	0.23	0.17	0.43	−0.12	0.18	0.16
	OCP	0.19	0.20	−0.26	0.24	0.23	0.02
	VAR	−0.76	−0.19	−0.10	−0.07	−0.41	−0.34
	sroFeP	0.58	−0.02	−0.04	0.51	0.55	0.21
	adsP–BOE	0.20	0.18	−0.16	0.16	−0.42	0.79
	P_o	0.21	0.08	0.00	−0.82	0.49	0.15
Mediterranean woodland	HypAp	0.65	−0.09	−0.43	0.33	−0.17	0.24
	BRU	−0.17	−0.64	0.09	−0.19	−0.24	−0.25
	OCP	0.14	0.11	0.14	−0.28	−0.20	−0.67
	VAR	0.64	0.41	−0.61	0.05	0.11	−0.09
	sroFeP	0.51	0.47	0.19	−0.37	0.57	−0.08
	adsP–BOE	−0.16	−0.30	−0.03	0.23	0.34	−0.05
	adsP–GOE	−0.51	0.33	0.43	0.24	−0.56	0.29
	P_o	−0.80	0.03	0.35	0.05	−0.03	0.32

Humid–temperate forest	sroAlP	0.41	−0.03	0.06	0.24	−0.24	0.06
	VAR	−0.11	0.55	0.22	−0.27	−0.38	−0.58
	sroFeP	−0.34	−0.48	0.16	0.38	0.43	−0.33
	adsP−Al_clay	−0.15	0.00	−0.68	0.14	0.12	−0.30
	adsP−BOE	−0.43	−0.01	0.09	0.15	0.02	−0.08
	adsP−SOM	−0.41	−0.08	0.35	−0.18	0.20	0.70
	adsP−FER	−0.22	0.19	−0.31	−0.03	−0.32	0.60
	adsP−GOE	−0.19	0.04	−0.28	0.00	−0.04	−0.09
	P_o	0.94	−0.09	0.01	−0.12	−0.05	−0.11

Table: S 2.2.4: Scores of explained variables (loadings) on redundancy analysis (RDA) axes. The values are a measure for how much variance of the variable is represented by the respective axis. Results are shown for the arid shrubland, Mediterranean woodland and humid−temperate forest. Values are presented in type II scaling. Therefore, they allow to infer correlation with explaining variables. For correlation between explaining end explained variables see Table: S 2.2.6.

Site	Variable	RDA1	RDA2	RDA3	RDA4	RDA5	RDA6
Arid shrubland	Oxalic	−0.97	−0.14	0.02	−0.35	0.03	0.02
	Malic	−1.02	−0.17	−0.12	0.03	−0.10	−0.06
	Citric	−1.09	−0.28	−0.08	0.24	0.09	0.02
	MBC	0.10	−0.29	−0.19	0.03	−0.09	0.08
	V_{max}	0.05	−0.69	0.43	0.03	−0.03	0.00
	K_m	0.73	−0.75	−0.26	−0.08	0.04	−0.03
Mediterranean woodland	Oxalic	−0.85	0.27	−0.44	0.04	0.21	0.01
	Malic	0.35	0.50	0.03	0.46	−0.04	−0.04
	Citric	0.08	0.70	0.43	−0.22	0.09	−0.02
	MBC	−1.01	−0.40	0.36	0.12	0.08	−0.10
	V_{max}	−0.99	0.07	0.27	0.12	−0.06	0.14
	K_m	−1.01	0.32	−0.21	−0.13	−0.21	−0.06
Humid−temperate forest	Oxalic	1.01	0.18	−0.21	0.01	0.16	−0.06
	Malic	1.09	0.14	0.14	0.18	−0.15	−0.05
	Citric	1.04	0.20	0.05	0.32	0.03	0.08
	MBC	1.00	−0.14	0.41	−0.44	0.02	0.02
	V_{max}	0.76	−0.24	−0.55	−0.22	−0.08	0.02
	K_m	0.27	−0.84	0.08	0.24	0.04	−0.01

Table: S 2.2.5: Standard deviation, explained variance per axis and cumulative explained variance from the redundancy analysis (RDA) for the arid shrubland, Mediterranean woodland and humid−temperate forest.

Site		RDA1	RDA2	RDA3	RDA4	RDA5	RDA6
Arid shrubland	SD	1.74	1.01	0.50	0.40	0.16	0.10
	Proportion	0.67	0.23	0.06	0.04	0.01	0.00
	Cumulative	0.67	0.90	0.96	0.99	1.00	1.00
Mediterranean woodland	SD	1.64	0.86	0.66	0.46	0.27	0.16
	Proportion	0.64	0.18	0.10	0.05	0.02	0.01
	Cumulative	0.64	0.82	0.93	0.98	0.99	1.00
Humid−temperate forest	SD	1.96	0.82	0.65	0.58	0.22	0.10
	Proportion	0.72	0.13	0.08	0.06	0.01	0.00
	Cumulative	0.72	0.85	0.93	0.99	1.00	1.00

Table: S 2.2.6: Correlations between explaining and explained variables from the redundancy analysis expressed as the cosine of the angle between the arrows resulting from the scores of predictor variables (Table: S 2.2.3) and scores of explained variables (Table: S 2.2.4) (90 ° = independent, 0 ° = collinearity). Note that for the P species adsP−AlOH no values are reported. This is due to missing dependent variables for the two samples for which this P species was found.

Site	Variable	HydAp	OCP	BRU	sroAl−P	VAR	sroFe−P	adsP−Al_clay	adsP−AlOH	adsP−BOE	adsP−SOM	adsP−FER	adsP−GOE	Po
Arid shrubland	Oxalic	0.99	−0.79	−0.88	n.d.	0.99	−0.98	n.d.	n.d.	−0.83	n.d.	n.d.	n.d.	−0.98
	Malic	1.00	−0.80	−0.89	n.d.	1.00	−0.98	n.d.	n.d.	−0.84	n.d.	n.d.	n.d.	−0.98
	Citric	1.00	−0.85	−0.93	n.d.	1.00	−0.96	n.d.	n.d.	−0.88	n.d.	n.d.	n.d.	−0.99
	MBC	−0.09	−0.46	−0.30	n.d.	−0.08	0.36	n.d.	n.d.	−0.40	n.d.	n.d.	n.d.	−0.03
	V_{max}	0.17	−0.67	−0.53	n.d.	0.18	0.11	n.d.	n.d.	−0.62	n.d.	n.d.	n.d.	−0.29
	K_m	−0.51	−0.03	0.14	n.d.	−0.50	0.73	n.d.	n.d.	0.04	n.d.	n.d.	n.d.	0.40
Mediterranean woodland	Oxalic	−0.99	−0.55	−0.05	n.d.	−0.64	−0.50	n.d.	n.d.	0.18	n.d.	n.d.	0.97	0.96
	Malic	0.46	0.96	−0.94	n.d.	0.93	0.98	n.d.	n.d.	−0.99	n.d.	n.d.	−0.05	−0.55
	Citric	−0.03	0.71	−0.99	n.d.	0.62	0.75	n.d.	n.d.	−0.93	n.d.	n.d.	0.45	−0.07
	MBC	−0.87	−0.95	0.59	n.d.	−0.98	−0.93	n.d.	n.d.	0.76	n.d.	n.d.	0.59	0.92
	V_{max}	−1.00	−0.73	0.18	n.d.	−0.80	−0.69	n.d.	n.d.	0.40	n.d.	n.d.	0.88	1.00
	K_m	−0.99	−0.55	−0.05	n.d.	−0.64	−0.50	n.d.	n.d.	0.18	n.d.	n.d.	0.97	0.96
Humid−temperate forest	Oxalic	n.d.	n.d.	n.d.	0.97	−0.02	−0.71	−0.98	n.d.	−0.99	−1.00	−0.64	−0.92	0.96
	Malic	n.d.	n.d.	n.d.	0.98	−0.06	−0.68	−0.99	n.d.	−1.00	−1.00	−0.68	−0.94	0.98
	Citric	n.d.	n.d.	n.d.	0.96	0.00	−0.72	−0.98	n.d.	−0.99	−1.00	−0.63	−0.92	0.96
	MBC	n.d.	n.d.	n.d.	1.00	−0.32	−0.46	−0.99	n.d.	−0.99	−0.95	−0.84	−1.00	1.00
	V_{max}	n.d.	n.d.	n.d.	0.97	−0.47	−0.31	−0.96	n.d.	−0.95	−0.89	−0.92	−1.00	0.98
	K_m	n.d.	n.d.	n.d.	0.37	−0.99	0.60	−0.31	n.d.	−0.27	−0.13	−0.85	−0.50	0.39

Table: S 2.2.7: P species results from the linear combination fitting (LCF) of phosphorus K-edge X-ray absorption near edge structure spectroscopy (XANES). The upper part shows the percentage of each species in total P. In the lower part of the table this is multiplied by the total P content in each sample and given as content per kg of soil [mg kg^{-1}]. Data are subdivided by sampling sites (arid shrubland, Mediterranean woodland and humid-temperate forest), therein by sampling depth (topsoil, subsoil and saprolite) and in each depth by three distances to the root (0–2 mm, 2–4 mm, and 4–6 mm). The LCF was restricted to a maximum of four standards per sample. If a P pool was not detected in a sample this is indicated by n.d. (not determined).

Site	Facing	Depth	Root proximity	HydAp	OCP	BRU	sroAl-P	VAR	sroFe-P	adsP-Al_clay	adsP-AlOH	adsP-BOE	adsP-SOM	adsP-FER	adsP-GOE	Po
			[mm]							(%)						
Arid shrubland	South	Topsoil	0–2	n.d.	30	7	n.d.	30	33	n.d.	n.d.	n.d.	n.d.	n.d.	n.d.	n.d.
			2–4	27	n.d.	n.d.	n.d.	31	13	n.d.	n.d.	n.d.	n.d.	n.d.	n.d.	29
			4–6	43	n.d.	n.d.	n.d.	26	21	n.d.	n.d.	10	n.d.	n.d.	n.d.	n.d.
		Subsoil	0–2	46	n.d.	n.d.	n.d.	54	n.d.	n.d.	n.d.	n.d.	n.d.	n.d.	n.d.	n.d.
			2–4	46	n.d.	n.d.	n.d.	54	n.d.	n.d.	n.d.	n.d.	n.d.	n.d.	n.d.	n.d.
			4–6	n.d.	23	22	n.d.	n.d.	38	n.d.	n.d.	n.d.	n.d.	n.d.	n.d.	17
		Saprolite	0–2	n.d.	7	n.d.	n.d.	26	35	n.d.	n.d.	n.d.	n.d.	n.d.	n.d.	32
			4–6	42	n.d.	n.d.	n.d.	58	n.d.	n.d.	n.d.	n.d.	n.d.	n.d.	n.d.	n.d.
	North	Topsoil	0–2	34	n.d.	10	n.d.	45	n.d.	n.d.	n.d.	n.d.	n.d.	n.d.	n.d.	10
			2–4	38	n.d.	n.d.	n.d.	25	36	n.d.	n.d.	n.d.	n.d.	n.d.	n.d.	n.d.
			4–6	31	n.d.	n.d.	n.d.	36	33	n.d.	n.d.	n.d.	n.d.	n.d.	n.d.	n.d.
		Saprolite	0–2	31	n.d.	n.d.	n.d.	69	n.d.	n.d.	n.d.	n.d.	n.d.	n.d.	n.d.	n.d.
			4–6	57	n.d.	n.d.	n.d.	43	n.d.	n.d.	n.d.	n.d.	n.d.	n.d.	n.d.	n.d.
Mediterranean woodland	South	Topsoil	0–2	n.d.	n.d.	n.d.	n.d.	n.d.	n.d.	n.d.	n.d.	n.d.	8	n.d.	18	74
			2–4	8	n.d.	n.d.	n.d.	24	22	n.d.	n.d.	n.d.	n.d.	n.d.	n.d.	45
			4–6	24	n.d.	n.d.	n.d.	27	16	n.d.	n.d.	33	n.d.	n.d.	n.d.	n.d.
		Subsoil	0–2	11	26	n.d.	n.d.	42	20	n.d.	n.d.	n.d.	n.d.	n.d.	n.d.	n.d.
			2–4	34	n.d.	n.d.	n.d.	56	11	n.d.	n.d.	n.d.	n.d.	n.d.	n.d.	n.d.
			4–6	34	n.d.	n.d.	n.d.	39	17	n.d.	n.d.	10	n.d.	n.d.	n.d.	n.d.
		Saprolite	0–2	27	n.d.	n.d.	n.d.	25	24	n.d.	n.d.	24	n.d.	n.d.	n.d.	n.d.
			2–4	31	n.d.	n.d.	n.d.	43	12	n.d.	n.d.	n.d.	n.d.	n.d.	n.d.	14
			4–6	29	n.d.	n.d.	n.d.	42	22	n.d.	n.d.	n.d.	n.d.	n.d.	n.d.	7
	North	Topsoil	0–2	n.d.	n.d.	n.d.	n.d.	22	10	n.d.	n.d.	19	n.d.	n.d.	n.d.	49
			2–4	n.d.	14	n.d.	n.d.	28	37	n.d.	n.d.	n.d.	n.d.	n.d.	n.d.	21
			4–6	n.d.	n.d.	10	n.d.	n.d.	n.d.	n.d.	n.d.	n.d.	18	42	n.d.	30

		Saprolite	0–2	7	n.d.	n.d.	n.d.	38	36	n.d.	n.d.	n.d.	n.d.	n.d.	n.d.	19
			2–4	n.d.	6	n.d.	n.d.	28	42	n.d.	n.d.	n.d.	n.d.	n.d.	n.d.	24
			4–6	18	n.d.	n.d.	n.d.	51	31	n.d.	n.d.	n.d.	n.d.	n.d.	n.d.	n.d.
Humid–temperate forest	South	Topsoil	0–2	n.d.	n.d.	n.d.	17	n.d.	n.d.	n.d.	n.d.	n.d.	n.d.	n.d.	n.d.	83
			2–4	n.d.	n.d.	n.d.	n.d.	n.d.	n.d.	33	n.d.	n.d.	n.d.	n.d.	n.d.	67
			4–6	n.d.	n.d.	n.d.	n.d.	n.d.	n.d.	n.d.	n.d.	51	15	n.d.	n.d.	34
		Subsoil	0–2	n.d.	n.d.	n.d.	n.d.	10	n.d.	25	n.d.	34	n.d.	n.d.	n.d.	30
			2–4	n.d.	n.d.	n.d.	21	n.d.	n.d.	36	n.d.	n.d.	n.d.	n.d.	9	34
			4–6	n.d.	n.d.	n.d.	n.d.	n.d.	n.d.	14	n.d.	36	39	n.d.	n.d.	10
		Saprolite	0–2	n.d.	n.d.	n.d.	n.d.	n.d.	n.d.	31	n.d.	n.d.	21	26	n.d.	21
			2–4	n.d.	n.d.	n.d.	n.d.	n.d.	n.d.	28	12	n.d.	47	n.d.	n.d.	14
			4–6	n.d.	n.d.	n.d.	n.d.	n.d.	n.d.	54	19	n.d.	7	n.d.	n.d.	20
	North	Topsoil	0–2	n.d.	n.d.	n.d.	11	n.d.	n.d.	n.d.	n.d.	n.d.	23	n.d.	n.d.	65
			2–4	n.d.	n.d.	n.d.	n.d.	n.d.	9	n.d.	n.d.	n.d.	54	n.d.	n.d.	37
			4–6	n.d.	n.d.	n.d.	n.d.	44	n.d.	n.d.	n.d.	27	n.d.	n.d.	n.d.	29
		Saprolite	0–2	n.d.	n.d.	n.d.	n.d.	n.d.	n.d.	12	n.d.	n.d.	57	22	n.d.	9
			2–4	n.d.	n.d.	n.d.	n.d.	n.d.	24	n.d.	n.d.	45	31	n.d.	n.d.	n.d.
			4–6	n.d.	n.d.	n.d.	n.d.	n.d.	16	47	n.d.	n.d.	n.d.	n.d.	n.d.	37

Site		Depth	Root proximity	HydAp	OCP	BRU	sroAl–P	VAR	sroFe–P	adsP–Al_clay	adsP–AlOH	adsP–BOE	adsP–SOM	adsP–FER	adsP–GOE	Po	P_{tot}
			[mm]	[mg kg^{-1}]													
Arid shrubland	South	Topsoil	0–2	n.d.	91.4	21.3	n.d.	91.4	100.5	n.d.	n.d.	n.d.	n.d.	n.d.	n.d.	n.d.	304.5
			2–4	79.9	n.d.	n.d.	n.d.	91.7	38.5	n.d.	n.d.	n.d.	n.d.	n.d.	n.d.	85.8	295.8
			4–6	144.3	n.d.	n.d.	n.d.	87.3	70.5	n.d.	n.d.	33.6	n.d.	n.d.	n.d.	n.d.	335.7
		Subsoil	0–2	165.3	n.d.	n.d.	n.d.	194.0	n.d.	n.d.	n.d.	n.d.	n.d.	n.d.	n.d.	n.d.	359.3
			2–4	167.2	n.d.	n.d.	n.d.	196.2	n.d.	n.d.	n.d.	n.d.	n.d.	n.d.	n.d.	n.d.	363.4
			4–6	n.d.	62.8	60.1	n.d.	n.d.	103.8	n.d.	n.d.	n.d.	n.d.	n.d.	n.d.	46.4	273.2
		Saprolite	0–2	n.d.	21.6	n.d.	n.d.	80.2	108.0	n.d.	n.d.	n.d.	n.d.	n.d.	n.d.	98.8	308.6
			4–6	123.1	n.d.	n.d.	n.d.	170.0	n.d.	n.d.	n.d.	n.d.	n.d.	n.d.	n.d.	n.d.	293.1
	North	Topsoil	0–2	99.9	n.d.	29.4	n.d.	132.3	n.d.	n.d.	n.d.	n.d.	n.d.	n.d.	n.d.	29.4	293.9
			2–4	159.5	n.d.	n.d.	n.d.	104.9	151.1	n.d.	n.d.	n.d.	n.d.	n.d.	n.d.	n.d.	419.7
			4–6	125.4	n.d.	n.d.	n.d.	145.7	133.5	n.d.	n.d.	n.d.	n.d.	n.d.	n.d.	n.d.	404.6

		Saprolite	0–2	136.3	n.d.	n.d.	n.d.	303.3	n.d.	n.d.	n.d.	n.d.	n.d.	n.d.	n.d.	n.d.	439.6
			4–6	191.7	n.d.	n.d.	n.d.	144.6	n.d.	n.d.	n.d.	n.d.	n.d.	n.d.	n.d.	n.d.	336.3
Mediterranean woodland	South	Topsoil	0–2	n.d.	n.d.	n.d.	n.d.	n.d.	n.d.	n.d.	n.d.	n.d.	23.8	n.d.	53.6	220.3	297.7
			2–4	12.8	n.d.	n.d.	n.d.	38.5	35.3	n.d.	n.d.	n.d.	n.d.	n.d.	n.d.	72.3	160.6
			4–6	31.8	n.d.	n.d.	n.d.	35.7	21.2	n.d.	n.d.	43.7	n.d.	n.d.	n.d.	n.d.	132.4
		Subsoil	0–2	37.4	88.4	n.d.	n.d.	142.7	68.0	n.d.	n.d.	n.d.	n.d.	n.d.	n.d.	n.d.	339.9
			2–4	89.1	n.d.	n.d.	n.d.	146.7	28.8	n.d.	n.d.	n.d.	n.d.	n.d.	n.d.	n.d.	262.0
			4–6	95.8	n.d.	n.d.	n.d.	109.8	47.9	n.d.	n.d.	28.2	n.d.	n.d.	n.d.	n.d.	281.6
		Saprolite	0–2	53.3	n.d.	n.d.	n.d.	49.3	47.4	n.d.	n.d.	47.4	n.d.	n.d.	n.d.	n.d.	197.3
			2–4	67.9	n.d.	n.d.	n.d.	94.1	26.3	n.d.	n.d.	n.d.	n.d.	n.d.	n.d.	30.6	218.9
			4–6	111.3	n.d.	n.d.	n.d.	161.3	84.5	n.d.	n.d.	n.d.	n.d.	n.d.	n.d.	26.9	383.9
	North	Topsoil	0–2	n.d.	n.d.	n.d.	n.d.	62.1	28.2	n.d.	n.d.	53.6	n.d.	n.d.	n.d.	138.3	282.3
			2–4	n.d.	40.4	n.d.	n.d.	80.8	106.7	n.d.	n.d.	n.d.	n.d.	n.d.	n.d.	60.6	288.5
			4–6	n.d.	n.d.	30.1	n.d.	n.d.	n.d.	n.d.	n.d.	n.d.	54.2	126.4	n.d.	90.3	301.1
		Saprolite	0–2	16.9	n.d.	n.d.	n.d.	91.7	86.9	n.d.	n.d.	n.d.	n.d.	n.d.	n.d.	45.9	241.4
			2–4	n.d.	11.5	n.d.	n.d.	53.5	80.3	n.d.	n.d.	n.d.	n.d.	n.d.	n.d.	45.9	191.2
			4–6	37.0	n.d.	n.d.	n.d.	104.9	63.8	n.d.	n.d.	n.d.	n.d.	n.d.	n.d.	n.d.	205.7
Humid-temperate forest	South	Topsoil	0–2	n.d.	n.d.	n.d.	59.6	n.d.	n.d.	n.d.	n.d.	n.d.	n.d.	n.d.	n.d.	290.9	350.5
			2–4	n.d.	n.d.	n.d.	n.d.	n.d.	n.d.	82.4	n.d.	n.d.	n.d.	n.d.	n.d.	167.2	249.6
			4–6	n.d.	n.d.	n.d.	n.d.	n.d.	n.d.	n.d.	n.d.	74.3	21.9	n.d.	n.d.	49.6	145.8
		Subsoil	0–2	n.d.	n.d.	n.d.	n.d.	50.6	n.d.	126.4	n.d.	171.9	n.d.	n.d.	n.d.	151.7	505.7
			2–4	n.d.	n.d.	n.d.	74.3	n.d.	n.d.	127.3	n.d.	n.d.	n.d.	n.d.	31.8	120.3	353.7
			4–6	n.d.	n.d.	n.d.	n.d.	n.d.	n.d.	30.8	n.d.	79.1	85.7	n.d.	n.d.	22.0	219.9
		Saprolite	0–2	n.d.	n.d.	n.d.	n.d.	n.d.	n.d.	87.4	n.d.	n.d.	59.2	73.3	n.d.	59.2	281.9
			2–4	n.d.	n.d.	n.d.	n.d.	n.d.	n.d.	81.4	34.9	n.d.	136.6	n.d.	n.d.	40.7	290.6
			4–6	n.d.	n.d.	n.d.	n.d.	n.d.	n.d.	159.2	56.0	n.d.	20.6	n.d.	n.d.	59.0	294.8
	North	Topsoil	0–2	n.d.	n.d.	n.d.	68.2	n.d.	n.d.	n.d.	n.d.	n.d.	142.7	n.d.	n.d.	403.3	620.4
			2–4	n.d.	n.d.	n.d.	n.d.	n.d.	34.7	n.d.	n.d.	n.d.	208.3	n.d.	n.d.	142.7	385.7
			4–6	n.d.	n.d.	n.d.	n.d.	139.8	n.d.	n.d.	n.d.	85.8	n.d.	n.d.	n.d.	92.1	317.7
		Saprolite	0–2	n.d.	n.d.	n.d.	n.d.	n.d.	n.d.	42.0	n.d.	n.d.	199.5	77.0	n.d.	31.5	349.9
			2–4	n.d.	n.d.	n.d.	n.d.	n.d.	199.1	n.d.	n.d.	373.2	257.1	n.d.	n.d.	n.d.	829.4
			4–6	n.d.	n.d.	n.d.	n.d.	n.d.	148.2	435.4	n.d.	n.d.	n.d.	n.d.	n.d.	342.8	926.4

Table: S 2.2.8: Absolute contents of low-molecular-weight organic acids (LMWOA; oxalic-, malic-, citric-acid), MBC, V_{max} and K_m values of acid phosphatase, and LMWOA contents normalized by MBC are shown in the table. Values are averaged over four soil pits in each site ±the standard error. At North facing soil pits only topsoil and the saprolite were sampled. At South facing all three depths (topsoil, subsoil, saprolite) were sampled. In the saprolite of the arid shrubland only root distances 0–2 mm and 4–6 mm were sampled, in all other sites sampled root distances were 0–2 mm, 2–4 mm, and 4–6 mm. If a value is missing this is indicated by 'n.d.' (not detected).

Site	Depth	Distance [mm]	Oxalic	Malic [µg g−1]	Citric	MBC	Oxalic/MBC	Malic/MBC [ng µg^{-1}]	Citric/MBC	V_{max}	K_m
Arid shrubland	Topsoil	0–2	5.6±1.8	4.6±4.2	1.1±0.8	275.2±34.4	22.9±8.8	19.4±18	4.4±3.3	153.5±79.1	4.3±1
		2–4	3.9±0.9	1.4±1.1	0.4±0.3	207.6±32	18.5±2.6	6.2±4.4	1.9±1.2	94.2±31.2	4.6±1.3
		4–6	4.2±0.7	1.9±1.2	1.2±0.5	261.3±37.9	16.8±3.2	7.4±5	5±1.7	143.1±43.2	4.4±0.3
	Subsoil	0–2	7.7±1.4	5.8±2.3	2.9±0.8	278±36.2	27.4±1.8	19.6±7	10.1±2	104.8±14.1	2.9±0.3
		2–4	5.8±0.4	2.8±1.2	0.8±0.4	142±25.1	42.8±5.5	22.4±9.4	6.8±4	103.9±26.9	3.1±0.4
		4–6	3.8±0.3	1.9±1.2	1.2±0.9	168.7±40.1	25.3±6.6	12.8±6.4	7.5±4.3	98.5±18	2.7±0.4
	Saprolite	0–2	8.5±2.1	12.2±5.4	5.9±2	164.5±40.7	64.5±25	105.2±64.1	45.2±16.7	93.4±3.6	2.3±0.4
		4–6	3.3±1.1	1.9±0.8	0.8±0.3	4.5±0.8	818.4±277.3	487.3±242.9	178.2±70.6	n.d.	n.d.
Mediterranean woodland	Topsoil	0–2	24.7±2.5	8.1±3	8.5±3.4	1163.4±321.4	31.3±13.4	7.3±2.6	7.2±2.4	348.4±43.8	7.1±0.6
		2–4	11.8±4.2	6.1±3.8	4.7±0.8	817.4±207.1	15.5±7.6	10.1±7.2	6.4±1.5	233.9±41.8	3.4±0.5
		4–6	11.4±1.3	2.9±0.8	3±1	1092.2±205.1	11.5±2.1	2.4±0.6	2.5±0.7	254.3±39.9	4.1±0.3
	Subsoil	0–2	18.4±2.3	6.6±2.2	6.8±2.3	250.3±91.8	93±32.7	38.1±20.5	31±13.5	164.8±20.1	5.9±0.4
		2–4	10.5±3	6.3±2.6	3.5±1.6	180.2±19.7	63.7±25.2	38.7±19.8	21.3±11.1	150.8±9.7	5.3±0.9
		4–6	5.2±1.7	3.8±1.2	3.9±1.8	143.9±22.2	37.6±11.1	29.3±12.1	31.9±17.9	121.2±16.9	4.7±1.5
	Saprolite	0–2	15.5±5.6	4.7±1.2	8.1±4	177.4±68.2	96.4±25.9	30.8±8.8	39.6±17.2	111±38.5	10.4±5.6
		2–4	6.3±1.5	7.4±1.3	8.4±6.9	427.9±355.7	71.4±36.3	97.6±56.7	65.1±63.7	100.2±74.1	2.4±0.9
		4–6	6.1±2.3	2.3±0.9	2.8±2.3	70.3±43.6	167.8±107.1	67.6±47.6	26.9±11.9	55.8±38.9	3.6±1.5
Humid-temperate forest	Topsoil	0–2	42.4±15.1	10.8±2.9	19.5±8.2	2187.5±440.8	20.4±6.6	5.1±1.1	9.7±4.1	1277±506.4	9.7±0.7
		2–4	39.3±11.8	7.8±3	12.5±5.7	1734.1±320.6	21.8±4.9	4±1.1	6±2.2	898.4±391.1	3.6±0.8
		4–6	32.6±12.9	9.3±4.6	16.4±11.3	1073.9±484.7	71.5±46.5	20.3±14.4	20.6±10.9	1030.3±489.9	3.2±1.4
	Subsoil	0–2	11.4±2.8	3.3±0.2	3±1.5	393.1±100.3	30.1±3.7	9.8±2.9	8.9±4	526.1±189.2	2.4±0.1
		2–4	10±1.7	0.9±0.7	1.2±1	251.1±68.9	46.5±13	2.6±1.8	3.2±2.5	627±291.1	5.3±1.7
		4–6	6.7±1.6	1.2±0.6	1.4±1.1	212.5±41.1	40.5±14.4	8.2±0.4	1.7±0	512.1±307.4	3.5±0.2
	Saprolite	0–2	7.6±2	3±2.5	2.8±2.5	161.5±51.1	71.7±43.4	49.8±45.8	46.6±46.3	n.d.	n.d.
		2–4	3.9±0.9	0.7±0.5	1.1±0.8	97.9±86.3	266.8±243.6	90.3±86.2	148.3±147	n.d.	n.d.
		4–6	2.9±0.7	1.3±0.8	1.6±0.9	437.5±431.4	226.6±220.8	146.1±142.4	333.1±332.1	n.d.	n.d.

Table: S 2.2.9: Parameters from linear models examining the effect of distance from the roots on microbial biomass carbon (MBC), low−molecular−weight organic acids (oxalic, malic, citric), and phosphatase kinetics (V_{max}, K_m). Significant p values are bolded and italicized.

Site	Depth	Variable	Slope	Intercept	r^2	p	n
Arid shrubland	Topsoil	MBC	−7.18	257.53	0.25	0.175	6
	Subsoil	MBC	−23.21	235.71	0.15	0.451	3
	Saprolite	MBC	−44.05	222.83	1.00	***0.000***	4
	Topsoil	Oxalic	−0.21	4.32	−0.18	0.660	6
	Subsoil	Oxalic	−0.14	5.52	−0.78	0.783	3
	Saprolite	Oxalic	−1.96	11.48	0.43	0.211	4
	Topsoil	Malic	−0.07	0.37	0.07	0.304	6
	Subsoil	Malic	−0.43	2.08	0.97	***0.082***	3
	Saprolite	Malic	−0.71	4.18	0.35	0.248	4
	Topsoil	Citric	0.04	0.20	−0.22	0.762	6
	Subsoil	Citric	−0.33	1.43	0.47	0.342	3
	Saprolite	Citric	−0.53	3.44	0.21	0.313	4
	Topsoil	V_{max}	−13.84	246.13	−0.19	0.688	6
	Subsoil	V_{max}	−4.73	97.01	0.33	0.394	3
	Saprolite	V_{max}	n.d.	n.d.	n.d.	n.d.	n<3
	Topsoil	K_m	−0.38	7.06	0.28	0.163	6
	Subsoil	K_m	0.06	3.17	0.96	***0.095***	3
	Saprolite	K_m	n.d.	n.d.	n.d.	n.d.	n<3
Mediterranean woodland	Topsoil	MBC	−17.71	1078.30	−0.20	0.713	6
	Subsoil	MBC	−26.24	274.37	0.51	0.330	3
	Saprolite	MBC	−27.08	305.60	−0.14	0.570	6
	Topsoil	Oxalic	−2.94	23.22	0.15	0.244	6
	Subsoil	Oxalic	−2.82	19.56	0.20	0.435	3
	Saprolite	Oxalic	−2.82	18.75	0.19	0.213	6
	Topsoil	Malic	−0.44	3.81	0.00	0.379	6
	Subsoil	Malic	−0.04	7.12	−1.00	0.986	3
	Saprolite	Malic	−0.91	8.05	0.09	0.286	6
	Topsoil	Citric	−1.16	7.72	0.10	0.282	6
	Subsoil	Citric	−1.38	11.23	0.83	0.187	3
	Saprolite	Citric	−1.91	15.28	−0.01	0.381	6
	Topsoil	V_{max}	−19.23	279.56	0.12	0.261	6
	Subsoil	V_{max}	4.52	120.93	0.85	0.174	3
	Saprolite	V_{max}	−19.74	170.30	0.09	0.324	5
	Topsoil	K_m	−0.90	8.07	0.36	0.121	6
	Subsoil	K_m	−0.64	6.29	0.47	0.345	3
	Saprolite	K_m	−0.32	5.01	−0.20	0.598	5
Humid−temperate forest	Topsoil	MBC	−279.08	2501.08	0.99	***0.000***	6
	Subsoil	MBC	−46.95	337.59	0.99	***0.049***	3
	Saprolite	MBC	34.50	12.75	0.48	***0.077***	6
	Topsoil	Oxalic	−6.68	49.16	−0.07	0.463	6
	Subsoil	Oxalic	−0.66	8.39	−0.38	0.624	3
	Saprolite	Oxalic	−0.98	6.45	0.31	0.145	6
	Topsoil	Malic	−2.31	13.24	0.25	0.177	6
	Subsoil	Malic	−0.74	3.33	0.62	0.287	3
	Saprolite	Malic	−0.05	0.28	0.12	0.262	6

Topsoil	Citric	−5.07	26.83	0.15	0.240	6
Subsoil	Citric	0.22	1.46	−0.89	0.848	3
Saprolite	Citric	0.06	0.34	−0.21	0.746	6
Topsoil	V_{max}	−60.37	689.36	−0.13	0.546	6
Subsoil	V_{max}	−68.40	478.54	0.22	0.428	3
Saprolite	V_{max}	−43.95	434.12	0.88	0.155	3
Topsoil	K_m	−1.08	7.76	0.31	0.146	6
Subsoil	K_m	0.30	2.19	0.37	0.380	3
Saprolite	K_m	0.43	3.84	−0.86	0.832	3

Table: S 2.2.10: Parameters from linear models examining the effect of distance from the roots on P species (Ca−P = calcium phosphates, Al−P = Al−phosphates, sorb Al−P = orthophosphate sorbed to Al−(oxy)hydroxides, Fe−P = Fe−phosphates, sorb Fe−P = orthophosphates sorbed to Fe−(oxy)hydroxides, Po = organically bound P). Significant p values are bolded and italicized.

Site	Depth	Facing	Variable	Slope	Intercept	r	p	n
Arid shrubland	Topsoil	North	Ca−P	−0.04	0.49	1.00	***0.000***	3
	Topsoil	South	Ca−P	0.02	0.31	−0.72	0.758	3
	Subsoil	South	Ca−P	0.00	0.46	0.50	0.333	3
	Saprolite	North	Ca−P	n.d.	n.d.	n.d.	n.d.	n<3
	Saprolite	South	Ca−P	n.d.	n.d.	n.d.	n.d.	n<3
	Topsoil	North	Fe−P	0.08	−0.02	0.36	0.381	3
	Topsoil	South	Fe−P	−0.03	0.31	−0.29	0.593	3
	Subsoil	South	Fe−P	0.10	−0.16	0.50	0.333	3
	Saprolite	North	Fe−P	n.d.	n.d.	n.d.	n.d.	n<3
	Saprolite	South	Fe−P	n.d.	n.d.	n.d.	n.d.	n<3
	Topsoil	North	Al−P	−0.02	0.42	−0.60	0.703	3
	Topsoil	South	Al−P	−0.01	0.32	0.14	0.454	3
	Subsoil	South	Al−P	−0.14	0.77	0.50	0.333	3
	Saprolite	North	Al−P	n.d.	n.d.	n.d.	n.d.	n<3
	Saprolite	South	Al−P	n.d.	n.d.	n.d.	n.d.	n<3
	Topsoil	North	sorbFe−P	n.d.	n.d.	n.d.	n.d.	n.d.
	Topsoil	South	sorbFe−P	n.d.	n.d.	n.d.	n.d.	n.d.
	Subsoil	South	sorbFe−P	n.d.	n.d.	n.d.	n.d.	n.d.
	Saprolite	North	sorbFe−P	n.d.	n.d.	n.d.	n.d.	n<3
	Saprolite	South	sorbFe−P	n.d.	n.d.	n.d.	n.d.	n<3
	Topsoil	North	sorbAl−P	n.d.	n.d.	n.d.	n.d.	n.d.
	Topsoil	South	sorbAl−P	0.03	−0.04	0.50	0.333	3
	Subsoil	South	sorbAl−P	n.d.	n.d.	n.d.	n.d.	n.d.
	Saprolite	North	sorbAl−P	n.d.	n.d.	n.d.	n.d.	n<3
	Saprolite	South	sorbAl−P	n.d.	n.d.	n.d.	n.d.	n<3
	Topsoil	North	Po	−0.03	0.11	0.50	0.333	3
	Topsoil	South	Po	0.00	0.10	−1.00	1.000	3
	Subsoil	South	Po	0.04	−0.07	0.50	0.333	3
	Saprolite	North	Po	n.d.	n.d.	n.d.	n.d.	n<3
	Saprolite	South	Po	n.d.	n.d.	n.d.	n.d.	n<3
Mediterranean woodland	Topsoil	North	Ca−P	0.03	0.00	−0.04	0.512	3
	Topsoil	South	Ca−P	0.06	−0.07	0.93	0.121	3
	Subsoil	South	Ca−P	−0.01	0.38	0.50	0.333	3
	Saprolite	North	Ca−P	0.03	0.02	0.36	0.381	3

	Saprolite	South	Ca–P	0.00	0.28	−0.50	0.667	3
	Topsoil	North	Fe–P	−0.03	0.23	−0.86	0.832	3
	Topsoil	South	Fe–P	0.04	0.01	−0.01	0.503	3
	Subsoil	South	Fe–P	−0.01	0.18	−0.79	0.788	3
	Saprolite	North	Fe–P	−0.01	0.40	−0.59	0.700	3
	Saprolite	South	Fe–P	−0.01	0.21	−0.95	0.901	3
	Topsoil	North	Al–P	−0.06	0.33	0.11	0.464	3
	Topsoil	South	Al–P	0.07	−0.03	0.66	0.269	3
	Subsoil	South	Al–P	−0.01	0.48	−0.95	0.894	3
	Saprolite	North	Al–P	0.03	0.29	−0.36	0.619	3
	Saprolite	South	Al–P	0.04	0.24	0.41	0.365	3
	Topsoil	North	sorbFe–P	0.11	−0.18	0.50	0.333	3
	Topsoil	South	sorbFe–P	−0.05	0.20	0.50	0.333	3
	Subsoil	South	sorbFe–P	n.d.	n.d.	n.d.	n.d.	n.d.
	Saprolite	North	sorbFe–P	n.d.	n.d.	n.d.	n.d.	n.d.
	Saprolite	South	sorbFe–P	n.d.	n.d.	n.d.	n.d.	n.d.
	Topsoil	North	sorbAl–P	0.00	0.13	−1.00	0.970	3
	Topsoil	South	sorbAl–P	0.06	−0.05	0.05	0.483	3
	Subsoil	South	sorbAl–P	0.03	−0.04	0.50	0.333	3
	Saprolite	North	sorbAl–P	n.d.	n.d.	n.d.	n.d.	n.d.
	Saprolite	South	sorbAl–P	−0.06	0.26	0.50	0.333	3
	Topsoil	North	Po	−0.05	0.48	−0.12	0.537	3
	Topsoil	South	Po	−0.19	0.95	0.97	0.079	3
	Subsoil	South	Po	n.d.	n.d.	n.d.	n.d.	n.d.
	Saprolite	North	Po	−0.05	0.29	0.13	0.460	3
	Saprolite	South	Po	0.02	0.02	−0.50	0.667	3
Humid–temperate forest	Topsoil	North	Ca–P	n.d.	n.d.	n.d.	n.d.	n.d.
	Topsoil	South	Ca–P	n.d.	n.d.	n.d.	n.d.	n.d.
	Subsoil	South	Ca–P	n.d.	n.d.	n.d.	n.d.	n.d.
	Saprolite	North	Ca–P	n.d.	n.d.	n.d.	n.d.	n.d.
	Saprolite	South	Ca–P	n.d.	n.d.	n.d.	n.d.	n.d.
	Topsoil	North	Fe–P	0.00	0.03	−1.00	1.000	3
	Topsoil	South	Fe–P	n.d.	n.d.	n.d.	n.d.	n.d.
	Subsoil	South	Fe–P	n.d.	n.d.	n.d.	n.d.	n.d.
	Saprolite	North	Fe–P	0.04	0.01	−0.14	0.546	3
	Saprolite	South	Fe–P	n.d.	n.d.	n.d.	n.d.	n.d.
	Topsoil	North	Al–P	0.08	−0.06	0.04	0.488	3
	Topsoil	South	Al–P	−0.04	0.18	0.50	0.333	3
	Subsoil	South	Al–P	−0.03	0.18	−0.55	0.684	3
	Saprolite	North	Al–P	n.d.	n.d.	n.d.	n.d.	n.d.
	Saprolite	South	Al–P	n.d.	n.d.	n.d.	n.d.	n.d.
	Topsoil	North	sorbFe–P	n.d.	n.d.	n.d.	n.d.	n.d.
	Topsoil	South	sorbFe–P	n.d.	n.d.	n.d.	n.d.	n.d.
	Subsoil	South	sorbFe–P	0.00	0.03	−1.00	1.000	3
	Saprolite	North	sorbFe–P	−0.06	0.24	0.50	0.333	3
	Saprolite	South	sorbFe–P	−0.07	0.28	0.50	0.333	3
	Topsoil	North	sorbAl–P	0.01	0.32	−0.97	0.924	3
	Topsoil	South	sorbAl–P	0.17	−0.17	1.00	***0.000***	3
	Subsoil	South	sorbAl–P	0.08	0.38	−0.35	0.612	3

Saprolite	North	sorbAl−P	−0.06	0.81	0.06	0.482	3
Saprolite	South	sorbAl−P	0.07	0.52	0.19	0.439	3
Topsoil	North	Po	−0.09	0.71	0.81	0.198	3
Topsoil	South	Po	−0.12	0.98	0.92	0.126	3
Subsoil	South	Po	−0.05	0.40	0.21	0.433	3
Saprolite	North	Po	0.07	−0.06	0.05	0.483	3
Saprolite	South	Po	0.00	0.19	−0.97	0.916	3

Table: S 2.2.11: Results of linear models examining the effect of soil depth on the parameters microbial biomass carbon (MBC), oxalic−, malic−, and citric acid content, maximum reaction rate of acid phosphatase (Vmax), and half saturation constant of acid phosphatase (Km) , calculated per study site. The table shows the p values of the overall model and of the post−hoc least square means (with "Tukey" correction) pairwise comparison. Significant p values are bolded and italicized.

Site	Variable	P−value of the overall linear model	Topsoil − Subsoil	Topsoil − Saprolite	Subsoil − Saprolite
Arid shrubland	MBC	***0.02***	0.31	***0.01***	0.31
	Oxalic	0.66	0.82	0.66	0.98
	Malic	0.12	0.77	0.11	0.43
	Citric	0.12	0.98	0.12	0.26
	V_{max}	0.25	0.26	0.61	0.99
	K_m	***0.01***	***0.01***	***0.04***	0.92
Mediterranean woodland	MBC	***<0.01***	***<0.01***	***<0.01***	0.96
	Oxalic	0.71	0.86	0.70	0.99
	Malic	***0.09***	***0.10***	0.22	0.68
	Citric	0.31	0.77	0.28	0.82
	V_{max}	***0.03***	0.14	***0.03***	0.86
	K_m	0.57	0.78	0.56	0.98
Humid−temperate forest	MBC	***<0.01***	***<0.01***	***<0.01***	0.94
	Oxalic	0.12	0.30	0.12	0.98
	Malic	***0.07***	0.24	***0.07***	0.94
	Citric	0.19	0.42	0.19	0.97
	V_{max}	0.41	0.48	0.56	0.99
	K_m	0.64	0.73	0.95	0.63

Table: S 2.2.12: Results of linear models examining the effect of study site in each soil depth on the parameters microbial biomass carbon (MBC), oxalic−, malic−, and citric acid content, maximum reaction rate of acid phosphatase (V_{max}), and half saturation constant of acid phosphatase (K_m) , calculated per study site. The table shows the p values of the overall model and of the post−hoc least square means (with "Tukey" correction) pairwise comparison. Significant p values are bolded and italicized.

Variable	Depth	P−value of the overall linear model	Humid−temperate forest − Mediterranean woodland	Mediterranean woodland − Arid shrubland	Humid−temperate forest − Arid shrubland
MBC	Topsoil	***<0.01***	***0.01***	***<0.01***	***<0.01***
MBC	Subsoil	0.85	1.00	0.88	0.87
MBC	Saprolite	0.21	0.32	0.25	0.95
Oxalic	Topsoil	0.10	0.40	0.61	***0.09***
Oxalic	Subsoil	0.29	0.45	0.30	0.93
Oxalic	Saprolite	0.19	0.18	0.49	0.86
Malic	Topsoil	***0.05***	0.24	0.57	***0.04***
Malic	Subsoil	***0.04***	***0.06***	***0.05***	0.99
Malic	Saprolite	***<0.01***	***<0.01***	***0.09***	0.39

Citric	Topsoil	0.15	0.39	0.76	0.13
Citric	Subsoil	***0.02***	***0.05***	***0.02***	0.60
Citric	Saprolite	***0.02***	***0.02***	***0.07***	0.91
V_{max}	Topsoil	***0.05***	***0.08***	0.99	***0.06***
V_{max}	Subsoil	0.14	0.29	0.81	0.13
V_{max}	Saprolite	***0.03***	***0.03***	0.99	0.14
K_m	Topsoil	0.56	0.79	0.91	0.54
K_m	Subsoil	0.29	0.30	0.45	0.93
K_m	Saprolite	0.73	0.83	0.91	0.74

Table: S 2.2.13: Results of linear models examining the effect of soil depth on P compound classes (Ca−P = calcium phosphates, Al−P = Al−phosphates, sorb Al−P = orthophosphate sorbed to Al−(oxy)hydroxides, Fe−P = Fe−phosphates, sorb Fe−P = orthophosphates sorbed to Fe−(oxy)hydroxides, Po = organically bound P) was calculated per study site. Distance from the roots was set as a fixed effect, with random slopes and random intercept. The table shows the results of the post−hoc least square means (with "Tukey" correction) pairwise comparison (p values). Significant p values are bolded and italicized.

Site	Variable	P−value of the overall linear model	Topsoil − Subsoil	Topsoil − Saprolite	Subsoil − Saprolite
Arid shrubland	Ca−P	0.25	0.61	0.61	0.23
	Fe−P	0.83	0.81	0.96	0.96
	Al−P	0.82	0.92	0.81	0.95
	sorbFe−P	n.d.	n.d.	n.d.	n.d.
	sorbAl−P	0.51	0.54	0.61	1.00
	P_o	0.79	0.95	0.90	0.77
Mediterranean woodland	Ca−P	***0.01***	***0.01***	***0.05***	0.57
	Fe−P	0.62	0.87	0.59	0.87
	Al−P	***0.06***	***0.05***	0.18	0.63
	sorbFe−P	0.42	0.48	0.48	1.00
	sorbAl−P	0.65	0.63	0.86	0.90
	P_o	0.14	0.15	0.24	0.92
Humid−temperate forest	Ca−P	n.d.	n.d.	n.d.	n.d.
	Fe−P	n.d.	n.d.	n.d.	n.d.
	Al−P	0.37	0.78	0.70	0.35
	sorbFe−P	0.54	0.92	0.52	0.74
	sorbAl−P	0.25	0.44	0.24	0.87
	P_o	***0.04***	***0.07***	***0.04***	0.89

Table: S 2.2.14: Results of linear models examining the effect of study site in each soil depth on P compound classes (Ca−P = calcium phosphates, Al−P = Al−phosphates, sorb Al−P = orthophosphate sorbed to Al−(oxy)hydroxides, Fe−P = Fe−phosphates, sorb Fe−P = orthophosphates sorbed to Fe−(oxy)hydroxides, Po = organically bound P) was calculated. Distance from the roots was set as a fixed effect, with random slopes and random intercept. The table shows the results of the post−hoc least square means (with "Tukey" correction) pairwise comparison (p values). Significant p values are bolded and italicized.

Variable	Depth	P−value of the overall linear model	Humid−temperate forest − Mediterranean woodland	Mediterranean woodland − Arid shrubland	Humid−temperate forest − Arid shrubland
Ca−P	Topsoil	***<0.01***	***0.07***	***<0.01***	***<0.01***
Ca−P	Subsoil	***<0.01***	***<0.01***	***<0.01***	***<0.01***
Ca−P	Saprolite	***<0.01***	***0.04***	0.19	***<0.01***
Fe−P	Topsoil	***0.02***	0.18	0.44	***0.02***
Fe−P	Subsoil	0.35	0.35	0.95	0.50
Fe−P	Saprolite	***0.03***	***0.03***	***0.08***	0.96
Al−P	Topsoil	***0.05***	0.80	0.14	***0.05***
Al−P	Subsoil	0.16	0.15	0.82	0.32
Al−P	Saprolite	***<0.01***	***<0.01***	0.28	***<0.01***
sorbFe−P	Topsoil	0.17	0.22	0.22	1.00
sorbFe−P	Subsoil	0.42	0.48	1.00	0.48
sorbFe−P	Saprolite	0.17	0.21	1.00	0.28
sorbAl−P	Topsoil	***0.01***	***0.09***	0.44	***0.01***
sorbAl−P	Subsoil	***0.01***	***0.01***	0.96	***0.01***
sorbAl−P	Saprolite	***<0.01***	***<0.01***	0.85	***<0.01***
Po	Topsoil	***<0.01***	0.39	***0.06***	***<0.01***
Po	Subsoil	***0.04***	***0.04***	0.75	0.10
Po	Saprolite	0.53	0.68	0.94	0.54

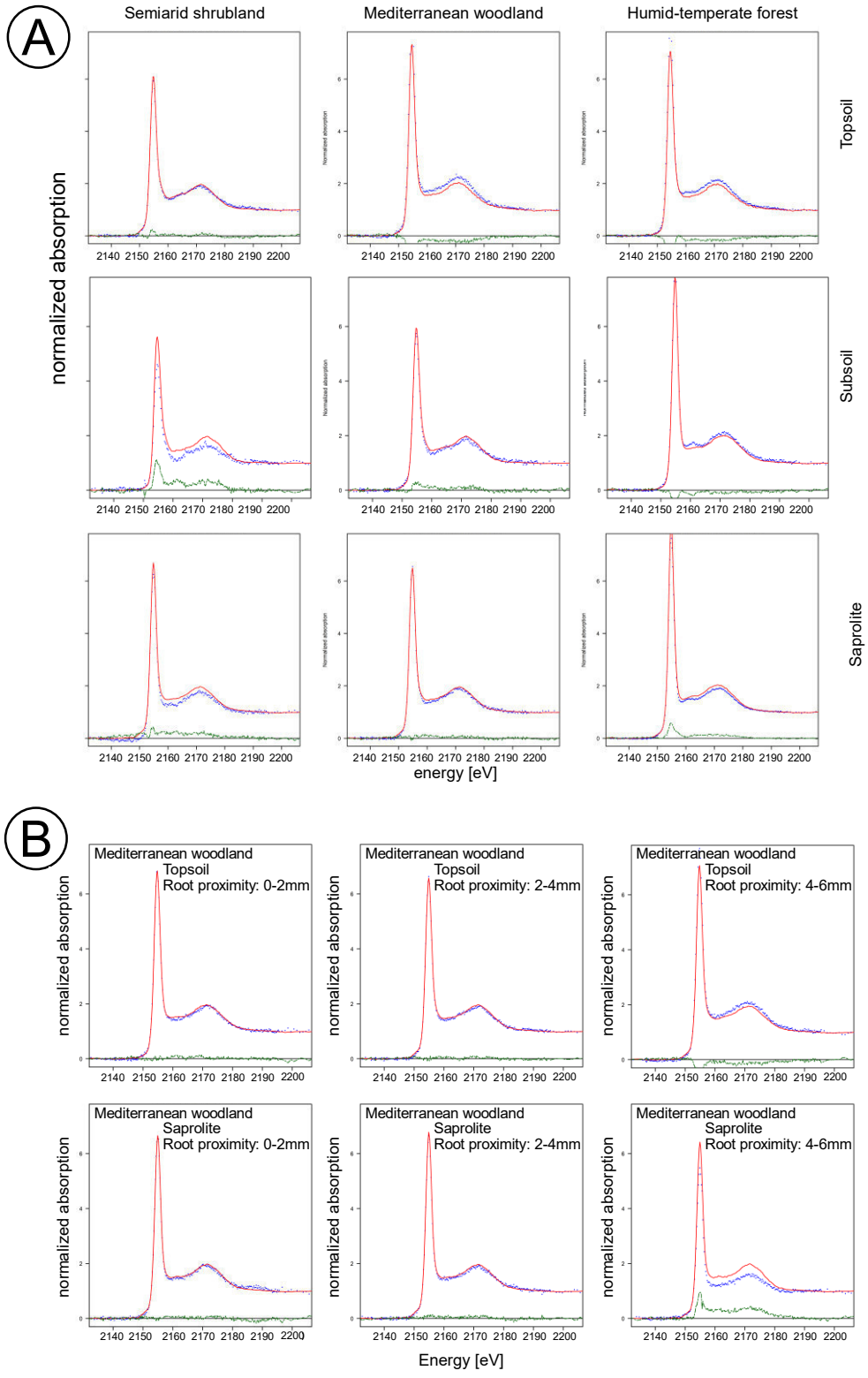

Figure: S 2.2.1: Exemplary phosphorus K−edge X−ray absorption near edge structure spectroscopy (XANES) spectra along the ecosequence (A) from all three soil depths (distance 0−2 mm from roots) and (B) from the Mediterranean woodland in topsoil, and saprolite for all three distances from roots (0−2 mm, 2−4 mm, and 4−6 mm). Black dots represent the measured data, the red curve is the best fit chosen by the lowest R factor. Green dots show the residual from the data to the fit (R−factor).

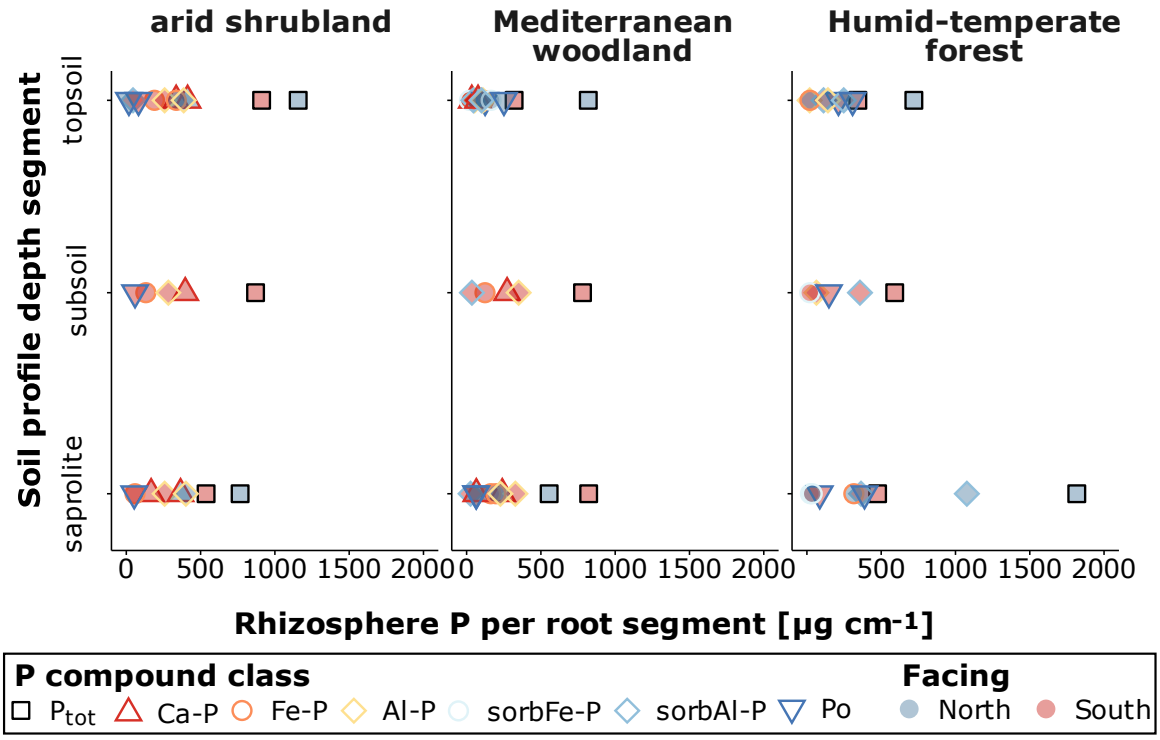

Figure: S 2.2.2: Pools of rhizosphere P per root segment (total P, calcium–phosphates (Ca–P), Fe– and Al–phosphates (Fe–P, Al–P), orthophosphates sorbed to Fe– and Al–(oxy)hydroxides (sorbFe–P, sorbAl–P), and organic P (P_o) were calculated for a cylinder around roots. Contents in each distance to the root were converted to rhizosphere P per root length by multiplying with bulk density and the respective volume of the cylinder sheathing the root. Average root thickness was set to 2 mm. For the arid shrubland ('shrubland'), Mediterranean woodland ('woodland'), and humid–temperate forest ('forest'). In each site for the topsoil, subsoil, and saprolite.

2.3. Microbial mobilization and utilization of sorbed inorganic phosphorus in soils of granodioritic origin formed under hyperarid to humid–temperate climate (Study 2)

Authors: Moritz Koester[1,2], Michaela A. Dippold[2], Yue Hu[2,3], Werner Häusler[4], Francisco Matus[5,6], Francisco Nájera[7,8], Svenja C. Stock[2,9], Sandra Spielvogel[10]

[1]Instiute of Geography, University of Bern, Bern, Switzerland

[2]Biogeochemistry of Agroecosystems, University of Goettingen, Goettingen, Germany

[3]Genebank Department, Leibniz Institute of Plant Genetics and Crop Plant Research (IPK), Rostock, Germany

[4]Research Department Ecology and Ecosystem Management, Chair of Soil Science, Technical University of Munich, Freising, Germany

[5]Laboratory of Conservation and Dynamic of Volcanic Soils, Universidad de La Frontera, Chile

[6]Network for Extreme Environment Research, NEXER–Chile, Universidad de La Frontera, Chile

[7]Department of Chemical Sciences and Natural Resources, Universidad de La Frontera, Chile

[8]Faculty of Agricultural Sciences, Universidad de Chile, Santiago, Chile

[9]Institute of Geography and Geoecology, Karlsruhe Institute of Technology, Karlsruhe

[10]Institute for Plant Nutrition and Soil Science, Christian–Albrechts University Kiel, Kiel, Germany

Corresponding author:

Moritz Koester
Affiliations: Biogeochemistry of Agroecosystems, University of Goettingen, Goettingen, Germany.
Adress: Buesgenweg 2, 37077 Goettingen
E–mail: moritzkoester@posteo.de
Tel: +49 551 39–33519

2.3.1. Abstract

Phosphor (P) sorption in soil is a multivariate process strongly dependent on soil mineralogy, organic carbon (C) content, free surface area, and pH, all of which are influenced by climate. This study aimed to examine differences in inorganic P sorption capacity of four soils along an aridity gradient and, subsequently, microbial P utilization. To investigate the differences in inorganic P sorption capacity and microbial P uptake, a combined approach of an ^{33}P isotope-exchange kinetics determination, and a consecutive laboratory incubation experiment were conducted. The experimental setup included a subset of mesocosms in the incubation experiment, which received a defined amount of glucose to simulate root exudation and supply microorganisms with labile C required to fuel P mobilization mechanisms.

P sorptivity was highest in the hyperarid and humid site. The large sorption capacity of the hyperarid site was associated with calcium carbonates and elevated clay content compared to an arid and Mediterranean site. At the humid site, high P sorptivity coincided with high contents of clay, total organic carbon, oxalate extractable aluminum, ferrihydrite, and a large free surface area. Microbial inorganic P uptake was below the detection limit in the hyperarid desert and highest in the Mediterranean woodland soil. The results indicate P limitation of microbial growth in the hyperarid desert's topsoil, possibly due to high $CaCO_3$ content. Isotopic dilution of desorbable P in the humid-temperate forest soil, likely by mineralized organic P, indicated highest importance of organic P for microbial P nutrition. At the Mediterranean site, microbial P mobilization was C limited, as indicated by enhanced microbial utilization of sorbed inorganic P under glucose addition. This study provides an insight in P sorption and microbial P utilization processes in soils from similar parent material but with different weathering history due to disparities in historical and present climate. The results imply that P cycling processes are highly site specific and consequences of changing climate on P cycling cannot be predicted by linear means.

Keywords: isotope techniques; soil mineralogy; Fe speciation in soil; soil incubation studies; microbial phosphorus (P) cycling in soil; climate dependent phopshorus (P) adsorption in soil

Highlights:

- P sorption is highest in soils under arid and humid climate.
- Microbial utilization of sorbed inorganic P is highest under Mediterranean climate.
- Under arid and Mediterranean climate microbial P utilization is C-limited.
- Under humid climate organic P is utilized and C limitation is relieved

Conceptual Figure:

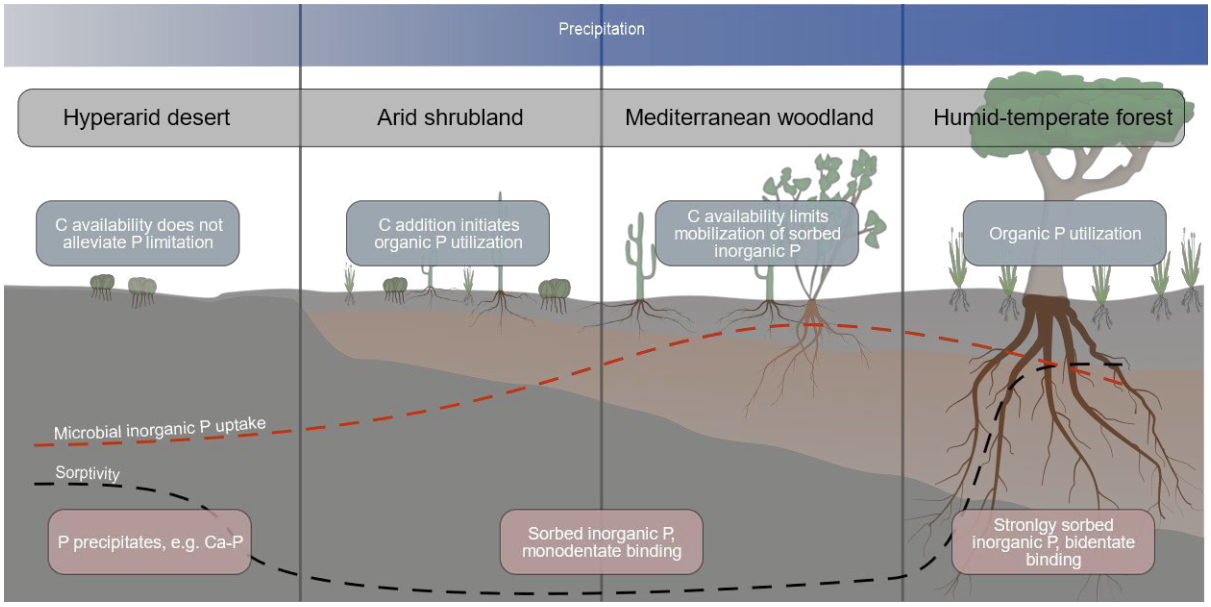

Figure 2.3.1: Conceptual Figure for study 2.

2.3.2. Introduction

Phosphorus (P) is an essential nutrient in all ecosystems and important for the cellular energy cycle (Marschner and Marschner, 2012). Unlike other macronutrients, the availability of P is highly dependent on soil type and status of pedogenesis. In natural ecosystems, the availability of P is determined by two factors: i) the initial content in the parent material and ii) the immobilization by secondary minerals and weathering products, i.e., the speciation of pedogenic sesquioxides and the surface area available for sorption processes (Vitousek and Farrington, 1997; Walker and Syers, 1976). P mobility in most soils is low because of rapid sorption to positive charged surfaces of sesquioxides and organo–mineral complexes or precipitation with polyvalent cations (Gerke and Hermann, 1992; Sims and Pierzynski, 2005; Violante and Pigna, 2002). While initial adsorption is fast, strong sorption to minerals requires longer times to manifest. Short–range order minerals are particularly important for strong sorption processes. In some cases, e.g., in soils with andic properties or otherwise highly reactive sesquioxides, this sorption can even be irreversible (Okajima et al., 1983). Data on the types of sesquioxides in a soil therefore not only allow conclusions to be drawn about rapid sorption processes, but also about the long–term availability of P (Gérard, 2016). The speciation of iron (Fe) and aluminum (Al) in soils depends on both, the parent material and weathering processes controlled by past and present climatic conditions. Water availability and temperature are among the main abiotic drivers of weathering processes (Goudie and Viles, 2012; Wu et al., 2013). Mean annual precipitation (MAP) and mean annual temperature (MAT) influence vegetation (cover and composition), soil pH, and total soil organic carbon (TOC)

content, which are important biological and physicochemical parameters for mineral weathering and formation of secondary sesquioxides.

Plant P availability is determined by sorption strength to the soil solid phase on the one hand and the capacity of microorganisms to solubilize P on the other hand (Richardson and Simpson, 2011). For biota's P nutrition, inorganic P, weakly adsorbed to the soil solid phase is a critical parameter to determine P availability in a soil. This is because if P from the soil solution is taken up by biota it is replenished by P weakly adsorbed to the soil's solid phase. Due to the strong immobilization by sorption in many soils, the P content in these soils is high, but the P availability is low. This distinct behavior of P requires adaptations of organisms to mobilize P. Microorganisms are known to modify chemical conditions in soil to mobilize inorganic P, for example by acidification and exudation of chelating compounds (Richardson and Simpson, 2011). It has been shown that biological P acquisition strategies are an ecosystem property and depend largely on climatic conditions (Koester et al., 2021). Microorganisms play a crucial role in P mobilization and liberation for subsequent plant uptake (Spohn and Kuzyakov, 2013). Microbial P uptake in bulk soil represents the basal biotic P mobilization as it is not influenced by (seasonal) input of labile root–derived carbon. In contrast, the rhizosphere provides a spatially constrained environment where biochemical energy in the form of low molecular compounds (covering a substrate spectrum from carbohydrates to organic acids) is provided to microorganisms and used as energy source to utilize P pools that would otherwise not be accessible. Understanding microbial inorganic P mobilization and uptake in an ecosystem, therefore, is a prerequisite to infer P availability to plants. The capacity of microorganisms to actively access the pool of sorbed inorganic P may be an indicator for the P limitation in an ecosystem (Pistocchi et al., 2018).

This study was carried out with soils collected along an ecosequence comprising four study sites in the Chilean Coastal Cordillera. The ecosystems under study were a hyperarid desert in the north an arid shrubland and Mediterranean woodland in central Chile and a humid–temperate forest in the south all developed on the same parent material. This study setup allowed us to study microbial inorganic P uptake in soils which are largely different in their mineralogy, C content and quality, pH, and other climate dependent variables. As the soils of the ecosequence originate from the same parent material, differences in soil mineralogy can be related to different climatic conditions under which the respective soil developed. It remains to be studied how altered carbon availability affects the microbial ability to mobilize P from the soils in the ecosystems studied and, furthermore, how microbial uptake of inorganic P adsorbed to the soil's solid phase differs as a function of the climatically determined mineralogy.

We hypothesize that (I) the sorption capacity along the ecosequence will be highest in the humid ecosystem, which contains the highest amount of pedogenic Fe– and Al– minerals, and gradually declines towards drier ecosystems. (II) Microbial uptake of inorganic P will be highest in the hyperarid desert ecosystem, due to high contents of inorganic P and low P sorptivity in the soil. (III) The addition of glucose will lead to an increased uptake of inorganic P in all ecosystems, as the input of readily available C stimulates P mobilization mechanisms such as organic acid exudation.

To test the hypotheses, two sequential laboratory studies were conducted. First the sorption of P to the soil's solid phase was determined by measuring P isotope–exchange kinetics (IEK). P has only one stable isotope (^{31}P) and two radioactive isotopes (^{32}P and ^{33}P) which do not occur in nature and can only be produced artificially. The radioactive isotopes have half–lives of less than a month. Therefore, short–term batch observations with radioactive P isotopes, to determine P IEK of sterile soils, are an excellent opportunity to measure abiotic P sorptivity of soils (Fardeau, 1993; Lopez–Hernandez et al., 1998). The ^{33}P labeled soil for the incubation experiment was also prepared by adsorbing P to sterilized soils. With the incubation experiment we pursued the goal to determine microbial P mobilization and incorporation, depending on climate driven soil mineralogy. Furthermore, we created rhizosphere–resembling conditions in half of the mesocosms by adding glucose to imitate the input of labile C by roots and determine its effect on microbial P mobilization.

2.3.3. Material and Methods

Study sites and sampling

The geological properties of all sites were described by Bernhard et al. (2018) and Oeser et al. (2018). Basic parameters of the soils are shown in . Mean annual precipitation of the four sites increases from north to south from 12 mm y^{-1} in the hyperarid desert, to 66 mm yr^{-1} in the arid shrubland, 367 mm yr^{-1} in the Mediterranean woodland, and 1469 mm yr^{-1} in the humid–temperate forest. Mean annual temperature decreases with increasing precipitation from 16.8 °C in the hyperarid desert, 13.7 °C in the arid shrubland, 14.1 °C in the Mediterranean woodland to 6.6 °C in the humid–temperate forest (Bernhard et al., 2018).

Samples were collected at each site from a south facing soil profile in midslope position. About 2 kg well mixed soil from A and B horizon were taken per site. Soils were air dried directly after sampling and roots were removed after soils were sieved to < 2 mm. About 250 g of soil from each site and horizon were sterilized by γ–irradiation (min. 50 kGy, STERIS, Radeberg, Germany) to be used in the IEK measurement.

Table 2.3.1: Basic soil parameter of the four study sites along the aridity gradient: hyperarid desert, arid shrubland, Mediterranean woodland, and humid–temperate forest ecosystem. Mean annual precipitation (MAP) and mean annual temperature (MAT) are taken from Fick and Hijmans (2017). Climate classification from Moreira-Munoz (2011) and Owen et al. (2011). Vegetation-, soil type, pH, and grain size classes are derived from Bernhard et al. (2018a, 2018b). Free surface area and iron (Fe) speciation were measured as part of the present study. The abbreviations for the Fe species are: Fe_{Si} for silicate bound Fe, Fe_{FH} for ferrihydrite, Fe_{GOE} for goethite, and Fe_{HM} for hematite and magnetite together.

Site	MAP[a]	MAT[a]	Climate[b,c]	Vegetation[d]	Soil-type[d]	pH[d]	Al_{ox}[d]	TOC	Sand[d]	Silt[d]	Clay[d]	Free surface area	Fe_{Si}	Fe_{FH}	Fe_{GOE}	Fe_{HM}
	[mm]	[°C]					mg g^{-1}	%	%	%	%	m^2 g^{-1}	%	%	%	%
Hyperarid desert	12	16.8	Arid	Biocrusts, small desert shrubs	Regosol	8.13	260	0.21	64	24	12	4.8	10.8	0.0	88.4	1.7
						8.28	221	0.16	81	11	8	5.3	8.6	0.0	91.4	0.7
Arid shrubland	66	13.7	Semi-arid	Sclerophyllous shrubs, cacti	Cambisol/ Leptosol	6.4	317	0.49	77	15	8	5.9	35.1	15.0	1.3	21.4
						6.3	218	0.22	73	14	11	13.0	49.3	10.5	4.3	18.8
Mediterranean woodland	367	14.1	Mediterr-anean	Deciduous forest, sclerophyllous shrubs	Cambisol	5.5	535	2.74	73	18	10	3.5	43.5	10.3	11.1	13.8
						5.0	447	0.26	78	13	9	5.4	48.5	12.1	8	12.7
Humid-temperate forest	1469	6.6	Humid	Coniferous forest	orthodystric Umbrisol/ umbric Podzol	4.3	10^4	7.92	56	21	23	18.7	41.8	29.3	5.5	7.0
						4.6	4741	0.66	82	11	7	26.6	52.6	20.6	12.9	2.9

a) (Fick, 2017)

b) (Muñoz et al., 2007)

c) (Owen et al., 2011)

d) (Bernhard et al., 2018a, 2018b)

Experimental Setup

In this study, two sequential experiments were conducted. First, the soils' sorption capacity for P was determined in an IEK experiment. With the IEK experiment the P pool (de)sorbable solely by physicochemical processes were determined. Moreover, the observed sorption kinetics allowed to analyze the underlying sorption processes (Randriamanantsoa et al., 2015). The ^{33}P labeled soil of the IEK experiment was mixed with unlabeled soil and used in an incubation study to determine microbial inorganic P uptake. In addition to analyzing basal microbial P mobilization in the incubation experiment, conditions in the rhizosphere were mimicked by adding glucose to a subset of mesocosm (Landi et al., 2006).

Isotope–exchange–kinetics

For the IEK study, a mixture of 1 g of sterile soil with 10 g double distilled water (ddH_2O) was placed on a shaker and allowed to equilibrate for 16 h. At the start of the experiment, 35 kBq g^{-1} of ^{33}P suspended in 100 µl 0.1 M $H_3PO_4^-$ solution (carrier solution) was added to the soil. Aliquots of 1 ml were taken from the suspension at 1, 5, 10, 30, 70, and 100 minutes after addition of the tracer. Samples were centrifuged at 20,000 g for 2 minutes to stop the sorption process immediately after aliquots were taken. The supernatant was transferred to a fresh vial, and the centrifugation was repeated. Three replicates per sampling time were measured. The radioactivity in solution was measured on a scintillation counter (HIDEX 300 SL, Hidex Deutschland Vertrieb GmbH, Germany). IEK were obtained by fitting a curve according to Equation 2.3.1 to the measured radioactivity (Bünemann, 2015).

$$\frac{r(t)}{R} = \mathrm{m} * \left(t + m^{\frac{1}{n}}\right)^{n} + \frac{r_{inf}}{R} \qquad \text{Equation 2.3.1}$$

Where r(t)/R is the ratio of radioactivity remaining in soil solution after the time t and the total added radioactivity (relative specific activity), and r_{inf}/R is the ratio of radioactivity at the end of the IEK study and the total radioactivity added to the soil. Parameters *m, n,* and r_{inf} were determined by the fit and used in the later analysis.

Incubation experiment

The same procedure as described for the IEK study, without sampling individual time points, was done to prepare ^{33}P labeled soil for the incubation study (three times 80 g soil and 400 ml ddH_2O per soil horizon). For the incubation study, unsterile soil from A and B horizons was pre–incubated for 14 days at 15 °C and at 42% of water holding capacity (WHC). The pre–incubated soils were mixed with the ^{33}P labeled sterile soil in a ratio of 7:1 (unsterile:sterile, w:w). The homogenized soil was then filled into a plastic ring (diameter of 5 cm and a volume

of 100 cm³) mounted on a ceramic plate. A weight of 1.5 kg was used to apply a defined pressure (≈7500 N m^{-2}) via a stamp to equalize bulk density of samples from the same site and horizon. The installation was placed in a sealed jar with a sand covered bottom. A quantity of water corresponding to 50% of WHC was applied to the soil from top. An additional 5 ml were added to the sand layer at the bottom of the mesocosms to saturate the soil through the ceramic plate to field capacity (100% WHC) (mesocosm preparation as in Apostel et al. (2017) and Najera et al. (2020)). A schematic experimental setup is shown in Figure: S 2.3.1. The incubation study run for 25 days with the first sampling after mixing the sterile and unsterile soil (t=−5), the second sampling time at the day of glucose addition (t=0), and subsequent sampling times 2, 7, and 20 days after the addition of glucose (t=2, t=7 and t=20). Four replicate mesocosms were prepared per harvesting time point and treatment. Half of the mesocosms from all sites and horizons received glucose on day 5 after the start of the incubation. The amount of glucose corresponded to 50 % of the respective mass of microbial biomass carbon (C_{mic}) as determined by DNA contents described in Koester et al. (2021).

Laboratory analyses

Microbial biomass phosphor (P_{mic}) and microbial biomass carbon (C_{mic})

From an aliquot of 3−5 g from each mesocosm microbial biomass phosphor (P_{mic}) was extracted by hexanol−resin fumigation following the protocol of Bünemann et al. (2016), which is a modification of the method published by Kouno et al. (1995). To correct for sorption of P during extraction, aliquots were spiked with $H_3PO_4^-$ solution, with an amount of P in the range of the expected P content of fumigated samples. Total inorganic P in the extracts of fumigated and unfumigated samples was determined photometrically by the malachite green method (Ohno and Zibilske, 1991). The ^{33}P content in the extract of fumigated and unfumigated samples for P_{mic} determination was measured by adding 8 ml of scintillation cocktail (Rotiscint eco plus, Carl Roth GmbH & co. KG, Karlsruhe, Germany) to 3 ml of the extract and mixing in a plastic vial. Quantification was done with a scintillation counter (HIDEX 300 SL, Hidex Deutschland Vertrieb GmbH, Germany).

P_{mic} was calculated according to Equation 2.3.2 for the stable isotope ^{31}P and the radioactive isotope ^{33}P.

$$P_{mic} = (P_{hex} - P_{resin})/\alpha \qquad \text{Equation 2.3.2}$$

P_{hex} and P_{resin} are the ^{31}P and ^{33}P concentrations of the hexanol−fumigated and unfumigated extract, respectively. The factor α is given by the recovery of the spiked P (Equation 2.3.3), where

P_{spike} is the concentration of ^{31}P in the spiked sample and P_{added} is the amount of ^{31}P initially added to the spiked sample.

$$\alpha = \frac{\sum P_{spike} - \sum P_{resin}}{n} / P_{added} \quad \text{Equation 2.3.3}$$

Inorganic P taken up from the ^{33}P labeled pool at the soil solid phase was calculated by Equation 5.

$$P_{uptake} = \frac{^{31}P_w}{^{33}P_w} * {}^{33}P_{mic} \quad \text{Equation 2.3.4}$$

$^{31}P_w$ and $^{33}P_w$ are the concentrations of the respective isotope of P in the unfumigated sample and $^{33}P_{mic}$ is the radioactivity taken up by the microbial biomass following from Equation 2.3.2. Equations 2, 3 and 4 are taken from Bünemann et al. (2016). We also calculated the ratio of P_{resin} from the P_{mic} extracts to the equilibrium concentration of P in soil solution without biological activity (C_p) from the IEK experiment. C_p was measured at the end of the IEK study after 45 h of isotopic exchange. The ratio was used to infer P uptake efficiency of plants and microorganisms from the soil solution.

Microbial biomass carbon (C_{mic}) was extracted from each timepoint and horizon as chloroform fumigated microbial biomass carbon following the procedure of Vance et al. (1987). Extracts were stored at −20 °C until analysis of total C concentration at a TOC/TIC analyzer (Multi N/C2100, Analytik Jena, Germany). C_{mic} was calculated by subtracting the C concentration of the non−fumigated sample from the fumigated one and applying a correction factor of 0.45 (J. Wu et al., 1990).

Microbial biomass nitrogen (N_{mic}) values were taken from (Stock et al., 2021). Microbial element ratios (C_{mic}:N_{mic}, C_{mic}:P_{mic}, N_{mic}:P_{mic}) were calculated as averages over all time points in each site, horizon, and treatment, respectively (Table 2.3.2). Microbial elements stoichiometry serves to identify possible growth limitations of microorganisms by one element.

Microbial respiration

Microbial respiration over the course of the experiment was assessed by CO_2 traps which consisted of a plastic tube containing 5 ml of 0.5 mol l^{-1} NaOH. A trap was placed in each of the mesocosms that were harvested at the end of the experiment and replaced every 3 – 5 days (time between CO_2 sampling was reduced after glucose addition as this was expected to increase the CO_2 flux). CO_2 respired by microorganisms was measured with a non−dispersive

infrared (NDIR) gas analyzer (TOC 5050, Shimadzu Corporation, Kyoto, Japan). For this, 0.4 ml of each CO_2 trap was diluted 1:10 (v:v) with ddH_2O.

Calculating long− and short−term exchangeable P

Inorganic P exchangeable within one minute (E_1) was calculated using Equation 2.3.5 (Fardeau, 1993).

$$E(t) = 5 * C_P * \frac{R}{r(t)} \qquad \text{Equation 2.3.5}$$

For E(1), the radioactivity in soil solution after one minute from the IEK experiment was used. The factor 5 corrects for the ratio of soil:solution to obtain values in µg g^{-1} soil. Values for exchangeable P within 25 days (intermediate timescale) and total exchangeable P (calculated by inserting r_{inf} for r(t)) are given in Table: S 2.3.1.

Soil mineralogy parameters

The total "free surface area" (Chiou et al., 1990) was measured according to the method described by Brunauer et al. (1938). It serves as one parameter determining the sorption capacity for P in soil. The method determines the amount of N_2 that is adsorbed to a soil sample. A free surface area was calculated from the N_2−soil sorption.

Fe speciation in soils was measured by Moessbauer spectroscopy. Samples were ball milled at 200 rpm for 2 min to obtain a homogenous powder. Spectra reported here were recorded at 4.2 K. Least square fit of the data was done by the PC−Mos II software (Fast Comtec GmbH, Oberhaching, Germany) using appropriate superpositions of Lorentzian lines grouped into quadrupole doublets or magnetic sextets. Some components of the spectra were fitted with Voigt line shapes, which were calculated by summing over many sextets with Lorentzian lines corresponding to Gaussian distributions of magnetic hyperfine fields (Filimonova et al., 2016).

The method allows to distinguish between Fe^{II+} and Fe^{III+} integrated in silicate minerals (Fe_{Si}) and four Fe−(hydr)oxides: ferrihydrite (Fe_{FH}), goethite (Fe_{GOE}), hematite, and magnetite (grouped for results as Fe_{HM}). Clay content, total organic carbon, pH, and oxalate extractable Al are taken from Bernhard et al. (2018).

The contribution of clay minerals to P sorption capacity is accounted for by using the content of clay sized particles in the soils. The influence of pedogenic Al−(hydr)oxides is evaluated by oxalate extractable Al. Both data sets are taken from Bernhard et al. (2018)

Statistics

All statistics were done in the language R (R Core Team, 2017) using the graphical user interface R Studio (RStudio Team, 2018). The fitting to the data points from the IEK study to obtain the parameters *m*, *n*, and *inf* of the sorption kinetics was done using the *nls* function from the 'stats' package (R Core Team, 2017). The 95% confidence interval of the fit was calculated by the function *predictNLS* from the package 'propagate' (Spiess, 2018).

To investigate the complex interplay between soil properties and sorption kinetics, radar charts were calculated (Figure 2.3.3). They depict relative values of explaining variables for P sorptivity in the soils. Relative values were obtained by dividing each value by the highest value in all samples of each variable. The following variables were considered to determine P sorption capacity: free surface area 'Area', oxalate leachable Al 'Al_{ox}', percentage of goethite in total Fe 'Fe_{GOE}', percentage of ferrihydrite in total Fe 'Fe_{FH}', percentage of hematite and magnetite in total Fe 'Fe_{HM}', percentage of silicate bound Fe in total Fe 'Fe_{Si}', $CaCO_3$ content in the soil '$CaCO_3$', percentage of clay in all grain sizes below 2 mm 'Clay', and total soil organic carbon 'TOC'. We calculated the sorptivity for each soil as the inverse of the theoretical value of radioactivity remaining in soil solution at completed isotopic exchange (r_{inf}) divided by the total radioactivity added to the soil (R; r_{inf}/R was determined by the fit). Statistical differences between treatments (reference vs. glucose addition) and sites were investigated by an analysis of variance (ANOVA), using the function *aov* from the package 'stats'.

2.3.4. Results

Free surface area and Fe mineralogy

The free surface area was 4.8 $m^2\ g^{-1}$ and 5.3 $m^2\ g^{-1}$ in the hyperarid desert's, 6.0 $m^2\ g^{-1}$ and 13.0 $m^2\ g^{-1}$ in the arid shrubland's, and 3.5 $m^2\ g^{-1}$ and 5.4 $m^2\ g^{-1}$ in the Mediterranean woodland's A and B horizons, respectively. The free surface area was very similar between these sites and horizons except of the arid shrubland's B horizon, which was more than twice as high as the A horizon in the arid shrubland (). The free surface area in the humid–temperate forest soil was in the A horizon 5.4 times (18.7 $m^2\ g^{-1}$), in the B horizon 4.9 times (26.64 $m^2\ g^{-1}$) higher than in the adjacent Mediterranean woodland soil.

Moessbauer spectroscopy revealed that most of the Fe in the hyperarid desert soil was goethite (88% and 91% for A and B horizon, respectively). The rest was mainly bound in silicate minerals (Fe_{Si}). The arid shrubland soil showed high contents of Fe_{Si} (35% and 49% for A and B horizon, respectively). The remaining Fe was mainly ferrihydrite (15% and 11% for A and B horizon, respectively), and magnetite (18% and 17% for A and B horizon, respectively). In the Mediterranean woodland and humid–temperate forest, 40–50% of the Fe were bound in

silicates (Fe_{Si}). The Mediterranean woodland soils contained approximately 10% of ferrihydrite and goethite in both horizons, about 5% of hematite and 8% of magnetite. In the humid–temperate forest, the amount of ferrihydrite was highest among all sites (29% and 21% for A and B horizon, respectively). Goethite constituted 6% of total Fe in the topsoil and 13% in the subsoil, while hematite had only a share of less than 3%, and magnetite 4% and 2% in A and B horizon, respectively.

Sorption kinetics

P sorption capacity of sterile soils decreased from the hyperarid desert to the arid shrubland and the Mediterranean woodland but increased sharply again towards the humid–temperate forest (Figure 2.3.2) P sorptivity of the soil in the hyperarid desert was weaker in the B horizon (36%) than in the A horizon (65 %). The soil from the B horizon of the arid shrubland adsorbed only 25% of the added tracer, while in the A horizon 35% was adsorbed, same as in both horizons of the Mediterranean woodland. P sorptivity was highest in the humid–temperate forest soil (>98% in both horizons). Another parameter for P availability in soils is the amount of P that is exchangeable, i.e., sorbed to the soil within 1 min (E_1) (Table: S 2.3.1 and Figure: S 2.3.2). The amount of E_1 in the B horizon of the humid–temperate forest soil is significantly higher than all others. E_1 was lowest in the A horizon of the hyperarid desert soil.

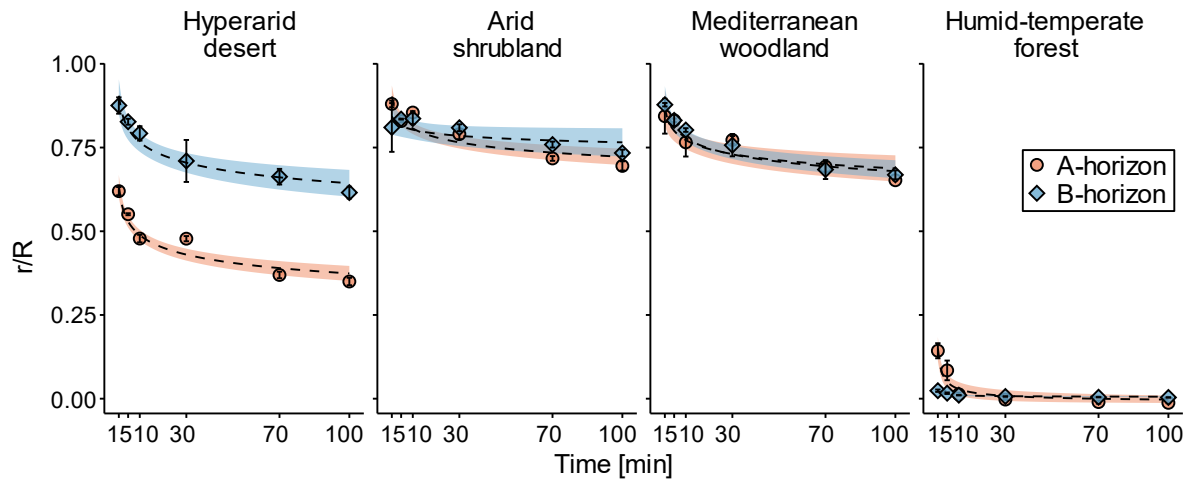

Figure 2.3.2: Sorption kinetics derived from a short–term batch experiment, measuring isotope–exchange kinetics (IEK) of ^{33}P in the soil solution for the hyperarid desert, arid shrubland, Mediterranean woodland, and humid–temperate forest, each for A– (green) and B horizon (orange), respectively. The y–axis depicts the ratio of radioactivity remaining in solution (r) to the total added radioactivity (R). The IEK experiment lasted 100 minutes. Whiskers indicate the standard errors of the mean. The dashed line is the product of a curve fitting, the light ribbon around each curve represents the 95 % confidence interval of the fit.

Figure 2.3.3 gives an overview over variables that possibly influenced P sorption in soil (Area, Al_{ox}, Fe_{GOE}, Fe_{FH}, Fe_{HM}, Fe_{Si}, $CaCO_3$, Clay, TOC). Sorption capacity was highest in the two endmembers of the aridity gradient, the hyperarid desert and the humid–temperate forest. The

hyperarid desert was the only site in which $CaCO_3$ was detected and it was found in both horizons. Furthermore, most of the Fe was goethite, as well in both horizons. Despite a relatively high sorptivity the free surface area at this site was low. The soils with low P sorption capacity in the arid shrubland and the Mediterranean woodland were characterized by low free surface area, low clay content, high proportions of Fe being bound in silicates, hematite, and magnetite. The humid–temperate forest was the site with the highest sorption capacity, it showed high TOC, large free surface area, high clay content, and a great amount of short–range order Al– and Fe minerals (oxalate soluble Al and ferrihydrite), but also silicate bound Fe in the A horizon. The B horizon, which had an even higher sorptivity than the A horizon, was characterized by large free surface area, and silicate bound Fe, but intermediate contents of clay, ferrihydrite, and oxalate soluble Al.

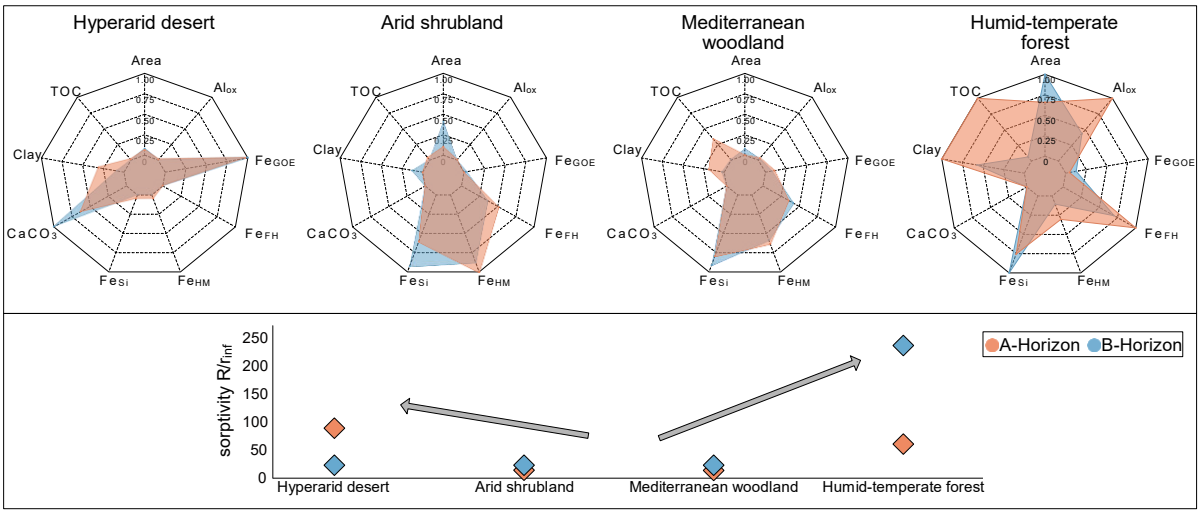

Figure 2.3.3: Radar charts of variables determining P sorption (upper part) and P sorptivity (lower part) for the hyperarid desert, arid shrubland, Mediterranean woodland, and humid–temperate forest, for the A and B horizons at each site. The depicted variables are (from top clockwise): Free surface area 'Area' (27 $m^2\ g^{-1}$), oxalate leachable Al 'Al_{ox}' (10589 mg kg^{-1}l), percentage of goethite in total Fe 'Fe_{GOE}' (91%), percentage of ferrihydrite in total Fe 'Fe_{FH}' (29%), percentage of hematite and magnetite in total Fe 'Fe_{HM}' (21%), percentage of silicate bound Fe in total Fe 'Fe_{Si}' (53%), $CaCO_3$ content in the soil '$CaCO_3$' (12%), percentage of clay in all grain sizes 'Clay' (27%), and total organic carbon 'TOC' (8%). Numbers in parentheses represent maximum values of the respective variable among all sites and horizons. The measured variables were normalized to the respective maximum value of all measurements of that variable. The lower part of the figure shows the sorption strength of the soils as the inverse of the radioactivity remaining in soil solution at steady state (calculated from the isotope–exchange kinetics determination (batch experiment)) divided by the total radioactivity added to the soil for the isotope–exchange kinetics determination. Grey arrows in the lower figure highlight the trend of increasing sorption strength towards the most arid and most humid study site.

Microbial biomass C and microbial element ratios

Irrespective of C amendment, the C_{mic} content in the A horizons increased along the aridity gradient towards more humid climate (Figure 2.3.4). During the experiment, the C_{mic} content fluctuated only slightly in samples that received no glucose, with exception of the subsoils of the hyperarid desert and Mediterranean woodland. The daily respired CO_2 varied even less between sampling times in the reference samples, with exception of the B horizon in the

humid–temperate forest (Figure: S 2.3.3). This corroborates the boundary assumption of steady state conditions in the non–glucose treatment during the experiment. A positive effect of glucose addition on microbial biomass C contents was statistically significant at sampling time 7 in all soils except in the arid shrubland (Figure 2.3.4). The effect of glucose addition on microbial biomass C decreased after sampling time 7 in all soils.

The C_{mic}:P_{mic} and N_{mic}:P_{mic} ratios without the addition of glucose first were wider with decreasing aridity, reaching their maxima in the Mediterranean woodland's A horizon, and decreasing again to the humid–temperate forest. The C_{mic}:N_{mic} ratio showed a less clear trend over the gradient. Glucose addition did not affect microbial stoichiometry in soils from the hyperarid desert and the arid shrubland. In the A horizon of the Mediterranean woodland, C_{mic}:P_{mic} and N_{mic}:P_{mic} ratios decreased by a factor of about 10, when glucose was added. In the humid–temperate forest soil, the C_{mic}:P_{mic} ratio became wider by factors of 3.8 and 2.2 after glucose addition, and the N_{mic}:P_{mic} ratio widened by factors of 3.3 and 2.0 for the A and B horizons, respectively.

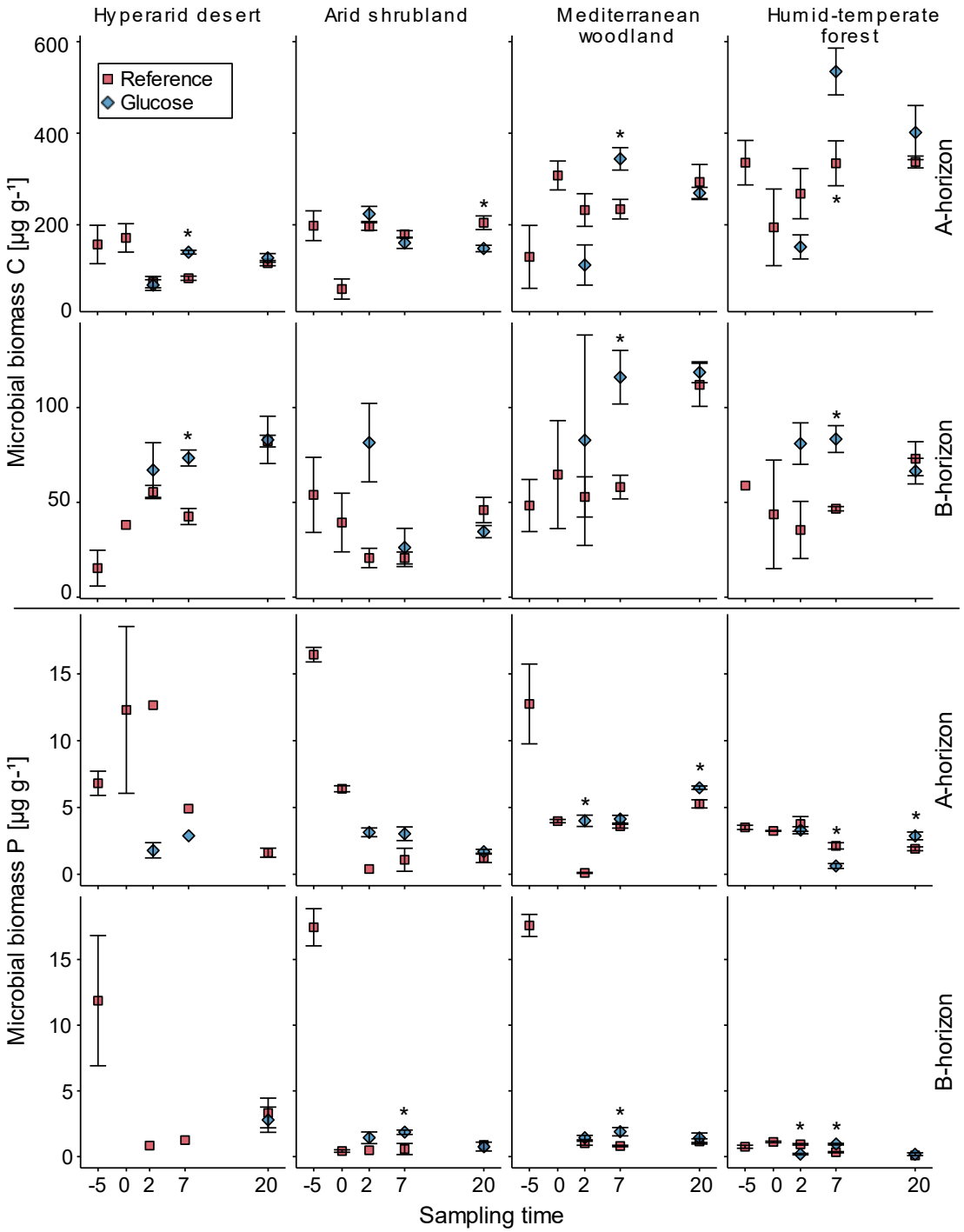

Figure 2.3.4: Microbial biomass carbon (C_{mic}) and microbial biomass phosphorus (P_{mic}) in the hyperarid desert, arid shrubland, Mediterranean woodland, and humid–temperate forest, each in A and B horizon. Red markers show the contents of C_{mic} and P_{mic} without the addition of glucose, blue markers the contents of C_{mic} and P_{mic} from the treatment with glucose addition. The x–axis shows the timeline with the start of the incubation experiment when sterile and non–sterile soil was mixed (–5), the day of glucose addition (0) and sampling times 2, 7, and 20 days after the glucose was added to half of the mesocosms. Error bars indicate standard errors of the mean. Missing data points for P_{mic} are due to P_{mic} contents partly being below the detection limit in the hyperarid desert and problems with the laboratory analysis for sampling point 0 at the Mediterranean woodland's B horizon.

Table 2.3.2: Microbial element ratios as combinations of the microbial contents of C, N, and P (C_{mic}, N_{mic}, P_{mic}) in the hyperarid desert, arid shrubland, Mediterranean woodland, and humid–temperate forest, in each site for the A and B horizon, respectively. Data represent mean values over all time points in the respective site, horizon, and treatment. Mean values are displayed with standard errors. The number in brackets behind the ratio is the number of samples from which the ratio was calculated. In the hyperarid desert the P_{mic} content was often below the detection limit, therefore, in some cases only three replicates were available.

Variable	Treatment	Hyperarid desert		Arid shrubland		Mediterranean woodland		Humid–temperate forest	
		Horizon							
		A	B	A	B	A	B	A	B
C_{mic}:N_{mic}	Reference	5.7±0.7 (20)	19.3±8.3 (13)	6.2±0.5 (16)	25.2±5.9 (11)	7.4±0.6 (19)	9.7±0.8 (15)	7.8±0.8 (17)	31.7±17.2 (12)
	Glucose	8.4±0.4 (11)	19.6±4.2 (9)	5.7±0.3 (12)	13.7±3.5 (9)	9.5±1.2 (9)	9.4±1.8 (11)	10.2±1.3 (10)	13.5±2.5 (12)
C_{mic}:P_{mic}	Reference	34.4±10.4 (11)	34.2±12.7 (3)	187.1±78.2 (15)	93.3±42.1 (11)	480.2±253.0 (17)	60.4±12.2 (15)	117.3±13.2 (18)	156.5±70.9 (11)
	Glucose	48.7±10.2 (3)	33.3±12.2 (3)	73.1±5.7 (12)	218.7±136.2 (10)	52.3±8.1 (12)	73.5±13.0 (11)	447.3±161.3 (11)	347.7±86.6 (10)
N_{mic}:P_{mic}	Reference	5.6±1.1 (11)	2.9±1.1 (8)	18.9±9.1 (15)	2.2±0.7 (12)	51.7±26.1 (17)	6.3±1.9 (15)	16.0±1.5 (19)	12.7±6.6 (11)
	Glucose	5.8±0.9 (3)	3.6±1.7 (3)	12.9±1.0 (12)	19.1±16.4 (12)	5.2±1.3 (12)	9.4±1.7 (12)	52.5±21.0 (11)	25.3±5.5 (10)

Microbial inorganic P uptake

Microbial P uptake from the soil solid phase differed significantly between sites and was affected by glucose addition (Figure 2.3.5). Microbial uptake of inorganic P was below the detection limit in the hyperarid desert soil and peaked in the soil from the Mediterranean woodland ecosystem. Microbial P uptake was always higher in topsoils compared to subsoils at each site. Shortly after mixing the sterilized soil with the microbially–active soil (time point –5), the microbial uptake of inorganic P from A and B horizons was similar between sites with 9.5 mg kg^{-1} and 0.42 mg kg^{-1} in the arid shrubland, 9.8 mg kg^{-1} and 11.4 mg kg^{-1} in the Mediterranean woodland, and 15.4 mg kg^{-1} and 8.6 mg kg^{-1} in the humid–temperate forest, respectively. During the experiment, microbial P uptake increased continuously in the Mediterranean woodland topsoil up to 30.5 mg kg^{-1} at sampling time 20, whereas in the humid–temperate forest topsoil it decreased from the start (15.4 mg kg^{-1}) towards the end of the experiment (3.5 mg kg^{-1}). A significant positive effect of glucose addition on microbial inorganic P uptake was observed in the arid shrubland's A horizon 5 days after glucose amendment. This effect was negative at sampling times 7 and 20 (not significant at sampling time 20). In the Mediterranean woodland soil, glucose addition enhanced microbial P uptake in both horizons, this effect was significant at sampling time 7. Glucose addition did not affect microbial inorganic P uptake in the humid–temperate forest.

Water soluble P extracted by anion–exchange membranes (P_{resin}) was mostly below 10% of the equilibrium concentration of P in soil solution without biological activity (C_p), in the hyperarid desert and Mediterranean woodland soils (Figure: S 2.3.4). The lowest values were observed in the B horizon of the hyperarid desert soil (less than 2%). In the arid shrubland soil, the P_{resin} to C_p ratio was about 1.6 times higher in the A horizon than in the B horizon. In contrast, in the humid–temperate forest soil, the P_{resin} to C_p ratio in the A horizon was only about one third of that in the B horizon. Highest ratios of anion–exchange membrane–extractable P relative to the equilibrium concentration of P without biological activity along the aridity gradient were measured in the B horizon of the humid–temperate forest (up to 69%). In the A horizon of the arid shrubland, Mediterranean woodland, and humid–temperate forest, a significant negative effect of glucose addition on P_{resin} proportions was revealed 2 and 7 days after glucose addition. In contrast, in the B horizon of the hyperarid desert, the P_{resin} proportion under glucose addition was significantly higher than in the sample without glucose addition at the end of the experiment. The P_{resin} proportions in samples from the arid shrubland's and Mediterranean woodland's B horizon 7 days after glucose amendment were significantly lower when glucose was added. In the humid–temperate forest, this was true in both horizons 2 and 7 days after glucose was added.

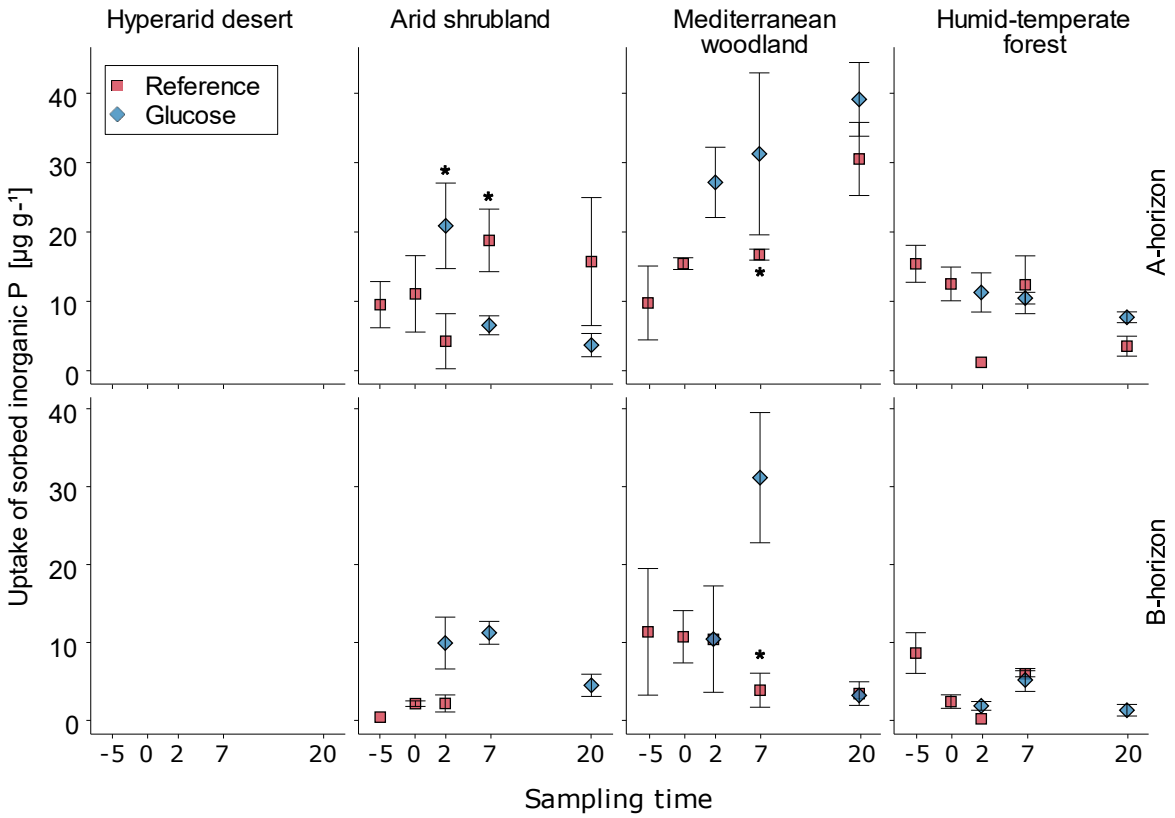

Figure 2.3.5: Phosphorus (P) incorporated in microbial biomass (P_{uptake}) calculated from the amount of ^{33}P in microbial biomass. The figure shows the microbial uptake of sorbed inorganic P for the hyperarid desert, the arid shrubland, the Mediterranean woodland, and the humid–temperate forest, each for the A– and B horizon. Red markers represent the amount of microbially taken up sorbed inorganic P without the addition of glucose (reference), blue markers the values from the treatment with glucose addition (glucose). The x–axis shows the timeline with the start of the incubation experiment when sterile and non–sterile soil was mixed (–5), the day of glucose addition (0) and sampling times 2, 7, and 20 days after the glucose was added to half of the mesocosms. Error bars indicate the standard error of the mean. Due to missing values the data points of reference samples for the arid shrubland B horizon at sampling points 7 and 20 and for the humid–temperate forest B horizon at sampling point 20 are missing. When error bars are missing the datapoint represents the value of a single sample.

Discussion

Sorption kinetics

The sorption of inorganic P to the solid phase can be exclusively attributed to abiotic physicochemical reactions as sterile soil was used in this study. Further, the reverse process of P desorption can be excluded due to the short duration (45 h) of the experiment (Oehl et al., 2001). The most important soil parameters for soil's P sorption capacity are the content and speciation of Al– and Fe–(hydr)oxides, clay content, pH, and free surface area (Achat et al., 2016; Gérard, 2016). P sorption capacity of Fe– and Al–oxides correlates negatively with pH (for a pH range from about 4 to 10; for common clay minerals from about pH 5 to 10) (Gérard, 2016). Along the studied aridity gradient, the pH drops linearly, from 8.1 to 4.3 in the A horizons of the hyperarid desert to the humid–temperate forest ecosystem (). As the sorption capacity is higher in the hyperarid desert (pH 8.1) than in the arid shrubland (pH 6.4) and the Mediterranean woodland (pH 5.5), P sorptivity in the hyperarid desert is controlled by factors other than pH (Figure 2.3.3 and). The free surface area in the A horizon increases linearly along the aridity

gradient. The clay content shows a unimodal distribution with the lowest values in the Mediterranean woodland (9.5% of total size fractions in the A horizon) and higher values in the hyperarid desert (12.1% of total size fractions in the A horizon) and the humid–temperate forest (22.5% of total size fractions in the A horizon). This coincides with higher sorption capacity of sites with high clay content (Figure 2.3.3). In the humid–temperate forest, the higher sorption capacity in the B horizon compared to the A horizon cannot be explained by the clay content, which decreases from the A to the B horizon. It might partly be caused by preferential migration of the smallest clay particles to the B horizon which have a relatively higher surface area. Another explanation would be that the A horizon contains more negatively charged organic compounds which occupy binding sites in the A horizon.

TOC is high in the A horizon of the humid–temperate forest but low in the B horizon at this site and the A horizon of the hyperarid desert, which show the highest P sorption. Therefore, the TOC content is not a good measure for P sorption in the studied soils. In the A horizon of the humid–temperate forest, high TOC values are accompanied by high contents of oxalate extractable Al, which represents short–range order pedogenic Al oxides (Figure 2.3.3). It is likely that organic carbon forms Al–humus complexes in the A horizon of the humid–temperate forest, which are known to provide sorption sites for P (Takahashi and Dahlgren, 2016). This is in accordance with results from another study at the same sites (Koester et al., 2021), who measured highest content of P sorbed to Al–(hydr)oxides in the humid–temperate forest soils and with findings by Helfenstein et al. (2018), who found increasing levels of P Al–oxide–humic complexes along a Hawaiian precipitation gradient from about 500 mm y^{-1} to >3000 mm y^{-1}. It has been shown that soils can exhibit hysteresis in P sorption, i.e., release less P by desorption than was initially adsorbed (Okajima et al., 1983). Villapando and Graetz (2001) found that the strength of the hysteresis effect is strongly positively correlated with oxalate extractable Al, which was abundant in the humid–temperate forest. It is also likely that some volcanic material (allophane, imogolite) was deposited at the humid–temperate forest site and has migrated to the B horizon of this soil. The higher free surface area and the lower clay content in the B horizon than in the A horizon point in this direction (Figure 2.3.3). In fact, P concentration and ^{33}P in the soil solution at the end of the IEK study were at the lower end of the quantifiable range and pointed to a partly irreversible adsorption occurring in the humid–temperate forest soil. This is particularly important in the B horizon, where only 2.4 % of the initially added radioactivity remained in the soil solution after only one minute of adsorption, indicating a kinetically rapid immobilization process. Moreover, in the humid–temperate forest ecosystem. Fe was mostly found in silicate forms (potentially in pedogenic clay minerals) and as ferrihydrite (short–range order mineral) (Figure 2.3.3), both of which are typically formed under conditions of continuous

water supply. The high sorption capacity in the B horizon of the humid–temperate forest cannot be explained by Fe mineralogy alone as the ferrihydrite content is lower than in the A horizon. As mentioned above, the size fractionation of migrating clay particles might favor higher sorption capacity per clay particle in the B horizon. Regardless of the reason for the strong sorption in the humid–temperate forest, it can lead to a strong overestimation of E_1 values (this is the P exchangeable at the soil solid phase within one minute) (Figure: S 2.3.2 and Table: S 2.3.1) for this site, as the calculation (Equation 2) assumes that all P which was sorbed is also desorbable. However, it has been shown that organic substances can compete for sorption sites with P (Achat et al., 2016; Grierson, 1992; Jones and Darrah, 1994). This seems to be the relevant process in the Mediterranean woodland's A horizon, where P sorption is low, but the TOC content is 2.7%, the second highest value in the studied soils (Table 2.3.1).

The high $CaCO_3$ contents in the hyperarid desert likely favored the goethite formation at this site (Blume et al., 2010). $CaCO_3$ and goethite both provide sorption sites for P ions and seem to be the reason for the moderate to strong P sorption in the hyperarid desert. The sorption capacity of goethite is only about one fourth of that of ferrihydrite (Blume et al., 2010), which is consistent with both, the lower sorption capacity, and the lower free surface area of the hyperarid desert soil compared to the humid–temperate forest soil (Figure 2.3.3). The slow kinetics of the strong P immobilization observed at the hyperarid site points towards additional, slow immobilization mechanisms such as, precipitation or co–precipitation with free Ca^{2+} in the soil solution.

The hypothesized linear increase in P sorption along the ecosequence from hyperarid to humid climate had to be rejected. The dependency of P sorption on multiple variables resulted in the strongest sorption in the most arid and most humid sites. The abiotic P immobilization processes, however, are largely different between the sites.

Microbial inorganic P uptake

Microbial uptake of inorganic P from the soil solid phase strongly varied across biomes (Figure 2.3.5). In the hyperarid desert, the ^{33}P content in P_{mic} and, therefore, microbial inorganic P uptake, was below the detection limit. P is not considered a limiting element in ecosystems where mineral weathering is in its initial state according to most ecological concepts (Vitousek and Farrington, 1997; Walker and Syers, 1976). Nevertheless, in the strongly P immobilizing A horizon of the hyperarid desert, a higher C_{mic}:P_{mic} ratio under high C availability (i.e., with glucose addition) supports the idea that P is limiting microbial growth if, for example, root exuded sugars alleviate C limitation (Table 2.3.2). Simultaneously, the C_{mic}:N_{mic} ratio remained constant, pointing to sufficient N supply even if the C availability is increased (Table 2.3.2). This is in line

with results from Bernhard et al. (2018), who found narrow soil C:N ratios (about 1.8 to 10) pointing to a sufficient N supply for microbial growth in relation to C in the hyperarid desert.

In the arid shrubland soil, microbial inorganic P uptake without C addition increased slightly over the course of the experiment (Figure 2.3.5), while at the same time C_{mic} values remained constant during the incubation (Figure 2.3.4). This suggests continuous utilization of P in bulk soil at this site. While the amount of microbial biomass C remained constant following the C pulse, the microbial biomass P was increased at the sampling times 2 and 7 (Figure 2.3.4). When microorganisms had access to an easily available C source, the microbial inorganic P uptake in the A horizon of the arid shrubland initially was increased over the control (sampling time 2) but thereafter decreased again (sampling times 7 and 20, Figure 2.3.5), and was significantly lower than the non−glucose treatment at sampling time7. The constant P_{mic} content from sampling time 2 to 7, while at the same time the inorganic P uptake decreased, indicates, that an alternative P source other than the inorganic P sorbed at the soil solid phase was exploited after the preferred use of the sorbed inorganic P at sampling time 2. One reason for this could be that after a boost in microbial activity due to the input of labile C (as confirmed by the elevated daily CO_2 release, Figure: S 2.3.3), the microbial community switches back to the P source that is preferentially utilized under steady−state conditions of scarce labile C (here likely primary P (apatite) or organic P). The gradual decline of microbial P under the addition of glucose from sampling point 2 to 20 corroborates the assumption made by Koester et al. (2021) that low organic P contents in the arid shrubland indicate effective P recycling from organic sources. This is probably achieved by rapid remineralization of the microbial biomass P. Therefore, the uptake of sorbed inorganic P (Figure 2.3.5) may have been overestimated, due to the fast recycling of necromass ^{33}P (especially at the two later sampling times) in this ecosystem with low organic P content (Brucker and Spohn, 2019). In terms of nutrient limitations in the arid shrubland, the decreasing C_{mic}:P_{mic} ratio under the addition of glucose (Table 2.3.2) leads to the conclusion that P becomes available if the supply of readily degradable C is sufficient. Both, the primary− and the organic P pool were important for microbial P nutrition in the arid shrubland. Our findings were confirmed by the results of Brucker et al. (2020), who found that C availability constrains P solubilization in this ecosystem.

Microbial uptake of sorbed inorganic P in the A horizon of the Mediterranean woodland increased steadily over the course of the experiment (Figure 2.3.5). The ratio of the biologically available P pool (P_{resin}) to the abiotic equilibrium concentration of P in soil solution without microbial activity (C_p) (Figure: S 2.3.4) was always smaller than 20%. This indicated that microbes lower the concentration of P in the soil solution by efficient microbial uptake systems.

Moreover, the addition of glucose significantly reduced the concentration of P in the soil solution (Figure: S 2.3.4) and increased microbial uptake of sorbed inorganic P (Figure 2.3.5). Because the input of labile C strongly favors the uptake of sorbed inorganic P, we conclude that this P pool is preferred for microbial P nutrition at this site. At none of the other sites was such a strong effect of glucose addition on microbial uptake of sorbed inorganic P observed. This immediate and efficient uptake of sorbed inorganic P in response to C addition in the Mediterranean woodland soil shows that this pool would be the preferred P pool to be utilized in the rhizosphere, where readily available C is released by the roots. It remains unknown whether microorganisms actively desorb P from the soil solid phase (e.g., by the exudation of low–molecular weight organic substances) or if the mobilization is due to the efficient uptake from the soil solution and subsequent physicochemical desorption. Furthermore, the increase in microbial biomass C with elevated P uptake during the incubation points towards a P limitation of microbial growth in the Mediterranean woodland's A horizon if no labile carbon (e.g., root–derived) is available to induce the above–described strong P mobilization. The narrowed C_{mic}:P_{mic} ratio (Table 2.3.2) corroborates that P is limiting microbial growth when labile root derived C is scarce. Low uptake of sorbed inorganic P at the end of the experiment in the B horizon of the Mediterranean woodland soil indicates that the labile C is already completely utilized. The differences in microbial biomass C and P between the reference and the glucose samples vanished towards the end of the incubation (Figure 2.3.4). This difference again points towards a strong dependence of the microbial community on the input of easily available root derived C, which is rapidly consumed if only given as a single–pulse addition.

The microbial uptake of sorbed inorganic P in the humid–temperate forest soils was low in both horizons and not significantly different under the addition of labile C. In both horizons, the microbial inorganic P uptake decreased over time. Moreover, high microbial biomass C (Figure 2.3.4) and the largest CO_2 efflux among the study sites (Figure: S 2.3.3) indicated that microbial activity along the ecosequence was highest in the humid–temperate forest. Because microbial uptake of sorbed inorganic P is low and primary P is not available (Brucker and Spohn, 2019) and secondary Fe– and Al–phosphates have low equilibrium concentrations at the pH values encountered at this site, the high microbial activity indicated that the utilization of organic P is an important source of P for microorganisms in this ecosystem. The utilization of organic P is also in line with a study by Koester et al. (2021), who found high organic P contents of up to 80% of total P, and Stock et al. (2019), who reported high activity of acid phosphatase in these soils. As outlined in the discussion part about P sorption, it must be assumed, that P fixation, i.e., irreversible abiotic immobilization, occurs in the humid–temperate forest soil. Therefore, the pool of (labeled) desorbable P is likely to be small and the ^{33}P would be rapidly exploited. This

pointed to constant microbial uptake of sorbed inorganic P over the course of the experiment but a depletion in ^{33}P of the small pool of desorbable P, thus, with microbial turnover also the P incorporated in microbial biomass. The addition of glucose in both horizons of the humid–temperate forest soil neither influenced the microbial uptake of sorbed inorganic P (except immediately after addition) nor microbial biomass P content. In the A horizon, the pulse–addition of glucose induced an increase in microbial biomass C towards the end of the incubation. In the B horizon, however, this effect occurred somewhat earlier at the intermediate time points. At the same time, the N_{mic}:P_{mic} ratio increased with the addition of glucose. This increase indicated that the input of labile root derived C in this ecosystem leads to an instantaneous increase of microbial activity and that P availability is sufficient to sustain this elevated microbial activity. However, stoichiometric ratios as well as increased biomass C reflect, that the provided labile C led only to a short–term overcoming of growth limiting factors. The wide C_{mic}:P_{mic} ratios after glucose addition (Table 2.3.2) also implies that for continuous growth, microbes may as well be P limited. Hence, the microbial community in the humid–temperate forest soil seems to be co–limited by P and other nutrients, which to identify is beyond the power of this study.

In summary, the first hypothesis must partly by rejected, since the P sorption capacity along the aridity gradient followed a unimodal instead of a simple linear relationship, with the highest P sorption capacity of the soil measured in the hyperarid desert and humid–temperate forest. Contrary to hypothesis two, microbial uptake of sorbed inorganic P was not highest in the hyperarid desert but in the Mediterranean woodland, where sorbed and immobilized P seems to be a key P resource for the biota. The third hypothesis assuming higher microbial inorganic P uptake under glucose addition can only be confirmed in the A horizon of the Mediterranean woodland soil, where this P resource requires C provision to be effectively used. In the other sites, either other P sources or other nutrients are limiting microbial growth and thus strongly interact with the availability of readily accessible C.

2.3.6. Conclusion

The P sorption capacity varied considerably among the soils of the aridity gradient, with the highest values found at the two endmembers of the ecosequence. P sorption capacity in the hyperarid desert was high but kinetically slow, presumably partially driven by precipitation of P with Ca ions. In contrast, P immobilization in the humid–temperate forest was fast and strong, and probably sorption driven.

Microbial uptake of sorbed inorganic P from the soil's solid phase was below the detection limit in the hyperarid desert soil and highest in the A horizon of the Mediterranean woodland soil. We

identified organic P as a preferred P source in the humid–temperate forest and potentially also in the arid shrubland. Moreover, inorganic P sorbed to the soil solid phase was most intensively utilized in the Mediterranean woodland soil. Our results indicate that in the A horizon of the Mediterranean woodland P limitation can be overcome when readily available C is exuded in the rhizosphere. In contrast, the microbiota in the other ecosystems along the ecosequence were either not primarily P limited or relied on different P sources. Consequently, although all these soils developed on identical parent material, P speciation, availability, and stoichiometric nutrient constraints are highly specific for each of the four sites and no systematic trends along the ecosequence could be identified. This suggests that shifts in abiotic boundary conditions (i.e., climate change) will alter all of these factors (P speciation, availability, and stoichiometric nutrient constraints) in nonlinear ways, making predictions of biogeochemical cycling highly complex and experimental approaches that simulate changing conditions essential.

2.3.7. Acknowledgment

We thank the Chilean National Park Service Corporación Nacional Forestal (CONAF) for granting permission to work in the National parks Nahuelbuta and La Campana. We also thank the Center for Advanced Research in Arid Zones (CEAZA) for the opportunity to work in the Nacional Reserve Santa Gracia. We express our gratitude to Karin Schmid and Susann Enzmann for supporting our laboratory analysis and Klaus Jarosch for fruitful discussions.

2.3.8. Funding

This study was funded by the German Research Foundation (DFG) within the frame of the priority program 1803, EarthShape: Earth surface shaping by biota (DFG SPP 1803; project number 255469939) under the subprojects KU 1184/36–1, DI 2136–11, and DI 2136/11. Michaela Dippold was funded by the Robert–Bosch Junior Professorship 2017.

2.3.9. Declaration of competing interests

The authors have no conflict of interest to declare. The, the research was conducted in the absence of any commercial or financial relationships that could be construed as a potential conflict of interest.

2.3.10. References

Achat, D.L., Pousse, N., Nicolas, M., Brédoire, F., Augusto, L., 2016. Soil properties controlling inorganic phosphorus availability: general results from a national forest network and a global compilation of the literature. Biogeochemistry 127 (2-3), 255–272.

Apostel, C., Dippold, M.A., Bore, E., Kuzyakov, Y., 2017. Sorption of Alanine changes microbial metabolism in addition to availability. Geoderma 292, 128–134.

Bernhard, N., Moskwa, L.-M., Schmidt, K., Oeser, R.A., Aburto, F., Bader, M.Y., Baumann, K., Blanckenburg, F. von, Boy, J., van den Brink, L., Brucker, E., Büdel, B., Canessa, R., Dippold, M.A., Ehlers, T.A., Fuentes, J.P., Godoy, R., Jung, P., Karsten, U., Köster, M., Kuzyakov, Y., Leinweber, P., Neidhardt, H., Matus, F., Mueller, C.W., Oelmann, Y., Oses, R., Osses, P., Paulino, L., Samolov, E., Schaller, M., Schmid, M., Spielvogel, S., Spohn, M., Stock, S.C., Stroncik, N., Tielbörger, K., Übernickel, K., Scholten, T., Seguel, O., Wagner, D., Kühn, P., 2018. Pedogenic and microbial interrelations to regional climate and local topography: New insights from a climate gradient (arid to humid) along the Coastal Cordillera of Chile. CATENA 170, 335–355.

Blume, H.-P., Brümmer, G.W., Horn, R., Kandeler, E., Kögel-Knabner, I., Kretzschmar, R., Stahr, K., Wilke, B.-M., Thiele-Bruhn, S., Welp, G., 2010. Lehrbuch der Bodenkunde, 16. Auflage ed. Spektrum Akademischer Verlag, Heidelberg, 578 pp.

Brucker, E., Kernchen, S., Spohn, M., 2020. Release of phosphorus and silicon from minerals by soil microorganisms depends on the availability of organic carbon. Soil Biology and Biochemistry 143, 107737.

Brucker, E., Spohn, M., 2019. Formation of soil phosphorus fractions along a climate and vegetation gradient in the Coastal Cordillera of Chile. CATENA 180, 203–211.

Brunauer, S., Emmett, P.H., Teller, E., 1938. Adsorption of Gases in Multimolecular Layers. J. Am. Chem. Soc. 60 (2), 309–319.

Bünemann, E.K., 2015. Assessment of gross and net mineralization rates of soil organic phosphorus – A review. Soil Biology and Biochemistry 89, 82–98.

Bünemann, E.K., Augstburger, S., Frossard, E., 2016. Dominance of either physicochemical or biological phosphorus cycling processes in temperate forest soils of contrasting phosphate availability. Soil Biology and Biochemistry 101, 85–95.

Chiou, C.T., Lee, J.F., Boyd, S.A., 1990. The surface area of soil organic matter. Environ. Sci. Technol. 24 (8), 1164–1166.

Fardeau, J.C., 1993. Le phosphore assimilable des sols : sa représentation par un modèle fonctionnel à plusieurs compartiments. Agronomie 13 (4), 317–331.

Filimonova, S., Kaufhold, S., Wagner, F.E., Häusler, W., Kögel-Knabner, I., 2016. The role of allophane nano-structure and Fe oxide speciation for hosting soil organic matter in an allophanic Andosol. Geochimica et Cosmochimica Acta 180, 284–302.

Gérard, F., 2016. Clay minerals, iron/aluminum oxides, and their contribution to phosphate sorption in soils — A myth revisited. Geoderma 262, 213–226.

Gerke, J., Hermann, R., 1992. Adsorption of Orthophosphate to Humic-Fe-Complexes and to Amorphous Fe-Oxide. J. Plant Nutr. Soil Sci. 155 (3), 233–236.

Goudie, A.S., Viles, H.A., 2012. Weathering and the global carbon cycle: Geomorphological perspectives. Earth-Science Reviews 113 (1-2), 59–71.

Grierson, P.F., 1992. Organic acids in the rhizosphere of Banksia integrifolia L.f. Plant Soil 144 (2), 259–265.

Helfenstein, J., Tamburini, F., Sperber, C. von, Massey, M.S., Pistocchi, C., Chadwick, O.A., Vitousek, P.M., Kretzschmar, R., Frossard, E., 2018. Combining spectroscopic and isotopic techniques gives a dynamic view of phosphorus cycling in soil. Nature communications 9 (1), 3226.

Jones, D.L., Darrah, P.R., 1994. Role of root derived organic acids in the mobilization of nutrients from the rhizosphere. Plant Soil 166 (2), 247–257.

Koester, M., Stock, S.C., Nájera, F., Abdallah, K., Gorbushina, A., Prietzel, J., Matus, F., Klysubun, W., Boy, J., Kuzyakov, Y., Dippold, M.A., Spielvogel, S., 2021. From rock eating to vegetarian ecosystems — Disentangling processes of phosphorus acquisition across biomes. Geoderma 388, 114827.

Kouno, K., Tuchiya, Y., Ando, T., 1995. Measurement of soil microbial biomass phosphorus by an anion exchange membrane method. Soil Biology and Biochemistry 27 (10), 1353–1357.

Landi, L., Valori, F., Ascher, J., Renella, G., Falchini, L., Nannipieri, P., 2006. Root exudate effects on the bacterial communities, CO2 evolution, nitrogen transformations and ATP content of rhizosphere and bulk soils. Soil Biology and Biochemistry 38 (3), 509–516.

Lopez-Hernandez, D., Brossard, M., Frossard, E., 1998. P-Isotopic exchange values in relation to Po mineralisation in soils with very low P-sorbing capacities. Soil Biology and Biochemistry 30 (13), 1663–1670.

Marschner, P., Marschner, H. (Eds.), 2012. Marschner's mineral nutrition of higher plants, 3rd ed. ed. Academic press, Amsterdam, London, 3 pp.

Najera, F., Dippold, M.A., Boy, J., Seguel, O., Koester, M., Stock, S.C., Merino, C., Kuzyakov, Y., Matus, F., 2020. Effects of drying/rewetting on soil aggregate dynamics and implications for organic matter turnover. Biol Fertil Soils.

Oehl, F., Oberson, A., Sinaj, S., Frossard, E., 2001. Organic Phosphorus Mineralization Studies Using Isotopic Dilution Techniques. Soil Sci. Soc. Am. J. 65 (3), 780–787.

Oeser, R.A., Stroncik, N., Moskwa, L.-M., Bernhard, N., Schaller, M., Canessa, R., van den Brink, L., Köster, M., Brucker, E., Stock, S.C., Fuentes, J.P., Godoy, R., Matus, F.J., Oses Pedraza, R., Osses McIntyre, P., Paulino, L., Seguel, O., Bader, M.Y., Boy, J., Dippold, M.A., Ehlers, T.A., Kühn, P., Kuzyakov, Y., Leinweber, P., Scholten, T., Spielvogel, S., Spohn, M., Übernickel, K., Tielbörger, K., Wagner, D., Blanckenburg, F. von, 2018. Chemistry and microbiology of the Critical Zone along a steep climate and vegetation gradient in the Chilean Coastal Cordillera. CATENA 170, 183–203.

Ohno, T., Zibilske, L.M., 1991. Determination of Low Concentrations of Phosphorus in Soil Extracts Using Malachite Green. Soil Sci. Soc. Am. J. 55 (3), 892–895.

Okajima, H., Kubota, H., Sakuma, T., 1983. Hysteresis in the phosphorus sorption and desorption processes of soils. Soil Science and Plant Nutrition 29 (3), 271–283.

Pistocchi, C., Mészáros, É., Tamburini, F., Frossard, E., Bünemann, E.K., 2018. Biological processes dominate phosphorus dynamics under low phosphorus availability in organic horizons of temperate forest soils. Soil Biology and Biochemistry 126, 64–75.

R Core Team, 2017. R: A Language and Environment for Statistical Computing. R Foundation for Statistical Computing, Vienna, Austria.

Randriamanantsoa, L., Frossard, E., Oberson, A., Bünemann, E.K., 2015. Gross organic phosphorus mineralization rates can be assessed in a Ferralsol using an isotopic dilution method. Geoderma 257-258, 86–93.

Richardson, A.E., Simpson, R.J., 2011. Soil microorganisms mediating phosphorus availability update on microbial phosphorus. Plant physiology 156 (3), 989–996.

RStudio Team, 2018. RStudio: Integrated Development Environment for R. RStudio, Inc., Boston, MA.

Sims, J.T., Pierzynski, G.M., 2005. Chemistry of Phosphorus in Soils, in: Tabatabai, M.A., Sparks, D.L. (Eds.), SSSA Book Series Soil Science Society of America, pp. 151–192.

Spiess, A.-N., 2018. propagate: Propagation of Uncertainty.

Spohn, M., Kuzyakov, Y., 2013. Phosphorus mineralization can be driven by microbial need for carbon. Soil Biology and Biochemistry 61, 69–75.

Stock, S.C., Koester, M., Boy, J., Godoy, R., Nájera, F., Matus, F., Merino, C., Abdallah, K., Leuschner, C., Spielvogel, S., Gorbushina, A.A., Kuzyakov, Y., Dippold, M.A., 2021. Plant carbon investment in fine roots and arbuscular mycorrhizal fungi: A cross-biome study on nutrient acquisition strategies. Science of The Total Environment 781, 146748.

Stock, S.C., Köster, M., Dippold, M.A., Nájera, F., Matus, F., Merino, C., Boy, J., Spielvogel, S., Gorbushina, A., Kuzyakov, Y., 2019. Environmental drivers and stoichiometric constraints on enzyme activities in soils from rhizosphere to continental scale. Geoderma 337, 973–982.

Takahashi, T., Dahlgren, R.A., 2016. Nature, properties and function of aluminum–humus complexes in volcanic soils. Geoderma 263, 110–121.

Vance, E.D., Brookes, P.C., Jenkinson, D.S., 1987. An extraction method for measuring soil microbial biomass C. Soil Biology and Biochemistry 19 (6), 703–707.

Villapando, R.R., Graetz, D.A., 2001. Phosphorus Sorption and Desorption Properties of the Spodic Horizon from Selected Florida Spodosols. Soil Sci. Soc. Am. J. 65 (2), 331–339.

Violante, A., Pigna, M., 2002. Competitive Sorption of Arsenate and Phosphate on Different Clay Minerals and Soils. Soil Sci. Soc. Am. J. 66 (6), 1788–1796.

Vitousek, P.M., Farrington, H., 1997. Nutrient limitation and soil development: Experimental test of a biogeochemical theory. Biogeochemistry 37 (1), 63–75.

Walker, T.W., Syers, J.K., 1976. The fate of phosphorus during pedogenesis. Geoderma 15 (1), 1–19.

Wu, J., Joergensen, R.G., Pommerening, B., Chaussod, R., Brookes, P.C., 1990. Measurement of soil microbial biomass C by fumigation-extraction—an automated procedure. Soil Biology and Biochemistry 22 (8), 1167–1169.

Wu, W., Zheng, H., Yang, J., Luo, C., Zhou, B., 2013. Chemical weathering, atmospheric CO2 consumption, and the controlling factors in a subtropical metamorphic-hosted watershed. Chemical Geology 356, 141–150.

2.3.11. Supplementary

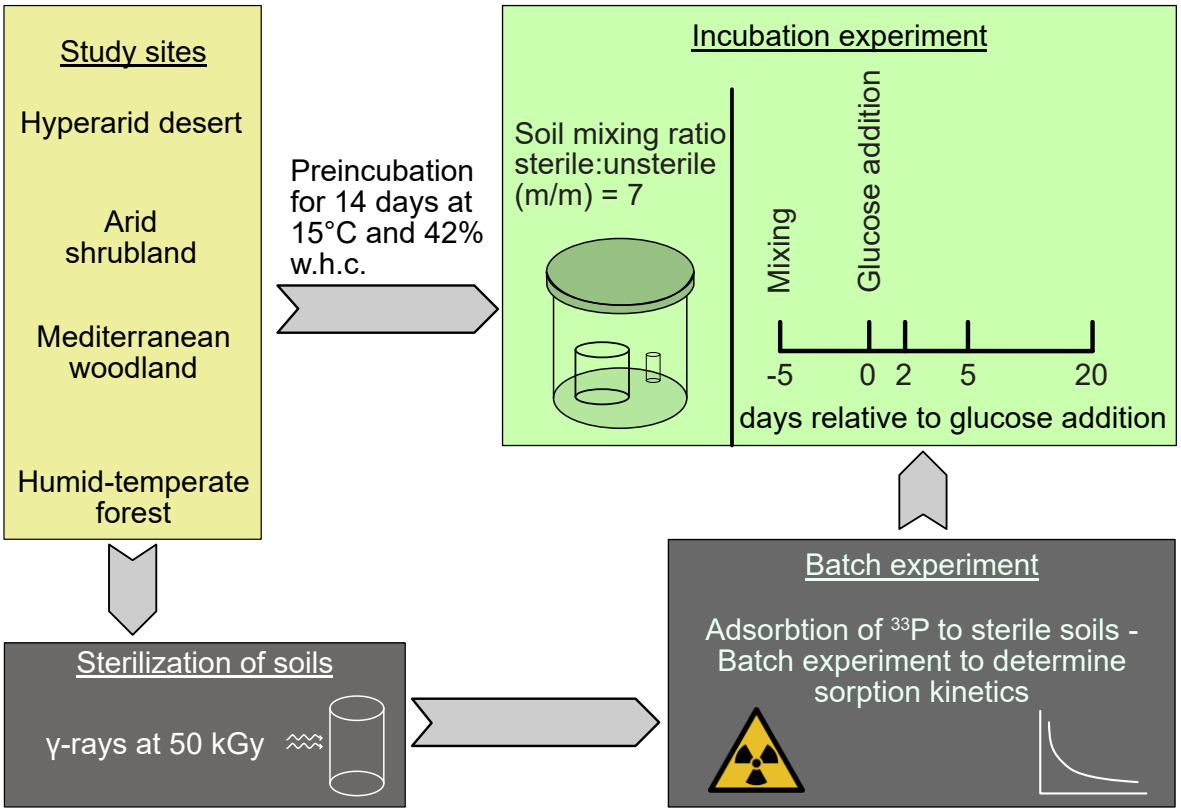

Figure: S 2.3.1: Schematic figure of the study design (Study 2). The study comprised four sites along an aridity gradient (hyperarid desert, arid shrubland, Mediterranean woodland and humid−temperate forest), in each of which the A and B horizon was investigated. A subsample of each soil was irradiated with gamma−rays to sterilize the soil for subsequent determination of abiotic inorganic P sorption. For a subsequent incubation experiment the sterile soils, labelled with ^{33}P were mixed with unsterile soils from the same site and horizon and microbial inorganic P uptake was measured. In addition, a subset of mesocosms was treated with glucose to investigate the effect of high labile carbon availability on microbial inorganic P uptake (calculated by ^{33}P in microbial biomass P and total microbial biomass P) and microbial parameters (microbial biomass carbon, microbial CO_2 release).

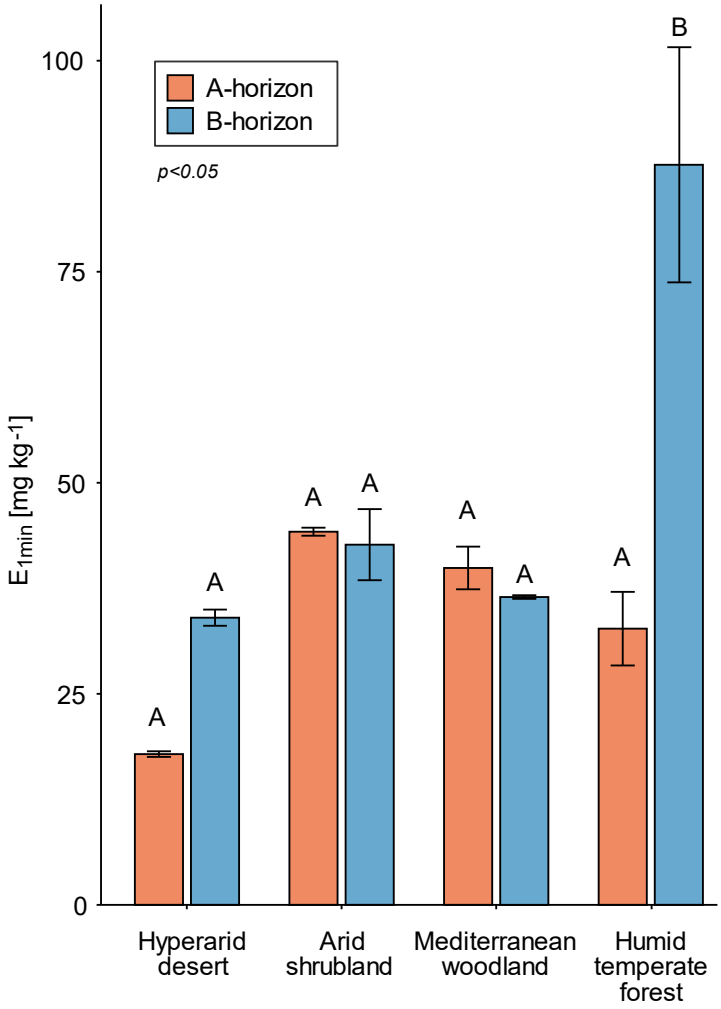

Figure: S 2.3.2: Phosphorus exchangeable within one minute for the hyperarid desert, arid shrubland, Mediterranean woodland and humid–temperate forest, each with A (green markers) and B horizon (orange markers) along the aridity gradient. Error bars indicate the standard errors of the mean.

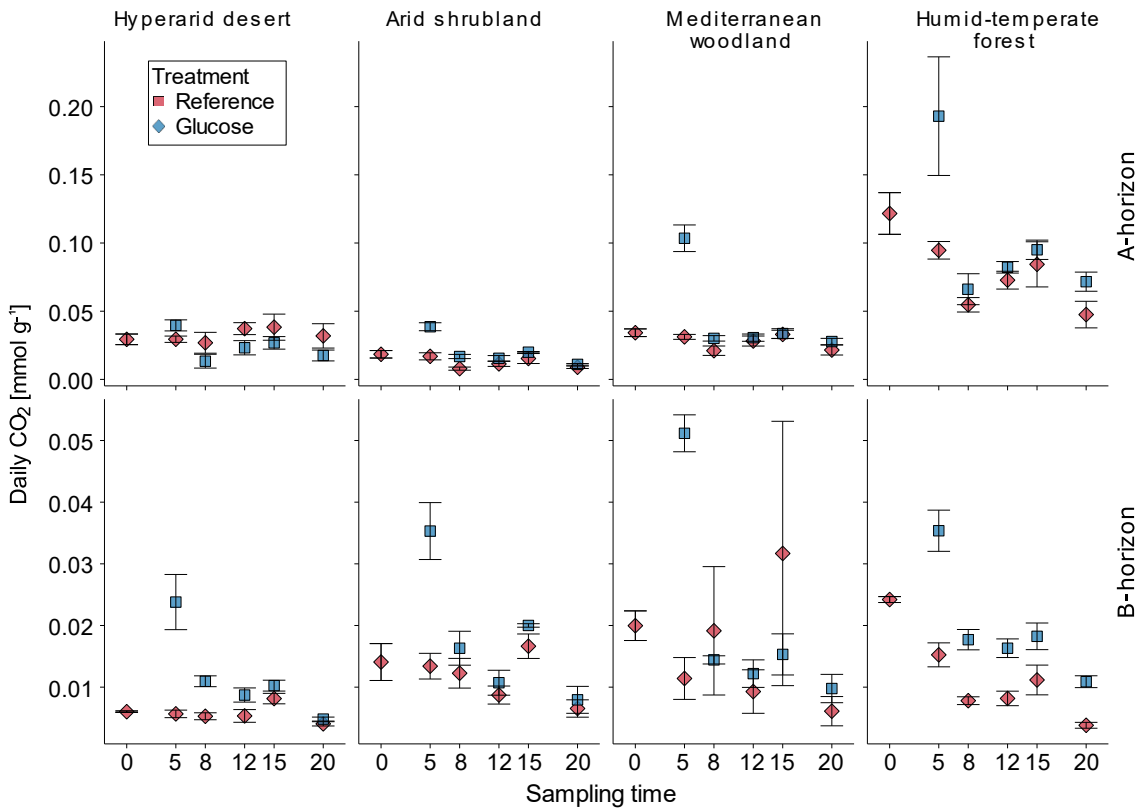

Figure: S 2.3.3: Daily carbon dioxide (CO_2) efflux from the soils in the hyperarid desert, arid shrubland, Mediterranean woodland, and humid temperate forest, each for the A and B horizon along the ecosequence. Red markers represent the amount of CO_2 respired without the addition of glucose (reference) while blue markers represent values from the treatment with glucose addition (glucose). Error bars indicate standard errors of the mean

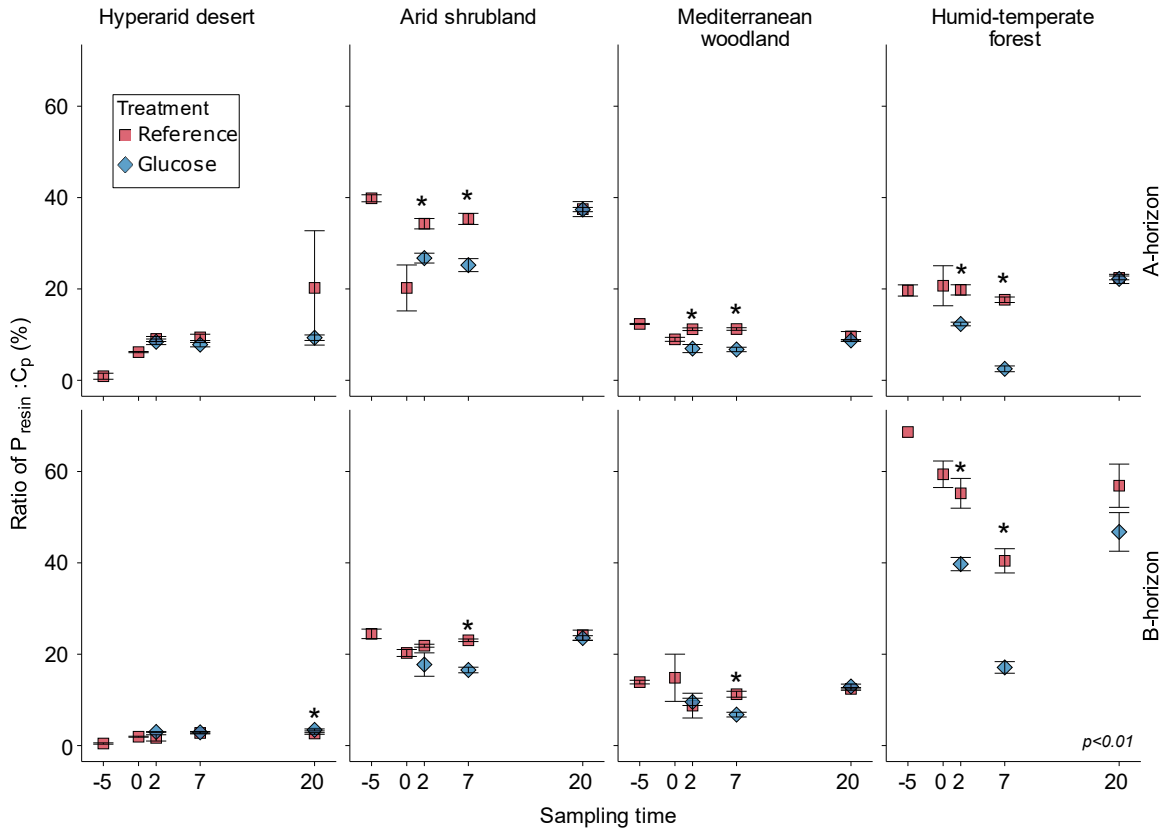

Figure: S 2.3.4: Comparison of water extractable P (C_p) at the end of the batch experiment (after 45 h of adsorption) to water extractable P from P_{mic} measurements (P_{resin}) in the in the hyperarid desert, arid shrubland, Mediterranean woodland, and humid–temperate forest, in each site for A and B horizon. Red markers represent the percentage of P_{resin} related to C_p without the addition of glucose (reference), blue markers show the ratio P_{resin}/C_p in percent from the treatment with glucose addition. Error bars indicate standard errors of the mean. Significant differences between the treatments are marked by an asterisk (*p<0.01*).

Table: S 2.3.1: Overview over the parameters derived from an isotope–exchange kinetics experiment at four soils along an aridity gradient with study sites at a hyperarid desert, arid shrubland, Mediterranean woodland, and humid–temperate forest. Each soil variable was determined for the A and B horizon, respectively. 'Pi' is the total amount of inorganic P in soil, 'C_p' the amount of P in water at the end of the experiment (equilibrium concentration without biological activity). 'sorbed P' is the share of inorganic P sorbed to the soil relative to the total added P in the short–term batch experiment. 'm', 'n', and 'r_{inf}/R' are parameters derived from fitting a curve to the ratio of ^{33}P in soil solution to the total added ^{33}P at the various sampling times in the sorption experiment, 'r_1/R' is the value obtained after one minute of sorption. E_{1min}, E_{25d}, and E_{total} are the amounts of exchangeable P within one minute, 25 days and three months, respectively. Equation 2 was used for the calculation of these values.

Variable	Hyperarid desert		Arid shrubland		Mediterranean woodland		Humid–temperate forest	
	Horizon							
	A	B	A	B	A	B	A	B
P_i [mg/kg]	964.8	578.7	384.5	535.4	321.8	458.8	305.5	480.2
C_p[[mg/kg]	10.9	29.7	37.9	34.0	32.6	32.0	5.2	2.0
sorbed P (%)	64.1	38.5	31.6	26.6	35.7	33.1	98.2	99.6
m	0.617	0.864	0.781	0.780	0.745	0.836	0.158	0.021
n	0.111	0.082	0.053	0.023	0.056	0.065	0.599	0.526
r_{inf}/R	0.011	0.051	0.099	0.063	0.101	0.070	0.017	0.004
r_1/R	0.6128	0.8756	0.8579	0.8100	0.8235	0.8779	0.1642	0.0238
E_{1min}	17.8	34.0	44.2	41.9	39.6	36.5	31.6	83.6
E_{25d}	53.6	71.4	69.6	50.1	63.4	65.6	300.3	470.8
E_{total}	964.8	578.7	384.5	535.4	321.8	458.8	305.5	480.2

2.4. Plant allocation of freshly assimilated C to roots, microorganisms, and weathering agents along an aridity gradient depends on prevailing P forms (Study 3)

Authors: Moritz Koester[a,b], Svenja C. Stock[b,c], Francisco Nájera[d,e], Francisco Matus[i,j], Jens Boy[l], Yakov Kuzyakov[c], Sandra Spielvogel[a,m], Michaela A. Dippold[b]

Affiliations:

[a]Instiute of Geography, University of Bern, Bern, Switzerland

[b]Biogeochemistry of Agroecosystems, University of Goettingen, Goettingen, Germany

[c]Soil Science of Temperate Ecosystems, Agricultural Soil Science, University of Goettingen, Goettingen, Germany

[d]Department of Chemical Sciences and Natural Resources, Universidad de La Frontera, Chile

[e]Faculty of Agricultural Sciences, Universidad de Chile, Santiago, Chile

[i]Laboratory of Conservation and Dynamic of Volcanic Soils, Universidad de La Frontera, Chile

[j]Network for Extreme Environment Research, NEXER–Chile, Universidad de La Frontera

[l]Institute of Soil Science, Leibniz Universität Hannover, Hannover, Germany

[m]Institute for Plant Nutrition and Soil Science, Christian–Albrechts University Kiel, Kiel, Germany

Corresponding Author:

Moritz Koester

Affiliation: Biogeochemistry of Agroecosystems, University of Goettingen, Goettingen, Germany

Adress: Buesgenweg 2, 37077 Goettingen

E–mail: moritzkoester@posteo.de

Tel: +49 551 39–33519

Fax +49 551 39 18 255 95

2.4.1. Abstract

P availability in soil determined by classical wet–chemical extractions suggests that P availability in soils is often low. However, plants and microorganisms posses a large set of mechanisms to mobilize P (by physical or chemical alteration of soil conditions) which is classically seen as hardly– or even unavailable to biota. This study focused on determining the exudation of low–molecular–weight organic acids (LMWOA) and the allocation of freshly assimilated C to LMWOA by plants, fungi, and bacteria. The aim was to understand which biological entities are best in mobilizing a certain P pool and how the C flow from the plant to the three biological compartments is steered by the available P forms and climate in a natural ecosystem. A sequence of ecosystems (ecosequence) from arid shrubland, over Mediterranean woodland, to humid–temperate forest on granodioritic parent material along the Chilean Coastal Cordillera was investigated. A field pulse labeling experiment was conducted, in which selected representative plant species per site were exposed to a $^{13}CO_2$ enriched atmosphere for up to 2h. LMWOA were sequentially extracted from the soils as free and sorbed LMWOA. LMWOA were determined quantitatively and for ^{13}C enrichment by tracer derived ^{13}C. Moreover, the soils P pools were quantified as water extractable and $NaHCO_3$ extractable P (together referred to as plant available P), ammonium–oxalate extractable P, dithionite–citrate bicarbonate extractable P, and total P (NH_3 pressure digestion). P in the arid shrubland was mainly present as hardly available P in adsorbed and precipitated form while under humid–temperate forest the proportion of plant available P was greatest. The LMWOA content increased with decreasing aridity from the arid shrubland towards the Mediterranean woodland and humid–temperate forest. ^{13}C allocation to LMWOA was similar under Mediterranean woodland and humid–temperate forest but lower under arid shrubland. ^{13}C allocation to oxalic acid was identified as an indicator for biological weathering of precipitated and sorbed inorganic P in the Mediterranean woodland and arid shrubland. Our results indicate the utilization of organic P in the humid–temperate forest and a high microbial diversity and, therefore a plethora of P mobilizing processes. In the Mediterranean woodland and arid shrubland on the contrary P mobilization is more specific and mainly governed by roots and fungi.

Keywords: Aridity gradient, P acquisition mechanisms, P pool determination, P bioavailability, root exudates, photoassimilates

2.4.2. Introduction

The availability of nutrients to plants depends on various soil and climate parameters, among which water availability is of utmost importance. In the last decades, many regions globally experienced droughts with higher frequency or severity. Future climate prediction models forecast an intensification of this trend due to climate change (Shukla et al., 2019). When water is sparse, the diffusivity of nutrients in soil is greatly reduced (Rouphael et al., 2012). Moreover, the desorption is reduced because nutrient concentrations in the soil solution are higher. Plants developed a wealth of adaptations to cope with seasonal or general water shortage. The input of energy as photosynthetically fixed carbon (C) into soils is the gateway by which plants transfer energy from above– to below–ground and feed all processes which are related to mobilization of nutrients in soils by root litter input but, moreover, by root exudates. It has been shown that up to 40% of photosynthetically fixed carbon end up as root exudates in soils (Kuzyakov and Domanski, 2000). Root exudates are the driver of interactions between plants and rhizosphere inhabiting microorganisms. It has been shown that plants exuded up to 1.7 times more C under drought compared to a control with sufficient water supply, while C allocation to plant biomass was reduced by a factor of 0.84 (Henry et al., 2007). Different soil properties cause greater variations in root exudate's chemical composition of a variety of grass and forb species than interspecific variations (Herz et al., 2018). Also, the life strategy of plants has a great influence on the exudation rate of the roots. Williams and Vries (2020) in their review on plant root exudation under drought worked out that fast growing plants have a higher rate of root exudation compared to slow growing plants. They attribute this to the strong dependence of fast–growing plants on plant growth promoting rhizobacteria (PGPR) for nutrient mineralization and, hence, nutrient supply to plants.

Root exudates comprise a wide variety of compounds among which sugars are quantitatively most important (Paterson, 2003). Root deposited sugars are mainly consumed by microorganisms in the rhizosphere and, thereby, promote nutrient mobilization (Gunina and Kuzyakov, 2015). Besides these quantitatively dominant compounds, there are less abundant, but more specific substances released to the soil, e.g., exoenzymes and low–molecular–weight–organic acids (LMWOA), which are released to directly enhance nutrient mobility in soil (Burns et al., 2013; Hinsinger, 2001; Jones and Darrah, 1994). LMWOA are important in a variety of processes in soil. Malic acid is released to maintain charge balance upon cation uptake. Enhanced exudation of malic acid was found to be an effective chemoattractant for the plant beneficial *Bacillus subtilis (Henry et al., 2007)*. Oxalic and malic acid are important for nitrate reduction (Marschner and Marschner, 2012). Moreover, oxalic,

malic and citric acid enhance the solubility of Ca–phosphates and improve organic P mobilization in soil (Hinsinger, 2001; Jones and Darrah, 1994; Wei et al., 2010).

As described above it exists a general understanding about the effect of drought on root exudation rates and, therefore, nutrient mobilization. However, it remains unclear how nutrient mobilization changes when climatic conditions become more arid. Therefore, the present study focused on an ecosystem gradient along the Chilean Coastal Cordillera, where differences in lithology are minimal, and changes in soil properties and plant species composition between sites are mainly attributed to varying climate (increasing aridity from south to north).

The objective of this study was to determine plant's C allocation to LMWOA and the microbial community, possibly also producing LMWOA, in the rhizosphere to understand P acquisition mechanisms along an ecosystem gradient. We hypothesize that (I) in ecosystems under dry climate the ^{13}C uptake by microorganisms is faster than in humid ecosystems because the microbial community is C limited and relies on labile C from root exudates. (II) Moreover, as aridity increases the production of LMWOA (weathering agents) shifts from bacteria to plants and fungi because fast growing plants demand a high flux of P from the soil to the roots to compensate for a strongly reduced diffusivity under drought, therefore, plants exploit P sources which are in spatial vicinity to roots and fungal hyphae. Moreover, fungi can exploit a greater soil volume than roots alone.(III) Under humid climate biota prefer organic P sources, whereas under Mediterranean and arid climate they exploit precipitated and sorbed inorganic P. This is because a greater proportion of P is in the organic pool under humid climate and enzymatic activity is higher when water and C are not limiting plant and microbial activity.

2.4.3. Material and Methods

Experimental sites

We focused on three study sites that represent a gradient across biomes (ecosequence) and extend from 29 ° to 38 ° of southern latitude. They are located along the Coastal Cordillera of Chile, and all soils have developed from granodioritic parent material. Mean annual precipitation (MAP) increases from 66 mm yr^{-1} to 1469 mm yr^{-1} and mean annual temperature (MAT) decreases from 13.7 °C to 6.6 °C, from north to south (Fick and Hijmans, 2017) (Table 2.4.1). The study sites comprise an ecosequence from *arid shrubland* (Reserva Nacional Santa Gracia) in the north to *Mediterranean woodland* (Parque Nacional La Campana) and *humid–temperate forest* (Parque Nacional Nahuelbuta) in the most southern site. Important site specifics are shown in Table 2.4.1. For a comprehensive description of vegetation, soils and geology see Bernhard et al. (2018b) and Oeser et al. (2018).

Table 2.4.1: Most important climate and vegetation characteristics of the three study sites.

Site	MAT[a] [°C]	MAP[a] [mm a^{-1}]	Aridity index[b]	Soil type[c]	Vegetation type[c]	Labelled plant species
Arid shrubland	13.7	66	0.0047 (arid)	Cambisol/ Leptosol	Sclerophyllous shrubs, cacti	*Gutierrezia resinosa* (Hooker & Arnott) Blake
Mediterranean woodland	14.1	367	0.2365 (semiarid)	Cambisol	Deciduous forest, sclerophyllous shrubs	*Erigeron fasciculatus* (Colla)
Humid–temperate forest	6.6	1469	1.4 (humid)	Orthodystric Umbrisol/ Umbric Podzol	Mixed broadleaved–coniferous forest	*Araucaria araucana* (Molina) K. Koch

a) (Fick and Hijmans, 2017)
b) (Trabucco and Zomer, 2019)
c) (Bernhard et al., 2018)

$^{13}CO_2$ pulse labeling and sampling

Pulse labeling of plants with ^{13}C enriched CO_2 is a widely used technique to quantify belowground C allocation by plants (Gavito and Olsson, 2003; Kuzyakov and Domanski, 2000), and meanwhile also established for woody vegetation in forests (Sommer et al., 2017). In this study, we used a cubic chamber with a site length of 60 cm. The chamber was built from polyethylene foil to let pass photosynthetic active radiation. The labeling was conducted in November 2016, at the start of the growing season on the southern hemisphere. ^{13}C labeled CO_2 was provided by the dissolution of 3 g of $Na_2{}^{13}CO_2$ (^{13}C enrichment 99%, Sigma Aldrich, Munich, Germany) in 50 ml H_2O. The solution was placed inside the chamber which was subsequently sealed airtight. To release the $^{13}CO_2$ from the solution 5 M H_2SO_4 was added by a syringe perforating the polyethylene foil with a thin needle. The hole was closed with adhesive tape after application of the acid. To control Temperature within the chambers to a maximum of 10 °C above ambient, icepacks and a small fan were placed within the chambers. The fan also served to maintain a homogenous distribution of $^{13}CO_2$ within the chamber. The labelling time differed among the sites, depending on weather conditions and temperature (Table 2.4.2). Plants were labeled on south and north facing slopes, with a sample size of four specimen per slope. Soil samples were taken before labeling (at plants which were not subject to labeling (same species)) and one, three, and fourteen days after labeling. Sampling was done with a soil core auger with a diameter of 8 cm down to a depth of 30 cm. The soil core was divided in three depths increments of 10 cm each. The samples were directly frozen in the field. Later samples were thawed, sieved to 2 mm and roots were separated. Samples were frozen again until analysis.

Table 2.4.2: Dates of labeling, weather conditions and duration of labeling.

Site	Date (dd.mm.jjjj)	Duration [h]	T_{air} [°C]*	Air pressure [hPa]*	Precipitation [mm]*	Solar radiation [W m^{-2}]*
Arid shrubland	12./13.11.2016	1.5	17–18.5	950	0	540–770
Mediterranean woodland	17./18.11.2016	1	22–33	965	0	890–915
Humid–temperate forest	25./26.11.2016	2	8–9.5	875	0–0.2	280–400

* data from EarthShape weather stations (Ehlers et al., 2017)

Labeled plant species

C investments to belowground processes as well as plant nutrient acquisition strategy vary strongly between plant morphological traits (herb, forbs, shrubs, trees) (Sala et al., 2012). To best represent the respective ecosystems nutritional strategy, we aimed to investigate a dominant plant species at each site. However, to reduce trait–based, strongly influencing factors, we selected only woody species in our experiment, we excluded plants which host nitrogen fixing bacteria and we selected only species which use the C3 photosynthetic pathway. Only species which accounted for at least 10% of the vegetation cover were selected. We sampled only plants between 40 and 60 cm in height to reduce variability based on plants age and size. The species *Gutierrezia resinosa* (Hooker & Arnott) Blake was chosen for labeling at the arid shrubland site. The perennial species belongs to the *Asteracea* family and has a habitus of a woody shrub, the growth height is up to 1.5 m (Solbrig, 1966). The plant is found at low altitude on sandy, alkaline to neutral soils with low C and N content (Solbrig, 1966). *G. resinosa* accounted for 15% of the plant cover at the arid shrubland site while the overall plant cover was 40% of the area.

At the Mediterranean woodland, the species *Erigeron fasciculatus* (Colla) was selected for labeling. The area was completely covered by vegetation, for 10% of the area *E. fasciculatus* accounted responsible. The species reaches a growth height of 70 cm, belongs to the *Asteracea* family and is endemic to mid and low altitudes in the Coquimbo–Valparaiso region (Andrus et al., 2009; Solbrig, 1962; Valdebenito et al., 1986).

At the HTR, the coniferous tree species *Araucaria araucana* (Molina) K. Koch was labeled. The species belongs to the *Araucariacea* family and grows in mid and high elevation (from the tree line until down to about 600 m a.s.l.) and under sufficient water supply of 1100 to 4000 mm a^{-1} (Diehl and Fontenla, 2010; Veblen, 1982). *A. araucana* accounted for 40% of the understory vegetation, the total plant cover at the site was 100%, the single trees can reach a growth height of up 45 m and a lifespan of about 1000 years (Aguilera–Betti et al., 2017; Veblen, 1982).

Analysis

LMWOA extraction

LMWOAs were extracted based on a method after Szmigielska et al. (1997) with modifications. LMWOAs were extracted with 0.5 M HCl in methanol (MeOH) with a soil to solution ratio of 1:1 (v/v) by shaking for one hour. After centrifugation at 950 *g* for 15 min the supernatant was transferred to a reaction vessel and dried under a gentle stream of N_2. For derivatization, 3 ml of MeOH and 300 µl of H_2SO_4 (50%) were added to the samples, vials were screw-capped with a Teflon coated lid and placed in a heating block at 60 °C for 30 min. Analytes were purified by liquid–liquid extraction using chloroform ($CHCl_3$) as final solvent. Subsequent analysis was done on a gas chromatograph mass spectrometer (GC–MS) (GC 7890A, MS 7000A Series Triple Quad, Agilent Technologies, Waldbronn, Germany) with a capillary column (DB–FFAP, 30 m length, 1 µm film thickness, 0.25 mm diameter, Agilent Technologies, Waldbronn, Germany). Standard solutions contained the following organic acids: oxalic–, malonic–, fumaric–, succinic–, maleic–, malic– and citric acid. The isotopic fingerprint of C of the analytes (^{13}C to ^{12}C ratio) was determined by a GC–isotope ratio mass spectrometer (IRMS) (Delta plus Thermo Fisher Scientific, Bremen, Germany). Contents and $^{13}C/^{12}C$ ratios of LMWOAs were determined for north and south facing slopes at each site and four replicate plant specimen per slope. As organic acids as well as their anions are co–extracted by the presented approach, the abbreviation for LMWOAs refers to acids and their respective anions.

PLFA extraction

Cell membranes constitute of phospholipid fatty acids (PLFA) which can be used as a biomarker to specify microbial functional groups in soil (Gavito and Olsson, 2003; Olsson et al., 1995). Phospholipidic fatty acids (PLFA) were extracted following the method introduced by Frostegård and Bååth (1996) with modification after Gunina et al. (2014). Briefly, 6 g of fresh soil were subject to extraction with a solution of modified protocol of methanol, chloroform, and citrate/KOH buffer (pH 4, v/v/v = 1:2:0.8) (E. Bligh and W. Dyer, 1959). PLFA were separated and purified by solid phase extraction, using activated silica gel (heated to 110°C for 10 h). The purified PLFA were hydrolyzed and methylated to their corresponding fatty acid methyl esters (FAMEs). Samples were quantified on a GC–MS (GC 7820A, MS 5977B, Agilent Technologies, Waldbronn, Germany). The isotopic fingerprint of C of the analytes (^{13}C to ^{12}C ratio) was determined by a GC–IRMS (Delta plus Thermo Fisher Scientific, Bremen, Germany). The raw data were drift corrected and µg FAME g^{-1} soil and at%^{13}C were calculated as described by Dippold and Kuzyakov (2016).

Total bacterial and fungal PLFA were calculated by summarizing the respective specific PLFA for either group. The PLFA 16:1ω5c is frequently used as an arbuscular mycorrhizal fungi (AMF)−specific PLFA but can also be produced by bacteria. To investigate the origin of this PLFA in our samples the ratio of 16:1ω5c PLFA to 16:1ω5c NLFA was calculated (Stock et al., 2021). The ratio was always >1 for all sites and depths. Hence, fungal PLFA were calculated as the sum of PLFAs 16:a. Total bacteria derived PLFAs were calculated as the sum of PLFAs i14:0, a14:0, 14:1ω5c, i15:0, a15:0, i16:0, a16:0, 16:1ω7c, 10Me16:0, i17:0, a17:0, 18:1ω9c, 18:1ω7c, and 10Me18:0.

Calculation of ^{13}C incorporation

Incorporation of the applied tracer into roots, PLFA, and LMWOA was calculated by the following equation (Gearing et al., 1991):

$$^{13}C_{inc} = \frac{at\%_{lab} - at\%_{ref}}{at\%_{tracer} - at\%_{ref}} * 1000\ [‰] \qquad \text{Equation 2.4.1}$$

were the $at\%_{lab}$ is the percentage of ^{13}C on total C in the labeled samples, $at\%_{ref}$ in the unlabeled samples, and $at\%_{tracer}$ the percentage of ^{13}C on total C of the CO_2 in the labeling chamber. Since the CO_2 in the labeling chamber is a mixture of atmospheric CO_2 ($[CO_2]_{air}$) and $Na_2{}^{13}CO_2$ born CO_2 ($[CO_2]_{input}$); $at\%_{tracer}$ was calculated by the following equations:

$$at\%_{tracer} = \{at\%CO_2\}_{air} \frac{[CO_2]_{air}}{[CO_2]_{air} + \left[{}^{13}CO_2\right]_{input}} + [at\%CO_2]_{input} \frac{\left[{}^{13}CO_2\right]_{input}}{[CO_2]_{air} + \left[{}^{13}CO_2\right]_{input}} \qquad \text{Equation 2.4.2}$$

with:

$$[CO_2]_{air} = \frac{P_a}{R * T} * [CO_2] * 10^{-6} * V_{chamber} \qquad \text{Equation 2.4.3}$$

and:

$$[CO_2]_{input} = \frac{m_{input}}{M(^{13}CO_2)} * V_{chamber} \qquad \text{Equation 2.4.4}$$

where the percentage of ^{13}C in the atmosphere is given by $[at\%CO_2]_{air}$, and the percentage in the $Na^{13}CO_3$ derived CO_2 by $[at\%CO_2]_{input}$ with 99 at%. Pa is the atmospheric air pressure at the time

of measurement in [Pa], T the air temperature in [K], R the universal gas constant [J mol^{-1} K^{-1}], [CO_2] the concentration of CO_2 in the atmosphere [ppm], $V_{chamber}$ the volume of the chamber [m^{-3}], m_{input} the $^{13}CO_3$ mass of the added $Na_2{}^{13}CO_3$ [g], and M($^{13}CO_2$) the molar mass of ^{13}C enriched CO_2.

Phosphorus extraction

Water soluble P was extracted by using anion exchange membranes (AEM) (Anion exchange membranes, VWR International GmbH, Darmstadt, Germany). Out of historical reasons this P fraction is called P_{resin}. For all extractions, except total P, 1 g of dry soil was placed in a conical bottom flask made from polypropylene. Two anion–exchange membranes with an area of 3.5 cm^2 each were placed in the flask and 30 ml double distilled H_2O (ddH_2O) were added. Samples were shaken for 16 h, subsequently, the anion–exchange membranes were removed and carefully cleaned (rinsed with ddH_2O) to remove adherent soil particles. The anion–exchange membranes were placed into a fresh conical bottom flasks and 50 ml of 0.5 M HCl were added. After allowing for degassing samples were shaken again for 2 h, anion–exchange membranes were removed and P content in the solution was determined photometrically using malachite green as a dying agent (Ohno and Zibilske, 1991). Bioavailable P is often determined by extraction with 0.5 M $NaHCO_3$ and termed Olsen P (P_{olsen}) (Olsen et al., 1954). Briefly, 30 ml of 0.5 M $NaHCO_3$ were added to the soil, the mixture was shaken for 16 h. Subsequently, the suspension was centrifuges at 1500 g for 15 min, the supernatant was filtrated (round filter paper grade 589/2, quantitative, White Ribbon GE Whatman).

P bound to poorly crystalline and well crystalline Fe– and Al–(hydr)oxides was determined by ammonium–oxalate (NH_4–oxalate) extractable P (P_{ox}) and dithionite–citrate–bicarbonate (DCB) (P_{dith}) extractable P, respectively. P_{ox} was extracted following the procedure described by Schwertmann (1964) (modified after Tamm (1922)). In short, 50 ml of NH_4–oxalate solution were added to the soil and shaken for 1 h under light exclusion, pH was adjusted to 3.25. The suspension was filtrated (round filter paper grade 589/2, quantitative, White Ribbon GE Whatman), and the volume adjusted to 50 ml. P_{dith} was determined after a method described by Mehra and Jackson (1958). Briefly, 30 ml of Na–citrate and 7.5 ml of $NaHCO_3$ were added to the soil and heated in a sand bath to 75– 80 °C. Two spatulas of sodium dithionite ($Na_2S_2O_4$) were added to each sample, the sample was kept at 75–80 °C and frequently stirred with a glass stick. After cooling the suspension was centrifuged at 1500 g for 15 min and filtrated (round filter paper grade 589/2, quantitative, White Ribbon GE Whatman). The procedure was repeated 2 to 4 times until the soil showed a grey color. P_{olsen}, P_{ox}, and P_{dith} were analyzed on an inductively

coupled plasma–optical emission spectrometer (ICP–OES) (Thermo Scientific iCap 7040 DUO Series, Bremen, Germany).

Total P content was determined by pressure digestion with HNO_3 (König et al., 2014). Briefly, samples (100 mg) were placed into Teflon beakers and 2 ml of 65% HNO_3 were added. Beakers were tightly closed and heated to 190 °C for 12 h. Subsequently, the extract was diluted with double distilled water (ultrapure) and analyzed on an inductively coupled plasma–optical emission spectrometer (ICP–OES) (Thermo Scientific iCap 6000 Series, Bremen, Germany). The P standard (conc. 100 mg L^{-1}) for calibration was of certified reference material grade (Sigma Aldrich, Munich, Germany).

Statistical analyses

All statistical analyses were conducted using R Version 3.4.3 (R Core Team, 2017). To test for differences of P fractions and LMWOA between sites an ANOVA was calculated by using the '*aov*' function of the *'stats'* package. If the obtained *p* value was below 0.05 a Tukey post–hoc test was conducted to test which sites were different from the others. The level of significance was set to α=0.05. ^{13}C incorporation data were tested for outliers by a *maximum normalized residual test* with the function *'grubbs.test'* of the *'outlier'* package (Komsta, 2011). If values were indicated as outliers, they were excluded from further analysis.

A PCA was calculated with ^{13}C incorporation in H_2O and HCl extractable oxalic–, malic–, and citric acid, respectively, as well as ^{13}C incorporation in bacteria, fungi, and roots. The four P pools of water extractable P (P_{resin}), $NaHCO_3$ extractable (P_{olsen}), NH_4–oxalate, and DCB leachable P (P_{ox} and P_{dith}) were added to the PCA plot as supplementary variables. The PCA was calculated for each site separately because ^{13}C incorporation to the different reservoirs follows different mechanisms in the three sites. The function *'PCA'* of the package *'FactoMineR'* was used for calculating the PCA (Le Sebastien et al., 2008). Plots, except for the PCA, were done with the package *'ggplot2'* (Wickham, 2016).

2.4.4. Results

P content across biomes

Total P content was highest in the humid–temperate forest with 692 µg g^{-1} in both, 0–10, and 20–30 cm. It was 566 and 533 µg g^{-1} in the arid shrubland in 0–10 and 20–30 cm, respectively (Figure 2.4.1). Lowest P content in the topsoil was measured in the Mediterranean woodland with 375 and 383 µg g^{-1} in 0–10 and 20–30 cm, respectively. The sum of P_{resin} and P_{olsen}, the plant available pool, in both sampling depths was highest in the humid–temperate forest. NH_4–oxalate (P_{ox}) and DCB extractable P (P_{dith}) were about the same in the arid shrubland and

Mediterranean woodland and increased in the humid–temperate forest. In the humid–temperate forest the P_{ox} content was higher than P_{dith} (Figure 2.4.1).

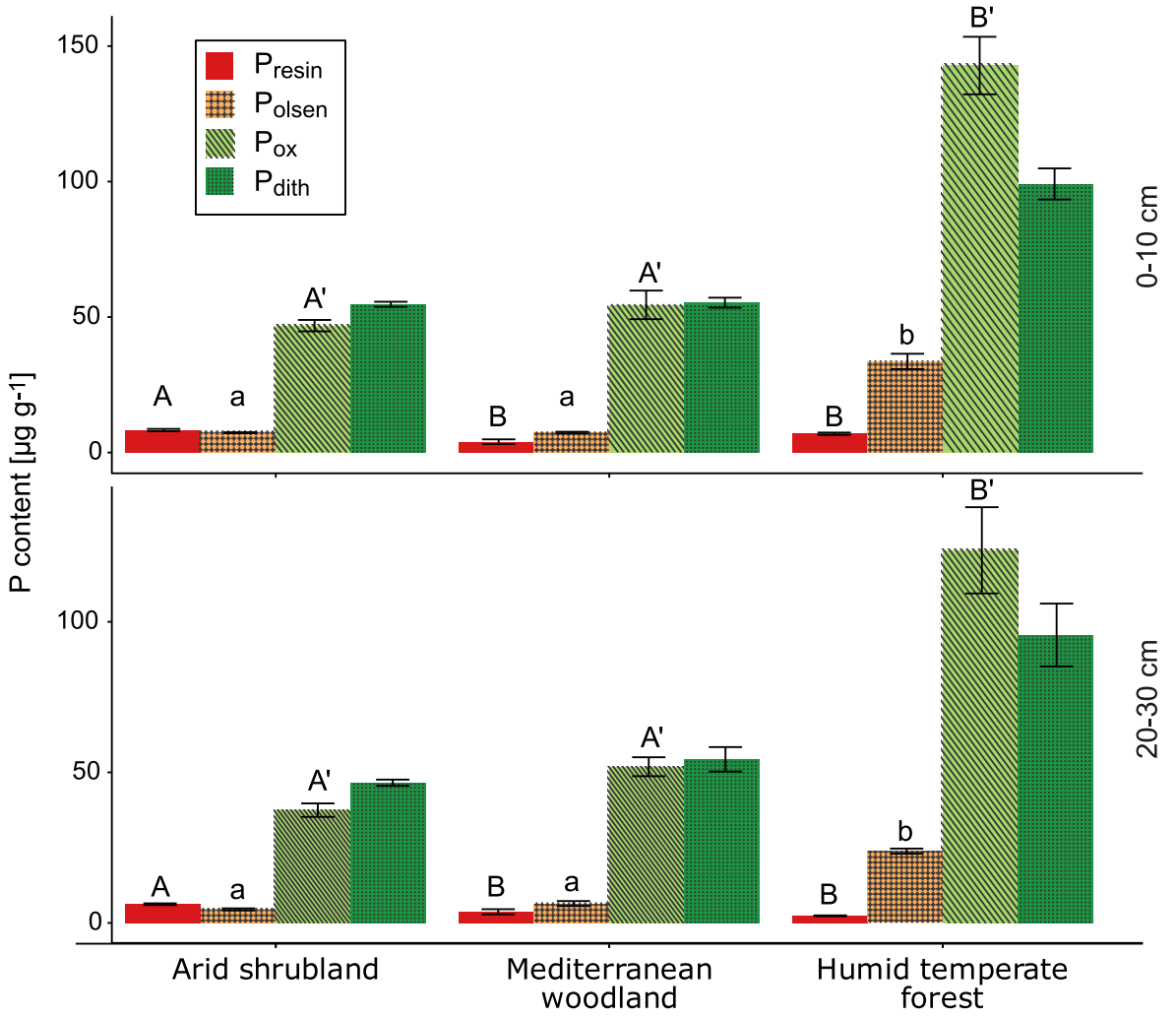

Figure 2.4.1: Phosphorus fractions for the three study sites in the soil depth 0–10 cm (top row) and 20–30 cm (bottom row). Plant available P is represented by water extractable P (Presin) in red and NaHCO3 extractable P (Polsen) in orange. NH4–oxalate leachable P(Pox), which is thought to be sorbed to poorly crystalline pedogenic oxides and crystalline AlPO4 surface precipitates, in light green and dithionite–citrate–bicarbonate extractable P (Pdith), which consists of P from poorly and well crystallized pedogenic oxides, in dark green. Significant differences between the same fraction in the three study sites is indicated by capital letters A and B for Presin, lower case letters a and b for Polsen and A' and B' for Pox ($p<0.05$).

Organic acid contents

Free and sorbed citric acid showed a strong increase with decreasing aridity in both sampling depths. Contents of water extractable citric acid increased from 1.8 µg g^{-1} in the arid shrubland, 2.5 µg g^{-1} in the Mediterranean woodland and 18.8 µg g^{-1} in the humid–temperate forest while contents of HCl extractable citric acid showed values of 0.4, 0.7, and 9.7 µg g^{-1} from arid to humid, all in 0–10 cm (Figure 2.4.2). The oxalic acid sorbed fraction increased from 3.5 and 6.4 µg g^{-1} in the arid shrubland to 11.5 and 13.8 µg g^{-1} in the humid–temperate forest in 0–10 cm and 20–30 cm, respectively. With exception of the H_2O extractable pool in the

humid–temperate forest in 0–10 cm and the Mediterranean woodland in 20–30 cm, oxalic acid was the most abundant organic acid (Figure 2.4.2). Free malic acid in both sampling depths showed the highest contents in the Mediterranean woodland (5.7 and 11.6 µg g^{-1}, respectively). The malic acid sorbed fraction increased from 0.4 µg g^{-1} in the arid shrubland to 1.4 µg g^{-1} in the humid–temperate forest (Figure 2.4.2).

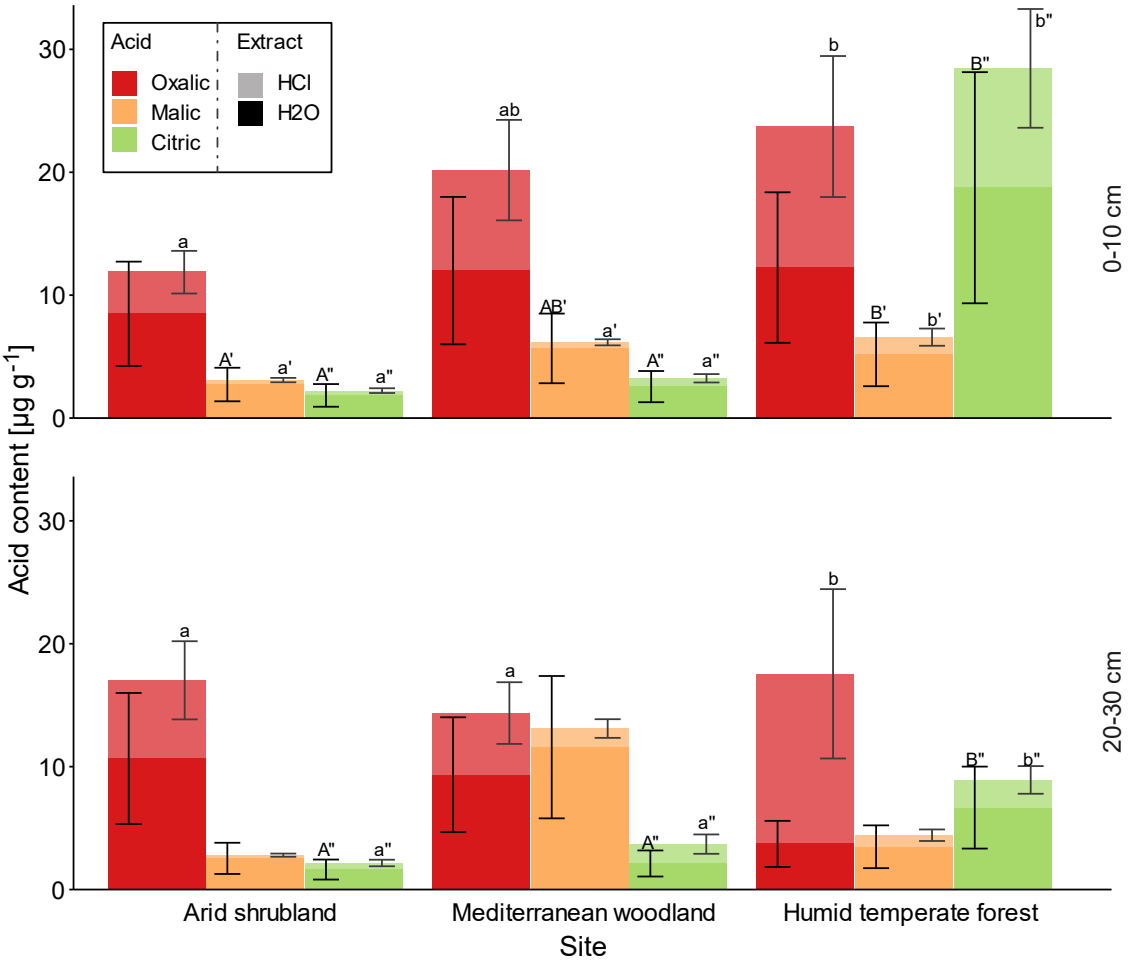

Figure 2.4.2: Low–molecular–weight organic acid (LMWOA) contents in soil at the three study sites in 0–10 cm (top) and 20–30 cm (bottom). The pools of free and sorbed LMWOA were extracted sequentially as H2O extractable free organic acids (solid color) and HCl extractable sorbed organic acids (light color). Significant differences between acid contents are indicated by capital letters for the H2O extracts and lowercase letters for the HCl extract. A and B for oxalic acid, A' and B' for malic acid and A" and B" for citric acid ($p<0.05$).

^{13}C dynamics

In the arid shrubland and Mediterranean woodland ^{13}C incorporation into bacterial PLFA was higher than the humid–temperate forest at all time points. At the arid shrubland the ^{13}C incorporation decreased over time from 7.17 µg g^{-1} one day after labeling to 1.32 µg g^{-1} 14 days after labeling in the upper 10 cm (Figure 2.4.3). No such decrease with time was observed for the Mediterranean woodland and at the humid–temperate forest ^{13}C incorporation into bacterial biomass was highest three days after labeling. Generally, ^{13}C incorporation into fungal biomass

was lower than in bacterial biomass. In the arid shrubland and Mediterranean woodland ^{13}C incorporation in fungal biomass in 0–10 cm sampling depth was highest one day after labeling, in the humid–temperate forest at was highest three days after the tracer was applied. Incorporation of ^{13}C in root tissue (in µg ^{13}C cm^{-3} soil) increased with decreasing aridity. At the arid shrubland it was 0.05 µg cm^{-3}, at the Mediterranean woodland 0.30 µg cm^{-3}, and at the humid–temperate forest 0.62 µg cm^{-3} one day after labeling in 0–10 cm sampling depth (Figure 2.4.3).

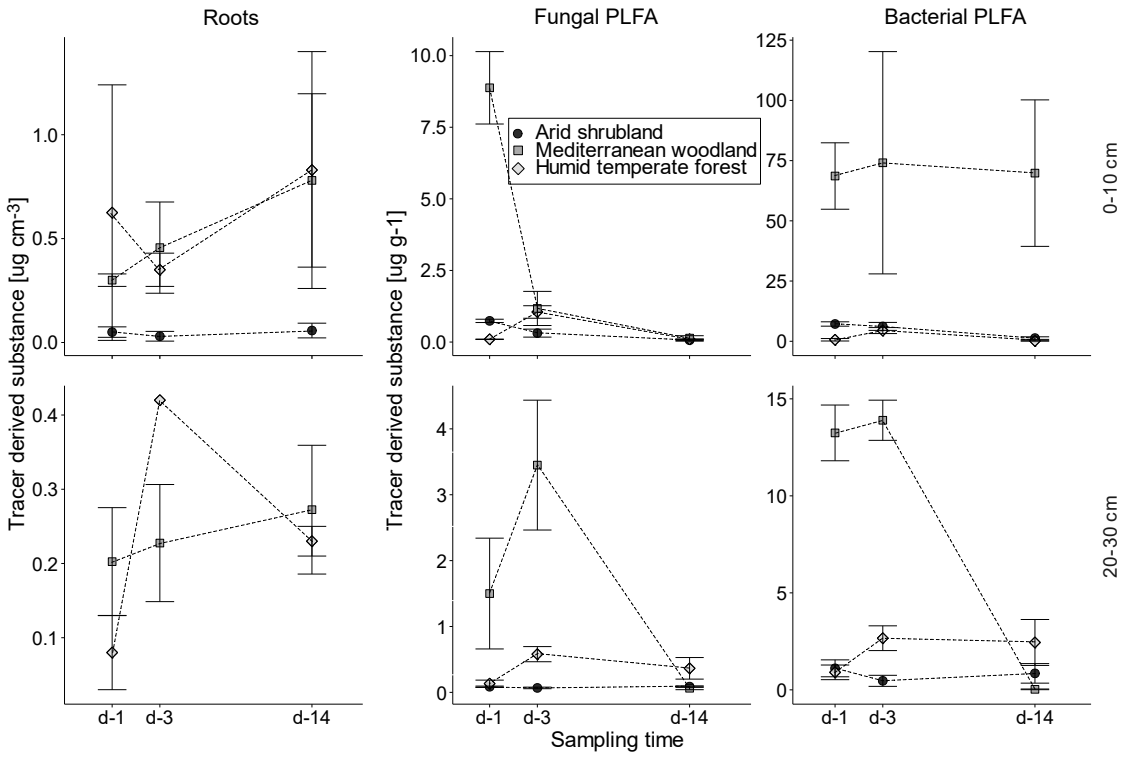

Figure 2.4.3: Incorporation of ^{13}C from CO_2 pulse labeling in roots, fungal PLFA, and bacterial PLFA for all sites (arid shrubland=black; Mediterranean woodland=dark grey, humid–temperate forest=light grey). The incorporation is shown for 0–10 cm sampling depth (top) and for 20–30 cm sampling depth (bottom). Values are given in µg 13C per cm^3 of soil for roots and in µg 13C per g dry soil for acids and microorganisms. Whiskers show the standard error of the mean (n=4).

Comparing the sampling time at one day with 14 days after tracer application the fraction of tracer derived C in roots was constant in the arid shrubland and humid–temperate forest but increased in the Mediterranean woodland (0.3 µg cm^{-3} at d–1 and 0.78 µg cm^{-3} at d–14). Incorporation of ^{13}C into organic acids, varied greatly among the study sites, while in the arid shrubland soils the incorporation was lowest the highest values were observed in the Mediterranean woodland and humid–temperate forest, depending the organic acid and its temporal dynamic, which varied greatly among the compounds: In the Mediterranean woodland, incorporation of ^{13}C in water extractable (free) organic acids in both sampling depths was low at the beginning of the experiment being 2.5, 1.3, and 0.7 µg g^{-1} for oxalic, malic, and

citric acid in 0–10 cm sampling depth, respectively. The values increased over time to 6.2, 8.3, and 1.3 µg g^{-1} for oxalic, malic, and citric acid 14 days after labeling in 0–10 cm sampling depth, respectively) (Figure 2.4.4). In both sites, the arid shrubland and Mediterranean woodland ^{13}C incorporation in HCl extractable (sorbed) oxalic acid in 0–10 cm was highest directly after labeling. This coincided with the highest allocation of ^{13}C to fungal biomass at these sites. At the humid–temperate forest soil incorporation of ^{13}C in organic acids was stable over the course of the experiment and higher in 0–10 cm than 20–30 cm sampling depth (Figure 2.4.4).

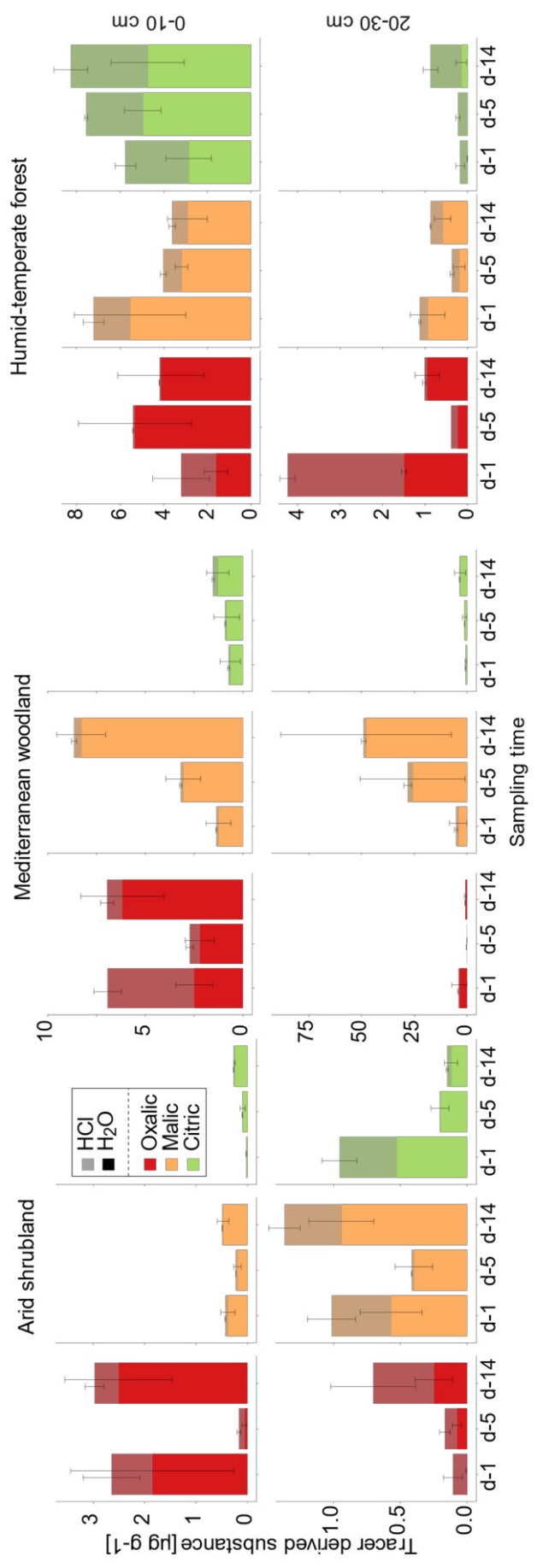

Figure 2.4.4: ^{13}C incorporation in free and sorbed low-molecular-weight organic acids (LMWOA) for the arid shrubland, Mediterranean woodland, and humid-temperate forest. For each compound incorporation is shown for 0–10 cm sampling depth (top) and for 20–30 cm sampling depth (bottom). The figure shows the incorporation of ^{13}C from CO_2 in oxalic-, malic-, and citric acid. The dark bars represent the free, H_2O extractable fraction of organic acids, the light bars the sorbed, HCl extractable fraction of organic acids from a sequential extraction of the acids. Note the difference in scaling of the x-axes. Whiskers show the standard error of the mean (n=4)

Relating P pools to ^{13}C incorporation

To investigate correlations between ^{13}C incorporation into root, microorganisms, and organic acids a PCA was calculated for each site separately. From each variable (^{13}C–Root, ^{13}C–Fungi, ^{13}C–Bacteria, ^{13}C–OxalicH2O, ^{13}C–OxalicHCl, ^{13}C–MalicH2O, ^{13}C–MalicHCl, ^{13}C–CitricH2O, ^{13}C–CitricHCl) the maximal value among all three sampling times was used in the PCA. The four P pools of water extractable P (P_{resin}), $NaHCO_3$ extractable P (P_{olsen}), NH_4–oxalate labile P (P_{ox}), and DCB extractable P (P_{dith}) were used as supplementary variables to investigate relationships between P speciation in soil and C allocation to plants, microorganisms, and organic acids (Figure 2.4.4).

The first principal component explained 50, 49 and 64%, the second principal component accounted for 18, 29, and 19% of the variation within the data at the arid shrubland, Mediterranean woodland, and humid–temperate forest, respectively. At the arid shrubland C allocation to bacteria and fungi was strongly correlated strongly with plant available P (P_{resin}, P_{olsen}), P bound in crystalline pedogenic metal–(hydr)oxides (P_{dith}), and, to a lower extend, with NH_4–oxalate leachable P (P_{ox}). ^{13}C allocation to roots correlated with ^{13}C in water soluble oxalic acid. ^{13}C allocation to roots and free oxalic acid was only weakly correlated with ^{13}C allocation to microorganisms (Figure 2.4.4). At the Mediterranean woodland C allocation to bacteria (^{13}C–Bacteria) and roots (^{13}C–Roots) correlated with ^{13}C in sorbed oxalic acid (^{13}C–$Oxalic_{HCl}$). These three variables correlated strongly with NH_4–oxalate leachable P (P_{ox}). P_{dith} was again strongly correlated with ^{13}C in fungi (^{13}C–Fungi). Polsen was strongly correlated with free oxalic acid (^{13}C–$Oxalic_{H2O}$) and plant available P in general correlated with ^{13}C in free and sorbed malic, citric acid (Figure 2.4.4). At the humid–temperate forest ^{13}C in bacteria and fungi was strongly correlated with ^{13}C in organic acids except for sorbed oxalic and malic acid. Moreover, ^{13}C in roots showed a moderate correlation with ^{13}C in microorganisms and organic acids, except for sorbed oxalic and malic acid. ^{13}C in microorganisms, roots, and organic acids, except of sorbed oxalic and malic acid, correlated with plant available P. (Figure 2.4.4).

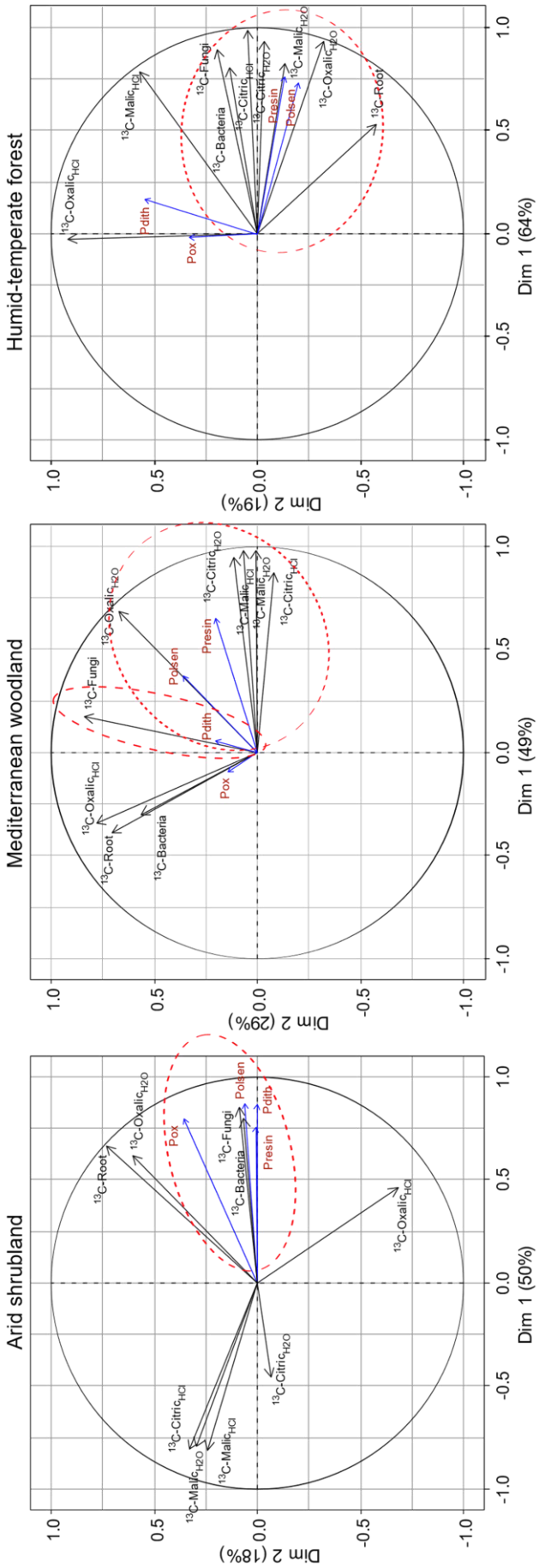

Figure 2.4.5: Biplot of a principal component analysis (PCA) with supplementary variables conducted at each of the three study sites separately. The PCA was calculated with the variables 13C in bacteria, 13C in fungi, 13C in roots, 13C in oxalic acid, 13C in malic acid, 13C in citric acid. The P fractions Presin, Polsen, Pox, and Pdith were included as supplementary variables. The angle between variables used in the PCA and supplementary variables can be interpreted in terms of correlation (the smaller the angle the higher the correlation between two variable).

2.4.5. Discussion

N and P availability/exploitation

Plant available P is highest in the humid–temperate forest, mainly due to high contents of $NaHCO_3$ extractable P (P_{olsen}) (Figure 2.4.1). The large P_{olsen} content goes along with a high content of NH_4–oxalate extractable P, which is in line with a study by Wuenscher et al. (2016) who found a good correlation between P_{olsen} and P_{ox} over a wide range of agricultural soils from central Europe. In the humid–temperate forest the high P_{ox} and P_{dith} contents are likely to be a result of high contents of poorly crystalline Al in the soil (Bernhard et al., 2018) and P adsorbed to Al–(hydr)oxides (Koester et al., 2020). P_{ox} was even higher than P_{dith} in this ecosystem which points towards a contribution of crystalline $AlPO_4$ surface precipitates and minerals in the order of the difference between P_{ox} and P_{dith} to the total P content (Prietzel, 2017). In summary this indicates that P taken up by plants originates from secondary P minerals and adsorbed P. However, biomass is highest among the three sites in the humid–temperate forest, hence, despite moderate availability, P is still limiting plant growth, as can be seen at high C:P ratios at this site (Stock et al., 2021). Moreover, our results are in contradiction to findings by Bernhard et al. (2018), who measured lowest plant available P at the humid–temperate forest compared to the Mediterranean woodland and arid shrubland by determining plant available P via extraction with 0.025 M HCl + 0.03 M NH_4F at pH 2.6 (Bray–1 extract). The pH values at the humid–temperate forest soil are around 4.5 (Bernhard et al., 2018). Therefore, the determination of plant available P at pH 2.6 likely gives more reliable results for this ecosystem. Thereby, the results by Bernhard et al. (2018) also point towards a P limitation of plant–growth at the humid–temperate forest. In addition to P, N as well is limiting plant growth in this ecosystem. Stock et al. (2021) reported C:N ratios of the samples from the same experiment of about 25 for the humid–temperate forest. The plant available P pool was lowest in the Mediterranean woodland, water extractable P and $NaHCO_3$ labile P together were 3.4 times lower than in the humid–temperate forest, indicating that plants are likely to experience an even higher P limitation in this ecosystem (Figure 2.4.1), considering that the biomass is high and plant cover is already 100% (Bernhard et al., 2018). Moreover, erosion (van Dongen et al., 2019) and soil denudation rates (Schaller et al., 2018) are the highest among the three study sites in the Mediterranean woodland imposing a high risk of nutrients being lost from the ecosystem. The specific root length in the upper 10 cm (Stock et al., 2021) is high which provides the prerequisite for fast nutrient uptake once they become available and reflect low P and water availability (Reich, 2014; Sharma et al., 2020) and high erosional losses at this site. This adaptation to fast nutrient uptake is also caused by the small pool of $NaHCO_3$ extractable P in the Mediterranean woodland which indicates that P is either in the soil solution or strongly

bound to the soil. In the Mediterranean woodland and arid shrubland the lack of water can lead to a change from monodentate to bidentate binding of P to Fe and Al in soil. The later binding is thought of being irreversible, meaning that P bound in this way is not longer plant available. The C:N ratio in the Mediterranean woodland and arid shrubland was in the range between 12–14, hence, did not indicate that plant–growth would be N limited at these two ecosystems. In both ecosystems this is likely a result of a relatively high abundance of diazotrophs (measured by nifH gene abundance, personal communication with K. Abdallah& S. Stock, "Soil nitrogen cycling along a precipitation gradient: from semi–desert to rainforest"). Especially in the arid shrubland the vegetation has a low demand, and the availability is likely to be stronger constrained by water availability and biological N nitrification than by N itself.

Plant C investment in P mobilization

^{13}C incorporation in roots and fungal PLFA in the Mediterranean woodland and humid–temperate forest in both sampling depth and in bacterial PLFA in the Mediterranean woodland and humid–temperate forest in 20–30 cm showed a pattern which is to expect when the tracer from a pulse labeling is flowing through a C pool, however, the kinetics of the individual pools were largely different. The magnitude of the ^{13}C incorporation in the arid shrubland was low in roots, fungal– and bacterial PLFA, therefore, the evaluation of tracer incorporation kinetics in this ecosystem is limited, however, the PCA allowed to draw some conclusions also for this ecosystem.

As we found similar incorporation of ^{13}C in all three LMWOAs in the humid–temperate forest, we conclude that the three acids were equally important in this ecosystem. The PCA gives indication that the acids were both, plant exuded but also produced by microorganisms (Figure 2.4.5). When comparing the ^{13}C incorporation kinetics in roots and microorganisms (Figure 2.4.3) on the one hand and LMWOA on the other hand (Figure 2.4.4) it becomes clear that oxalic and malic acid show a similar pattern as microorganisms and ^{13}C kinetics in citric acid resembles the ^{13}C incorporation into roots. At the same time ^{13}C in roots steadily increases, suggesting that plants' C allocation to roots is slow and controlled by a plant internal reservoir. Plant available P in the humid–temperate forest is highest among the three ecosystems. At the same time all P mobilization proxies correlate strongly with plant available P in the PCA (Figure 2.4.5). Moreover, strongly sorbed or precipitated P (P_{ox}, P_{dith}) was correlated only with sorbed oxalic acid. It has been shown that fungi intend to exploit nutrients, especially P, by colonizing nutrient rich minerals (Jongmans et al., 1997). Moreover, the microbial community around AMF colonized roots is different from that of a non mycorrhized root and that around hyphae (hyphosphere), which most likely also impacts chemical conditions and compounds produced

by the microbial community (Ouahmane et al., 2007). It was never shown that AMF themselves produce oxalic acid, but it was proven that they provide the conditions for bacteria in their hyphosphere to produce them. AMF feed phosphate solubilizing bacteria in their vicinity in exchange for P (Zhang et al., 2016) and an important mechanisms of P mobilization by bacteria is organic acid exudation. This indirect effect of fungi on oxalic acid production also explains, that despite high contents of oxalic acid in the humid–temperate forest soil there was little ^{13}C incorporated in oxalic acid at this site. Generally, we conclude that bacteria in soil do not directly dependent on input root derived photoassimilates. Moreover, we conclude that mineral bound P forms play only a minor role for biota's P nutrition in this ecosystem and that the primary P source in this ecosystem is organic P. This is in line with earlier studies from this site (Koester et al., 2020).

The ^{13}C incorporation to LMWOA in the Mediterranean woodland changed markedly over the course of the experiment. In 0–10 cm sampling depths the contents of ^{13}C in free LMWOA were highest two weeks after labeling (Figure 2.4.4). This was closely related to an increase of ^{13}C in root biomass in this ecosystem (Figure 2.4.3), pointing to a plant origin of these acids. The plant available P forms correlated with free oxalic acid but also had a high loading on the first dimension of the PCA, which represented free and sorbed malic and citric acid. Fungal PLFA on the contrary were highest enriched in ^{13}C at the first sampling time and decreased steadily over the sampling period (Figure 2.4.3), which coincided with a decrease of ^{13}C in sorbed oxalic acid from one day after tracer application to the last sampling time (Figure 2.4.4). The 2nd principal component in the Mediterranean woodland explains 13C in roots, fungal and bacterial PLFA, sorbed– and, to a lower extend, free oxalic acid (Figure 2.4.5). At the same time P_{dith} and P_{ox} correlated strongly with the 2nd dimension of the PCA, pointing to exploitation of hardly soluble P forms by roots and microorganisms. From the ^{13}C kinetics of roots and microorganisms (Figure 2.4.3) and LMWOA (Figure 2.4.4) we infer that ^{13}C in sorbed oxalic acid is related to ^{13}C in fungi, while it is independent from ^{13}C in roots and bacteria. Also, the PCA revealed a strong correlation of ^{13}C in fungi with DCB leachable P, pointing to elevated allocation of photoassimilates to fungi for the sake of fungal growth when DCB is high. The sorbed fraction of oxalic acid in the soil is actively participating in mineral dissolution processes as it is already adsorbed to sorption sites which potentially hosted phosphate ions in the first place. In the Mediterranean woodland the relative contribution of DCB– and NH_4–oxalate leachable P to total P in soil is higher than in the humid–temperate forest indicating a greater relevance of these P forms for biota in the soils of this ecosystem. Moreover, oxalic acid shows the highest content among the three acids in the Mediterranean woodland, confirming the high relevance of P solubilization by oxalic acid in the Mediterranean woodland. We must assume that biological P

uptake from the soil solution is very efficient because plant available P contents are low while the sorption capacity of the soil for P is also low compared to the humid–temperate forest (Koester, 2021). Therefore, our results corroborate that below ground C allocation to roots and microorganisms is important for P cycling in the Mediterranean woodland as this site had the lowest plant available P contents (Figure 2.4.1) while C allocation to roots was mostly highest along the ecosequence (Figure 2.4.3). C allocation by plants to root exudates is a well-known strategy for plants to deal with abiotic stress to keep nutrients available and have them accessible once the abiotic stress alleviates (Williams and Vries, 2020). In an artificial drought experiment root C exudation was enhanced despite a reduction of total C uptake and less assimilation of C to above ground biomass (Karlowsky et al., 2018). To which extend this is a general strategy and as well applicable to P cycling e.g., in more arid ecosystems, is not clear yet. Nevertheless, it is reasonable to assume that plants concentrate their resources below–ground when experiencing abiotic stress and keep the rhizosphere functioning to be ready to take up nutrients once surrounding conditions allow them to grow (Williams and Vries, 2020). Contrary to the humid–temperate forest in the Mediterranean woodland P mobilization strategies seem to be less divers. This is in accordance with a general decrease of microbial diversity and multifunctionality under increased aridity (Delgado–Baquerizo et al., 2016; Maestre et al., 2015).

Microbial activity in the arid shrubland performs at a much lower rate as in the other two ecosystems. The reason for this is a low C input to the soil mediated by the vegetation, which is water limited and, hence, the input of photoassimilates via roots is low (Bernhard et al., 2018; Canessa et al., 2020; Stock et al., 2019). With respect to temporal dynamics of ^{13}C incorporation in roots, microorganisms, and LMWOA only limited conclusions can be drawn as the contents of measured parameters are low and, therefore, only small differences occur. While incorporation of ^{13}C in bacteria and fungi decreases over the course of the experiment the incorporation in roots increases slightly. Incorporation in LMWOA is very heterogenous among the three acids and between the sorbed and free fraction of the acids, suggesting a mixt origin from plants as well as microorganisms. As in the Mediterranean woodland ^{13}C in fungi correlates strongly with DCB leachable P. Suggesting investment in fungal biomass when DCB leachable P is high. The content of plant available P, particularly P_{resin}, is higher than in the Mediterranean woodland, indicating less efficient uptake of P from the soil solution by biota. Overall, the patterns in the arid shrubland are very similar to those in the Mediterranean woodland but on a lower level, demonstrating that presumably already in the Mediterranean woodland drought adaptations and adaptations to related abiotic stresses are driving the

belowground C allocation and that these drivers are just much more expressed in the more dry, arid shrubland.

Conclusively, we found evidence that C allocation to the rhizosphere is decoupled from microbial activity in the humid–temperate forest while in the Mediterranean woodland and arid shrubland microorganisms are more tightly bound to plant activity. Microbial mineralization of nutrients in the humid–temperate forest is a steady process which does not directly rely on the input of energy in the form of photo–assimilated C but is moderated by a rich reservoir of organic matter present in soil. The two other ecosystems, however, have lower soil C contents and, this, the microbial community depends much stronger on the input of readily degradable C by roots. We found indications that nutrient availability along the aridity gradient is restricted by different factors, resulting in a unimodal curve of highest N and P availability in the Mediterranean woodland. This is likely a result of highest weathering rates at this site (van Dongen et al., 2019) supplying fresh rock–born nutrients and a high abundance of legumes delivering N to the ecosystem. At the same time water availability is sufficient for nutrients to diffuse towards roots which form a dense network of fine roots in the upper soil layer (Stock et al., 2021). Moreover, the rhizosphere is well supplied with root exudates during the growing season, enabling microbial activity to scavenge for nutrients. In the arid shrubland plant growth is limited by water availability. This cascades down to the microbial community which suffers from C limitation due to the lack of a dense vegetation cover. In the humid–temperate forest N and P availability are low because of proceeded pedogenesis (high fixation of nutrients in soil) and high precipitation, which results in high leaching losses, especially of N.

2.4.6. Conclusions

P forms in soil changed along the ecosequence from mainly precipitated and absorbed inorganic P in the arid shrubland to a a greater proportion of plant available P. We know from other studies at the same sites that also organic P is higher under humid than under Mediterranean and arid climate. LMWOA were significantly higher under humid temperate forest than Mediterranean woodland and arid shrubland but ^{13}C allocation to LMWOA was similar in the humid–temperate forest and Mediterranean woodland. ^{13}C allocation to oxalic acid was identified as an indicator for biological weathering of precipitated and sorbed inorganic P in the Mediterranean woodland and arid shrubland. Our results indicate the utilization of organic P in the humid–temperate forest and a high microbial diversity and, therefore a plethora of P mobilizing processes. In the Mediterranean woodland and arid shrubland on the contrary P mobilization is more specific and mainly governed by roots and fungi.

2.4.7. Acknowledgement

We thank the Chilean National Park Service Corporación Nacional Forestal (CONAF) for granting permission to work in the National parks Nahuelbuta and La Campana. We also thank the Center for Advanced Research in Arid Zones (CEAZA) for the opportunity to work in the Nacional Reserve Santa Gracia.

2.4.8. Funding

This study was funded by the German Research Foundation (DFG) within the frame of the priority program 1803, EarthShape: Earth surface shaping by biota (DFG SPP 1803; project number 255469939) under the subproject „Fire–Induced Redistribution and Losses of Elements in the Weathering Zone“ (DFG DI 2136/11)

2.4.9. Conflict of interest

The authors have no conflict of interest to declare, the research was conducted in the absence of any commercial or financial relationships that could be construed as a potential conflict of interest.

2.4.10. References

Aguilera–Betti, I., Muñoz, A.A., Stahle, D., Figueroa, G., Duarte, F., González–Reyes, Á., Christie, D., Lara, A., González, M.E., Sheppard, P.R., Sauchyn, D., Moreira–Muñoz, A., Toledo–Guerrero, I., Olea, M., Apaz, P., Fernandez, A., 2017. The First Millennium–Age Araucaria Araucana in Patagonia. trre 73 (1), 53–56.

Andrus, N., Tye, A., Nesom, G., Bogler, D., Lewis, C., Noyes, R., Jaramillo, P., Francisco–Ortega, J., 2009. Phylogenetics of Darwiniothamnus (Asteraceae: Astereae) – molecular evidence for multiple origins in the endemic flora of the Galápagos Islands. Journal of Biogeography 36 (6), 1055–1069.

Bernhard, N., Moskwa, L.–M., Schmidt, K., Oeser, R.A., Aburto, F., Bader, M.Y., Baumann, K., Blanckenburg, F. von, Boy, J., van den Brink, L., Brucker, E., Büdel, B., Canessa, R., Dippold, M.A., Ehlers, T.A., Fuentes, J.P., Godoy, R., Jung, P., Karsten, U., Köster, M., Kuzyakov, Y., Leinweber, P., Neidhardt, H., Matus, F., Mueller, C.W., Oelmann, Y., Oses, R., Osses, P., Paulino, L., Samolov, E., Schaller, M., Schmid, M., Spielvogel, S., Spohn, M., Stock, S., Stroncik, N., Tielbörger, K., Übernickel, K., Scholten, T., Seguel, O., Wagner, D., Kühn, P., 2018. Pedogenic and microbial interrelations to regional climate and local topography: New insights from a climate gradient (arid to humid) along the Coastal Cordillera of Chile. CATENA 170, 335–355.

Burns, R.G., DeForest, J.L., Marxsen, J., Sinsabaugh, R.L., Stromberger, M.E., Wallenstein, M.D., Weintraub, M.N., Zoppini, A., 2013. Soil enzymes in a changing environment: Current knowledge and future directions. Soil Biology and Biochemistry 58, 216–234.

Canessa, R., Brink, L., Saldaña, A., Rios, R.S., Hättenschwiler, S., Mueller, C.W., Prater, I., Tielbörger, K., Bader, M.Y., 2020. Relative effects of climate and litter traits on decomposition change with time, climate and trait variability. J Ecol.

Delgado–Baquerizo, M., Maestre, F.T., Reich, P.B., Jeffries, T.C., Gaitan, J.J., Encinar, D., Berdugo, M., Campbell, C.D., Singh, B.K., 2016. Microbial diversity drives multifunctionality in terrestrial ecosystems. Nat Commun 7 (1), 10541.

Diehl, P., Fontenla, S.B., 2010. Arbuscular mycorrhizal infection in two morphological root types of Araucaria araucana (Molina) K. Koch. Revista Argentina de Microbiología 42, 133–137.

Dippold, M.A., Kuzyakov, Y., 2016. Direct incorporation of fatty acids into microbial phospholipids in soils: Position−specific labeling tells the story. Geochimica et Cosmochimica Acta 174, 211–221.

E. Bligh, W. Dyer, 1959. A rapid method of total lipid extraction and purification. undefined.

Fick, S.E., Hijmans, R.J., 2017. WorldClim 2: new 1−km spatial resolution climate surfaces for global land areas. Int. J. Climatol 37 (12), 4302–4315.

Frostegård, A., Bååth, E., 1996. The use of phospholipid fatty acid analysis to estimate bacterial and fungal biomass in soil. Biol Fert Soils 22 (1–2), 59–65.

Gavito, M.E., Olsson, P.A., 2003. Allocation of plant carbon to foraging and storage in arbuscular mycorrhizal fungi. FEMS Microbiol Ecol 45 (2), 181–187.

Gearing, P.J., Gearing, J.N., Maughan, J.T., Oviatt, C.A., 1991. Isotopic distribution of carbon from sewage sludge and eutrophication in the sediments and food web of estuarine ecosystems. Environ. Sci. Technol. 25 (2), 295–301.

Gunina, A., Dippold, M.A., Glaser, B., Kuzyakov, Y., 2014. Fate of low molecular weight organic substances in an arable soil: From microbial uptake to utilisation and stabilisation. Soil Biology and Biochemistry 77, 304–313.

Gunina, A., Kuzyakov, Y., 2015. Sugars in soil and sweets for microorganisms: Review of origin, content, composition and fate. Soil Biology and Biochemistry 90, 87–100.

Henry, A., Doucette, W., Norton, J., Bugbee, B., 2007. Changes in crested wheatgrass root exudation caused by flood, drought, and nutrient stress. Journal of Environmental Quality 36 (3), 904–912.

Herz, K., Dietz, S., Gorzolka, K., Haider, S., Jandt, U., Scheel, D., Bruelheide, H., 2018. Linking root exudates to functional plant traits. PLOS ONE 13 (10), e0204128.

Hinsinger, P., 2001. Bioavailability of soil inorganic P in the rhizosphere as affected by root−induced chemical changes: a review. Plant and soil 237 (2), 173–195.

Jones, D.L., Darrah, P.R., 1994. Role of root derived organic acids in the mobilization of nutrients from the rhizosphere. Plant Soil 166 (2), 247–257.

Jongmans, A.G., van Breemen, N., Lundström, U., van Hees, P.A.W., Finlay, R.D., Srinivasan, M., Unestam, T., Giesler, R., Melkerud, P.−A., Olsson, M., 1997. Rock−eating fungi. Nature 389 (6652), 682–683.

Karlowsky, S., Augusti, A., Ingrisch, J., Hasibeder, R., Lange, M., Lavorel, S., Bahn, M., Gleixner, G., 2018. Land use in mountain grasslands alters drought response and recovery of carbon allocation and plant−microbial interactions. J Ecol 106 (3), 1230–1243.

Koester, M., Stock, S.C., Nájera, F., Abdallah, K., Gorbushina, A., Prietzel, J., Matus, F., Klysubun, W., Boy, J., Kuzyakov, Y., Dippold, M.A., Spielvogel, S., 2020. From rock eating to vegetarian ecosystems — Disentangling processes of phosphorus acquisition across biomes. Geoderma, 114827.

Komsta, L., 2011. outliers: Tests for outliers.

König, N., Blum, U., Symossek, F., Bussian, B., Furtmann, K., Gärtner, A., Groeticke, K., Gutwasser, F., Höhle, J., Hauenstein, M., Kiesling, G., Klingenberg, U., Klinger, T., Nack, T., Stahn, M., Trefz−Malcher, G., Wies, K., 2014. Handbuch Forstliche Analytik.

Kuzyakov, Y., Domanski, G., 2000. Carbon input by plants into the soil. Review. J. Plant Nutr. Soil Sci. 163 (4), 421–431.

Le Sebastien, Josse, J., Husson, F., 2008. FactoMineR: A Package for Multivariate Analysis. Journal of Statistical Software 25 (1), 1–18.

Maestre, F.T., Delgado−Baquerizo, M., Jeffries, T.C., Eldridge, D.J., Ochoa, V., Gozalo, B., Quero, J.L., García−Gómez, M., Gallardo, A., Ulrich, W., Bowker, M.A., Arredondo, T., Barraza−Zepeda, C., Bran, D., Florentino, A., Gaitán, J., Gutiérrez, J.R., Huber−Sannwald, E., Jankju, M., Mau, R.L., Miriti, M., Naseri, K., Ospina, A., Stavi, I., Wang, D., Woods, N.N., Yuan, X., Zaady, E., Singh, B.K., 2015. Increasing aridity reduces soil microbial diversity and abundance in global drylands. PNAS 112 (51), 15684–15689.

Marschner, P., Marschner, H.M.n.o.h.p. (Eds.), 2012. Marschner's mineral nutrition of higher plants, 3rd ed. ed. Academic Press, Amsterdam, London.

Mehra, O.P., Jackson, M.L., 1958. Iron Oxide Removal from Soils and Clays by a Dithionite–Citrate System Buffered with Sodium Bicarbonate. Clays and Clay Minerals 7 (1), 317–327.

Ohno, T., Zibilske, L.M., 1991. Determination of Low Concentrations of Phosphorus in Soil Extracts Using Malachite Green. Soil Sci. Soc. Am. J. 55 (3), 892–895.

Olsen, S.R., Cole, C.V., Watanabe, F.S., Dean, L.A., 1954. Estimation of available phosphorus in soils by extraction with sodium bicarbonate Circular 939. U.S. Dept. of Agriculture, Washington DC, USA, charts ; 23 cm.

Ouahmane, L., Thioulouse, J., Hafidi, M., Prin, Y., Ducousso, M., Galiana, A., Plenchette, C., Kisa, M., Duponnois, R., 2007. Soil functional diversity and P solubilization from rock phosphate after inoculation with native or allochtonous arbuscular mycorrhizal fungi. Forest Ecology and Management 241 (1–3), 200–208.

Paterson, E., 2003. Importance of rhizodeposition in the coupling of plant and microbial productivity. European Journal of Soil Science 54 (4), 741–750.

Prietzel, J., 2017. Mobilization of X-ray amorphous and crystalline aluminum and iron phosphates by common soil extraction procedures. Zeitschrift für Pflanzenernährung und Bodenkunde 180 (1), 14–17.

Reich, P.B., 2014. The world-wide 'fast–slow' plant economics spectrum: a traits manifesto. J Ecol 102 (2), 275–301.

Rouphael, Y., Cardarelli, M., Schwarz, D., Franken, P., Colla, G., 2012. Effects of Drought on Nutrient Uptake and Assimilation in Vegetable Crops, in: Aroca, R. (Ed.), Plant Responses to Drought Stress [recurso electrónico]. From Morphological to Molecular Features. Springer Healthcare Ltd; Imprint Springer, Alemania, pp. 171–195.

Sala, O.E., Golluscio, R.A., Lauenroth, W.K., Roset, P.A., 2012. Contrasting nutrient–capture strategies in shrubs and grasses of a Patagonian arid ecosystem. Journal of Arid Environments 82, 130–135.

Schaller, M., Ehlers, T.A., Lang, K., Schmid, M., Fuentes-Espoz, J.P., 2018. Addressing the contribution of climate and vegetation cover on hillslope denudation, Chilean Coastal Cordillera (26°–38°S). Earth and Planetary Science Letters 489, 111–122.

Schwertmann, U., 1964. Differenzierung der Eisenoxide des Bodens durch Extraktion mit Ammoniumoxalat-Lösung. Journal of Plant Nutrition and Soil Science 105 (3), 194–202.

Sharma, M., Pang, J., Wen, Z., Borda, A. de, Kim, H.S., Liu, Y., Lambers, H., Ryan, M.H., Siddique, K.H.M., 2020. A significant increase in rhizosheath carboxylates and greater specific root length in response to terminal drought is associated with greater relative phosphorus acquisition in chickpea. Plant Soil.

Shukla, P., Skea, J., Calvo Buendia, E., Masson-Delmotte, V., Pörtner, H.-O., Roberts, D.C., Zhai, P., Slade, R., Connors, S., Diemen, R. van, Ferrat, M., Haughey, E., Luz, S., Neogi, S., Pathak, M., Petzold, J., Portugal Pereira, J., Vyas, P., Huntley, E., Kissick, K., Belkacemi, M., Malley, J. (Eds.), 2019. IPCC, 2019: Climate Change and Land: an IPCC special report on climate change, desertification, land degradation, sustainable land management, food security, and greenhouse gas fluxes in terrestrial ecosystem. In press.

Solbrig, O.T., 1962. The South American Species of Erigeron. Contributions from the Gray Herbarium of Harvard University (191), 3–79.

Solbrig, O.T., 1966. The South American Species of Gutierrezia. Contributions from the Gray Herbarium of Harvard University (197), 3–42.

Sommer, J., Dippold, M.A., Zieger, S.L., Handke, A., Scheu, S., Kuzyakov, Y., 2017. The tree species matters: Belowground carbon input and utilization in the myco-rhizosphere. European Journal of Soil Biology 81, 100–107.

Stock, S.C., Koester, M., Boy, J., Godoy, R., Nájera, F., Matus, F., Merino, C., Abdallah, K., LEUSCHNER, C., Spielvogel, S., Gorbushina, A.A., Kuzyakov, Y., Dippold, M.A., 2021. Plant carbon investment in fine roots and arbuscular mycorrhizal fungi: A cross-biome study on nutrient acquisition strategies. Science of The Total Environment 781, 146748.

Stock, S.C., Köster, M., Dippold, M.A., Nájera, F., Matus, F., Merino, C., Boy, J., Spielvogel, S., Gorbushina, A., Kuzyakov, Y., 2019. Environmental drivers and stoichiometric constraints on enzyme activities in soils from rhizosphere to continental scale. Geoderma 337, 973–982.

Tamm, O., 1922. Eine Methode zur Bestim mung der anorganischen Komponenten des Gelkomplexes im Boden. Meddel. Statens Skogsforsoksanst. 19, 385–404.

Trabucco, A., Zomer, R., 2019. Global Aridity Index and Potential Evapotranspiration (ET0) Climate Database v2. Figshare. doi:10.6084/M9.FIGSHARE.7504448.V3.

Valdebenito, H., Lowrey, T.K., Stuessy, T.F., 1986. A New Species of Erigeron (Compositae: Astereae) from Chile. Brittonia 38 (1), 1.

van Dongen, R., Scherler, D., Wittmann, H., Blanckenburg, F. von, 2019. Cosmogenic 10 Be in river sediment: where grain size matters and why. Earth Surf. Dynam. 7 (2), 393–410.

Veblen, T.T., 1982. Regeneration Patterns in Araucaria araucana Forests in Chile. Journal of Biogeography 9 (1), 11.

Wei, L., Chen, C., Xu, Z., 2010. Citric acid enhances the mobilization of organic phosphorus in subtropical and tropical forest soils. Biol Fertil Soils 46 (7), 765–769.

Wickham, H., 2016. ggplot2: Elegant Graphics for Data Analysis.

Williams, A., Vries, F.T. de, 2020. Plant root exudation under drought: implications for ecosystem functioning. New Phytologist 225 (5), 1899–1905.

Wuenscher, R., Unterfrauner, H., Peticzka, R., Zehetner, F., 2016. A comparison of 14 soil phosphorus extraction methods applied to 50 agricultural soils from Central Europe. Plant Soil Environ. 61 (No. 2), 86–96.

Zhang, L., Xu, M., Liu, Y., Zhang, F., Hodge, A., Feng, G., 2016. Carbon and phosphorus exchange may enable cooperation between an arbuscular mycorrhizal fungus and a phosphate–solubilizing bacterium. New Phytologist 210 (3), 1022–1032.

2.5. Environmental drivers and stoichiometric constraints on enzyme activities in soils from rhizosphere to continental scale (Study 4)

Published in *Geoderma* (2019), 337, 973–982, doi: 10.1016/j.geoderma.2018.10.030

Svenja C. Stock [a]*, Moritz Köster [b], Michaela A. Dippold [b], Francisco Nájera [c], Francisco Matus [c], Carolina Merino [c], Jens Boy[d], Sandra Spielvogel [e], Anna Gorbushina [f], and Yakov Kuzyakov [a,g,h]

Affiliation

[a] Soil Science of Temperate Ecosystems, University of Göttingen, Göttingen, Germany

[b] Biogeochemistry of Agroecosystems, University of Göttingen, Göttingen, Germany

[c] Departamento de Ciencias Químicas y Recursos Naturales, Universidad de La Frontera, Temuco, Chile

[d] Institute of Soil Science, Leibniz University Hannover, Hannover, Germany

[e] Soil Science, University of Kiel, Kiel, Germany

[f] Department Materials and Environment, Federal Institute for Material Research and Testing, Berlin, Germany

[g] Institute of Environmental Sciences, Kazan Federal University, 420049 Kazan, Russia

[h] Agro–Technology Institute, RUDN University, Moscow, Russia

2.5.1. Abstract

Microbial activity and functioning in soils are strongly limited by the availability of C, of which a great proportion is released by roots. Root exudates stimulate microbial activity and growth, or shift the stoichiometric balance between C, N, and P. Thereby, exudates heighten microbial nutrient demand and acquisition of N and P, leading to an increase in enzyme production. Aim of this study was to determine environmental controls of extracellular enzyme production, and hence on potential enzyme activities (V_{max}) and substrate affinities (K_m). To determine the controlling factors, we worked on four scales from the microscale (i.e., rhizosphere) through the mesoscale (i.e., soil depth) and landscape scale (relief positions), and finally to the continental scale (1200 km transect within the Coastal Cordillera of Chile). Kinetics of seven hydrolyzing enzymes of the C, N, and P cycles (cellobiohydrolase, β–glucosidase, β–xylosidase, β–N–acetylglucosaminidase, leucine–aminopeptidase, tyrosine–aminopeptidase, and acid phosphatase) were related to soil texture, C and N contents, pH, and soil moisture via redundancy analysis (RDA). Potential activities of C, N, and P acquiring enzymes increased up

to 7–times on the continental scale with rising humidity of sites and C and N contents, while substrate affinities simultaneously declined. On the landscape scale, neither V_{max} nor K_m of any enzyme differed considerably between north and south slopes. From top– to subsoil (down to 120 cm depth) potential activities decreased (strongest of aminopeptidases under humid temperate conditions with up to 90%). Substrate affinities, however, increased with greater soil depth only for N and P acquiring enzymes. Affinities of cellobiohydrolase and β–xylosidase, on the contrary, were 1.5– to 3–times higher in top– than in subsoil. A rise of potential activities from bulk soil to root was observed for N and P acquiring enzymes and β–glucosidase. Simultaneously, substrate affinities of N and P acquiring enzymes declined, whereas affinities of β–glucosidase increased. These trends of activities and affinities in the rhizosphere were significant only for acid phosphatase. The RDA displayed a strong relation of potential activities of C and P acquiring enzymes and β–N–acetylglucosaminidase to C and N contents as well as to the silt and clay contents. Aminopeptidase activity was mainly dependent on soil moisture and pH. We conclude that substrate availability for microorganisms mainly determined enzyme activity patterns on the continental scale (i.e., the humidity gradient). Patterns on the meso– and microscale are primarily controlled by nutrient limitation, which is induced by a shift of the stoichiometric balance due to input of easily available C by roots in the rhizosphere.

Keywords: Extracellular enzymes, stoichiometric homeostasis, rhizosphere effect, nutrient acquisition, multi–scale study

2.5.2. Introduction

Extracellular enzymes, originating largely from plant roots and soil microorganisms (Burns et al., 2013), catalyze soil organic matter decomposition (SOM). Enzymes split organic polymers into soluble molecules and ions, which can be assimilated by microorganisms and taken up by plant roots (Allison and Vitousek, 2005; Sinsabaugh et al., 2008). Microbial activity in soil is mainly limited by available carbon (C) (Blagodatsky and Richter, 1998; Hodge et al., 2000; Schimel and Weintraub, 2003), of which root exudates and decaying litter are the largest source (Bertin et al., 2003; Kuzyakov, 2002a; Pausch and Kuzyakov, 2018). Exudates are easily degradable and are thus highly available substrate for microorganisms (Bertin et al., 2003; Schimel and Weintraub, 2003; Meier et al., 2017), which can stimulate microbial activity and growth (Blagodatskaya et al., 2014; de Graaff et al., 2010; 2014, de Nobili et al., 2001), and in

turn increase C demand and investment into C and nutrient acquisition (i.e., enzyme synthesis) (Hernández and Hobbie, 2010).

Labile C stimulates not only microbial activity as readily available energy source, but also shifts the stoichiometric balance between C, nitrogen (N), and phosphorus (P) (Cheng and Kuzyakov, 2005; Phillips et al., 2011; Sinsabaugh and Moorhead, 1994). Thereby, labile C heightens microbial nutrient demand, which can be compensated by an upregulation of enzyme synthesis and a degradation of nutrient−rich compounds to maintain stoichiometric homeostasis (Chen et al., 2014; Cheng and Kuzyakov, 2005; Phillips et al., 2011; Sinsabaugh and Follstad Shah, 2012; Sinsabaugh et al., 2014). The upregulation of enzyme synthesis does not necessarily aim to boost enzyme activities, but also to produce enzymatic systems with higher substrate affinities to strengthen the competitiveness of microorganisms by a more efficient SOM and litter decomposition (Klipp and Heinrich, 1994; Kuzyakov and Xu, 2013; Stone and Plante, 2014). Whether enzyme production is upregulated depends on the cost efficiency of resource allocation into enzyme production in relation to microbial growth (Moorhead et al., 2012; Sinsabaugh and Follstad Shah, 2012).

Biochemical reaction products or a high availability of the target element (e.g., C, N, or P) can suppress enzyme activity. If sufficient easily available compounds are present to cover the cells' energy demands, the synthesis of new extracellular enzymes can be inhibited, (Sinsabaugh et al., 1993), as reported for N and P acquiring enzymes (DeForest et al., 2012; Olander and Vitousek, 2000; Turner and Wright, 2014). Alternatively, enzyme activity can be stimulated by the presence of their target substrate (Allison and Vitousek, 2005; Kielak et al., 2013). Microbial nutrient acquisition strategies (i.e., the allocation of resources into the synthesis of specific enzymes), therefore, likely change according to substrate and nutrient availability.

Extracellular enzyme activities are affected further by abiotic factors such as soil moisture, pH, and soil particle size distribution (Acosta−Martínez and Tabatabai, 2000; Sanaullah et al., 2011; Stemmer et al. 1998). They either directly modify enzyme activities, e.g., via conformation changes, binding onto soil particles, or the dependence on diffusion rates (Davidson and Janssens, 2006; Quiquampoix et al., 1992; Turner, 2010), or indirectly such as via altering substrate solubility, substrate concentration and accessibility, or grazing pressure on microorganisms (Burns et al., 2013; Kuzyakov and Mason−Jones, 2018 (in press); Ruamps et al., 2011). Responses of enzyme activities to moisture and pH changes are complex and vary depending on the ecosystem settings, scales, and ambient conditions to which enzymes are adapted (Allison and Jastrow, 2006; Dick and Tabatabai. 1987; Burns et al., 2013; German et al., 2012; Turner, 2010), rising a challenge for studies on enzyme driven SOM decomposition and

nutrient release across and within ecosystems. Former and recent studies well covered the response of extracellular enzymes to moisture shifts (e.g., Burns et al., 2013; Sanaullah et al., 2011; Steinweg et al., 2012) as well as rhizosphere effects (e.g., Dakora and Phillips, 2002; Phillips et al., 2011; Tarafdar and Jungk, 1987; Weintraub et al., 2007). Studies on enzyme kinetics were conducted on several scales, ranging from a continental scale (as the global distribution of activities (e.g., Sinsabaugh et al., 2008)) to focusing on microscales (as activity distribution in the rhizosphere (e.g., Razavi et al., 2016)). Directions and responses, however, are not consistent and simultaneous measurements of enzyme activities on multiple scales are scares.

By working on four spatial scales, we aimed to gain deeper insights on the regulatory effects of substrate availability and stoichiometric constraints on extracellular enzyme activities. Therefore, we analyzed kinetics of seven hydrolyzing enzymes of the C, N, and P cycles, responsible for cellulose and hemicellulose degradation, chitin and protein decomposition, and P acquisition via dissociation of phosphoric acid, and which are representative for decomposers of easily and complex substrates, on four scales: continental, landscape, meso−, and microscale.

We hypothesize that (1) on the continental scale, i.e., across ecosystems with a strong gradient in mean annual precipitation (MAP) and vegetation cover, enzyme activities are stimulated while substrate affinities decrease in response to increasing precipitation and plant biomass (litter) input (i.e., substrate availability). (2) On the landscape scale, represented by opposite slopes with different vegetation cover induced by deviating moisture regime, we also expect enzyme activities to rise with higher soil moisture. (3) On the medium scale of the soil profile (characterized by decreasing C and N contents with depth), we hypothesize enzyme activities to decrease from top− to subsoil, while substrate affinities enhance, in response to substrate scarcity in the subsoil. (4) On the microscale, i.e., from bulk soil to rhizosphere characterized by a C, N, and C:N increase, we hypothesize enzyme activities are stimulated, while substrate affinities decline in response to higher substrate availability.

2.5.3. Material and Methods

Study area

Study areas are located within the Coastal Cordillera of Chile between 29 ° and 38 ° southern latitude (Figure 2.5.1). The study sites cover a climate gradient from humid temperate (*Parque*

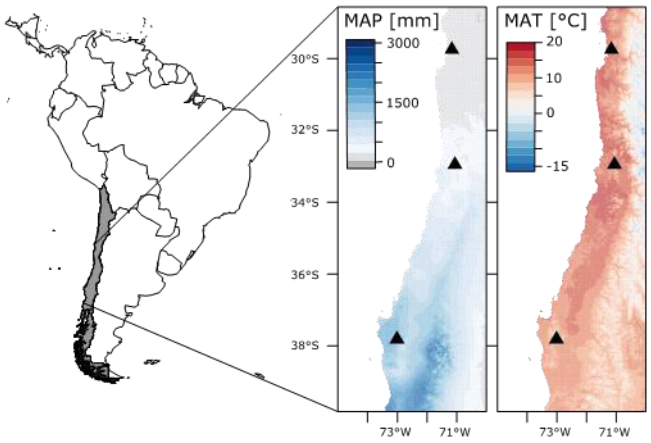

Figure 2.5.1: Study site overview. Showing mean annual precipitation (MAP) and mean annual temperature (MAT) along the continental gradient (WorldClima data, Hijmans et al., 2005). Study sites from north to south: Santa Gracia, La Campana, Nahuelbuta.

National Nahuelbuta (NA)) to Mediterranean (*Parque National La Campana* (LC)) and semiarid (*Reserva Santa Gracia* (SG)), with soils developed on granitoid parent material in all sites. Altitude and distance to the Pacific Ocean of the sites increase from north to south. In Nahuelbuta, Umbrisols and Podzols are present (pH 3.7–5.1), covered with a dense coniferous forest (Table: S 2.5.1; Bernhard et al., 2018). In La Campana, a patchy deciduous forest and evergreen sclerophyllous shrubs cover primarily Cambisols (pH 4.5–6.1) (Table: S 2.5.1; Bernhard et al., 2018). In Santa Gracia, the developed Cambisols (pH 5.48–7.0) are covered mainly with sclerophyllous shrubs and cacti (Table: S 2.5.1; Bernhard et al., 2018). For a more detailed description of the study sites see Table: S 2.5.1 as well as Bernhard et al. (2018) and Oeser et al. (2018).

Soil sampling and analyses

Soil samples were collected in summer 2016 from four soil pits in each study site; three on a south–exposed slope, arranged as a catena encompassing a soil pit at top–, mid–, and toe–slope positions, and one on a north–exposed slope at mid–slope position. Soil was sampled in three distances from channels of young living roots (0–2 mm, 2–4 mm, 4–6 mm), in three soil increments. Depth increments were chosen as percentage of depth until saprolite. The upper 30 % of the soil profile encompassed the topsoil, the increment between 30 % and 70 % the subsoil. The third increment encompassed the lower part of the soil profile down to the start of the saprolite. In total, 97 samples were collected. After sampling, the material was directly cooled and stored at 4 °C until analyses.

Gravimetric water content was determined by drying aliquots of the samples at 105 °C until constant weight. For determining C and N contents, aliquots of the samples were dried (50 °C) and subsequently ground milled. The measurement of C and N was conducted simultaneously by an elemental analyzer (NA1500, Fisons instruments, Milano, Italy). Soil particle size fraction and pH data were acquired by Bernhard et al. (2018) from samples taken in the same soil pits

and during the same time as our samples. These samples, however, were collected in different soil depth increments and not in rhizosphere gradients.

Enzyme assays

Activities of the extracellular enzymes were determined using synthetic fluorogenic substrates (Marx et al., 2001) (see Table 2.5.1). Subsamples (0.5 g) of the cooled (4 °C) soil samples were pre−incubated 24 h in sterile 100 ml jars. After pre−incubation, 50 ml of sterile water was added to the jars and shaken for 30 min. Subsequently, the soil solution was sonicated (40 J s^{-1}; 2 min) before aliquots of 50 µl were pipetted into black polystyrene 96−well microplates (Brand, Germany). Afterwards, 50 µl of buffer (0.1 *M* MES (pH 6.1) for 4−methylumbelliferone (MUF) linked substrates; 0.05 *M* TRIZMA (pH 7.8) for 7−amino−4−methylcoumarin (AMC) associated substrates) and 100 µl of substrate solution (0, 10, 20, 30, 40, 50, 100, and 200 µmol g^{-1}) were added. Three analytical replicates were measured for each sample at each substrate concentration. Fluorescence was measured by a microplate reader (Victor³ 1420−050 Multi label Counter; extinction: 355 nm, emission: 460 nm) immediately after substrate addition (t_0) and 2 h after addition (t_1). For calibration and accounting for quenching, standard plates were prepared with 50 µl of a composite soil solution (for each site and depth), with 150, 145, 140, 130, 100, 70, and 30 µl of buffer (MES or TRIZMA) and 0, 5, 10, 20, 50, 80, and 120 µl standard (MUF or AMC), respectively. Plates were measured at t_0 and t_1. With the regression slopes of the standard measurements, enzyme activities of the samples were calculated [nmol substrate g^{-1} soil h^{-1}]. Activities were fitted by the Michaelis−Menten Equation, which describes non−linear saturation curves:

$$V = \frac{(V_{max} * [S])}{(K_m + [S])} \qquad \text{Equation 2.5.1}$$

with S as the added substrate concentrations, V_{max} as the maximal rate of enzymatic activity under optimum substrate conditions, and K_m as the half−saturation constant as indicator for substrate affinity. The residual standard errors (RSE) of the fitted non−linear saturation curves are given in Table: S 2.5.2.

Table 2.5.1: Overview of extracellular enzymes with respective fluorogenic substrates (Marx et al., 2001) and ecological functions.

Enzyme	Fluorogenic substrate	Function
b–cellobiohydrolase (EC 3.2.1.91)	4–methylumbelliferone–b–D–cellobioside	hydrolysis of cellulose
b–glucosidase (EC 3.2.1.21)	4–methylumbelliferone–b–D–glucoside	hydrolysis of simple sugars
b–xylosidase (EC 3.2.2.37)	4–methylumbelliferone–b–D–xylopyranoside	hydrolysis of hemicellulose
b–N–acetylglucosaminidase (EC 3.2.1.14)	4–methylumbelliferone–acetyl–b–D–glucosaminide	hydrolysis of chitooligosaccharides into N–acetylglucosamine
leucine–aminope ptidase (EC 3.4.11.1)	L–leucine–7–amino–4–methylcoumarin	cleaving of peptide bonds in proteins
tyrosine–aminopeptidase (EC 3.4.11)	L–tyrosine–7–amino–4–methylcoumarin	cleaving of peptide bonds in proteins
acid phosphatase (EC 3.1.3.2)	4–methylumbelliferone–phosphate	P–acquisition via dissociation of phosphoric acid

Statistical analysis

All statistical analyses were conducted using R 3.4.3 (R Core Team, 2017). To evaluate the differences of soil parameters (C, N, C:N, soil moisture) and enzyme kinetics (V_{max} and K_m) between sites, slope aspects, soil depths, and root proximity, generalized linear mixed effect models (GLMM) were calculated using the R package 'lme4' (Bates et al., 2015). To determine the fixed effect 'site', we specified slope aspect as further fixed effect, and soil profile and soil depth as nested random effects. To determine the fixed effect of 'slope aspect', 'soil depth' and 'root proximity' (without interaction terms), we specified soil profile as nested random effect. *p* values were obtained by multiple comparisons with a general linear hypotheses test function using the R package 'multcomp' (Hothorn et al., 2008).

Redundancy analyses (RDA) were calculated to determine the effects of the soil variables C, N, C:N, moisture, pH, and particle size fractions on enzyme activities, as well as to test for the effects of these factors on C and N contents in soil. RDAs were conducted with the 'vegan' package (Oksanen et al., 2017) on scaled and log–transformed data. Type II scaling (correlation) plots are shown in the results including only significant constraining variables.

2.5.4. Results

Soil properties

C content in soil increased stronger on the continental and landscape scale than N content (3– to 4–times compared to 2– to 3–times) (Figure 2.5.2). On the mesoscale, C content decreased

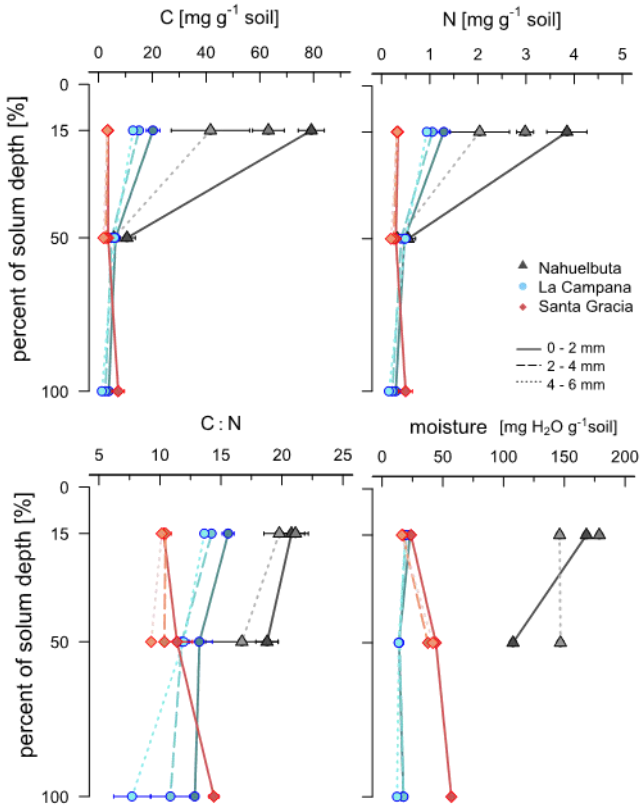

Figure 2.5.2: Depth profiles of carbon- nitrogen content, C:N ratio, and soil moisture in Nahuelbuta (black triangles), La Campana (blue circles), and Santa Gracia (red diamonds), separated by root proximities – 0–2 mm (darkest shade), 2–4 mm, and 4–6 mm (lightest shade). Data points represent means±SE of south–exposed slopes (n = 3). C and N content, as well as C:N show clear increase (*p<0.05*) from bulk soil to roots in the sites under humid temperate (Nahuelbuta) and under Mediterranean (La Campana) climate conditions; especially in the topsoil.

between 20% (in Santa Gracia) and 85% (in Nahuelbuta) from top– to subsoil, while N content declined between 25% (SG) and 80% (NA). On the microscale, C content was1.5– to 2–times

higher in root proximity than bulk soil, while N content was similar, resulting in 1.1– to 1.2–times higher C:N ratios in root proximity (0–2 mm) than in bulk soil (4–6 mm) (Figure 2.5.2).

Enzyme activities

Potential activities (V_{max}) of C, N, and P acquiring enzymes increased on the continental scale with higher soil moisture (Figure 2.5.3). The strongest rise (up to 7–times) was observed for β–xylosidase, β–N–acetylglucosaminidase, and acid phosphatase. On the landscape scale, activities of C, N, and P acquiring enzymes (except tyrosine–aminopeptidase) showed trends (*p*>0.05) of higher activities on the south than north slope at the sites under humid temperate (Nahuelbuta) and Mediterranean (La Campana) climate. Activities for most enzymes decreased from top– to subsoil (Figure 2.5.4). The strongest decrease was detected at the site under humid temperate climate conditions (up to 90 % for both aminopeptidases). Under semiarid climate conditions (Santa Gracia), only the protein degrading leucine–aminopeptidases decreased with soil depth. Root effects on enzyme activities (i.e., higher activities in root proximity than in bulk soil) were similar at sites under humid temperate and Mediterranean climate conditions, for C, N, and P acquiring enzymes (*p*>0.05) (Figure 2.5.5). Root effects on enzyme activities were mostly absent at the site under semiarid conditions (except for tyrosine–aminopeptidase).

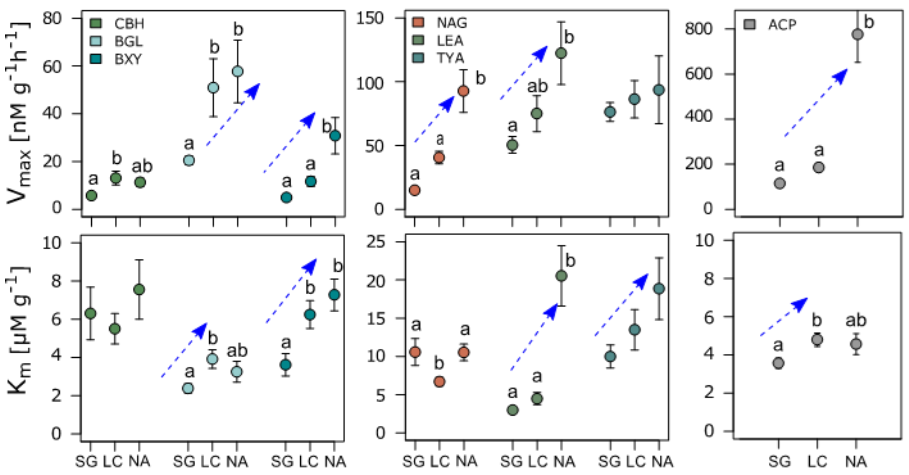

Figure 2.5.3: Continental gradients of potential activities (Vmax) and substrate affinities (Km) of the extracellular enzymes (from left to right): CBH = β−cellobiohydrolase, BGL = β−glucosidase, BXY = β−xylosidase, NAG = β−N−acetyl-glucosaminidase, LEA = leucine−amino-peptidase, TYA = tyrosine−amino-peptidase, ACP = acid phosphatase. Sites: Santa Gracia (SG), La Campana (LC), and Nahuelbuta (NA). Data present means±SE of north and south slopes and all soil depths and root distances (SG, LC: n = 36; NA: n = 24. Letters indicate significant ($p<0.05$) differences of activities and affinities between the study sites identified by GLMM. Activities of C−, N−, and P−acquiring enzymes increase with humidity, while substrate affinities decrease (i.e., increasing Km). Blue arrows show effects of the continental moisture gradient on the enzyme activities and affinities.

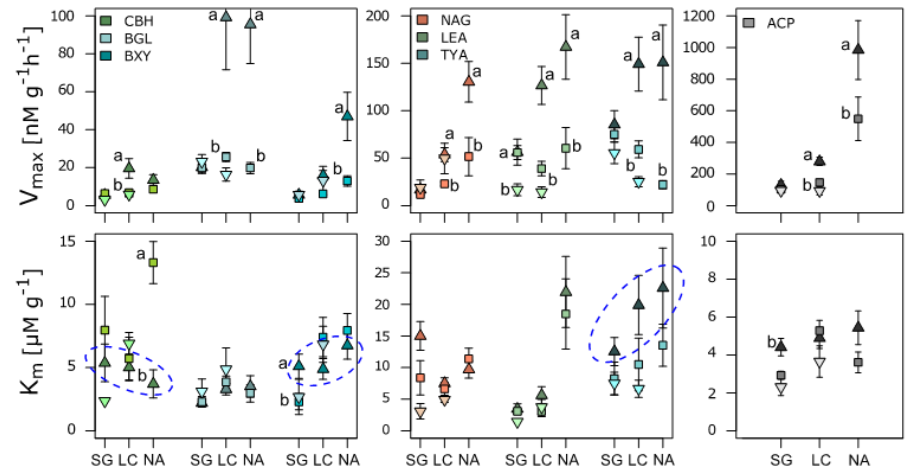

Figure 2.5.4: Potential activities (Vmax) and substrate affinities (Km) separated by soil depth (1 = topsoil, 2−3 = subsoil) of (from left to right): CBH = β−cellobiohydrolase, BGL = β−glucosidase, BXY = β−xylosidase, NAG = β−N−acetylgluco-saminidase, LEA = leucine−amino-peptidase, TYA = tyrosine−amino-peptidase, ACP = acid phosphatase. Sites: Santa Gracia (SG), La Campana (LC), and Nahuelbuta (NA). Soil depths: 1 = triangle, 2 = square, 3 = inverted triangle – Santa Gracia: 0−40 cm, 40−80 cm, 80−200 cm; La Campana: 0−60 cm, 60−120 cm, 120−200 cm; Nahuelbuta: 0−80 cm, 80−160 cm. Data present means±SE of both slopes and all root distances separated by soil depths (n = 12). Letters indicate significant differences ($p<0.05$) between soil depths. Activities of C−, N−, and P−acquiring enzymes are higher in the topsoil (depth 1) than subsoil (depth 2 and 3) at the sites under humid temperate (NA) and Mediterranean (LC) climate conditions. Substrate affinities of C−acquiring enzymes are tendential ($p>0.05$) higher in the topsoil than subsoil, while substrate affinities of N− and P−acquiring enzymes are tendential ($p>0.05$) lower in the topsoil and higher in the subsoil.

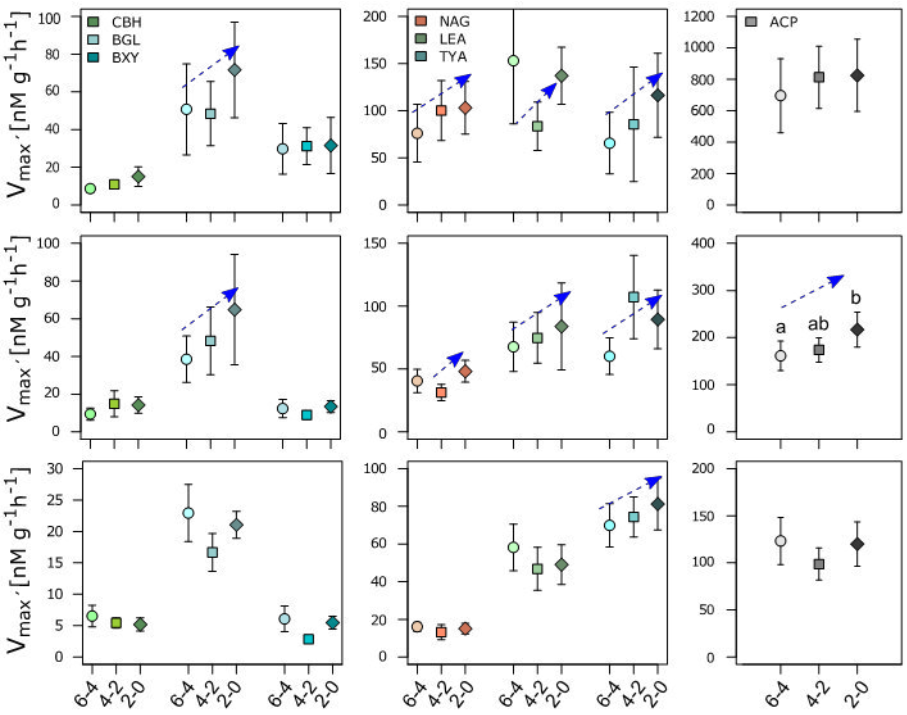

Figure 2.5.5: Enzyme activities (Vmax) from bulk soil (6–4 mm) to root proximity (2–0 mm). Nahuelbuta = top row; La Campana = middle row; Santa Gracia = bottom row. Data present means±SE from both slopes and all soil depths (SG, LC: n = 12; NA: n = 8). From left to right: CBH = β–cellobiohydrolase, BGL = β–glucosidase, BXY = β–xylosidase, NAG = β–N–acetylglucosaminidase, LEA = leucine–aminopeptidase, TYA = tyrosine–aminopeptidase, ACP = acid phosphatase. GLMM only identified activity differences of acid phosphatases in La Campana (Mediterranean climate conditions) as significant ($p<0.05$; indicated by letters). Blue arrows show effects of the rhizosphere gradient on enzyme activities. Trends ($p>0.05$) of increasing activities from bulk soil to roots of C–, N–, and P–acquiring enzymes were detected at the sites under humid temperate (Nahuelbuta) and Mediterranean (La Campana) climate conditions. At the site under semiarid conditions (Santa Gracia) only tyrosine–aminopeptidase activities showed an increasing trend ($p>0.05$) from bulk soil to roots.

Enzyme substrate affinities

Substrate affinities of C, N, and P acquiring enzymes declined (i.e., increasing K_m) on the continental scale from semiarid to humid climate conditions, while potential enzyme activities (V_{max}) grew (Figure 2.5.3). On the landscape scale, the only clear trend ($p>0.05$) was observed for β–cellobiohydrolase, which had lower substrate affinities on the south than north slope at the sites under humid temperate and Mediterranean conditions. N and P acquiring enzymes had generally higher substrate affinities in the subsoil, while substrate affinities of C acquiring enzymes were higher in the topsoil (up to 1.5– to 3–times) (Figure 2.5.4). Higher affinities of C acquiring enzymes in the subsoil than in the topsoil were common only under semiarid climate conditions. From root to bulk soil, affinities of C acquiring enzymes generally decreased ($p>0.05$), while affinities of N and P acquiring enzymes increased ($p>0.05$) (Figure 2.5.6).

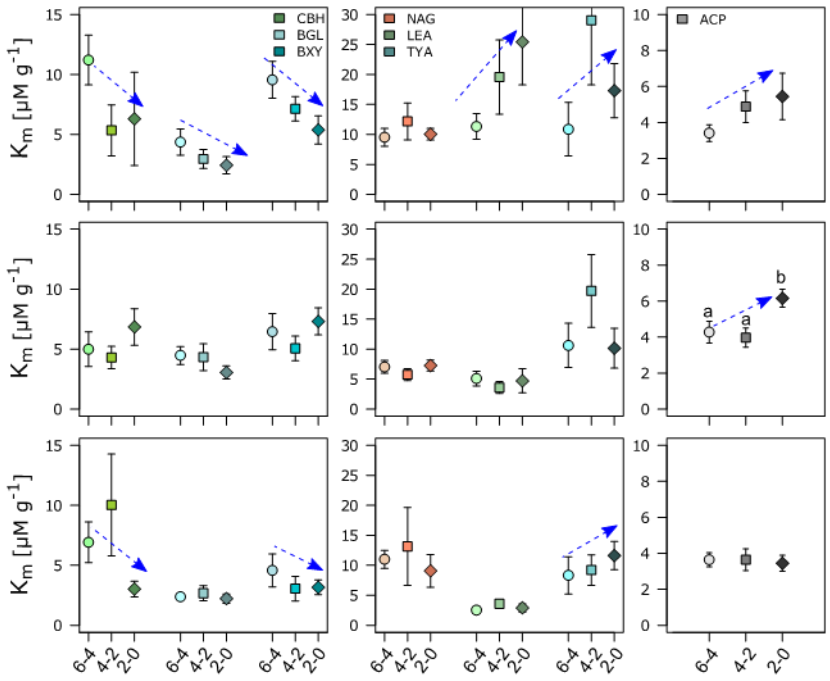

Figure 2.5.6: Substrate affinities (K_m) from bulk soil (0–6 mm) to root proximity (2–0 mm). Nahuelbuta = top row; La Campana = middle row; Santa Gracia = bottom row. Data present means±SE from both slopes and all soil depths (SG, LC: n = 12; NA: n = 8). From left to right: CBH = β–cellobiohydrolase, BGL = β–glucosidase, BXY = β–xylosidase, NAG = β–N–acetylglucosaminidase, LEA = leucine–aminopeptidase, TYA = tyrosine–aminopeptidase, ACP = acid phosphatase. GLMM only identified affinity differences of acid phosphatases in La Campana (Mediterranean climate conditions) as significant (*p<0.05*; indicated by letters). Blue arrows show effects of the rhizosphere gradient on substrate affinities. The strongest trends of substrate affinities were detected at the site under humid temperate conditions (Nahuelbuta): Affinities of C–acquiring enzymes increased from bulk soil to root, while affinities of N– and P–acquiring enzymes decreased.

Effects of abiotic and biotic factors on enzyme activities

Constrained axes of the RDA on potential enzyme activities were able to explain 57.1 % of their variation. The first and second axis of the RDA accounted for 41.4 % and 8.6 %, respectively (Figure 2.5.7). C and N contents strongly determine potential activities of all enzymes except of aminopeptidases (Figure 2.5.7). All these enzymes were primarily associated with the medium silt (6.3 – 20 µm), fine silt (2 – 6.3 µm), and clay (< 2µm) fraction of soil particles, whereas aminopeptidases were rather associated to the coarse silt fraction (20–63 µm) (Figure 2.5.7). Variance of aminopeptidases, and especially tyrosine–aminopeptidases, activities were primarily explained by soil moisture and pH (Figure 2.5.7). While soil moisture exerted a negative and pH a positive effect on aminopeptidase activities, these relations were reversed for the other enzymes. Only potential activities of β–glucosidase seemed less affected by pH (Figure 2.5.7).

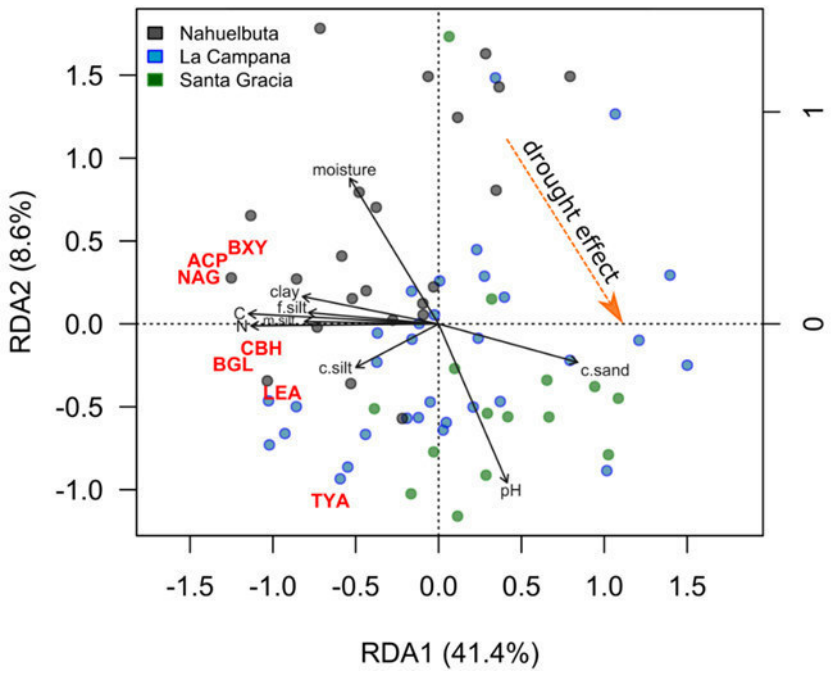

Figure 2.5.7: Redundancy analysis on potential activities of cellobiohydrolase (CBH), b-glucosidase (BGL), b-xylosidase (BXY), b-N-acetylglucosaminidase (NAG), leucine-aminopeptidase (LEA), tyrosine-aminopeptidase (TYA), and acid phosphatase (ACP) with C and N contents, soil moisture, pH, and particle size fractions as constraints. The overall RDA was significant with 999 permutations. A type II scaling (correlation) plot is shown, including only significant constraining variables. The constraining variables explained 57.1 % of the total variance.

Constrained axes of the RDA on C and N contents were able to explain 87.8 % of the variation. The first and second axis of the RDA accounted for 87.4 % and 0.4 % of the variation of C and N contents (Figure 2.5.8). C and N contents were strongest determined by small size soil particles (silt and clay fraction), whereas soil moisture and pH determined contents to a much lower extend (Figure 2.5.8). Soil particle size fractions strongest correlated with soil depth, while soil moisture and pH were stronger related to the factor site (Figure 2.5.8).

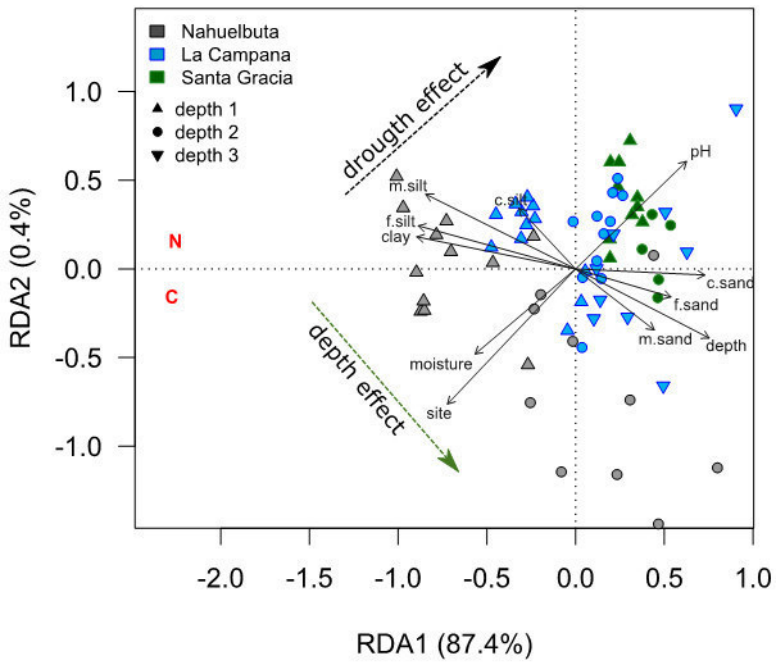

Figure 2.5.8: Redundancy analysis on C and N contents with soil moisture, pH, and particle size fractions as constraints. The overall RDA was significant with 999 permutations. A type II scaling (correlation) plot is shown, including only significant constraining variables. The constraining variables explained 87.8 % of the total variance.

2.5.5. Discussion

Activation of microbial activity in response to labile carbon

Microbial activity in soil is strongly limited by the availability of C (Blagodatsky and Richter, 1998; Hodge et al., 2000). On the continental scale, vegetation cover and plant species composition change fundamentally (Bernhard et al., 2018). Denser vegetation cover and higher productivity result in greater above– and belowground biomass input, which was apparent by higher C and N contents in the southern than in the northern sites (Figure 2.5.2). With greater amounts of biomass entering the soil, greater amounts of substrate and easily accessible C are available, enabling microorganisms to invest into nutrient acquisition (i.e., extracellular enzyme synthesis), as costs will be balanced off by energy and nutrients gained by soil organic matter decomposition (Allison et al., 2014; Hernández and Hobbie, 2010). In response, enzyme activities are stimulated, as was observed for C, N, and P acquiring enzymes on the continental scale from north to south (Figure 2.5.3). This was also displayed by the RDA as C and N contents explained a high degree of variances in enzyme activities (Figure 2.5.7) (Allison and Vitousek, 2005; Cheng et al., 2003; Hernández and Hobbie, 2010). Growing enzyme activities along with declining substrate affinities (i.e., high K_m) from north to south, suggest that especially on the continental scale the substrate availability is driving enzyme activities.

On the mesoscale – the soil depth profile – substrate availability, likewise, seemed to be a driving force for N and P acquiring enzymes in the subsoil. Enzymes with high substrate affinities in the subsoil, as seen for N and P acquiring enzymes (Figure 2.5.4), increase the competitiveness of microbes for nutrients under substrate limitation (Blagodatskaya et al., 2009; Hernández and Hobbie, 2010; Klipp and Heinrich, 1994).

Root exudates are one of the largest sources of labile C input (Bertin et al., 2003; Kuzyakov, 2002a; Pausch and Kuzyakov, 2018). Coinciding, measured C and N contents increased from bulk soil to root proximity (Figure 2.5.2). This rise of C content concurs with trends of ascending β–glucosidase and N and P acquiring enzyme activities from bulk soil to roots (Figure 2.5.5), indicating a stimulation of microbial activity by root–derived C (Blagodatskaya et al., 2010; Kuzyakov, 2002b; Meier et al., 2017). Root effects on enzyme activities were only significant for acid phosphatases under Mediterranean conditions, which is likely related to the sampling strategy. Razavi et al. (2016) and Ma et al. (2018) demonstrated that rhizosphere extension significantly differs for enzymes and plant species. Activity radii extended mostly less than 2 mm from roots, with the greatest extension detected for acid phosphatases (Razavi et al., 2016). The successful determination of phosphatase activities from rhizosphere to bulk soil,

however, suggests that activities for C and N cycling enzymes would be fully captured with a finer resolution of sampling distances.

Nutrient mining for stoichiometric homeostasis

Labile C does not only stimulate microbial activity as easily available energy source but can also induce a relative increase of microbial nutrient limitation by stoichiometric imbalance, which stimulates nutrient acquisition from other sources, e.g., from SOM (Cheng and Kuzyakov, 2005; Hernández and Hobbie, 2010; Phillips et al., 2011; Sinsabaugh and Moorhead, 1994). Activities of C acquiring enzymes did not only increase with higher C content (as shown in section 2.4.4.1) but also with greater N content, indicated by the strong relation observed in the RDA (Figure 2.5.7). In fact, the strong effect of N on C acquiring enzymes supports the conclusion that an upregulation of C acquisition in response to greater N availability is dominantly driving activities of these respective enzymes. Greater N availability (1) allows microorganisms to invest N into enzyme synthesis and (2) heightens the demand for C for microbial growth (Allison and Vitousek, 2005; Saiya–Cork et al., 2002; Sinsabaugh and Follstad Shah, 2012). C acquiring enzymes seemed to be driven by stoichiometric constraints on the meso– and microscale, which was supported by higher substrate affinities of β–cellobiohydrolase and β–xylosidase in topsoil and root proximity than in bulk soil (Figure 2.5.4, Figure 2.5.6). Increase of microbial activity and growth by labile carbon input surges microbial C demand (Hernández and Hobbie, 2010) and, thus, promotes the investment into C mining via enzyme production.

A similar dependence on stoichiometric constraints was also seen for N and P acquiring enzymes. Activities of N acquiring enzymes (Figure 2.5.3, Figure 2.5.5) increased towards places with great N limitation (i.e. site under humid temperate conditions, topsoil, root proximity) indicated by high C:N ratios (Figure 2.5.2). This elevation of activities in response to N limitation indicates an upregulation of N acquisition in response to stoichiometric imbalance, initiated by available C input and microbial activity stimulation (Loeppmann et al., 2016a; Sinsabaugh et al., 2009; Treseder and Vitousek, 2001). RDA results supported this response for activities of β–N–acetylglucosaminidases, as they C and N explained most of their variance (Figure 2.5.7). Patterns of activities of aminopeptidases, however, were better explained by pH and soil moisture (Figure 2.5.7).

Substrate affinities of N acquiring enzymes , which were lower in the topsoil than subsoil (Figure 2.5.4), and in root proximity than in bulk soil (Figure 2.5.6), indicate further that enzyme activities are not substrate limited but N demand driven (Loeppmann et al., 2016a; Stone and Plante, 2014). The same relations of affinities and activities as for N acquiring enzymes in the topsoil

and in root proximity were also seen for acid phosphatases. High activities but low substrate affinities indicate P demand to be driving the investment into enzymatic P acquisition.

Switch of N acquisition strategy on the continental scale

Higher activities of aminopeptidases, and especially of tyrosine–aminopeptidases, than of β–N–acetylglucosaminidases (Figure 2.5.3) in the northern (dry) site than in the southern sites, suggest that cleaving of amino acids is the dominant pathway of microorganisms to acquire N from organic sources at the moisture limited site. Peptides are the most important organic N source and easier to decompose than chitin (Derenne and Largeau, 2001; Kögel–Knabner, 2006; Sinsabaugh and Follstad Shah, 2012). In the site under semiarid (and also Mediterranean) conditions, peptides are more abundant than chitin due to less fungal biomass (seen as decrease of bacterial and fungal DNA from south to north; data not shown). Therefore, microorganisms need to primarily synthesize aminopeptidases to cover their basic N demand at the site under semiarid and Mediterranean conditions (Sinsabaugh and Follstad Shah, 2012). Ascending activities of β–N–acetylglucosaminidases with increasing humidity on the continental scale indicate a growing importance of chitin hydrolysis as N acquiring strategy as organic biomass input rises as well.

Soil moisture, pH, and soil particle size effect

Water availability affects plant productivity and, thus, organic matter input as litter and root–derived C into soil (Knapp et al., 2006) – this is on the continental scale. On the microscale, water limitation reduces water film thickness, reduces the substrate dissolution, and decreases its diffusion rates (Allison and Treseder, 2008; Davidson and Janssens, 2006; Schimel et al., 2007). Nutrient resources can, therefore, be accessed by roots and microorganisms only with sufficient water content in soil. Rising water availability stimulated potential activities of all enzymes except aminopeptidases (Figure 2.5.7). A positive effect of water availability on C content, but a negative effect on N content indicate that substrate availability (as C content) and the accessibility of N are modulated by water availability, which in turn can considerably affect enzyme activities (Figure 2.5.8).

Soil pH is an important factor regulating enzyme activities (Sinsabaugh et al., 2008). Acidity affects enzyme conformation (and thus its affinity to the substrate), binding of enzymes onto soil particles, breakdown of molecules, and nutrient availability (Carrino–Kyker et al., 2016; Quiquampoix et al., 1992; Turner, 2010). The RDA shows that pH had an especially marked effect on the activities of aminopeptidases (Figure 2.5.7), which coincided with the positive effect on N content (Figure 2.5.8).

Distribution of pores and particle size fractions are important for microbial habitats in soil (Kirchmann and Gerzabek 1999; Ruamps et al., 2011; Kravchenko and Guber, 2017). Depending on the size, microhabitats within pores can markedly differ in water supply, availability of substrates, or grazing pressure on microorganisms (Kuzyakov and Mason–Jones, 2019; Ruamps et al., 2011). Smaller particles are associated with greater C and N contents (Kandeler et al., 1999; Stemmer et al., 1998) and microbial biomass (Seesitsch et al., 2001; vanGestel et al., 1996). Smaller soil particles can form stable complexes with organic compounds, such as extracellular enzymes. Enzyme immobilization reduces their efficiency but protects them from decomposition and stabilizes their activity for a longer period (Demkina et al. 2017; Dick and Tabatabai 1987; Tietjen and Wetzel 2003). Greater proportions of silt and clay increased enzyme activities: 20 – 63 µm fraction for aminopeptidases, and <2 – 20 µm for the other enzymes (Figure 2.5.7).

2.5.6. Conclusions

Substrate availability and nutrient limitation (initiated by microbial activity stimulation and a shift in the stoichiometric balance) are two strong drivers of enzyme activities in soil. The results suggest that activities on the continental scale are mainly driven by substrate availability (i.e. belowground C input by plants). Additionally, from the arid north to the humid south, the chitin–based N acquisition got more relevant. Low potential activities and high substrate affinities of N and P acquiring enzymes in the subsoil and in the root free soil, suggested that substrate limitation is driving the investment into N and P acquisition on these scales. In the topsoil and in the rhizosphere, however, high potential activities and low substrate affinities of N and P acquiring enzymes, together with high C:N ratios, suggested that the C input increased microbial nutrient limitation, which primarily controlled activities of N and P acquiring enzymes at these sites. Likewise, stoichiometric constraints (i.e., C demand and N limitation) seemed to primarily control investment into cellulose and hemicellulose degrading enzymes on the meso– and microscale. A high degree of C and N contents being explained by clay and silt contents, and by soil moisture and pH to a smaller extent, indicated that the effects of substrate availability and nutrient limitation on the resource allocation for enzyme production indirectly depend on texture and are altered by water availability and acidity. A greater correlation of particle size fractions with soil depth than with study sites indicated further that texture becomes especially important when comparing enzyme activity patterns on the mesoscale, while the impact of soil moisture and pH dominates activity patterns stronger on the continental scale.

2.5.7. Acknowledgement

We thank the Chilean National Park Service Corporación Nacional Forestal (CONAF) for the possibility to work in the National Parks La Campana and Nahuelbuta. We also thank the Center for Advanced Research in Arid Zones (CEAZA) for the possibility to work in the National Reserve Santa Gracia. Further, we express our gratitude to Susann Enzmann for her help during laboratory work as well as the Centre for Stable Isotope Research and Analysis (KOSI). This work was supported by the German Research Foundation (DFG) [project number KU 1184/36–1] within the Priority Program 1803 'EarthShape: Earth Surface Shaping by Biota'.

2.5.8. References

Acosta–Martínez, V., Tabatabai, M.A., 2000. Enzyme activities in a limed agricultural soil. Biol. Fertil. Soils 31, 85–91. https://doi.org/10.1007/s003740050628

Allison, S.D., Chacon, S.S., German, D.P., 2014. Substrate concentration constraints on microbial decomposition. Soil Biol. Biochem. 79, 43–49. https://doi.org/10.1016/j.soilbio.2014.08.021

Allison, S.D., Jastrow, J.D., 2006. Activities of extracellular enzymes in physically isolated fractions of restored grassland soils. Soil Biol. Biochem. 38, 3245–3256. https://doi.org/10.1016/j.soilbio.2006.04.011

Allison, S.D., Treseder, K.K., 2008. Warming and drying suppress microbial activity and carbon cycling in boreal forest soils. Glob. Change Biol. 14, 2898–2909. https://doi.org/10.1111/j.1365–2486.2008.01716.x

Allison, S.D., Vitousek, P.M., 2005. Responses of extracellular enzymes to simple and complex nutrient inputs. Soil Biol. Biochem. 37, 937–944. https://doi.org/10.1016/j.soilbio.2004.09.014

Bates, D., Mächler, M., Bolker, B., Walker, S., 2015. Fitting Linear Mixed–Effects Models Using lme4. J. Stat. Softw. 67. https://doi.org/10.18637/jss.v067.i01

Bernhard, N., Moskwa, L.–M., Schmidt, K., Oeser, R.A., Aburto, F., Bader, M., Baumann, K., von Blanckenburg, F., Boy, J., van den Brink, L., Brucker, E., Büdel, B., Canessa, R., Dippold, M.A., Ehlers, T.A., Fuentes, J.P., Godoy, R., Jung, P., Karsten, U., Köster, M., Kuzyakov, Y., Leinweber, P., Neidhardt, H., Matus, F., Mueller, C.W., Oelmann, Y., Oses, R., Osses, P., Paulino, L., Samolov, E., Schaller, M., Schmid, M., Spielvogel, S., Spohn, M., Stock, S., Stroncik, N., Tielbörger, K., Übernickel, K., Scholten, T., Seguel, O., Wagner, D., Kühn, P., 2018. Pedogenic and microbial interrelations to regional climate and local topography: new insights from a climate gradient (arid to humid) along the Coastal Cordillera of Chile. Catena.

Bertin, C., Yang, X., Weston, L.A., 2003. The role of root exudates and allelochemicals in the rhizosphere. Plant Soil 256, 67–83. https://doi.org/10.1023/A:1026290508166

Blagodatskaya, E., Blagodatsky, S., Anderson, T.–H., Kuzyakov, Y., 2014. Microbial Growth and Carbon Use Efficiency in the Rhizosphere and Root–Free Soil. PLoS ONE 9, e93282. https://doi.org/10.1371/journal.pone.0093282

Blagodatskaya, E., Blagodatsky, S., Dorodnikov, M., Kuzyakov, Y., 2010. Elevated atmospheric CO_2 increases microbial growth rates in soil: results of three CO_2 enrichment experiments. Glob. Change Biol. 16, 836–848. https://doi.org/10.1111/j.1365–2486.2009.02006.x

Blagodatskaya, E.V., Blagodatsky, S.A., Anderson, T.–H., Kuzyakov, Y., 2009. Contrasting effects of glucose, living roots and maize straw on microbial growth kinetics and substrate availability in soil. Eur. J. Soil Sci. 60, 186–197. https://doi.org/10.1111/j.1365–2389.2008.01103.x

Blagodatsky, S.A., Richter, O., 1998. Microbial growth in soil and nitrogen turnover: a theoretical model considering the activity state of microorganisms. Soil Biol. Biochem. 30, 1743–1755. https://doi.org/10.1016/S0038–0717(98)00028–5

Burns, R.G., DeForest, J.L., Marxsen, J., Sinsabaugh, R.L., Stromberger, M.E., Wallenstein, M.D., Weintraub, M.N., Zoppini, A., 2013. Soil enzymes in a changing environment: Current knowledge and future directions. Soil Biol. Biochem. 58, 216–234. https://doi.org/10.1016/j.soilbio.2012.11.009

Carrino-Kyker, S.R., Kluber, L.A., Petersen, S.M., Coyle, K.P., Hewins, C.R., DeForest, J.L., Smemo, K.A., Burke, D.J., 2016. Mycorrhizal fungal communities respond to experimental elevation of soil pH and P availability in temperate hardwood forests. FEMS Microbiol. Ecol. 92, fiw024. https://doi.org/10.1093/femsec/fiw024

Chen, R., Senbayram, M., Blagodatsky, S., Myachina, O., Dittert, K., Lin, X., Blagodatskaya, E., Kuzyakov, Y., 2014. Soil C and N availability determine the priming effect: microbial N mining and stoichiometric decomposition theories. Glob. Change Biol. 20, 2356–2367. https://doi.org/10.1111/gcb.12475

Cheng, W., Johnson, D.W., Fu, S., 2003. Rhizosphere effects on decomposition. Soil Sci. Soc. Am. J. 67, 1418–1427.

Cheng, W., Kuzyakov, Y., 2005. Root effects on soil organic matter decomposition. Roots Soil Manag. Interact. Roots Soil 119–143.

Dakora, F.D., Phillips, D.A., 2002. Root exudates as mediators of mineral acquisition in low-nutrient environments. Plant Soil 245, 35–47. https://doi.org/10.1023/A:1020809400075

Davidson, E.A., Janssens, I.A., 2006. Temperature sensitivity of soil carbon decomposition and feedbacks to climate change. Nature 440, 165–173. https://doi.org/10.1038/nature04514

de Graaff, M.-A., Classen, A.T., Castro, H.F., Schadt, C.W., 2010. Labile soil carbon inputs mediate the soil microbial community composition and plant residue decomposition rates. New Phytol. 188, 1055–1064. https://doi.org/10.1111/j.1469-8137.2010.03427.x

de Graaff, M.-A., Jastrow, J.D., Gillette, S., Johns, A., Wullschleger, S.D., 2014. Differential priming of soil carbon driven by soil depth and root impacts on carbon availability. Soil Biol. Biochem. 69, 147–156. https://doi.org/10.1016/j.soilbio.2013.10.047

Demkina, E.V., Shanenko, E.F., Nikolaev, Y.A., El'-Registan, G.I., 2017. Model of the regulation of activity of immobilized enzymes (amylases) in soil. Microbiology 86, 231–240. https://doi.org/10.1134/S0026261717020060

De Nobili, M., Contin, M., Mondini, C., Brookes, P., 2001. Soil microbial biomass is triggered into activity by trace amounts of substrate. Soil Biol. Biochem. 33, 1163–1170. https://doi.org/10.1016/S0038-0717(01)00020-7

Derenne, S., Largeau, C., 2001. A REVIEW OF SOME IMPORTANT FAMILIES OF REFRACTORY MACROMOLECULES: COMPOSITION, ORIGIN, AND FATE IN SOILS AND SEDIMENTS. Soil Sci. 166, 833-847

Dick, W.A., Tabatabai, M.A., 1987. KINETICS AND ACTIVITIES OF PHOSPHATASE-CLAY COMPLEXES1. Soil Sci. 143, 5-15

German, D.P., Marcelo, K.R.B., Stone, M.M., Allison, S.D., 2012. The Michaelis-Menten kinetics of soil extracellular enzymes in response to temperature: a cross-latitudinal study. Glob. Change Biol. 18, 1468–1479. https://doi.org/10.1111/j.1365-2486.2011.02615.x

Hernández, D.L., Hobbie, S.E., 2010. The effects of substrate composition, quantity, and diversity on microbial activity. Plant Soil 335, 397–411. https://doi.org/10.1007/s11104-010-0428-9

Hodge, A., Robinson, D., Fitter, A., 2000. Are microorganisms more effective than plants at competing for nitrogen? Trends Plant Sci. 5, 304–308.

Hothorn, T., Bretz, F., Westfall, P., 2008. Simultaneous Inference in General Parametric Models. Biom J 50, 346–363.

Kandeler, E., Stemmer, M., Klimanek, E.-M., 1999. Response of soil microbial biomass, urease and xylanase within particle size fractions to long-term soil management. Soil Biol. Biochem. 31, 261–273. https://doi.org/10.1016/S0038-0717(98)00115-1

Kielak, A.M., Cretoiu, M.S., Semenov, A.V., Sørensen, S.J., van Elsas, J.D., 2013. Bacterial chitinolytic communities respond to chitin and pH alteration in soil. Appl. Environ. Microbiol. 79, 263–272. https://doi.org/10.1128/AEM.02546-12

Kirchmann, H., Gerzabek, M.H., 1999. Relationship between soil organic matter and micropores in a long-term experiment at Ultuna, Sweden. J. Plant Nutr. Soil Sci. 162, 493–498. https://doi.org/10.1002/(SICI)1522-2624(199910)162:5<493::AID-JPLN493>3.0.CO;2-S

Knapp, A.K., Burns, C.E., Fynn, R.W.S., Kirkman, K.P., Morris, C.D., Smith, M.D., 2006. Convergence and contingency in production–precipitation relationships in North American and South African C4 grasslands. Oecologia 149, 456–464. https://doi.org/10.1007/s00442-006-0468-2

Klipp, E., Heinrich, R., 1994. Evolutionary Optimization of Enzyme Kinetic Parameters; Effect of Constraints. J. Theor. Biol. 171, 309–323. https://doi.org/10.1006/jtbi.1994.1234

Kögel-Knabner, I., 2006. Chemical structure of organic N and organic P in soil. Nucleic Acids Proteins Soil 23–48.

Kravchenko, A.N., Guber, A.K., 2017. Soil pores and their contributions to soil carbon processes. Geoderma 287, 31–39. https://doi.org/10.1016/j.geoderma.2016.06.027

Kuzyakov, Y., 2002a. Factors affecting rhizosphere priming effects. J. Plant Nutr. Soil Sci. 165, 382–396.

Kuzyakov, Yakov, 2002b. Separating microbial respiration of exudates from root respiration in non-sterile soils: a comparison of four methods. Soil Biol. Biochem. 34, 1621–1631. https://doi.org/10.1016/S0038-0717(02)00146-3

Kuzyakov, Y., Mason-Jones, K., 2019. Nano-scale undead drivers of microbial life, biogeochemical turnover and ecosystem functions. Soil Biol. Biochem. https://doi.org/10.1016/j.soilbio.2018.09.032

Kuzyakov, Y., Xu, X., 2013. Competition between roots and microorganisms for nitrogen: mechanisms and ecological relevance. New Phytol. 198, 656–669. https://doi.org/10.1111/nph.12235

Loeppmann, S., Blagodatskaya, E., Pausch, J., Kuzyakov, Y., 2016. Enzyme properties down the soil profile – A matter of substrate quality in rhizosphere and detritusphere. Soil Biol. Biochem. 103, 274–283. https://doi.org/10.1016/j.soilbio.2016.08.023

Ma, X., Zarebanadkouki, M., Kuzyakov, Y., Blagodatskaya, E., Pausch, J., Razavi, B.S., 2018. Spatial patterns of enzyme activities in the rhizosphere: Effects of root hairs and root radius. Soil Biol. Biochem. 118, 69–78. https://doi.org/10.1016/j.soilbio.2017.12.009

Manzoni, S., Schimel, J.P., Porporato, A., 2012. Responses of soil microbial communities to water stress: results from a meta-analysis. Ecology 93, 930–938. https://doi.org/10.1890/11-0026.1

Marx, M.-C., Wood, M., Jarvis, S.., 2001. A microplate fluorimetric assay for the study of enzyme diversity in soils. Soil Biol. Biochem. 33, 1633–1640. https://doi.org/10.1016/S0038-0717(01)00079-7

Meier, I.C., Finzi, A.C., Phillips, R.P., 2017. Root exudates increase N availability by stimulating microbial turnover of fast-cycling N pools. Soil Biol. Biochem. 106, 119–128. https://doi.org/10.1016/j.soilbio.2016.12.004

Moorhead, D.L., Lashermes, G., Sinsabaugh, R.L., 2012. A theoretical model of C- and N-acquiring exoenzyme activities, which balances microbial demands during decomposition. Soil Biol. Biochem. 53, 133–141. https://doi.org/10.1016/j.soilbio.2012.05.011

Oeser, R.A., Stroncik, N., Moskwa, L.-M., Bernhard, N., Schaller, M., Canessa, R., van den Brink, L., Köster, M., Brucker, E., Stock, S., Fuentes, J.P., Godoy, R., Matus, F., Oses Pedraza, R., Osses McIntyre, P., Paulino, L., Seguel, O., Bader, M.Y., Boy, J., Dippold, M.A., Ehlers, T.A., Kühn, P., Kuzyakov, Y., Leinweber, P., Scholten, T., Spielvogel, S., Spohn, M., Übernickel, K., Tielbörger, K., Wagner, D., von Blanckenburg, F., 2018. Chemistry and Microbiology of the Critical Zone along a steep climate and vegetation gradient in the Chilean Coastal Cordillera. Catena.

Oksanen, J., Blanchet, G., Friendly, M., Kindt, R., Legendre, P., McGlinn, D., Minchin, P.R., O'Hara, R.B., Simpson, G.L., Solymos, P., Stevens, H.H., Szoecs, E., Wagner, H., 2017. vegan: Community Ecology Package.

Olander, L.P., Vitousek, P.M., 2000. Regulation of soil phosphatase and chitinase activity by N and P availability. Biogeochemistry 49, 175–191. https://doi.org/10.1023/A:1006316117817

Pausch, J., Kuzyakov, Y., 2018. Carbon input by roots into the soil: Quantification of rhizodeposition from root to ecosystem scale. Glob. Change Biol. 24, 1–12. https://doi.org/10.1111/gcb.13850

Phillips, R.P., Finzi, A.C., Bernhardt, E.S., 2011. Enhanced root exudation induces microbial feedbacks to N cycling in a pine forest under long−term CO2 fumigation: Rhizosphere feedbacks in CO2−enriched forests. Ecol. Lett. 14, 187–194. https://doi.org/10.1111/j.1461−0248.2010.01570.x

Quiquampoix, H., Staunton, S., Baron, M.−H., Ratcliffe, R.G., 1993. Interpretation of the pH dependence of protein adsorption on clay mineral surfaces and its relevance to the understanding of extracellular enzyme activity in soil. Colloids Surf. Physicochem. Eng. Asp. 75, 85–93. https://doi.org/10.1016/0927−7757(93)80419−F

R Core Team, 2017. R: A Language and Environment for Statistical Computing. Vienna, Austria.

Razavi, B.S., Zarebanadkouki, M., Blagodatskaya, E., Kuzyakov, Y., 2016. Rhizosphere shape of lentil and maize: Spatial distribution of enzyme activities. Soil Biol. Biochem. 96, 229–237. https://doi.org/10.1016/j.soilbio.2016.02.020

Rosseel, Y., 2012. lavaan : An R Package for Structural Equation Modeling. J. Stat. Softw. 48. https://doi.org/10.18637/jss.v048.i02

Ruamps, L.S., Nunan, N., Chenu, C., 2011. Microbial biogeography at the soil pore scale. Soil Biol. Biochem. 43, 280–286. https://doi.org/10.1016/j.soilbio.2010.10.010

Saiya−Cork, K.., Sinsabaugh, R.., Zak, D.., 2002. The effects of long term nitrogen deposition on extracellular enzyme activity in an Acer saccharum forest soil. Soil Biol. Biochem. 34, 1309–1315. https://doi.org/10.1016/S0038−0717(02)00074−3

Sanaullah, M., Blagodatskaya, E., Chabbi, A., Rumpel, C., Kuzyakov, Y., 2011. Drought effects on microbial biomass and enzyme activities in the rhizosphere of grasses depend on plant community composition. Appl. Soil Ecol. 48, 38–44. https://doi.org/10.1016/j.apsoil.2011.02.004

Schimel, J., Balser, T.C., Wallenstein, M., 2007. Microbial Stress−Response Physiology and Its Implications for Ecosystem Function. Ecology 88, 1386–1394.

Schimel, J., Weintraub, M.N., 2003. The implications of exoenzyme activity on microbial carbon and nitrogen limitation in soil: a theoretical model. Soil Biol. Biochem. 35, 549–563. https://doi.org/10.1016/S0038−0717(03)00015−4

Sessitsch, A., Weilharter, A., Gerzabek, M.H., Kirchmann, H., Kandeler, E., 2001. Microbial Population Structures in Soil Particle Size Fractions of a Long−Term Fertilizer Field Experiment. Appl. Environ. Microbiol. 67, 4215–4224. https://doi.org/10.1128/AEM.67.9.4215−4224.2001

Sinsabaugh, R.L., Antibus, R.K., Linkins, A.E., McClaugherty, C.A., Rayburn, L., Repert, D., Weiland, T., 1993. Wood Decomposition: Nitrogen and Phosphorus Dynamics in Relation to Extracellular Enzyme Activity. Ecology 74, 1586–1593. https://doi.org/10.2307/1940086

Sinsabaugh, R.L., Belnap, J., Findlay, S.G., Shah, J.J.F., Hill, B.H., Kuehn, K.A., Kuske, C.R., Litvak, M.E., Martinez, N.G., Moorhead, D.L., Warnock, D.D., 2014. Extracellular enzyme kinetics scale with resource availability. Biogeochemistry 121, 287–304. https://doi.org/10.1007/s10533−014−0030−y

Sinsabaugh, R.L., Follstad Shah, J.J., 2012. Ecoenzymatic Stoichiometry and Ecological Theory. Annu. Rev. Ecol. Evol. Syst. 43, 313–343. https://doi.org/10.1146/annurev−ecolsys−071112−124414

Sinsabaugh, R.L., Hill, B.H., Follstad Shah, J.J., 2009. Ecoenzymatic stoichiometry of microbial organic nutrient acquisition in soil and sediment. Nature 462, 795–798. https://doi.org/10.1038/nature08632

Sinsabaugh, R.L., Lauber, C.L., Weintraub, M.N., Ahmed, B., Allison, S.D., Crenshaw, C., Contosta, A.R., Cusack, D., Frey, S., Gallo, M.E., Gartner, T.B., Hobbie, S.E., Holland, K., Keeler, B.L., Powers, J.S., Stursova, M., Takacs−Vesbach, C., Waldrop, M.P., Wallenstein, M.D., Zak, D.R., Zeglin, L.H., 2008. Stoichiometry of soil enzyme activity at global scale. Ecol. Lett. 11, 1252–1264. https://doi.org/10.1111/j.1461−0248.2008.01245.x

Sinsabaugh, R.L., Moorhead, D.L., 1994. Resource allocation to extracellular enzyme production: A model for nitrogen and phosphorus control of litter decomposition. Soil Biol. Biochem. 26, 1305–1311. https://doi.org/10.1016/0038-0717(94)90211-9

Spiers, G.A., McGill, W.B., 1979. Effects of phosphorus addition and energy supply on acid phosphatase production and activity in soils. Soil Biol. Biochem. 11, 3–8. https://doi.org/10.1016/0038-0717(79)90110-X

Steinweg, J.M., Dukes, J.S., Wallenstein, M.D., 2012. Modeling the effects of temperature and moisture on soil enzyme activity: Linking laboratory assays to continuous field data. Soil Biol. Biochem. 55, 85–92. https://doi.org/10.1016/j.soilbio.2012.06.015

Stemmer, M., Gerzabek, M.H., Kandeler, E., 1998. Organic matter and enzyme activity in particle-size fractions of soils obtained after low-energy sonication. Soil Biol. Biochem. 30, 9–17. https://doi.org/10.1016/S0038-0717(97)00093-X

Stone, M.M., Plante, A.F., 2014. Changes in phosphatase kinetics with soil depth across a variable tropical landscape. Soil Biol. Biochem. 71, 61–67. https://doi.org/10.1016/j.soilbio.2014.01.006

Tarafdar, J.C., Jungk, A., 1987. Phosphatase activity in the rhizosphere and its relation to the depletion of soil organic phosphorus. Biol. Fertil. Soils 3, 199–204. https://doi.org/10.1007/BF00640630

Tietjen, T., G. Wetzel, R., 2003. Extracellular enzyme-clay mineral complexes: Enzyme adsorption, alteration of enzyme activity, and protection from photodegradation. Aquat. Ecol. 37, 331–339. https://doi.org/10.1023/B:AECO.0000007044.52801.6b

Treseder, K.K., Vitousek, P.M., 2001. EFFECTS OF SOIL NUTRIENT AVAILABILITY ON INVESTMENT IN ACQUISITION OF N AND P IN HAWAIIAN RAIN FORESTS. Ecology 82, 946–954. https://doi.org/10.1890/0012-9658(2001)082[0946:EOSNAO]2.0.CO;2

Tscherko, D., Hammesfahr, U., Marx, M.-C., Kandeler, E., 2004. Shifts in rhizosphere microbial communities and enzyme activity of Poa alpina across an alpine chronosequence. Soil Biol. Biochem. 36, 1685–1698. https://doi.org/10.1016/j.soilbio.2004.07.004

Turner, B.L., 2010. Variation in pH Optima of Hydrolytic Enzyme Activities in Tropical Rain Forest Soils. Appl. Environ. Microbiol. 76, 6485–6493. https://doi.org/10.1128/AEM.00560-10

Turner, B.L., Wright, J.S., 2014. The response of microbial biomass and hydrolytic enzymes to a decade of nitrogen, phosphorus, and potassium addition in a lowland tropical rain forest. Biogeochemistry 117, 115–130. https://doi.org/10.1007/s10533-013-9848-y

Weintraub, M.N., Scott-Denton, L.E., Schmidt, S.K., Monson, R.K., 2007. The effects of tree rhizodeposition on soil exoenzyme activity, dissolved organic carbon, and nutrient availability in a subalpine forest ecosystem. Oecologia 154, 327–338. https://doi.org/10.1007/s00442-007-0804-1

Van Gestel, M., Merckx, R., Vlassak, K., 1996. Spatial distribution of microbial biomass in microaggregates of a silty-loam soil and the relation with the resistance of microorganisms to soil drying. Soil Biol. Biochem. 28, 503–510. https://doi.org/10.1016/0038-0717(95)00192-1

Table: S 2.5.1: Study site description.

	Parque National Nahuebluta	Parque National La Campana	Reserva Santa Gracia	References
Abbreviation	NA	LC	SG	
Location	37.81°S, 73.01°W	32.96°S, 71.06°W	29.76°S, 71.14°W	
Altitude [m a.s.l.]	1240	730	680	
Distance to Pacific Ocean [km]				
	55	43	23	
Climate	humid	mediterranean	semiarid	Muñoz et al. 2007; Bernhard et al., 2018
MAT [°C]	6.1	13.6	13.9	WorldClim data, Hijmans et al., 2005
MAP [mm]	1600	358	81	WorldClim data, Hijmans et al., 2005
Parent material	granitoid	granitoid	granitoid	Bernhard et al., 2018; Oeser et al., 2018
Soil type	Umbrisol	Cambisol	Cambisol	Bernhard et al., 2018
Vegetation cover	coniferous forest	decidous forest	sclerophyllous shrubs	Bernhard et al., 2018
		sclerophyllous shrubs	cacti	
Dominant species				
south slopes	*Araucaria araucana*	*Colliguaja oderifera*	*Proustia cuneifolia*	Bernhard et al., 2018
	Nothofagus antarctica	*Lithrea caustic*	*Balbisia peduncularis*	
	Chusquea coleu	*Aristeguietia salvia*	*Senna cumingii*	
		Podanthus mitiqui		
north slopes	*Nothofagus obliqua*	*Lithrea caustic*	*Cordia decandra*	
	Araucaria araucana	*Jubaea chilensis*	*Adesmia spp.*	
	Gaultheria mucronata	*Retamilla trinervia*	*Baccharis paniculatum*	
			Eulychnia acida	
			Cumulopuntia sphaerica	

Table: S 2.5.2: Residual standard errors of the fitted non−linear saturation curves calculated by the Michaelis Menten equation. From left to right: CBH = β−cellobiohydrolase, BGL = β−glucosidase, BXY = β−xylosidase, NAG = β−N−acetylglucosaminidase, LEA = leucine−aminopeptidase, TYA = tyrosine−aminopeptidase, ACP = acid phosphatase.

site	slope aspect	slope position	soil depth [cm]	root proximity [mm]	CBH	BGL	BXY	NAG	LEA	TYA	ACP
NA	S	top	0−80	0−2	1.61	10.44	4.17	7.15	5.80	1.30	36.36
NA	S	top	0−80	2−4	3.23	14.65	6.65	6.89	4.49	1.41	58.61
NA	S	top	0−80	4−6	na	13.85	7.27	7.66	5.00	11.49	60.11
NA	S	mid	0−80	0−2	1.77	9.70	5.96	14.42	4.85	12.40	39.67
NA	S	mid	0−80	2−4	4.91	na	5.43	7.32	15.62	3.30	61.42
NA	S	mid	0−80	4−6	0.87	1.52	0.74	9.85	2.43	0.57	19.26
NA	S	bottom	0−80	0−2	4.50	11.48	7.37	9.09	8.52	7.22	106.56
NA	S	bottom	0−80	2−4	0.54	6.78	3.26	4.34	3.21	na	37.07
NA	S	bottom	0−80	4−6	1.57	14.80	6.57	8.40	5.39	1.83	61.79
NA	S	top	80−160	0−2	0.84	2.35	1.14	4.51	2.35	4.03	22.92
NA	S	top	80−160	4−6	0.76	1.28	1.14	1.09	3.53	2.28	14.54
NA	S	mid	80−160	0−2	1.76	1.82	0.93	3.80	8.32	0.68	12.24
NA	S	mid	80−160	2−4	1.35	1.51	1.10	10.76	1.79	1.58	19.25
NA	S	mid	80−160	4−6	0.88	0.99	0.77	0.74	na	na	3.60
NA	S	bottom	80−160	0−2	0.75	1.71	1.20	1.24	na	0.65	76.44
NA	S	bottom	80−160	2−4	1.22	1.63	1.62	1.82	1.96	0.45	43.96
NA	S	bottom	80−160	4−6	1.04	1.48	1.06	1.48	na	0.94	31.73
NA	N	mid	0−80	0−2	na	1.60	1.65	2.71	2.52	13.54	21.80
NA	N	mid	0−80	2−4	0.82	2.55	1.44	1.20	3.93	1.49	15.20
NA	N	mid	0−80	4−6	1.03	1.04	1.44	0.84	1.71	na	6.48
NA	N	mid	80−160	0−2	na	2.18	1.10	1.42	3.47	1.39	16.22
NA	N	mid	80−160	2−4	0.59	0.62	0.49	0.83	1.87	na	10.45
NA	N	mid	80−160	4−6	0.38	1.39	0.77	0.82	0.40	na	9.56
LC	S	top	0−60	0−2	4.30	35.92	2.05	6.03	7.14	2.79	38.46
LC	S	top	0−60	2−4	2.23	9.66	1.50	3.94	5.50	1.95	25.01
LC	S	top	0−60	4−6	1.95	8.05	2.10	10.04	12.67	9.66	19.69
LC	S	mid	0−60	0−2	0.79	1.55	2.31	4.88	4.00	3.01	26.96
LC	S	mid	0−60	2−4	1.45	4.34	1.68	2.95	8.60	18.71	18.37
LC	S	mid	0−60	4−6	1.12	6.34	2.72	5.67	3.27	1.38	16.72
LC	S	bottom	0−60	0−2	1.15	8.34	3.23	7.23	9.89	18.73	21.13
LC	S	bottom	0−60	2−4	1.41	5.19	2.34	5.46	8.06	3.62	24.50
LC	S	bottom	0−60	4−6	0.93	3.44	1.47	9.96	9.68	2.42	12.47
LC	S	top	60−120	0−2	0.51	1.72	1.10	2.94	2.51	2.37	12.58
LC	S	top	60−120	2−4	0.81	2.20	0.70	2.07	na	1.15	8.31
LC	S	top	60−120	4−6	0.58	1.54	0.97	1.57	1.36	0.73	7.35
LC	S	mid	60−120	0−2	na	1.12	0.88	0.76	na	5.00	9.77
LC	S	mid	60−120	2−4	0.48	1.37	2.45	1.77	na	4.61	8.10
LC	S	mid	60−120	4−6	0.74	1.57	0.79	2.35	na	14.51	4.27
LC	S	bottom	60−120	0−2	1.77	4.43	1.05	1.59	1.24	11.41	8.84
LC	S	bottom	60−120	2−4	0.92	4.55	0.86	1.53	2.28	0.92	5.32
LC	S	bottom	60−120	4−6	1.55	3.99	0.98	1.05	3.86	5.84	2.99

LC	S	mid	>120	0–2	0.51	1.45	1.22	3.09	2.11	na	4.99
LC	S	mid	>120	2–4	na	1.66	0.46	na	na	2.60	na
LC	S	mid	>120	4–6	na	0.66	0.45	1.07	na	na	4.05
LC	S	bottom	>120	0–2	na	0.69	0.74	na	na	1.50	3.34
LC	S	bottom	>120	2–4	na	1.01	6.93	na	0.42	2.63	3.06
LC	S	bottom	>120	4–6	na	0.54	2.18	na	0.19	0.42	na
LC	N	mid	0–60	0–2	0.76	2.82	1.13	1.13	1.93	1.17	6.20
LC	N	mid	0–60	2–4	0.60	2.71	0.82	1.49	3.49	3.81	13.59
LC	N	mid	0–60	4–6	1.35	1.40	1.22	1.27	1.37	2.44	11.57
LC	N	mid	60–120	0–2	0.56	1.57	0.50	1.34	na	2.21	10.53
LC	N	mid	60–120	2–4	0.96	2.25	0.65	1.35	1.44	0.94	9.50
LC	N	mid	60–120	4–6	na	2.23	0.31	na	1.01	0.65	14.74
LC	N	mid	>120	0–2	0.68	1.40	1.04	4.95	0.71	1.73	14.19
LC	N	mid	>120	2–4	0.89	1.64	0.99	4.65	1.63	1.91	8.28
LC	N	mid	>120	4–6	0.61	1.24	0.82	3.64	0.79	1.18	5.17
SG	S	top	0–40	0–2	1.38	3.07	0.76	1.25	8.00	14.14	6.96
SG	S	top	0–40	2–4	0.78	2.24	0.83	1.51	3.55	12.92	4.96
SG	S	top	0–40	4–6	na	2.30	1.21	1.99	3.40	5.60	6.72
SG	S	mid	0–40	0–2	0.70	5.86	1.07	2.63	4.76	1.24	7.74
SG	S	mid	0–40	2–4	0.49	2.30	0.77	na	na	1.45	4.85
SG	S	mid	0–40	4–6	1.04	1.57	0.92	1.20	na	6.90	10.63
SG	S	lower	0–40	0–2	na	0.94	0.75	na	2.58	1.50	5.10
SG	S	lower	0–40	2–4	na	1.19	0.67	na	1.91	5.94	3.59
SG	S	lower	0–40	4–6	0.88	0.76	1.08	na	na	1.00	3.00
SG	S	bottom	0–40	0–2	0.28	0.96	na	na	1.11	2.64	4.22
SG	S	bottom	0–40	2–4	0.44	1.84	0.57	0.99	1.05	3.53	2.25
SG	S	bottom	0–40	4–6	0.33	2.19	0.61	1.14	1.49	4.70	4.77
SG	S	top	40–80	0–2	2.03	1.57	1.19	0.86	6.00	5.49	4.24
SG	S	top	40–80	2–4	1.05	0.84	0.82	na	2.51	4.94	5.05
SG	S	top	40–80	4–6	0.55	1.25	11.20	na	2.15	5.78	2.09
SG	S	mid	40–80	0–2	na	2.58	0.60	0.67	5.24	1.85	7.89
SG	S	mid	40–80	2–4	na	9.47	0.47	na	1.41	5.37	2.60
SG	S	mid	40–80	4–6	na	1.52	0.39	na	1.02	0.75	3.73
SG	S	lower	40–80	0–2	0.43	1.66	0.70	0.83	2.78	4.59	8.90
SG	S	lower	40–80	2–4	na	1.51	0.88	2.01	0.88	3.61	5.63
SG	S	lower	40–80	4–6	0.71	2.49	0.95	1.29	1.45	3.71	7.05
SG	S	bottom	40–80	0–2	0.29	1.45	na	0.43	1.72	4.37	8.70
SG	S	bottom	40–80	2–4	0.72	1.77	14.12	1.45	3.59	4.04	6.05
SG	S	bottom	40–80	4–6	1.22	1.02	1.09	0.80	4.36	5.98	5.16
SG	S	top	>80	0–2	2.39	2.74	1.32	6.56	0.39	4.02	10.60
SG	S	mid	>80	0–2	0.71	2.23	1.09	6.87	na	1.43	16.66
SG	S	lower	>80	0–2	na	1.72	0.79	0.89	0.39	2.03	2.06
SG	S	bottom	>80	0–2	na	0.97	0.91	na	0.85	4.59	7.43
SG	N	mid	0–40	0–2	1.31	2.02	1.61	1.57	1.53	2.18	10.20
SG	N	mid	0–40	2–4	0.53	2.46	0.88	2.58	0.67	3.26	6.24

SG	N	mid	0–40	4–6	0.71	2.50	1.44	1.10	4.14	10.73	12.20
SG	N	mid	40–80	0–2	na	0.97	0.96	2.48	1.78	6.21	4.72
SG	N	mid	40–80	2–4	na	0.82	0.81	na	0.72	0.73	4.27
SG	N	mid	40–80	4–6	0.71	3.30	1.58	2.15	4.58	15.99	8.48
SG	N	mid	>80	0–2	0.26	1.64	0.69	3.77	1.67	4.76	3.40

2.6. Published and submitted co−authorships during the PhD

Published:

Stock, S.C., Koester, M., Boy, J., Godoy, R., Nájera, F., Matus, F., Merino, C., Abdallah, K., Leuschner, C., Spielvogel, S., Gorbushina, A.A., Kuzyakov, Y., Dippold, M.A., 2021. Plant carbon investment in fine roots and arbuscular mycorrhizal fungi: A cross−biome study on nutrient acquisition strategies. Science of The Total Environment 781, 146748.

Najera, F., Dippold, M.A., Boy, J., Seguel, O., Koester, M., Stock, S., Merino, C., Kuzyakov, Y., Matus, F., 2020. Effects of drying/rewetting on soil aggregate dynamics and implications for organic matter turnover. Biol Fertil Soils 56 (7), 893–905.

Matus, F., Stock, S., Eschenbach, W., Dyckmans, J., Merino, C., Nájera, F., Köster, M., Kuzyakov, Y., Dippold, M.A., 2019. Ferrous Wheel Hypothesis: Abiotic nitrate incorporation into dissolved organic matter. Geochimica et Cosmochimica Acta 245, 514–524

Bernhard, N., Moskwa, L.−M., Schmidt, K., Oeser, R.A., Aburto, F., Bader, M.Y., Baumann, K., Blanckenburg, F. von, Boy, J., van den Brink, L., Brucker, E., Büdel, B., Canessa, R., Dippold, M.A., Ehlers, T.A., Fuentes, J.P., Godoy, R., Jung, P., Karsten, U., Köster, M., Kuzyakov, Y., Leinweber, P., Neidhardt, H., Matus, F., Mueller, C.W., Oelmann, Y., Oses, R., Osses, P., Paulino, L., Samolov, E., Schaller, M., Schmid, M., Spielvogel, S., Spohn, M., Stock, S., Stroncik, N., Tielbörger, K., Übernickel, K., Scholten, T., Seguel, O., Wagner, D., Kühn, P., 2018. Pedogenic and microbial interrelations to regional climate and local topography: New insights from a climate gradient (arid to humid) along the Coastal Cordillera of Chile. CATENA 170, 335–355.

Oeser, R.A., Stroncik, N., Moskwa, L.−M., Bernhard, N., Schaller, M., Canessa, R., van den Brink, L., Köster, M., Brucker, E., Stock, S., Fuentes, J.P., Godoy, R., Matus, F.J., Oses Pedraza, R., Osses McIntyre, P., Paulino, L., Seguel, O., Bader, M.Y., Boy, J., Dippold, M.A., Ehlers, T.A., Kühn, P., Kuzyakov, Y., Leinweber, P., Scholten, T., Spielvogel, S., Spohn, M., Übernickel, K., Tielbörger, K., Wagner, D., Blanckenburg, F. von, 2018. Chemistry and microbiology of the Critical Zone along a steep climate and vegetation gradient in the Chilean Coastal Cordillera. CATENA 170, 183–203.

Submitted:

Khaled Abdallah; Svenja C. Stock; Felix Heeger; Moritz Koester; Francisco Nájera; Francisco Matus; Carolina Merino; Sandra Spielvogel; Anna Gorbushina; Yakov Kuzyakov; Michaela A. DippoldSoil nitrogen cycling along a precipitation gradient: from semi-desert to rainforest. Submitted to Geoderma on June 21st, 2021

Acknowledgements

First of all, I want to thank Sandra Spielvogel for giving me the opportunity to work on this fantastic topic and supporting me all along the way to this doctoral degree. Not less important was the support of Michaela Dippold who always had an open ear and never-ending patience. Thank you both for your dedication to this topic, great discussions and for always seeing a way to solve any problem.

I thank Kirstin Übernickel, Leandro Paulino, Friedhelm von Blanckenburg and Todd Ehlers for the excellent organization of all *Earthshape* meetings. I thank Jens Boy and Jörg Prietzel for great discussions and critical comments on my manuscripts. This work could not have been done without the support from our Chilean collaborators. A special thanks to Carolina Merino, Francisco Najera, Francisco Matus, and Roberto Godoy for fantastic support with field work, lab space and especially for your hospitality that made me feel welcome from the first second.

I am grateful for all the help from the laboratory staff at university of Goettingen. I thank Karin Schmidt for her great effort in measuring so many samples and for her amazing coffee and tea support. Also, Suzan Enzman thank you for always being supportive in the lab and you positive energy. Thank you to all my colleagues and friends from the Geographical Institute at the University of Bern and the University of Goettingen, to all my co-authors and people who contributed to this work. Thank you, Kyle Mason-Jones, for taking the time to comment on this thesis and for unforgettable climbs during our time in Goettingen. My thanks to Callum Banfield for the hours we spent together in the lab and your dedication to solving any lab problems that arose. A big thank to Svenja Stock for being such a good colleague and friend, for great field work campaigns and discussions on the data. To Pancho, who was a friend from the first minute and your unconditioned support. Thank you, Andy, Nina, Katha, Sara, Lingling, Joscha and Matthias for, moral support, movie evenings and so much more.

I thank my family for all the support they gave me through all the years. Thank you, Renee, for being with me on this journey.

Erklärung

(gemäß Promotionsreglement der Philosophisch–naturwissenschaftlichen Fakultät der Universität Bern (PromR Phil.–nat. 19) Artikel 18)

„Ich erkläre hiermit, dass ich diese Arbeit selbständig verfasst und keine anderen als die angegebenen Quellen benutzt habe. Alle Stellen, die wörtlich oder sinngemäss aus Quellen entnommen wurden, habe ich als solche gekennzeichnet. Mir ist bekannt, dass andernfalls der Senat gemäss Artikel 36 Absatz 1 Buchstabe r des Gesetzes über die Universität vom 5. September 1996 und Artikel 69 des Universitätsstatuts vom 7. Juni 2011 zum Entzug des Doktortitels berechtigt ist. Für die Zwecke der Begutachtung und der Überprüfung der Einhaltung der Selbständigkeitserklärung bzw. der Reglemente betreffend Plagiate erteile ich der Universität Bern das Recht, die dazu erforderlichen Personendaten zu bearbeiten und Nutzungshandlungen vorzunehmen, insbesondere die Doktorarbeit zu vervielfältigen und dauerhaft in einer Datenbank zu speichern sowie diese zur Überprüfung von Arbeiten Dritter zu verwenden oder hierzu zur Verfügung zu stellen."

Bern, den _____ _____

Moritz Köster